

**The geochemical response of sedimentary
archives to rapid recent glacier retreat at the
western Antarctic Peninsula (WAP): from source to
sink**

Geochemische Reaktion von Sedimentarchiven auf den
schnellen rezenten Gletscherrückzug auf der Westantarktischen
Halbinsel: von der Quelle zur Senke

Dissertation

zur Erlangung des Grades eines Doktors der Naturwissenschaften

– Dr. rer. nat. –

angenommen bei der Fakultät für Mathematik und Naturwissenschaften der
Carl von Ossietzky Universität Oldenburg

von

Patrick Monien

geboren am 15.02.1977 in Oldenburg

Erstgutachter: Prof. Dr. Hans-Jürgen Brumsack

Zweitgutachter: Prof. Dr. Jürgen Rullkötter

Eingereicht am: 02. Oktober 2013

Disputation am: 11. Februar 2014

Abstract

Since the middle of the 20th century the western Antarctic Peninsula (WAP) belongs to the regions with the most rapid warming on Earth and is therefore considered to be one of the hotspots of climate change. During the last six decades an increase in mean annual air temperatures of more than 3°C is observed along the WAP causing severe changes in local cryospheric and ecosystems. The overarching aim of this thesis is to assess, whether the documented temperature increase and associated glacier retreat at WAP is reflected in the geochemistry of sedimentary records and if such episodes did occur during other periods within the Holocene. Moreover, this work focusses on biogeochemical processes in maritime Antarctic sediments and their implications for local benthic and pelagic communities.

The rapid recent warming in the WAP region has already been related to significant changes in the distribution of one of the regions' upper-trophic level predators, such as the Chinstrap (*Pygoscelis antarctica*) Adélie (*P. adélieae*) and Gentoo (*P. papua*) penguins. In order to investigate the influence of past climate change on the distribution and occurrence of local penguin colonies lake sediments from Ardley Island and Fildes Peninsula, King George Island (KGI), were analysed for geochemical bioelements (As, Ba, Ca, Cd, Cu, Hg, P, TS, Se, Sr, and Zn) that are known to be characteristic for penguin guano. These element concentrations were used to reconstruct a high-resolution history of local penguin populations during the last 9,000 years. The results of this study let assume that Gentoo penguin colonies generally expanded to occupy more inland areas of Ardley Island during 'warmer' periods, particularly during the Mid-Holocene Hypsithermal when relative sea levels were c. 8-12 m higher. In addition to rapid and catastrophic crashes as a result of volcanic eruptions, low population episodes appear to have coincided with colder

phases with the expansion of land and sea-ice creating unfavourable breeding conditions for this species.

The assumption that this region has experienced short-term alternations in regional climate was supported by high-resolution investigation of marine sediments from Maxwell Bay, KGI. Palaeoclimatic interpretation of major and trace element distribution patterns and granulometric data allowed the identification of two main climatic events during the Late Holocene, synchronous in timing to the Little Ice Age (c. 550–50 cal yr BP) and the Medieval Warm Period (c. 1400–550 cal yr BP) of the Northern Hemisphere. Concurrent with the gradual glacier retreat and an enhanced input of eroded particulate material into coastal areas ^{210}Pb data moreover showed that sediment mass accumulation rates have almost tripled since the end of the 1930s.

In order to get insights into biogeochemical processes in coastal Antarctic sediments and to test whether they are influenced by the observed changes of the sedimentary environment, redox-sensitive trace metals, nutrients and terminal metabolic products were investigated in pore waters of surface sediments from Potter Cove, KGI. Their distribution revealed a high spatial variability in redox conditions at the study site. Particularly in the shallower areas of the bay significant correlation between sulphate depletion and total alkalinity indicates sulphate reduction to be the major pathway of organic matter mineralisation. In contrast, dissimilatory metal oxide reduction seems to be prevailing in the newly ice-free areas and the deeper troughs. Here dissolved iron concentrations of up to 700 μM were present, which are presumably responsible for high metal assimilation in benthic deposit feeders, like *Laternula elliptica*. It is suggested that the increased accumulation of fine-grained material with high amounts of reducible metal oxides in combination with a reduced availability of metabolisable organic matter and enhanced physical and biological disturbance by bottom water currents, ice scouring and burrowing organisms favours metal oxide reduction over sulphate reduction in these respective areas.

Based on modelled iron reduction rates an Antarctic shelf-derived input of potentially bioavailable iron to the Southern Ocean was calculated, which is in the same order of magnitude as the flux provided by icebergs and significantly higher than the input by aeolian dust. This makes suboxic shelf sediments a key source of iron for the high nutrient-low chlorophyll areas of the Southern Ocean.

Kurzfassung

Seit Mitte des 20. Jahrhunderts gehört die Westantarktische Halbinsel (WAH) zu den sich am stärksten erwärmenden Regionen der Erde, womit sie zu einer der Schlüsselregionen des Klimawandels zählt. In den vergangenen sechzig Jahren wurde im Bereich der WAH ein Anstieg der mittleren Jahrestemperatur von mehr als 3°C beobachtet, der zu weitreichenden Veränderungen lokaler Kryo- und Ökosysteme geführt hat. Das Hauptziel dieser Dissertation ist zu ermitteln, ob sich der dokumentierte Temperaturanstieg und der damit verbundene Gletscherrückzug in der Geochemie sedimentärer Archive widerspiegelt und ob solche Klimaepisoden bereits zu anderen Zeiten im Holozän aufgetreten sind. Zudem bildet die Untersuchung biogeochemischer Prozesse in Sedimenten der maritimen Antarktis und deren Einflüsse auf lokale, benthische und pelagische Lebensgemeinschaften einen Schwerpunkt dieser Arbeit.

Die schnelle rezente Erwärmung in der Region der WAH wurde bereits mit signifikanten Veränderungen in der Häufigkeit und Verteilung von Predatoren, wie Zügel- (*Pygoscelis antarctica*), Adélie- (*P. adeliae*) und Eselspinguinen (*P. papua*) in Verbindung gebracht. Um den Einfluss vergangener Klimawandel auf die Verteilung und das Auftreten von lokalen Pinguinkolonien zu untersuchen, wurden Seesedimente von Ardley Island und der Fildes Halbinsel, King George Island (KGI) auf geochemische Bioelemente (As, Ba, Ca, Cd, Cu, Hg, P, TS, Se, Sr und Zn) hin untersucht, die bekanntermaßen charakteristisch für Pinguinguano sind. Diese Elementkonzentrationen wurden für eine hochauflösende Rekonstruktion der lokalen Pinguinpopulation in den vergangenen 9000 Jahren verwendet. Die Ergebnisse dieser Studie lassen vermuten, dass die Eselspinguinkolonien in Warmphasen im Allgemeinen expandiert sind und Gebiete weiter im Inneren der Insel besiedelt haben.

Dies gilt insbesondere für die Mittlere Wärmezeit, in der der relative Meeresspiegel etwa 8-12 m höher gewesen ist. Neben schnellen und katastrophenartigen Populationseinbrüchen, die auf vulkanische Eruptionen zurückzuführen sind, scheinen Zeitabschnitte mit niedrigeren Populationszahlen mit kälteren Phasen, der Ausweitung von Land- und Meereis und den damit verbundenen ungünstigeren Brutbedingungen für diese Spezies verbunden zu sein. Die Vermutung, dass diese Region kurzfristige Änderungen in Bezug auf das regionale Klima erfahren hat, wurde durch hochauflösende Untersuchungen an marinen Sedimenten von der Maxwell Bay (KGI) bestätigt. Die paläoklimatische Interpretation von Haupt- und Spurenelementverteilungsmustern und granulometrischen Daten ermöglichten die Identifizierung von zwei Hauptklimaphasen während des späten Holozäns, die zeitgleich mit der "Kleinen Eiszeit" und der "Mittelalterlichen Warmzeit" der Nordhemisphäre auftraten. Einhergehend mit dem schrittweisen Gletscherrückzug und dem vermehrten Eintrag von erodiertem partikulärem Material in Küstengebiete zeigten ^{210}Pb Daten zudem, dass sich die Sedimentakkumulationsraten in diesem Gebiet seit dem Ende der 1930er Jahren fast verdreifacht hat.

Um Einblicke in biogeochemische Prozesse in antarktischen Küstensedimenten zu erhalten und um herauszufinden, ob diese durch die beobachteten Veränderungen der sedimentären Umwelt beeinflusst werden, wurden redox-sensitive Spurenmetalle, Nährstoffe und metabolische Endprodukte in Porenwässern von Oberflächensedimenten der Potter Cove (KGI) untersucht. Deren Verteilungen lassen eine hohe räumliche Variabilität der vorherrschenden Redoxbedingungen im Untersuchungsgebiet erkennen. Besonders in den flacheren Gebieten der Bucht zeigt die signifikante Korrelation zwischen Sulfatabnahme und Alkalinität, dass Sulfatreduktion den Hauptprozess der Mineralisierung von organischem Material darstellt. Demgegenüber scheint die dissimilatorische Reduktion von Metalloxiden in den neuen eisfreien Gebieten und den tieferen Senken der Bucht zu dominieren. Hier wurden Konzentrationen von gelöstem Fe von bis zu 700 μM gefunden,

die höchstwahrscheinlich auch für die erhöhte Metallaufnahme in benthischen Filtrierern wie *Laternula elliptica* verantwortlich sind. Es ist anzunehmen, dass die erhöhte Akkumulation von feinkörnigem Material mit hohem Anteil an reduzierbaren Metalloxiden in Kombination mit der verminderten Verfügbarkeit von metabolisierbarem organischem Material und einer erhöhten physikalischen und biologischen Störung des Sediments durch Bodenwasserströmungen, Eisberge und bioturbierende Organismen dafür sorgt, dass in diesen Gebieten Metalloxidreduktion gegenüber Sulfdatreduktion begünstigt wird. Basierend auf modellierten Eisenreduktionsraten wurde ein vom antarktischen Schelf verursachter Eintrag von bioverfügbarem Eisen in den Südozean berechnet, der in derselben Größenordnung liegt wie die Zufuhr mittels Eisbergen und der signifikant höher ist als der Eintrag durch äolischen Staub. Somit stellen suboxische Schelfsedimente eine wichtige Quelle für Eisen in den HNLC-Gebieten des Südozeans dar.

Table of contents

Abstract	i
Kurzfassung	iv
Table of contents	vii
Figure legend	xii
Table legend	xvi
1. Introduction	1
1.1. Regional settings	1
1.1.1. South Shetland Islands and King George Island	1
1.1.2. Maxwell Bay and adjacent coves	3
1.2. Recent changes at the WAP and their implications for local cryo- and ecosystems	4
1.3. Natural iron fertilisation in the Southern Ocean	6
1.4. Unlocking the past: Holocene climate variability at the WAP	9
1.5. Inferring past climate from historical penguin populations	12
1.6. Objectives of this thesis	15
2. Outline of the author's contribution	18
3. A geochemical record of late Holocene palaeoenvironmental changes at King George Island (maritime Antarctica)	24
3.1. Abstract	24
3.2. Introduction	25
3.3. Regional setting	26
3.4. Material and Methods	28
3.4.1. Sampling	28
3.4.2. Depth correction	29

3.4.3. Core description	29
3.4.4. Laboratory analyses	30
3.4.5. Calculation of SiO ₂ excess	32
3.4.6. Chemical Index of Alteration	33
3.4.7. Statistics	33
3.5. Results	34
3.5.1. Chronology	34
3.5.2. Lithogenic background	35
3.5.3. Vertical distributions of elements	36
3.5.4. Bioproductivity proxies	38
3.5.5. Geochemistry of sulphur and redox sensitive elements	39
3.5.6. Chemical weathering	40
3.6. Discussion	41
3.6.1. Lithogenic background and teprochronology	41
3.6.2. Alteration of potential proxies by early diagenesis	42
3.6.3. Controlling factors of bioproductivity in the coastal WAP region: reduced sea ice coverage and reduced sunlight penetration	44
3.6.4. Proxies for changes in provenance and glacier extents on Barton Peninsula	45
3.6.5. Geochemical proxies for the recent rapid warming along the WAP	48
3.7. Conclusions	49
3.8. Acknowledgements	50
3.9. Supplementary material	50
4. Penguin colony expansion on the western Antarctic Peninsula during Holocene warm phases curtailed by volcanic activity	51
4.1. Introduction	51
4.2. Results and Discussion	52

4.3.	Supplementary Information	62
4.3.1.	Supplementary Material and Methods	62
4.3.2.	Supplementary Results and Discussion	72
4.3.3.	Supplementary Figures	76
4.3.4.	Supplementary Tables	81
4.4.	Acknowledgements	86
5.	Redox conditions and trace metal cycling in coastal sediments from the maritime Antarctic	87
5.1.	Abstract	87
5.2.	Introduction	88
5.3.	Trace element geochemistry	90
5.3.1.	Iron	90
5.3.2.	Manganese	90
5.3.3.	Rhenium	91
5.3.4.	Molybdenum	91
5.3.5.	Uranium	91
5.4.	Regional Setting	92
5.5.	Material and Methods	93
5.5.1.	Sampling	93
5.5.2.	Pore water analyses	95
5.5.3.	Sediment analyses	96
5.5.4.	Calculation of sulphate depletion	96
5.5.5.	Estimation of sulphate and iron reduction rates	97
5.5.6.	Statistics	98
5.6.	Results and Discussion	99
5.6.1.	Pore water profiles and redox zonation of Potter Cove surface sediments	99
5.6.2.	Pore water stoichiometry and sulphate reduction rates	105

5.6.3. Spatial distribution of redox conditions in Potter Cove surface sediments	108
5.6.4. Factors controlling redox conditions in Potter Cove sediments	111
5.6.5. Coastal pore waters as a significant source of trace metals and micronutrients in the Antarctic region	115
5.7. Conclusions	117
5.8. Acknowledgements	118
6. Influence of the pore water geochemistry on Fe and Mn assimilation in <i>Laternula elliptica</i> at King George Island (Antarctica)	119
6.1. Abstract	119
6.2. Introduction	120
6.3. Material and Methods	122
6.3.1. Sample collection and experimental treatment	122
6.3.2. Element analysis	124
6.3.3. Standard reference material	125
6.3.4. Pore water and seawater analysis	126
6.3.5. Statistical analysis	128
6.4. Results	129
6.4.1. Iron withdrawal experiments	129
6.4.2. Element concentrations of hemolymph, pore water, and seawater samples	130
6.4.3. Tissue element analysis (Fe, Mn)	133
6.5. Discussion	134
6.5.1. What controls Fe accumulation in <i>L. elliptica</i> ?	134
6.5.2. Combined geochemical and physiological interpretation of Fe accumulation pattern in <i>L. elliptica</i>	136
6.5.3. Manganese assimilation by <i>L. elliptica</i>	140
6.6. Conclusions and Outlook	142

6.7. Acknowledgements	143
7. Climate fluctuations during the past two millennia as recorded in sediments from Maxwell Bay, South Shetland Islands, West Antarctica	145
8. A new Holocene relative sea level curve for the South Shetland Islands, Antarctica	147
9. The influence of sedimentation on metal accumulation and cellular oxidative stress markers in the Antarctic bivalve <i>Laternula elliptica</i>	149
10. On the phytoplankton bloom in coastal waters of southern King George Island (Antarctica) in January 2010: An exceptional feature?	151
11. Summary & Outlook	153
12. References	158
Danksagungen	195
Curriculum vitae	197
Eidesstattliche Erklärung	198

Figure legend

(abbreviated)

Fig. 1.1.	a) Map of Antarctica, b) the western Antarctic Peninsula with the South Shetland Islands, c) King George Island including tectonical block division after Birkenmajer et al. (2001) and d) Maxwell Bay with adjacent coves and peninsulas.	2
Fig. 1.2.	Scheme of sources and cycling of dissolved and particulate iron in the Southern Ocean modified after Tagliabue et al. (2010).	7
Fig. 1.3.	Compilation of Antarctic Peninsula climate records and syntheses derived from marine and lacustrine sedimentary records and ice cores.	11
Fig. 1.4.	Accumulation pathway of trace elements during the food chain and their deposition as ornithogenic soils in lake sediments.	13
Fig. 3.1.	Map of the study site with sediment core location.	27
Fig. 3.2.	Lithology of core PS 69/335. Radiographs of selected sections showing a) worm tube evidence for high bioturbation rates in the upper part of the core, b) the coarser grained tephra layer at 6.36 mcd, and c) evidence for flaser bedding at the bottom.	30
Fig. 3.3.	a) Age and linear sedimentation rate vs depth of core PS 69/335 according to radiocarbon and ^{210}Pb measurements. b) Mass accumulation rates of bulk sediment (MAR_{BS}) vs year AD in Maxwell Bay calculated using the ^{210}Pb dating model.	34
Fig. 3.4.	$(\text{Na}_2\text{O} + \text{K}_2\text{O})$ vs SiO_2 content of the BSi adjusted sedimentary deposits from Maxwell Bay compared with the composition of bedrock from the Fildes, Barton and Weaver Peninsula.	35

Fig. 3.5.	Trace element abundances of core PS 69/335 and bedrock from Barton, Weaver and Fildes Peninsula normalised to N-MORB (Sun & McDonough, 1989).	35
Fig. 3.6.	a) Vertical distribution of Ti/Al, K/Al, and Ca/Al of core PS 69/335 vs depth and age as determined by quantitative WD-XRF accompanied by photomicrographs of selected sediments at b) 442, c) 448, and d) 744 cal yr BP.	37
Fig. 3.7.	a) Comparison between selected bioproductivity proxies ($\text{SiO}_{2\text{xs}}$, BSi, TOC), Zr/Al, K/Al, Rb/Al, Ti/Al, and Mg/K ratios vs age in Maxwell Bay sediments and recorded climatic events of several studies along the WAP.	38
Fig. 3.8.	Vertical distribution of TS, TOC, and U/Al vs depth and age of core PS 69/335.	39
Fig. 3.9.	Cross plot of TOC and TS of Maxwell Bay sediments.	40
Fig. 3.10.	a) $\text{CaO}^* + \text{Na}_2\text{O} - \text{K}_2\text{O} - \text{Al}_2\text{O}_3$ diagram of the samples from Maxwell Bay and the average composition of the dominant bedrock of the Barton Peninsula, b) vertical distribution of the CIA vs age of core PS 69/335.	41
Fig. 4.1.	Overview maps showing a) Antarctica with b) the location of the western Antarctic Peninsula with the sampling site of core GC047/TC046 and the South Shetland Islands, c) King George Island (KGI) with d) the Fildes Peninsula and e) the sampling sites at Yanou Lake (KGI) and Ardley Lake, Ardley Island.	53
Fig. 4.2.	Downcore profiles of selected aluminium normalised guano-elements (P, Zn, As, Cu, TN, TS, TC, Ca, Sr, Hg, Se) and lithogenic elements (Si, Ti, Zr) of core ARD.	55
Fig. 4.3.	Proxies for changes in penguin occupation, sea-ice and Holocene climate at the Antarctic Peninsula.	57

Fig. 4.S1.	Classical age model, linear sedimentation rates and lithology of the Ardley Lake cores.	76
Fig. 4.S2.	Classical age model, linear sedimentation rates and lithology of the Yanou Lake cores.	77
Fig. 4.S3.	Developing regional tephrochronology for the Antarctic Peninsula region, ARD core F _{o.s.} profile from Ardley Lake (Fig. 4.3) compared to TOC, LOI ₅₅₀ and guano-associated bioelement/aluminium ratios vs age in core YAN.	78
Fig. 4.S4.	Results of R-mode cluster analysis for measured major and trace elements of a) core ARD and b) core YAN.	79
Fig. 4.S5.	a) C/N and b) C/P ratios b) of Ardley Lake sediments, local lichens, liverworts, mosses, vascular plants and different types of ornithogenic soils.	79
Fig. 4.S6.	Biplots of selected element/aluminium ratios of Ardley Lake sediments, ornithogenic soils and local bedrock.	80
Fig. 5.1.	Map of the study site with sampling locations. Sediment cores and surface samples were taken during austral summers 2009/2010 and 2010/2011.	93
Fig. 5.2.	Pore water profiles of nutrients (NO ₃ ⁻ , NH ₄ ⁺ , PO ₄ ³⁻), redox-sensitive trace metals (Fe, Mn, Mo, U, Re), sulphate depletion (SO ₄ ²⁻ _{dep}), H ₂ S, and total alkalinity (TA) from core P04 close to the tidewater glacier front.	100
Fig. 5.3.	Pore water profiles of nutrients (NO ₃ ⁻ , NH ₄ ⁺ , PO ₄ ³⁻), redox-sensitive trace metals (Fe, Mn, Mo, U, Re), sulphate depletion (SO ₄ ²⁻ _{dep}), H ₂ S, and total alkalinity (TA) from cores P05 and P08 obtained from the central Potter Cove.	103

Fig. 5.4.	Pore water profiles of nutrients (NO_3^- , NH_4^+ , PO_4^{3-}), redox-sensitive trace metals (Fe, Mn, Mo, U, Re), sulphate depletion (SO_4^{2-} dep), H_2S , and total alkalinity (TA) from cores P07 and K48 obtained close to the southern coast of Potter Peninsula.	105
Fig. 5.5.	Ratios of total alkalinity (TA) to sulphate depletion (SO_4^{2-} dep) in pore waters from Potter Cove sediments with best-fit linear regressions.	107
Fig. 5.6.	a) Pore water profiles of sulphate (SO_4^{2-}) and b) modelled sulphate reduction rates (SRR) for the upper 20 cm of cores P07, KX4, K23, and K48 using the REC model after Lettmann et al. (2012).	108
Fig. 5.7.	Contourplots of several pore water (Fe, Mn, SO_4^{2-} dep, PO_4^{3-} , TA) and solid phase parameters (TOC, TS) of Potter Cove sediments.	109
Fig. 6.1.	a) Map of the Antarctic Peninsula with b) King George Island, and c) Potter Cove including the sampling stations.	123
Fig. 6.2.	Iron concentrations in bivalve hemolymph during a 14 day withdrawal experiment in a) filtered seawater and b) filtered seawater spiked with $10 \mu\text{mol L}^{-1}$ Fe.	130
Fig. 6.3.	Iron concentrations in bivalve hemolymph.	131
Fig. 6.4.	Pore water profiles of Fe and Mn down to 11 cm below seafloor of four stations related to the sampling sites of <i>L. elliptica</i> .	132
Fig. 6.5.	Shell volume normalised Fe and Mn tissue contents: a) Fe contents in gills, b) Mn contents in gills, c) Fe contents in DG, d) Fe contents in mantle tissues.	133
Fig. 6.6.	Possible Fe and Mn uptake pathways for <i>L. elliptica</i> in Potter Cove related to diagenetic processes in the upper sediment layers.	143

Table legend

(abbreviated)

Table 1.1.	Standard Gibbs free energy (ΔG) of the principle respiratory pathways of natural organic matter mineralisation with acetate as an electron donor taken from Canfield and Thamdrup (2009).	8
Table 3.1.	Coring sites on cruise ANT-XXIII/4.	29
Table 4.S1.	Comparison of bio-elements found in ornithogenic sediments and penguin guano around Antarctica.	81
Table 4.S2.	Radiocarbon ages for a) the Ardley Lake sediment core, b) the Yanou Lake sediment core and c) marine cores from the Anvers.	82
Table 4.S3.	Correlation coefficients between the elements in Lake Ardley sediments.	84
Table 4.S4.	Correlation coefficients between the elements in Lake Yanou sediments.	85
Table 5.1.	Overview of pore water core locations, including sampling date, UTM coordinates (Zone Z21E; WGS84), water depth, coring gear and core length.	94
Table 5.2.	Precision and accuracy of pore water (Fe, Mn, Mo, Na, Re, U, PO_4^{3-} , NO_x^- , NO_2^- , NH_4^+ , SO_4^{2-}) and solid phase (TS, TC, TIC) analyses of Potter Cove sediments.	98
Table 5.3.	Iron reduction rates in the upper 20 cm of selected Potter Cove sediments estimated by using the REC model after Lettmann et al. (2012).	116

Table 6.1.	Results of the reference materials IAEA-A13 and IAEA407 analysed at two/three different laboratories.	126
Table 6.2.	Mean and range of Ca, Fe, K, Mn, Na, and Sr concentrations in bivalve hemolymph, pore water, and seawater.	131
Table 6.3.	Mean contents \pm 95% confidence intervals [mg kg ⁻¹ dry weight] of Fe and Mn in tissues of <i>L. elliptica</i> for all three stations.	139

1. Introduction

The western Antarctic Peninsula (WAP) belongs to one of the fastest warming regions on Earth representing a key area for studying the impact of changing climate on sea level, glacier dynamics and terrestrial and marine ecosystems (Clarke et al., 2007). During the last decades severe changes in the distribution of the local fauna and flora have been observed (e.g., Ducklow et al., 2007; Montes-Hugo et al., 2009). However, the lack of suitable long-term data series makes it difficult to put them into the context of climate change and to predict future scenarios. To date there are only a few geological data series from this highly sensitive area dealing with palaeoenvironmental conditions in the Holocene. Although most of the records suggest that the WAP has experienced widespread climate variability since the Last Glacial Maximum (e.g., Bentley et al., 2009; Michalchuk et al., 2009), the records available so far are often ambiguous, which complicates the search for respective driving mechanisms.

This thesis aims to shed more light on Holocene climate variability at the WAP and its past and recent impact on local cryo- and ecosystems. The eight papers comprised in this thesis will concentrate on inorganic geochemical proxies analysed in marine and lake sediment cores around King George Island, WAP. Moreover, recent biogeochemical processes in the water column and in pore waters of the Antarctic shelf, which have never been addressed before, and their implications on benthic and pelagic organisms, will be discussed.

1.1. Regional settings

1.1.1. South Shetland Islands and King George Island

The South Shetland Islands (SSI) represent a mature 550 km long Jurassic-Quaternary island arc located c. 100 km west of the northern Antarctic Peninsula (AP)

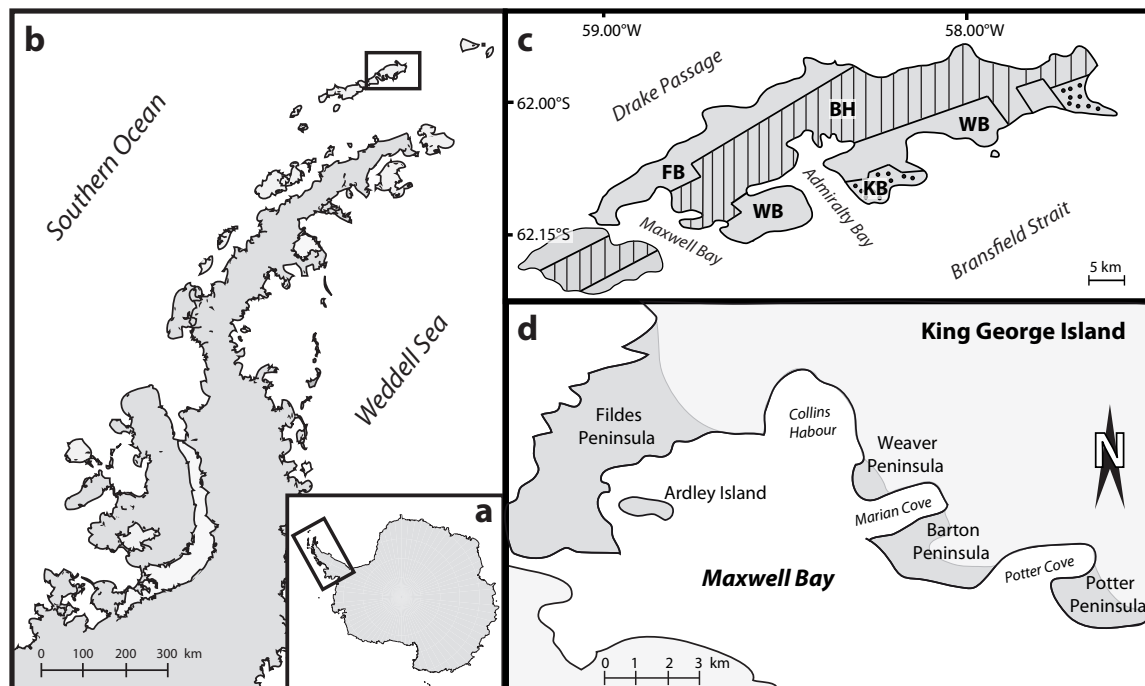


Fig. 1.1. a) Map of Antarctica, b) the western Antarctic Peninsula with the South Shetland Islands, c) King George Island including tectonical block division after Birkenmajer et al. (2001) and d) Maxwell Bay with adjacent coves and peninsulas. BH: Barton Horst, FB: Fildes Block, KB: Krakow Block, WB: Warszawa Block.

and 950 km southeast of the South American continent (Yeo et al., 2004; Machado et al., 2008). The arc is separated from the AP by the Bransfield Strait, a Cenozoic marginal basin, and founded on a basement of schists, gneiss and deformed sedimentary rocks (Birkenmajer, 1992; Lee et al., 2004; Machado et al., 2008). According to Ashcroft (1972) and Barker and Griffith (1972), there is geophysical evidence that the SSI are situated on a continental micro-plate, which may be connected to a back-arc spreading ridge in the Bransfield Basin in the southeast, and a now inactive oceanic trench in the northwest. King George Island (KGI), the study area, is the largest of the SSI (Smellie et al., 1984; Yeo et al., 2004). Its interior is mostly covered by a c. 600 m thick ice-cap and exposed outcrops and ice-free areas are only present in restricted zones along the shoreline (Yeo et al., 2004; Lee et al., 2004). In general, KGI can be divided into four main lithostratigraphic units that are separated by large-scale strike-slip faults: the Barton Horst, the

Fildes Block (Fildes Peninsula), the Warszawa Block (Potter Peninsula), and the Krakow Block (Birkenmajer, 1982; Birkenmajer, 2001) (Fig. 1.1). Geological studies revealed that the Fildes Block is characterised by Mesozoic-Cenozoic magmatic rocks, i.e., basalts to basaltic andesites, trachybasalts, porphyritic basalts, dacites, andesites and interbedded volcanic breccias (Machado et al., 2005). In contrast, Weaver Peninsula is dominated by basalts to basaltic andesites showing a more mafic composition, whereas the presence of more intermediate basaltic-andesitic rocks and the volcanoclastic Sejong Formation of Late Palaeocene–Eocene age is typical for the basement of Barton Peninsula (Chun et al., 1994; Lee et al., 2001; Yoo et al., 2001; Yeo et al., 2004). Moreover, in the northeast of Barton Peninsula, quartz-dioritic and granodioritic plutons of KGI apparently intruded into the volcanic strata (Jwa et al., 1992; Kim et al., 2000; Yeo et al., 2004; Machado et al., 2008). These intrusions likely caused hydrothermal alterations of the volcanic basement, leading to the formation of rocks containing quartz, pyrite, and clay minerals like kaolinite or illite. Finally, on Potter Peninsula, Lower Tertiary stratiform volcanic successions of basaltic–andesitic lavas and tuffs are present, overlain by Quaternary deposits including neoglacial moraines and marine sediments (Birkenmajer, 1998a; Birkenmajer, 1998b).

1.1.2. Maxwell Bay and adjacent coves

Maxwell Bay is a U-shaped, semi-enclosed fjord with a length of about 14 km and a width of 6-14 km, located at the western tip of KGI bordered by the Fildes Peninsula and Nelson Island (Yoon et al., 2000). Characterised by a flat bathymetry in its central part with water depths of 400 to 550 m, and a shallower zone with greater topographic irregularities in the north, it is separated from the adjacent Bransfield Strait in the southwest by a steep submarine sill of >430 m (Griffith and Anderson, 1989; Yoon et al., 2000). A couple of small fjords, namely Potter Cove, Marian Cove and Collins Harbour that currently receive input from calving tidewater

glaciers extend further inland from the main Maxwell Bay (Lee et al., 2004). Sea ice covers Maxwell Bay from July to September and usually starts to break up at the end of October (Khim et al., 1997; Khim and Yoon, 2003). The rest of the year the bay and its tributary inlets are free of ice, which allows for the development of two distinct water masses. Saline and relatively cold subsurface water ($<0^{\circ}\text{C}$, 34.0–34.5 psu) enters the bay from Bransfield Strait, generally following a wind-driven cyclonic circulation pattern (Chang et al., 1990; Khim et al., 1997; Roese and Drabble, 1998). It is covered by a warmer and less saline water mass ($0\text{--}1.04^{\circ}\text{C}$, 33.85–34.0 psu) influenced by glacial melt water and glacio-fluvial river water (Griffith and Anderson, 1989; Khim et al., 1997; Yoon et al., 1998). This surface layer is characterised by high loads of glacial melt water and glacio-fluvial river water (Griffith and Anderson, 1989; Khim et al., 1997; Yoon et al., 1998). This surface layer is characterised by high loads of glacial melt water plumes and surface runoff that, together with ice-rafted debris from the calving icebergs, significantly contribute to the sediment supply to these bays (Griffith and Anderson, 1989; Domack and Ishman, 1993; Yoon et al., 1998). Owing to the fact that Maxwell Bay has one of the thickest undisturbed marine sediment successions in this area (Milliken et al., 2009), it is considered to be a prime high-resolution archive of Pleistocene climate oscillations.

1.2. Recent changes at the WAP and their implications for local cryo- and ecosystems

Since the 1950s, annual average air temperatures at the Antarctic Peninsula (AP) have been increasing by $3.7 \pm 1.6^{\circ}\text{C}$ (Morris and Vaughan, 2003; Vaughan et al., 2003; Turner et al., 2005), which is six times the global average of $0.6 \pm 0.2^{\circ}\text{C}$ (Houghton et al., 2001). Highest warming rates were recorded during austral fall and winter, with a rise in average decadal air temperature of up to 1.09°C (King and Harangozo, 1998; Turner et al., 2005; Ding and Steig, 2013). This fact makes the Antarctic Peninsula one of the fastest warming areas worldwide, and therefore a model area for the investigation of climate-related changes and their implications on

marine and terrestrial ecosystems. One of the consequences of the local warming trend is a significant increase in land and sea ice melting. The duration of the annual sea ice season in the Bellingshausen Sea (AP), for example, is already three months shorter than in 1979 (Parkinson, 2002; Stammerjohn et al., 2008; Stammerjohn et al., 2012). Moreover, several authors reported a rapid retreat and break-up of major ice shelves, like Larsen A and Larsen B in the northwestern Weddell Sea (e.g., Rott et al., 1996; Rott et al., 2002; Scambos et al., 2003; Rack and Rott, 2004), which has led to further destabilisation and increased flow rates of outlet and valley glaciers on land (Rignot et al., 2004; Scambos et al., 2004). Consequently, a negative glacial mass balance has been observed during this period, even showing an increase in the last decade (Shepard et al., 2003; Scambos et al., 2004; Rignot et al., 2008). At present, up to 87% of the local glaciers show an overall retreat (Cook et al., 2005), and these changes have also affected the nature of the glaciers. Formerly subpolar glaciers with typical discharge values between 0.2 and $0.4 \text{ m}^3 \text{ s}^{-1} \text{ km}^{-2}$ are turning into temperate ones, characterised by discharge values of up to $1.1 \text{ m}^3 \text{ s}^{-1} \text{ m}^{-2}$ during the summer months (Dominguez et al., 2007). This shift is not only documented by increases in the subglacier circulation and the glacier slide speed, but also by the response of glacier ice, and the occurrence of new crevasses and moulins (Dominguez et al., 2007).

The consequences of these changes are extensive and are affecting both local terrestrial and marine ecosystems. New ice-free areas are formed on previously ice-covered bedrock (Braun and Gossmann, 2002; Rückamp et al., 2011) where pedogenesis and the colonisation of primary plants like moss and lichens are favoured. The rising significance of soil formation and chemical weathering under a more humid and warmer climate was already shown in certain areas of maritime Antarctica (Beyer et al., 2000; Navas et al., 2008). The retreat of local glaciers is moreover accompanied by an enhanced melt water flux to coastal areas (Dierssen et al., 2002; Dominguez et al., 2007; Meredith et al., 2008). Particularly at the WAP,

the resulting lower surface water salinities are typically linked with a transition from a system dominated by large diatoms to a system characterised by smaller cryptophytes (Moline et al., 2004). Presumably, this restructuring of the phytoplankton community observed in recent years will have implications on zooplankton communities and higher trophic levels as well as on biogeochemical cycles (Montes-Hugo et al., 2009), considering that large diatoms make up to 80% of the particulate organic carbon export in the Southern Ocean (Jin et al., 2006).

Along with increased rock erosion, these melt waters transport huge loads of fine suspended particulate matter into coastal waters, resulting in a rise of the vertical nearshore sediment flux. In several studies it was shown that increasing sediment accumulation rates, although not quantified to date, may have a severe impact on the local benthic community (Ahn et al., 1996; Pakhomov et al., 2003; Ahn et al., 2004; Tatian et al., 2008; Torre et al., 2012). In addition, a higher turbidity and light diminution caused by an increased amount of suspended particles in the water column are assumed to be one of the major reasons for low primary production in some nearshore regions of the AP (Schloss et al., 1999; Schloss and Ferreyra, 2002; Dierssen et al., 2002). However, particularly in more hemipelagic zones around the islands, the input of essential micronutrients by glacier effluents may have a positive impact on phytoplankton bloom development as well.

1.3. Natural iron fertilisation in the Southern Ocean

Iron is an important micronutrient limiting ocean productivity in high nutrient-low chlorophyll (HNLC) regions like the Southern Ocean (Martin et al., 1990; Lancelot et al., 2009). Mesoscale iron fertilisation experiments in this area revealed that the supply of iron is able to significantly stimulate local phytoplankton growth (Bakker et al., 2005; Boyd et al., 2007). Controlling the development of algal blooms in this region, the supply of iron might therefore be a fundamental factor for atmospheric CO₂ drawdown, as observed in ice cores during the Last Glacial Maximum (LGM)

(Martin et al., 1990). In oxic seawater iron is generally present in its stable oxidised form Fe(III), which undergoes strong hydrolysis and precipitates as Fe (oxyhydr) oxides (e.g., Millero et al., 1995; Waite, 2001). This particulate iron, though not directly available to organisms, may be transferred into a bioavailable form by long-term dissolution processes, which include a coupled organic ligand-photochemical mechanism (Borer et al., 2005). These organic ligands are either degradation products released during organic matter mineralisation (Rue and Bruland, 1995) or siderophores, ligands that are produced by hetero- or autotrophic bacteria to support iron uptake (Mawji et al., 2008). After iron has been acquired via siderophores or in its colloidal or dissolved form, it is rapidly cycled in the water column by heterotrophic flagellates, ciliates and mesozooplankton (Wilhelm, 1995; Nodwell and Price, 2001; Shaked et al., 2005).

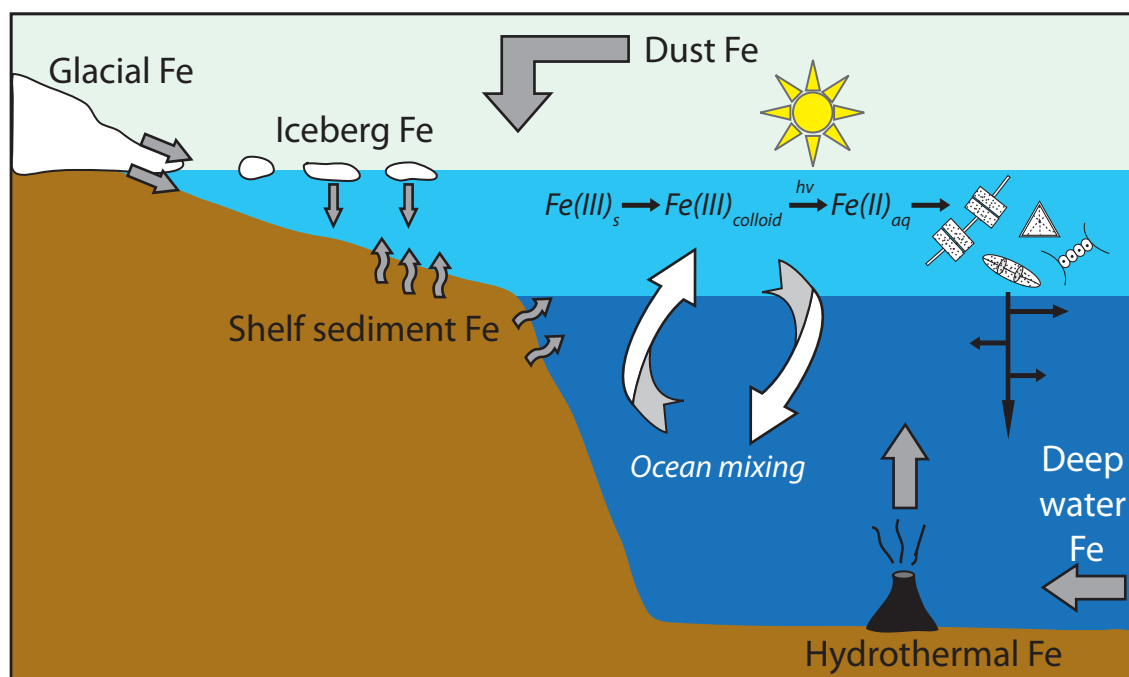


Fig. 1.2. Scheme of sources and cycling of dissolved and particulate iron in the Southern Ocean modified after Tagliabue et al. (2010).

As shown in figure 1.2 there are several potential sources of iron in the Southern Ocean. In addition to the aeolian input by dust (e.g., Wagener et al., 2008), the

supply of iron-bearing glacial sediments is considered to be of high relevance for ocean productivity around Antarctica. Raiswell et al. (2006) and Death et al. (2013), for example, could show that (sub-) glacial melt waters, basal ice, and supra-glacial and pro-glacial sediments deliver large amounts of bioavailable Fe (oxyhydr)oxides to the open ocean. Shaw et al. (2011) demonstrated that free drifting icebergs carrying significant amounts of labile and potentially bioavailable ferrihydrite may represent a major contributor of iron in Antarctic waters. In addition, Dold et al. (2013) stresses the importance of increased acid rock drainage resulting from the microbially catalysed oxidation of sulphide minerals as local iron source. Moreover, suboxic shelf sediments are discussed as potential sources of bioavailable iron to the ocean (Tagliabue et al., 2010; Shaw et al., 2011; de Jong et al., 2012; Measures et al., 2012). The background for this is the oxidation of organic material in coastal shelf sediments, which is coupled to electron acceptors (e.g., Froelich et al., 1979). According to the energy yield of the respective mineralisation pathway, aerobic respiration is followed by denitrification, the reduction of Mn(IV) and Fe(III) oxides, sulphate reduction and methanogenesis (Table 1.1; Froelich et al., 1979). Generally, sulphate reduction is considered to be the major pathway of organic matter

Table 1.1. Standard Gibbs free energy (ΔG) of the principle respiratory pathways of natural organic matter mineralisation with acetate as an electron donor taken from Canfield and Thamdrup (2009). Note that ΔG values are standardised to a 4e- transfer equivalent to the oxidation of one mole of organic carbon with an oxidation state of 0, as in carbohydrates. Calculation conditions: 25°C, and unit activity for all reactants and products, with a pH of 7.

		kJ per reaction ΔG (acetate)
Oxic respiration	$O_2 + 1/2 C_2H_3O_2^- \rightarrow HCO_3^- + 1/2 H^+$	-402
Denitrification	$4/5 NO_3^- + 3/5 H^+ + 1/2 C_2H_3O_2^- \rightarrow 2/5 N_2 + HCO_3^- + 1/5 H_2O$	-359
Mn reduction (pyrolusite)	$7/2 H^+ + 2 MnO_2 + 1/2 C_2H_3O_2^- \rightarrow 2 Mn^{2+} + HCO_3^- + 2 H_2O$	-385
Fe reduction (freshly precipitated amorphous FeOOH)	$15/2 H^+ + 4 FeOOH + 1/2 C_2H_3O_2^- \rightarrow 4 Fe^{2+} + HCO_3^- + 6 H_2O$	-241
Sulphate reduction	$1/2 H^+ + 1/2 SO_4^{2-} + 1/2 C_2H_3O_2^- \rightarrow 1/2 H_2S + HCO_3^-$	-43.8
Methanogenesis	$1/2 H_2O + 1/2 C_2H_3O_2^- \rightarrow 1/2 CH_4 + 1/2 HCO_3^-$	-19.9

degradation in coastal sediments (e.g., Jørgensen, 1982). However, particularly in sediments rich in reactive Mn and Fe oxides, dissimilatory metal oxide reduction may play a dominant role (Canfield et al., 1993; Vandieken et al., 2006; Canfield and Thamdrup, 2009). In the ferruginous zones of these sediments, the reduction of Fe(III) causes an accumulation of dissolved Fe(II) (dFe) in the pore waters, which may escape via the sediment-water interface into the water column (Canfield and Thamdrup, 2009; Raiswell and Canfield, 2012). Whereas only a small amount of Fe(II) will be complexed by organic ligands, most of the iron will be rapidly re-oxidised in oxic waters forming very reactive nanoparticulate ferrihydrite (Raiswell and Anderson, 2005). By resuspension, lateral transport by currents and upwelling, these labile Fe phases may be transported into the euphotic zone, where they will be transferred into bioavailable forms by biological and photochemical processes as described above (Lam and Bishop, 2008; Boyd and Ellwood, 2010 and references therein; Lam et al., 2012).

Although considered to be of high relevance, there are only few studies on the contribution of Antarctic shelf sediments to the iron pool of the Southern Ocean so far. Most of these investigations and models are based on general fluxes of dFe obtained from incubation experiments on the California shelf determined by Elrod et al. (2004), or dFe concentration measurements in the water column (Blain et al., 2007; Lancelot et al., 2009; Tagliabue et al., 2010; de Jong et al., 2012). However, Fe reduction rates in sediments of the Antarctic shelf based on pore water data are not available to date.

1.4. Unlocking the past: Holocene climate variability at the WAP

In view of the dramatic environmental changes at the AP, it is also of utmost importance to unravel the climate and glacial history of this region to learn how this system has responded to past climatic events. There are several palaeoenvironmental records along the Antarctic Peninsula, including ice cores as well as lacustrine and

marine sedimentary archives. Each of them provides different insights into, e.g., past atmospheric temperatures, precipitation and regional sea-ice extent (Aristarain et al., 1986; Shevenell et al., 1996; Aristarain et al., 2004; Mulvaney et al., 2012; Abram et al., 2013), onset of deglaciation on land and changes in relative sea-levels (Hjort et al., 1997; Roberts et al., 2011), and variations in bioproductivity, diatom and foraminiferal assemblages in lake and marine sediments (Björck et al., 1991a; Björck et al., 1991c; Leventer et al., 1996; Björck et al., 1996; Jones et al., 2000; Yoon et al., 2000; Taylor et al., 2001; Leventer et al., 2002; Taylor and Sjunneskog, 2002; Khim et al., 2002; Heroy et al., 2008; Milliken et al., 2009; Michalchuk et al., 2009; Sterken et al., 2012). Other studies deal with changes in the quantity and sedimentological characteristics of suspended particulate matter input into coastal waters induced by glacial melting (e.g., Domack et al., 1994; Domack et al., 2001), advance and retreat of local ice shelves (Domack et al., 1995), sea surface temperature variability (e.g., Shevenell et al., 2011), and modifications of ocean current systems such as the Antarctic Circumpolar Current (ACC), including changes in frontal positions and water mass distributions on the AP shelf (Anderson, 1999; Howe and Pudsey, 1999; Shevenell and Kennett, 2002; Hemming et al., 2007). Although most records demonstrate that the WAP region has undergone significant changes in climate since the Last Glacial Maximum (LGM), the timing, duration and even occurrence of different Holocene warm and cold periods differ strongly from each other (Fig. 1.3). The diachroneity of major climate events across this area, though widely present in palaeoenvironmental WAP archives such as the 'Early Holocene Climate Optimum' (11.5–9.5 cal kyr BP) and the 'Mid-Holocene Hypsithermal' (4.5–2.8 cal kyr BP), was also emphasised by Bentley et al. (2009) in a recent review paper. Particularly the presence of Late Holocene climate fluctuations, like Southern Hemisphere equivalents of the 'Little Ice Age' and the 'Medieval Warm Period' in these records, is still controversially discussed (Leventer et al., 1996; Domack et al., 2001; Khim et al., 2002; Jones and Mann, 2004; Milliken et al., 2009; Bentley et al., 2009).

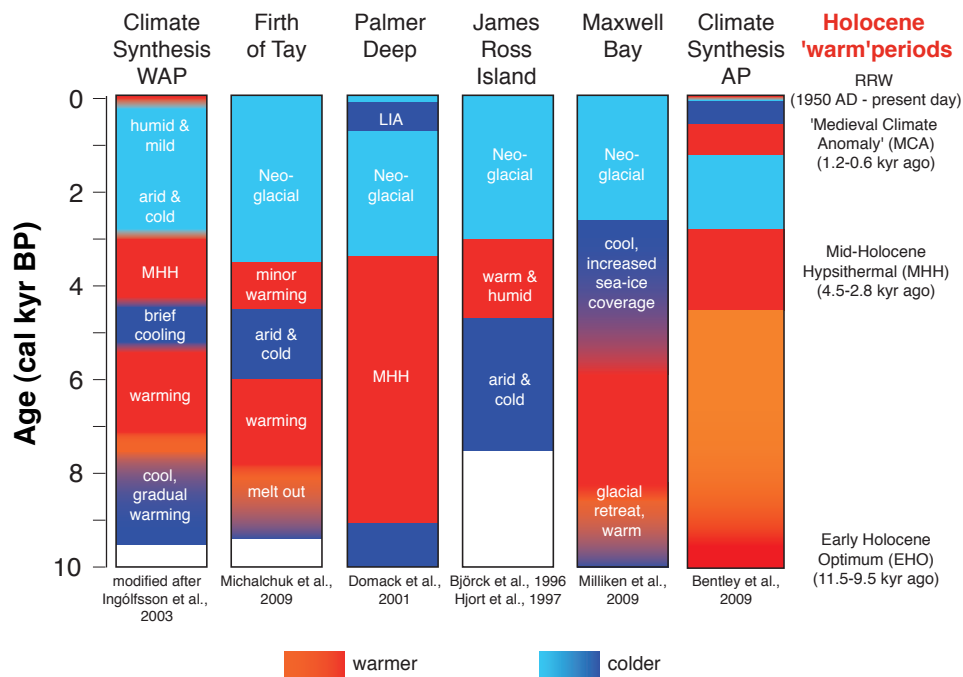


Fig. 1.3. Compilation of Antarctic Peninsula climate records and syntheses derived from marine and lacustrine sedimentary records and ice cores. RRW: 'Recent Regional Warming', LIA: 'Little Ice Age', MCA: 'Medieval Climate Anomaly', MHH: 'Mid-Holocene Hypsithermal', EHO: 'Early Holocene Optimum'.

Although inorganic geochemical proxies bear a high potential for reconstructing palaeoenvironmental conditions and changes in glacier extent, up to the present day their application in Subantarctic records is rare. Jaccard et al. (2013), for instance, used Ca/Fe and Ba/Fe ratios in sediments from the Sub-Antarctic Zone (Ocean Drilling Project sites 1090 and 1094) obtained by XRF core scanning to infer changes in ocean productivity and glacial-interglacial cycles over the past million years. By performing a geochemical provenance analysis on fine-grained sediments from the Ross Sea, Monien et al. (2012) were able to reconstruct palaeo-ocean currents and -ice flows related to local climate variability during the past 14 million years. Early Miocene palaeoenvironmental changes in the McMurdo Sound region were investigated by Talarico and Sandroni (2011) using geochemical data of basement clasts. The authors could show that fluctuation in these proxy records are most probably related to changes in provenance caused by alternating climate, sea-ice

extent, and current regimes. No comparable investigations exist for the Antarctic Peninsula.

1.5. Inferring past climate from historical penguin populations

The rapid recent warming in the WAP region has already been related to significant changes of the local ecosystem, which includes the distribution of one of the regions' upper trophic level predators, such as the Chinstrap (*Pygoscelis antarctica*), Adélie (*P. adeliae*), and Gentoo (*P. papua*) penguins (Smith et al., 1999; Ducklow et al., 2007; Trivelpiece et al., 2011). Although long-term data series dealing with penguin populations are only available for a few locations across the AP (Barbosa et al., 2012), it was shown that breeding populations of Chinstrap and Adélie penguins are generally in decline, whereas Gentoo penguin populations seem to be stable or increasing during the last 30 years (Woehler et al., 2001; Ducklow et al., 2007; Trivelpiece et al., 2011; Barbosa et al., 2012). These observed trends are mainly attributed to changes in regional sea-ice extent, which are positively correlated to the availability of prey species, like krill (*Euphausia superba*) (Fraser et al., 1992; Fraser and Hofmann, 2003; Weimerskirch et al., 2003; Forcada et al., 2006). Moreover, variations in snow and ice coverage limiting the availability of suitable breeding sites (Williams, 1995; Smith et al., 1999; Bricher et al., 2008), the reduction or recovering of marine mammal stocks competing for krill by fisheries (Trivelpiece et al., 2011), but also disturbance by research activity and tourism (Micol and Jouventin, 2001; Bricher et al., 2008) are discussed. Since the variability in the size of penguin populations is considered to reflect direct or indirect responses to climate change (Croxall et al., 2002), the knowledge about historical penguin population sizes may give valuable insights into local palaeoenvironmental conditions. Radiocarbon dated organic relics found in abandoned Adélie and Gentoo penguin rookeries of the Antarctic Peninsula and around the Ross Sea have already been used to estimate historical population dynamics at the Antarctic Peninsula and around the Ross Sea

(Baroni and Orombelli, 1994; Emslie, 2001; Emslie and Woehler, 2005; Emslie et al., 2007; Emslie et al., 2011). In another promising approach, geochemical data were obtained from highly preserved sedimentary archives of lakes influenced by ornithogenic (bird-formed) soils. It could be shown that these soils found around the penguin rookeries are characterised by a very specific assemblage of bio-elements, which are accumulated during the course of the food chain and finally excreted by top predators, like penguins (Fig. 1.4) (Tatur and Keck, 1990; Ancora et al., 2002; Sun et al., 2004). Mineralogical investigations of soils deposited around the nesting

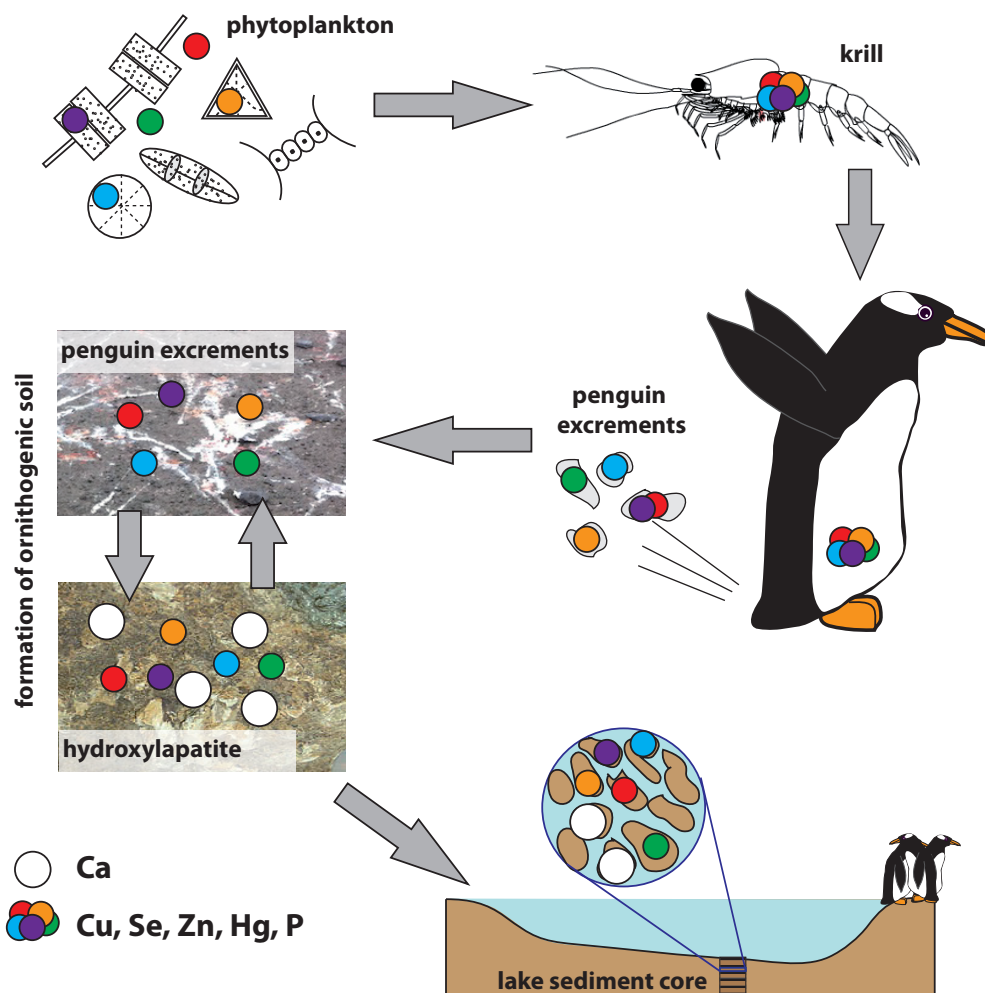


Fig. 1.4. Accumulation pathway of trace elements during the food chain and their deposition as ornithogenic soils in lake sediments.

sites showed high abundances of apatite, a calcium phosphate, which is particularly present as hydroxylapatite ($\text{Ca}_5(\text{PO}_4)_3(\text{OH})$) (Myrcha et al., 1985; Tatur et al., 1997) and which is formed during the microbial degradation of penguin guano (Myrcha et al., 1985; Föllmi, 1996). Moreover, other phosphates, such as struvite ($\text{Mg}(\text{NH}_4)\text{PO}_4 \times 6 \text{H}_2\text{O}$) or leukophosphate ($(\text{K},\text{NH}_4)(\text{Fe}_3,\text{Al})_2(\text{PO}_4)_2 \times 2 \text{H}_2\text{O}$), resulting from dissolution processes and chemical reactions with surrounding rocks and soils are present as well (Myrcha et al., 1985). During the precipitation of authigenic apatite in the upper soil layers, an ion exchange between Ca^{2+} , PO_4^{3-} , F^- , and OH^- with elements, like Ag, Ba, Br, Cd, Cu, Cr, I, Na, Mg, Mo, Pb, S, Se, Sr, U, V, Y, and Zn is possible (Jarvis et al., 1994; Sauer et al., 1997; Abratis et al., 2004; Tribovillard et al., 2006). Consequently, elements enriched in penguin guano (e.g., As, Cd, Cu, P, S, Se, Zn) are incorporated and fixed in these apatite-bearing ornithogenic soils (Fig. 1.4). When these soils are transported via surface runoff and deposited into nearby lakes, the presence of guano-related elements in undisturbed lake sediments that are considered immobile in lacustrine archives (e.g., Sun et al., 2000) may directly reflect the presence of penguin populations in the lake catchment area (Sun and Xie, 2001; Liu et al., 2007; Liu et al., 2011b). Moreover, the amount of ornithogenic soil input into these lakes was shown to be proportional to the penguin population size present during the time of deposition (e.g., Liu et al., 2011a). Taking advantage of this fact, Huang et al. (2009; 2011), Liu et al. (2005; 2006; 2011b; 2013), Zhu et al. (2005), Zale (1994) and Sun et al. (2000; 2004) were able to reconstruct historical penguin population sizes and corresponding climate events by using bio-element and rare earth element (REE) patterns in short lacustrine depositional sequences of the WAP, the Ross Sea region and Vestfold Hills, East Antarctica. However, particularly at the WAP, these records do only cover the past c. 3,000 years, and no information could be inferred from these data about the response of local penguin populations on warm phases in the Early and Mid-Holocene, which are assumed to represent a widespread phenomenon across the AP.

1.6. Objectives of this thesis

This thesis forms part of the multi-national project IMCOAST (IMPact of climate induced glacial melting on marine COASTal systems in the western Antarctic Peninsula region), involving working groups of different scientific fields from Germany, Poland, Spain, United Kingdom, Belgium, The Netherlands, Brazil and Argentina. The main objective of this interdisciplinary cooperation is to study past, recent, and future climate-induced changes of land ice masses and sedimentary run-off, and their effects on coastal benthic and pelagic ecosystems in the King George Island coastal area by combining different geochemical, sedimentological, biological, and physico-hydrographical indicators. The aim of this thesis was to assess whether the rapid recent warming trend at the WAP has already been recorded by the geochemistry of local sediments and pore waters, and how these changes may affect benthic and pelagic ecosystems. Moreover, inorganic geochemical proxies were applied on marine and lacustrine sedimentary records in order to get insights into palaeoenvironmental changes in this highly climate-sensitive area.

Chapter 3 presents the first comprehensive, high-resolution geochemical study of sediments from the AP. Major and trace element distribution patterns were obtained from a c. 9 m long sediment core taken in Maxwell Bay off King George Island, WAP. By comparing inorganic geochemical data of local bedrock and nearshore deposits, small-scaled changes in provenance are assessed in order to reveal climate-induced retreats and re-advances of local glaciers during the last two millenia. These investigations are linked to granulometric studies conducted on the same core, which compare the occurrence of simultaneous climate phases in both hemispheres since c. 2,000 cal years BP (chapter 7). In addition, naturally occurring lead isotopes (^{210}Pb) were measured in surface sediments to evaluate whether the observed rapid recent glacier retreat is reflected in enhanced accumulation of melt water or subglacially derived glacial material in coastal areas off King George Island.

Another subproject (chapter 4) deals with the impact of environmental changes on local penguin populations. Specific bio-element assemblages in lake sediments, which are characteristic for ornithogenic (bird-formed) soils, are used to unravel past variations in penguin occupation on Ardley Island, WAP, since the Last Glacial Maximum. By determining the key factors responsible for population changes of upper-trophic level predators like penguins in this region, this study may provide a basis for predicting future fluctuations and their consequences for the local ecosystem.

In chapters 5 and 6, this thesis focuses on the recent changes of the sedimentary environment and benthic communities due to the rapid warming. Pore water data of coastal surface sediments give first insights into redox conditions of nearshore deposits of maritime Antarctica and their implications on metal uptake by benthic filter feeders. Furthermore, in a unique approach combining trace element concentrations in pore waters from the WAP shelf and modelling of metabolic rates, we intend to shed light on the relevance of Antarctic shelf sediments as iron fertiliser for the high nutrient-low chlorophyll (HNLC) Southern Ocean.

To date, the local glacial and climatic history of the Antarctic Peninsula is still not fully unravelled, making it difficult to identify respective driving mechanism for past, recent and future changes. Moreover, there is little knowledge about biogeochemical processes in present Antarctic sedimentary environments and their implications on benthic and pelagic ecosystems. The overarching questions of this thesis are therefore:

- Can major and minor element distribution patterns and granulometric data in sedimentary archives from the western Antarctic Peninsula be used to reconstruct climate-related retreats and re-advances of local glaciers during the last c. 2,000 years?

- Is the recent rapid glacier retreat reflected in increasing accumulation of subglacially or surface run-off derived glacial material in coastal areas?
- Are changes in local penguin populations driven by alternations in climate, sea-ice extent, and relative sea level reconstructable from guano-related bio-element concentrations in Holocene lake sediments?
- What are the major biogeochemical processes and pathways of organic matter degradation in coastal sediments from the maritime Antarctic? How do these processes possibly affect element assimilation in benthic organisms?
- Do Antarctic shelf sediments represent a potential source of micronutrients, like iron, to the iron-limited HNLC regions of the Southern Ocean?

2. Outline of the author's contribution

The thesis is based on eight manuscripts, which deal with different aspects of past and recent changes in climate at the western Antarctic Peninsula and their implications for local cryogenic, terrestrial and marine ecosystems. Whereas four main manuscripts are displayed in more detail (chapters 3 to 6), additional publications and manuscripts that were developed in the framework of this thesis are attached as abstracts in chapters 7-10. In the following list the author's contribution to each manuscript are given.

Chapter 3

A geochemical record of late Holocene palaeoenvironmental changes at King George Island (maritime Antarctica)

This manuscript focusses on Late Holocene climate variability in the northern WAP as revealed by changes in provenance of sedimentary deposits off King George Island. It is to some extent based on the results of the diploma thesis of the author (Monien, 2008), which has been significantly revised, re-written, and complemented by new data and interpretations. The author wrote the manuscript and conducted all geochemical analyses, except for total organic carbon and biogenic silica determinations, which were done by Gerhard Kuhn and Rita Fröhlking (both Alfred Wegener Institute for Polar and Marine Research (AWI), Bremerhaven). Granulometric data and radiocarbon ages of the sediments were delivered by Christian Hass (Wadden Sea Research Station, AWI, Sylt). Andreas Klügel (Bremen University) assisted the author with petrological analyses of volcanic glass shards. Recovering of the sediment core was carried out by Gerhard Kuhn and the Polarstern crew during cruise ANT-XXIII/4 in 2006. All data were evaluated and interpreted by

the author himself with support by Bernhard Schnetger, Hans-Jürgen Brumsack and Christian Hass. In 2011 this manuscript has been published in *Antarctic Science*, **23**(3), 255-267.

Chapter 4

Penguin colony expansion on the western Antarctic Peninsula during Holocene warm phases curtailed by volcanic activity

This study deals with the reconstruction of historical penguin populations on Ardley Island, western Antarctic Peninsula using inorganic geochemical biomarkers in lake sediments. The concept of this study was developed by the author and Stephen Roberts (British Antarctic Survey (BAS), UK). Both undertook analytical work and data analysis with assistance from Julia Lofffield, Bernhard Schnetger and Hans-Jürgen Brumsack. The author wrote and edited the paper together with Stephen Roberts and Dominic Hodgson (BAS). Anne Hey (Cardiff University, UK) and Claire Allen (BAS) conducted diatom analyses on marine cores from the Anvers Shelf. Peter Fretwell (BAS) performed satellite vegetation mapping and DEM analysis. Ryszard Ochyra (Polish Academy of Science, Poland) identified moss used for radiocarbon dating. Steve Moreton (NERC Radiocarbon Facility, UK) undertook SUERC radiocarbon dating analyses. Fieldwork was conducted by Stephen Roberts, Peter Fretwell, Dominic Hodgson, Emma Hocking and Michael Bentley (both Durham University, UK). All authors contributed significantly to the interpretations and commented on the manuscript. The manuscript will be submitted to *Nature Geoscience*.

Chapter 5

Redox conditions and trace metal cycling in coastal sediments from the maritime Antarctic

This study addresses biogeochemical processes in coastal sediments from Potter Cove, King George Island and their implication on the Southern Ocean iron cycle. The author is responsible for the concept of this study, the data interpretation and the writing of the manuscript, supported by comments from Bernhard Schnetger and Hans-Jürgen Brumsack. All geochemical analyses of sediments and pore waters were conducted by the author except for nutrient measurements of pore waters, which were done by Sanja Asendorf and Donata Monien. Sampling of sediment cores was carried out by the author with support by Sanja Asendorf, Donata Monien, Oscar Gonzales (Instituto Antartico Argentino (IAA), Argentina) and the Argentine diving division "Prefectura". Heng Chai Lim supported the study with a current model of the sampling location and Karsten Lettmann helped with the modelling of biogeochemical reduction rates. This manuscript has been submitted to *Geochimica Cosmochimica Acta*.

Chapter 6

Influence of the pore water geochemistry on Fe and Mn assimilation in *Laternula elliptica* at King George Island (Antarctica)

This manuscript is about assimilation pathways of major and minor elements in the circum-Antarctic benthic deposit feeder *Laternula elliptica*. Harald Poigner, Doris Abele (both AWI, Bremerhaven), Dorothee Wilhelms-Dick (Bremen University) and Patrick Monien developed the concept of the study, Harald Poigner did the sampling of the bivalves with support by Oscar Gonzales (IAA) and the Argentine diving division "Prefectura" as well as the geochemical analyses on the bivalve tissues assisted

by Michael Kriews (AWI, Bremerhaven). Pore water and sea water samples were sampled and analysed for major and trace elements by Patrick Monien and Donata Monien, who also contributed to the interpretation of the data. Harald Poigner wrote the manuscript supported by comments of all co-authors. In 2013 the manuscript has been published in *Estuarine, Coastal and Shelf Science*, **135**, 285-295.

Chapter 7

Climate fluctuations during the past two millennia as recorded in sediments from Maxwell Bay, South Shetland Islands, West Antarctica

In this study Late Holocene climate fluctuations at the WAP are discussed using granulometric and geochemical data obtained from a sedimentary record from Maxwell Bay. Christian Hass is responsible for the concept of the study. He conducted the granulometric analyses and developed the radiocarbon age model. Recovering of the sediment core was carried out by Gerhard Kuhn during cruise ANT-XXIII/4 in 2006. He moreover delivered total organic carbon and biogenic silica data. Patrick Monien did all inorganic geochemical analyses of the sediments, conducted the hierarchical cluster analysis, developed the ^{210}Pb age model of surface sediments and assisted Christian Hass with the interpretation of the whole dataset. In this context data were also taken from his diploma thesis (Monien, 2008) and newly interpreted. Supported by all co-authors Christian Hass wrote the manuscript, which was published in *Geological Society, London, Special Publications*, **344**, 243-260 in 2010.

Chapter 8

A new Holocene relative sea level curve for the South Shetland Islands, Antarctica

This paper uses an interdisciplinary approach integrating sedimentary evidence from isolation basins with geomorphological evidence from raised beaches to reconstruct a new Holocene relative sea-level curve for the South Shetland Islands. Robert Larter (BAS), Dominic Hodgson and Michael Bentley developed the concept for this study, whereas field work was done by Emma Hocking (née Watcham), Stephen Roberts, Michael Bentley, Peter Fretwell and Dominic Hodgson. Moreover, Emma Hocking conducted diatom analyses and established the age model together with Steven Moreton. The mathematical models were provided by Pippa Whitehouse (Durham University, UK). Whereas Melanie Leng (NERC Isotope Geoscience Laboratory, UK) and Emma Hocking did the bulk geochemical analyses for all cores, Patrick Monien conducted the inorganic geochemical analyses of the Yanou lake core. Data evaluation and interpretation was done by Emma Hocking, Michael Bentley, Dominic Hodgson, Stephen Roberts, Jerry Lloyd (Durham University, UK), Robert Larter, Peter Fretwell and Patrick Monien. The manuscript which was written by Emma P. Hocking supported by comments of all co-authors was published in *Quaternary Science Reviews*, **30**, 3152-3170 in 2011.

Chapter 9

The influence of sedimentation on metal accumulation and cellular oxidative stress markers in the Antarctic bivalve *Laternula elliptica*

This study is about the impact of increasing sediment accumulation in coastal areas of the WAP on the assimilation of metals in the bivalve *Laternula elliptica*. Gunnar Husmann, Eva Philipp (both Kiel University) and Doris Abele developed the

concept of the study. All analyses with respect to the bivalve tissues were done by Gunnar Husmann, who was assisted by Eva Philipp and Michael Kriews. Donata Monien provided geochemical data of local sea water, whereas Patrick Monien is responsible for sampling, geochemical analyses and data evaluation of Potter Cove sediments. Furthermore, he assisted the first author with the interpretation of the data. Gunnar Husmann wrote the paper with the help of all co-authors. This paper was published in 2012 in *Estuarine, Coastal and Shelf Science*, **111**, 48-59.

Chapter 10

On the phytoplankton bloom in coastal waters of southern King George Island (Antarctica) in January 2010: An exceptional feature?

This manuscript deals with possible controlling factors of phytoplankton bloom development in coastal waters around King George Island, WAP. The conceptual model of this study was established by Irene Schloss, who is also responsible for all mathematical models in this manuscript, which were done in cooperation with Dany Dumont and Claudie-Ann Michaud Tremblay (all Quebec University, Canada). Water sampling was conducted by Oscar Gonzáles, Alejandro Ulrich (both IAA), Donata and Patrick Monien and the Arctowski Station field crew. Gastón Almandoz (La Plata University, Argentina) and Elsbietta Kopckynska (Polish Academy of Science, Poland) conducted the diatom analyses and Aga Wasilowska (Warsaw University, Poland) supplied nutrient data from Admiralty Bay. Nutrient data of Potter Cove surface waters were provided by Donata and Patrick Monien, who moreover contributed significantly to the interpretation of the data used in this study. Irene Schloss wrote the manuscript together with all co-authors. The manuscript has been published in *Limnology & Oceanography*, **59**(1), 195-210 in 2014.

3. A geochemical record of late Holocene palaeoenvironmental changes at King George Island (maritime Antarctica)

Patrick Monien^a, Bernhard Schnetger^a, Hans-Jürgen Brumsack^a, H. Christian Hass^b, Gerhard Kuhn^c

^aInstitute for Chemistry and Biology of the Marine Environment (ICBM), PO Box 2503, D-26111 Oldenburg, Germany

^bAlfred Wegener Institute for Polar and Marine Research, Wadden Sea Research Station, Hafenstrasse 43, D-25992 List, Germany

^cAlfred Wegener Institute for Polar and Marine Research, Am Alten Hafen 26, D-27568 Bremerhaven, Germany

This chapter is published in *Antarctic Science*, **23**(3), 255-267 (2011).

3.1. Abstract

During RV Polarstern cruise ANT-XXIII/4 in 2006, a gravity core (PS 69/335-2) and a giant box core (PS 69/335-1) were retrieved from Maxwell Bay off King George Island (KGI). Comprehensive geochemical (bulk parameters, quantitative XRF, Inductively Coupled Plasma Mass Spectrometry) and radiometric dating analyses (¹⁴C, ²¹⁰Pb) were performed on both cores. A comparison with geochemical data from local bedrock demonstrates a mostly detrital origin for the sediments, but also points to an overprint from changing bioproductivity in the overlying water column in addition to early diagenetic processes. Furthermore, ten tephra layers that were most probably derived from volcanic activity on Deception Island were identified. Variations in the vertical distribution of selected elements in Maxwell Bay sediments further indicate a shift in source rock provenance as a result of changing glacier extents during the past c. 1,750 years that may be linked to the Little Ice Age and the Medieval Warm Period. Whereas no evidence for a significant increase in chemical

weathering rates was found, ^{210}Pb data revealed that mass accumulation rates in Maxwell Bay have almost tripled since the 1940s ($0.66 \text{ g cm}^{-2} \text{ yr}^{-1}$ in AD 2006), which is probably linked to rapid glacier retreat in this region due to recent warming.

3.2. Introduction

The western Antarctic Peninsula (WAP) region is one of the most sensitive and dynamic areas of the Earth's surface, where ecological and cryospheric systems respond rapidly to climatic changes (Domack et al., 2001). Since the middle of the 20th century a mean atmospheric warming of nearly 3°C is observed along the WAP (e.g., Meredith and King, 2005), which is significantly higher than the average global warming trend of $0.6 \pm 0.2^\circ\text{C}$ over the last 100 years (Houghton et al., 2001). The most recent reconstructions confirm this, showing a warming trend of 0.17°C per decade for West Antarctica between 1957 and 2006 (Steig et al., 2009). One of the consequences of the local warming trend is a significant increase in melting of land and sea ice. Since the late 1960s, a reduction of sea ice as well as a dramatic retreat of glaciers is reported that has accelerated in the last decade (Rignot et al., 2008). These changes are regionally accompanied by the creation of new ice-free areas (Braun and Gossmann, 2002; Cook et al., 2005) favouring soil formation on previously ice-covered bedrock. Whereas on continental Antarctica chemical weathering is still negligible (Y. Il Lee et al., 2004), it is suggested that particularly under warmer and more humid conditions along the WAP, pedogenesis and weathering processes may have been more significant. Furthermore, along with enhanced melt water discharge, an increase in rock erosion has been observed. At Potter Cove, King George Island (KGI), for example, sub-, peri-, and proglacial melt water streams transport suspended material of c. 0.14 kg m^{-3} ($0.0042\text{--}0.532 \text{ kg s}^{-1}$) into coastal waters during the melting period (Schloss et al., 2002), which may have direct effects on marine ecosystems. In light of the sensitive character of this region, geochemical studies of sedimentary archives may provide critical information on the response of

ecological and cryospheric systems to alternating environmental conditions along the WAP. High-resolution palaeoenvironmental records may be used to indicate to what extent this rapid regional warming is recorded by coastal sediments and whether similar events may have occurred in the recent past. Vertical distributions of major and minor elements in marine sediments serve as palaeoclimatic proxies and may reveal changes in bioproductivity, the origin and weathering of source rocks, glacier advance and retreat, sediment transportation processes, redox conditions, and diagenesis. To date, however, comprehensive geochemical investigations in this area are nonexistent or restricted to bulk parameters, like total organic carbon (TOC), nitrogen, carbonate and opal (e.g., Yoon et al., 2010, 2000), granulometric data (Hass et al., 2010), and rare earth elements (REE) patterns of surface sediments (Santos et al., 2007).

In this study a first comprehensive geochemical characterisation of Holocene sediments from Maxwell Bay, KGI is presented. Inorganic geochemical data is used for provenance analyses to reconstruct possible local glacier extents during the last two millennia. Furthermore, in the context of the rapid warming trend of the past 50 years, shifts in the quantity and nature of the vertical sediment flux as well as the degree of chemical weathering in the supply area are examined. The results of this investigation may allow a better understanding of the impact of global climate change on regional terrestrial and marine ecosystems along the WAP in the past and future.

3.3. Regional setting

King George Island (62°23'S, 58°27'W) is the largest of the South Shetland Islands (SSI), a Jurassic–Quaternary magmatic island arc forming a 550 km long archipelago separated from the WAP by the Bransfield Strait. The interior of the island is mostly occupied by a 600 m thick ice cap covering the basement, which is mainly composed of igneous rocks of pyroclastic, volcanic or plutonic origin (Yeo et

al., 2004). According to Fig. 3.1, KGI can be divided into three main tectonic blocks with different lithostratigraphies: the Barton Horst (Barton and Weaver peninsulas), the Fildes Block (Fildes Peninsula) at the north-west end, and the Warszawa Block

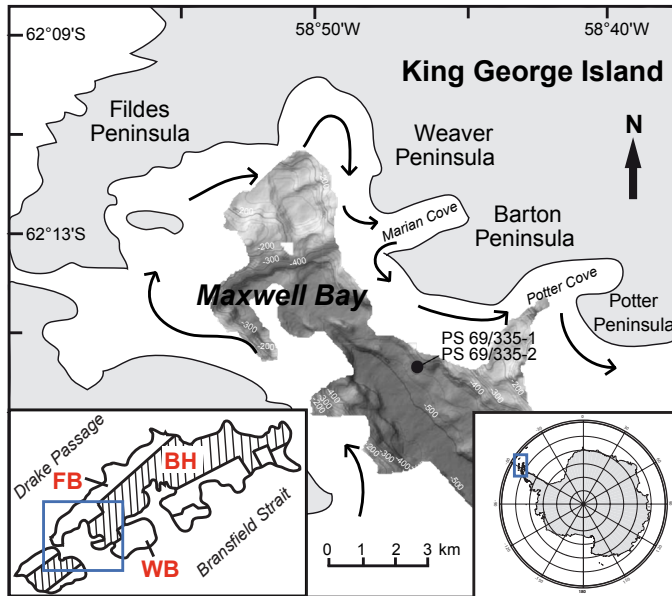


Fig. 3.1. Map of the study site. The black dot marks the sediment core location. Black arrows indicate general ocean currents in Maxwell Bay and adjacent coves according to Chang et al. (1990) and Roese & Drabble (1998). Bathymetric data is from Hass et al. (2010). FB = Fildes Block, BH = Barton Horst, WB = Warszawa Block.

(Potter Peninsula) in the south-east (Santos et al., 2007 and references therein). Geological investigations on Fildes Peninsula showed that the Fildes Block is dominated by basalts to basaltic andesites, trachybasalts, porphyritic basalts, and dacites and andesites interbedded volcanic breccias (Machado et al., 2005). Whereas Weaver Peninsula is characterised by basalts to basaltic andesites showing a relative mafic composition

(Yeo et al., 2004), the bedrock of Barton Peninsula located close to the study site consist of more intermediate basaltic-andesitic rocks and the volcanoclastic Sejong Formation of late Palaeocene–Eocene age. In the central northern parts plutonic rocks (granodiorites) of Middle Eocene age dominate (Yeo et al., 2004 and references therein). Maxwell Bay, a U-shaped embayment with a length of 14 km and a width of 6–14 km, is located at the southwestern end of KGI, enclosed by Nelson Island and the Fildes Peninsula (Yoon et al., 2000). It is separated from the Bransfield Strait by a deep submarine sill (>430 m) and characterised by a flat central part with water depths ranging from 400–550 m and a shallower part at the northern end displaying greater topographic irregularities (Griffith and Anderson,

1989; Yoon et al., 2000). More than half of the coastline of the bay is governed by headlands and rocky beaches. Tidewater glaciers are only found in more protected tributary inlets, like Potter and Marian coves (Griffith and Anderson, 1989). From July–September the bay is completely covered by sea ice, which begins to break up in late October (Griffith and Anderson, 1989; Khim and Yoon, 2003). During summer (November–February) the bay is ice-free and two different water masses may be distinguished. Relatively cold and saline open ocean water (subsurface water) enters the bay from the Bransfield Strait ($<0^{\circ}\text{C}$, 34.0–34.5 psu) generally showing wind driven cyclonic circulation patterns (Roese and Drabble, 1998). It is overlain by a surface layer of warmer and less saline water ($0\text{--}1.04^{\circ}\text{C}$, 33.9–34.0 psu) that is mixed with freshwater discharging from melting glaciers and surface runoff (Khim and Yoon, 2003 and references therein). Sediment laden plumes are reported adjacent to most of the tidewater glaciers in the protected inlets during this period (Griffith and Anderson, 1989). Today KGI is characterised by a maritime cold climate that is more humid and warmer than in other Antarctic areas, particularly compared to the Antarctic continent. It is characterised by a high relative humidity (89%), an annual precipitation rate of 437.6 mm water equivalent and a mean annual air temperature of -1.8°C (Lee et al., 2004). With summer temperatures frequently above 0°C it is one of the very few Antarctic regions with substantial summer melting.

3.4. Material and Methods

3.4.1. Sampling

During RV Polarstern cruise ANT-XXIII/4 in April 2006, a gravity core (SL, PS 69/335-2) and a giant box core (GKG, PS 69/335-1) were recovered at a water depth of 450 m in Maxwell Bay off KGI (Gohl, 2007) (Table 3.1, Fig. 3.1). The gravity core was cut in 1 m sections onboard where wet bulk density was determined with a multi-sensor core logger (GEOTEK Ltd, UK) via gamma ray attenuation. Stored at 4°C the cores were transported to Bremerhaven, opened, and split for further

analyses. Samples for the determination of geochemical and sedimentological parameters were taken from the working halves of the gravity core sections and a 60 cm long subcore obtained from the GKG. Sampling was performed at fixed intervals of 5 cm (SL) and 10 cm (GKG) using 10 cm³ syringes. After being freeze-dried and weighed, the samples were ground and homogenised in agate ball mills.

Table 3.1. Coring sites on cruise ANT-XXIII/4.

Core	Gear	Location	Longitude and latitude (deg/min/s)	Water depth (m)	Core length (m)
PS 69/335-1	GKG	Maxwell Bay	58°46'23.4"W 62°15'30.6"S	447	0.60
PS 69/335-2	SL	Maxwell Bay	58°46'20.4"W 62°15'30.0"S	446	9.43

3.4.2. Depth correction

In order to correct for the loss of surface sediment and compressional effects during the coring process of gravity core PS 69/335-2, an undisturbed surface sediment subcore taken from GKG PS 69/335-1 was used for substitution. Based on high-resolution colour reflectance data (b^*) and using the AnalySeries 2.0.4.2 software (Paillard et al., 1996) both cores were combined to one synthetic core 'PS 69/335'. For further details see Hass et al. (2010). In the following original core depths of PS 69/335-2 are converted to metres composite depth (mcd) with an offset of +0.24 m.

3.4.3. Core description

Figure 3.2 shows the lithology and selected radiographs (see <http://doi.pangaea.de/10.1594/PANGAEA.509895>) of core PS 69/335 that were taken at the Alfred Wegener Institute, Bremerhaven using a Faxitron X-ray Inspection System (Hewlett Packard, USA). The core PS 69/335 has a composite length of 9.51 m and it is dominated by homogenous brown-green-greyish silty clay with comparably few

scattered ice rafted debris (average value for the fraction >63 mm is 1.1%, only four samples exceeding 5%) (Hass et al., 2010). In the upper 8 mcd bioturbation is moderate to high, which is supported by radiographs revealing worm tubes (Fig. 3.2). The lower part displays weak lamination and evidence for flaser bedding. At 6.36–6.37 mcd a dark brown to black stratum was recognised which included coarser grained sediment with higher amounts of silt (67%), fine sand (20%) and volcanic glass shards and represents most probably a tephra layer.

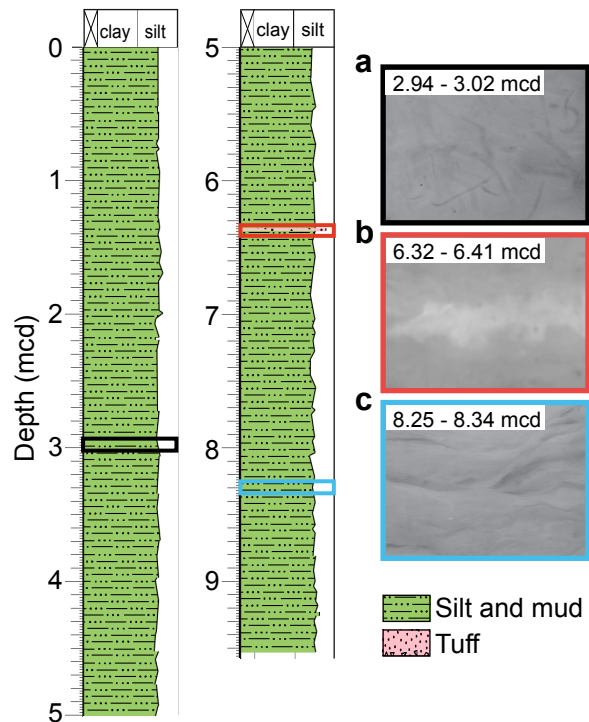


Fig. 3.2. Lithology of core PS 69/335. Radiographs of selected sections showing a) worm tube evidence for high bioturbation rates in the upper part of the core, b) the coarser grained tephra layer at 6.36 mcd, and c. evidence for flaser bedding at the bottom.

3.4.4. Laboratory analyses

The content of total sulphur (TS) was determined using a carbon and sulphur analyser (ELTRA CS 500, Germany) equipped with a solid-state infrared detector. Total organic carbon was determined with a CS-analyser (LECO, Germany) after calcareous material had been removed from sample splits by adding concentrated HCl ($\geq 37\%$). Quantitative X-ray fluorescence (XRF) analysis was carried out with a conventional wavelength dispersive XRF (WD-XRF) spectrometer (Philips PW 2400). Glass beads were prepared from the samples with di-lithium tetraborate

according to Schnetger et al. (2000) and measured in random order to avoid artificial trends. Further element analyses (REE, Cs, Nb, Th, U) of selected samples were performed by Inductively Coupled Plasma Mass Spectrometry (ICP-MS) at 5000-fold dilution using an Element 2 mass spectrometer (Thermo Fisher GmbH, Germany). Sample preparation was conducted following Schnetger (1997) with slight modifications using 1 ml HClO₄ (70%, subboiled) and 3 ml HF (40%, Suprapur®) for acid digestions. Based on the water content of each sample, element contents were corrected for seawater salt assuming seawater composition and a salinity of 34‰, which is consistent with the subsurface salinity found at Maxwell Bay (Roese and Drabble, 1998). This method was checked using 13 selected samples, which were washed with 18.2 MΩ water and ultrasonicated three times to dissolve the sea salts. Chloride and sulphate concentrations of the filtrate were then quantified by ion chromatography using a DIONEX ion chromatograph. Both methods agreed within 11% based on a linear correlation between water content and measured chloride concentration with $r^2 = 0.974$. Smear slides of selected sediment layers were prepared for petrographic investigations. Sediment samples were taken from the undisturbed archive half. After fixation with Canada balsam at 130°C the samples were analysed at Bremen University, Germany using a LEICA DMRX polarisation microscope (Leica Camera AG, Germany). Photomicrographs were taken with a LEICA DFC 320 digital camera system and processed with IM50 software (Leica Camera AG, Germany). The Accelerator Mass Spectrometry ¹⁴C chronology of core PS 69/335-2 is based on the age model after Hass et al. (2010). For the sediments from Maxwell Bay a reservoir effect of 1,100 years was assumed (Hass et al., 2010), which is consistent with literature where reservoir effects between c. 1,000 and 1,400 years (Björck et al., 1991b) were found for this area. In addition, ²¹⁰Pb analyses were carried out for eight samples obtained from both cores. Activities of radionuclides were measured by gamma spectrometry (Ge-detector, GWC 2522-7500 SL, Canberra Industries Inc., USA) and processed with GENIE 2000 3.0

(Canberra Industries Inc., USA). Counting statistics were better than 5% for the samples except those with very low ^{210}Pb activity ($<0.08 \text{ Bq g}^{-1}$). The accuracy of this method was tested by using a standard reference material similar in matrix composition to the WAP samples (UREM-11). It averaged 10% for all radioisotope concentrations, which were corrected for the samples by factors calculated using the certified reference values. To take account of changing sedimentation rates with time, the age of each sediment slice was determined according to the constant rate of supply model after Appleby & Oldfield (1978). Compaction effects were taken into account by correcting the ^{210}Pb excess activities with the dry bulk density. The total ^{210}Pb inventory was determined by integration of the corrected ^{210}Pb activity data versus the depth profile, whereas ^{210}Pb excess values of lacking sediment samples were interpolated at 1 cm steps. Mass accumulation rates of the bulk sediment (MAR_{BS}) were calculated from the product of the linear sedimentation rate and the dry bulk density. Analytical data are available at <http://doi.pangaea.de/10.1594/PANGAEA.737926>, 737995, 733677, 738106, and 738123.

3.4.5. Calculation of SiO_2 excess

SiO_2 excess ($\text{SiO}_{2\text{xs}}$), which represents the biogenic, nonlithogenic fraction of total SiO_2 and thus the content of biogenic silica (BSi), was calculated after Böning et al. (2005):

$$\text{SiO}_{2\text{xs}} (\%) = \text{SiO}_{2\text{sample}} (\%) - [\text{SiO}_2/\text{Al}_2\text{O}_{3\text{lithogenic}} \cdot \text{Al}_2\text{O}_{3\text{sample}} (\%)] \quad (3.1)$$

In keeping with an average bedrock calculation, a lithogenic $\text{SiO}_2/\text{Al}_2\text{O}_3$ ratio of 3.07 was assumed. $\text{SiO}_{2\text{xs}}$ was chosen as a proxy for biosiliceous production for different reasons: particularly for wet alkaline extraction, the precision and accuracy of the BSi determination vary depending on the extraction time, the solid to solution ratio, and the pH (Liu et al., 2002 and references therein). In addition, the variable

amounts of reactive Si-containing components, including quartz, clay minerals, aluminosilicates and volcanic glasses, leached by this procedure may bias the results (Koning et al., 2002).

3.4.6. Chemical Index of Alteration

In order to estimate the degree of chemical weathering of the source material the Chemical Index of Alteration (CIA) after Nesbitt & Young (1982) was calculated. Usually, the CIA ranges between <50 for fresh rocks and 100 for highly residual clays. An increase in this index therefore reflects a decreasing primary mineral content and increasing amount of secondary phases. Thus, high values indicate intensive chemical weathering due to high precipitation and air temperatures, whereas low values may evidence a colder and/or more arid climate where physical weathering prevails.

3.4.7. Statistics

In order to guarantee the precision and accuracy of the methods at least eightfold measurements of several carefully selected in-house (PS-S, UT-S, TW-TUC, Loess, DR-BS) and international reference standards (BIR-1, JA-2, JB-1, PACS-1, JG-1a, IAPSO Standard Seawater 35%) were conducted. To determine the degree of statistical spread and therefore the precision of a method, the relative standard deviation was used (Skoog and Leary, 1996). In the case of TS and XRF analyses multiple determinations of reference material were performed to calculate the pooled estimated relative standard deviation after Skoog & Leary (1996). To get an idea of the accuracy of a method, the relative systematic error (f) representing the variation from the certified value was determined (Skoog and Leary, 1996). Statistical evaluation is summarised in Table S1 (supplementary data will be found on www.journals.cambridge.org/jid_ANS). Precision was better than 1% for major elements (Si, Ti, Al, Fe, Mn, Mg, Ca, K, P) and <5% for minor elements (Cs, Rb, Sr, Th, U, Y,

Zr, REE; Nb and Ba 5–6%) and bulk parameters (TS, TOC). In general, accuracy ranged from -0.98 to 1.6% (major elements) and -6.5 to 5.8% (minor elements and bulk parameter), except for U, SO_4^{2-} and Cl^- ($|f| < 10\%$).

3.5. Results

3.5.1. Chronology

According to the age model described above, the core spans the Late Holocene period (c. 1,700 calendar (cal) yr BP to present, Fig. 3.3a) (Hass et al., 2010). Linear sedimentation rates calculated from this model range between 0.34 and 1.67 cm yr^{-1} (average = 0.55 cm yr^{-1}) and were verified by data obtained by ^{210}Pb excess activity of the surface sediments (0.2–1.0 cm yr^{-1} , Fig. 3.3a). These data moreover reveal that during the last 100 years sediment mass accumulation rates have gradually increased from 0.2 $\text{g cm}^{-2} \text{yr}^{-1}$ at the beginning of the 1910s to 0.66 $\text{g cm}^{-2} \text{yr}^{-1}$ between AD 2005 and AD 2006 (Fig. 3.3b). The highest increases are observed between c. AD 1940 and AD 1980 (0.0049 $\text{g cm}^{-2} \text{yr}^{-2}$) as well as during the last decade (0.0151 $\text{g cm}^{-2} \text{yr}^{-2}$).

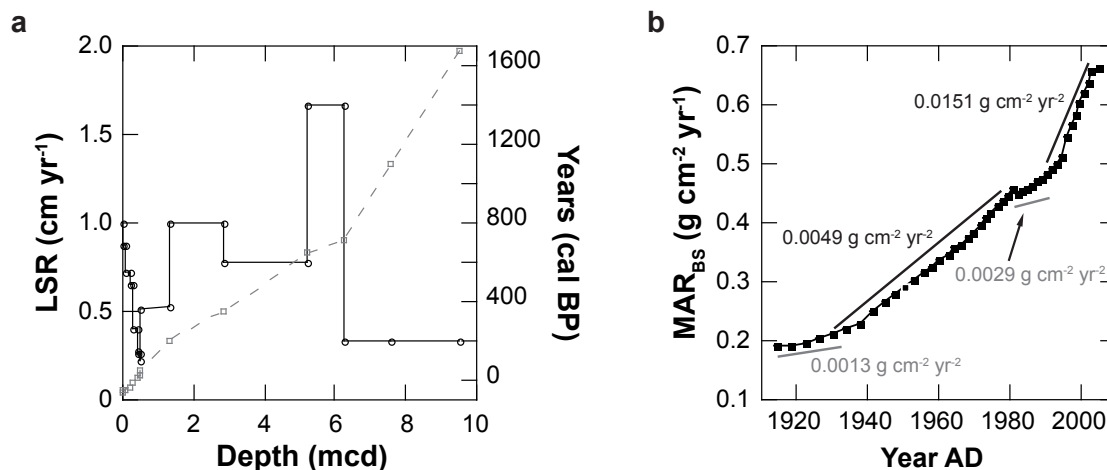


Fig. 3.3. a) Age (grey squares) and linear sedimentation rate (LSR) vs depth of core PS 69/335 according to radiocarbon and ^{210}Pb measurements. b) Mass accumulation rates of bulk sediment (MAR_{BS}) vs year AD in Maxwell Bay calculated using the ^{210}Pb dating model and including interpolated sediment depths.

3.5.2. Lithogenic background

In Fig. 3.4 the $(\text{Na}_2\text{O} + \text{K}_2\text{O})$ vs SiO_2 contents of core PS 69/335 samples are shown and compared to the composition of the local bedrock. To establish a better comparability of source and sink material the sediment composition was corrected for sea salt and for BSi to avoid artefacts (e.g., Na_2O , K_2O) and dilution effects. Because individual samples from the source rocks of the island are highly variable in composition, median and quartiles (25% and 75%) were calculated, which are more robust to outliers. Figure 3.4 shows that the sediments of core PS 69/335 plot in the field of tholeiitic basaltic andesites

and in the red box representing the variability of Barton Peninsula bedrock. Generally, the NMORB-normalised distribution patterns of the sediments follow the trends of

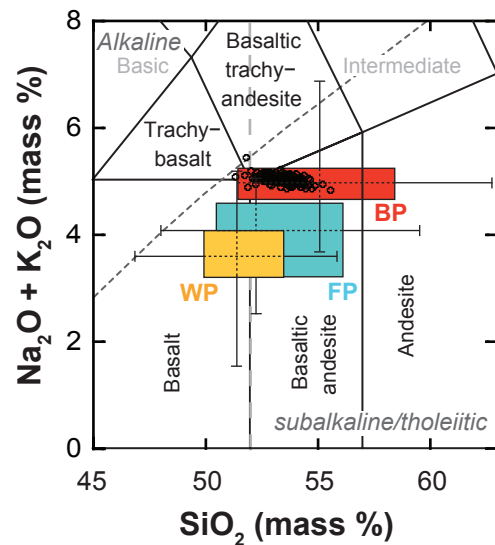


Fig. 3.4. $(\text{Na}_2\text{O} + \text{K}_2\text{O})$ vs SiO_2 content of the BSi adjusted sedimentary deposits from Maxwell Bay (black circles) compared with the composition of bedrock from the Fildes (FP), Barton (BP) and Weaver Peninsula (WP). Source rock data were compiled using the data from Machado et al. (2005), Yeo et al. (2004), and Lee et al. (2004) and are given as median, quartiles (box) and 95% confidence interval (whiskers). Fields for volcanic rock classification are from Le Bas et al. (1986).

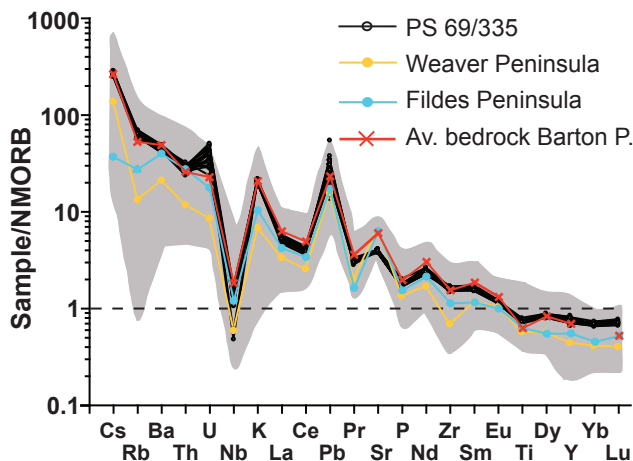


Fig. 3.5. (Trace element abundances of core PS 69/335 and bedrock from Barton, Weaver and Fildes Peninsula normalised to N-MORB (Sun & McDonough, 1989). Shaded area represents the total variability of western KGI bedrock types. Mean source rock data are from Lee et al. (2004), Yeo et al. (2004), and Machado et al. (2005).

the source rocks found in the study area (Fig. 3.5, grey area). However, the highest correlation is given for an average Barton Peninsula bedrock (Fig. 3.5, red line), which is calculated based on the geochemical data compiled by Lee et al. (2004). The calculation was done with respect to the spatial distribution of the different types of bedrock found on Barton Peninsula (51% basaltic andesite 2 (BA-2), 20% basaltic andesite 1 (BA-1), 10% granodiorite, 14% Sejong Formation, 5% lapilli tuff) using the geological map published in Lee et al. (2004). All samples are relatively enriched in large ion lithophile elements, such as Cs, Rb, Ba, U, K, Pb, Sr, and light rare earth elements (La, Ce, Pr and Nd) and show a negative Nb trough in the spider diagram. In addition, it is evident that uranium shows even higher than expected values for KGI volcanic rocks.

3.5.3. Vertical distributions of elements

In general the geochemistry of Maxwell Bay sediments reveals minor variations with depth. However, significant deviations with regard to selected element/aluminium (E/Al) ratios are evident in discrete sediment layers (Fig. 3.6a). Slightly higher Ti/Al and Ca/Al, and lower K/Al values are typical for some intervals in the upper part of the core (226, 231, 246, 276, 281, 286, 378, and 442 calendar yr BP) and at 1,274 cal yr BP, whereas the assumed tephra layer at 6.36 mcd (744 cal yr BP) is characterised by increased Ca/Al and decreased K/Al and Ti/Al ratios. Photomicrographs of selected samples moreover indicate that significant amounts of brownish and pristine volcanic glass shards are present in the pronounced layers (442 cal yr BP (30–50%) and 744 cal yr BP (c. 50%), Fig. 3.6b & d) but could not be found in the remaining samples where biological material (diatoms) prevails (e.g., 448 cal yr BP, Fig. 3.6c). After these layers were removed from the dataset, some distinct distribution patterns are apparent in several element ratios (Fig. 3.7a). The Mg/K ratio in the lithogenic background ranges between 1.54 and 1.78. The highest values are found between c. 550 and 50 cal yr BP and before 1,400 cal yr BP.

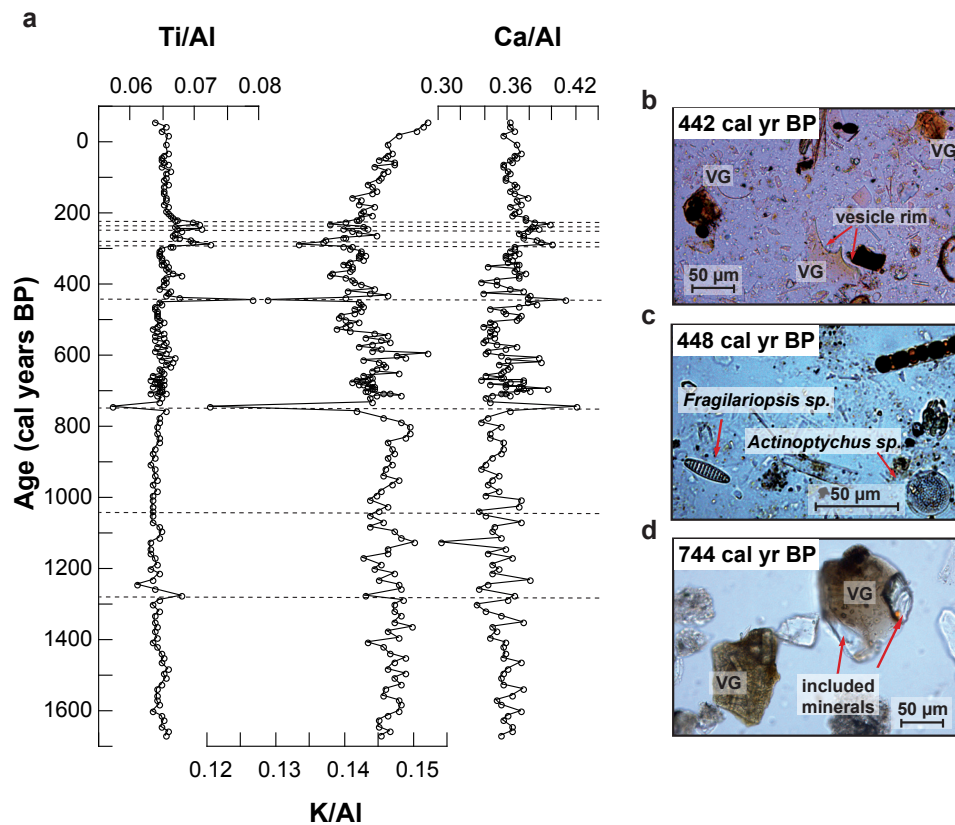


Fig. 3.6. a) Vertical distribution of Ti/Al, K/Al, and Ca/Al of core PS 69/335 vs depth (mcd) and age (cal yr BP) as determined by quantitative WD-XRF accompanied by photomicrographs of selected sediments at b) 442, c) 448, and d) 744 cal yr BP. VG = volcanic glass.

It generally follows the distribution of the mean grain size (12–21 µm), which is largest in the intervals mentioned above (Hass et al., 2010). Similar characteristics are also observed in the tephra corrected Ti/Al record (0.063–0.068, average = 0.065). In contrast, rather opposing trends are recognised in the Rb/Al ($r = -0.58$) and Zr/Al ($r = -0.39$) profiles where slightly lower values (13×10^{-4} (Zr/Al) and 3.5×10^{-4} (Rb/Al)) are correlated with a higher mean grain size (16–21 µm). This is also true for K/Al, which shows a positive correlation to Rb/Al ($r = 0.83$). In particular for the Mg/K record, lower ratios between c. 550 and 1,400 cal yr BP and a significant decrease during the last 50 years are apparent.

3.5.4. Bioproductivity proxies

A higher downcore variability was observed for bioproductivity proxies, like TOC and $\text{SiO}_{2\text{xs}}$ (Fig. 3.7a). Figure 3.7a reveals that $\text{SiO}_{2\text{xs}}$ (4.1–9.4%, average = 6.4%) correlates quite well with BSi (2.6–9.6%, average = 6.2%), which was re-calculated from opal data taken from Hass et al. (2010). However, compared to $\text{SiO}_{2\text{xs}}$ ($1\sigma = 1.1$) the BSi record ($1\sigma = 1.4$) shows a greater variability. It cannot be excluded that this is solely a result of the lower precision of the leaching method. Consequently, in this study $\text{SiO}_{2\text{xs}}$ has been used as it is probably more reliable than BSi as a proxy for

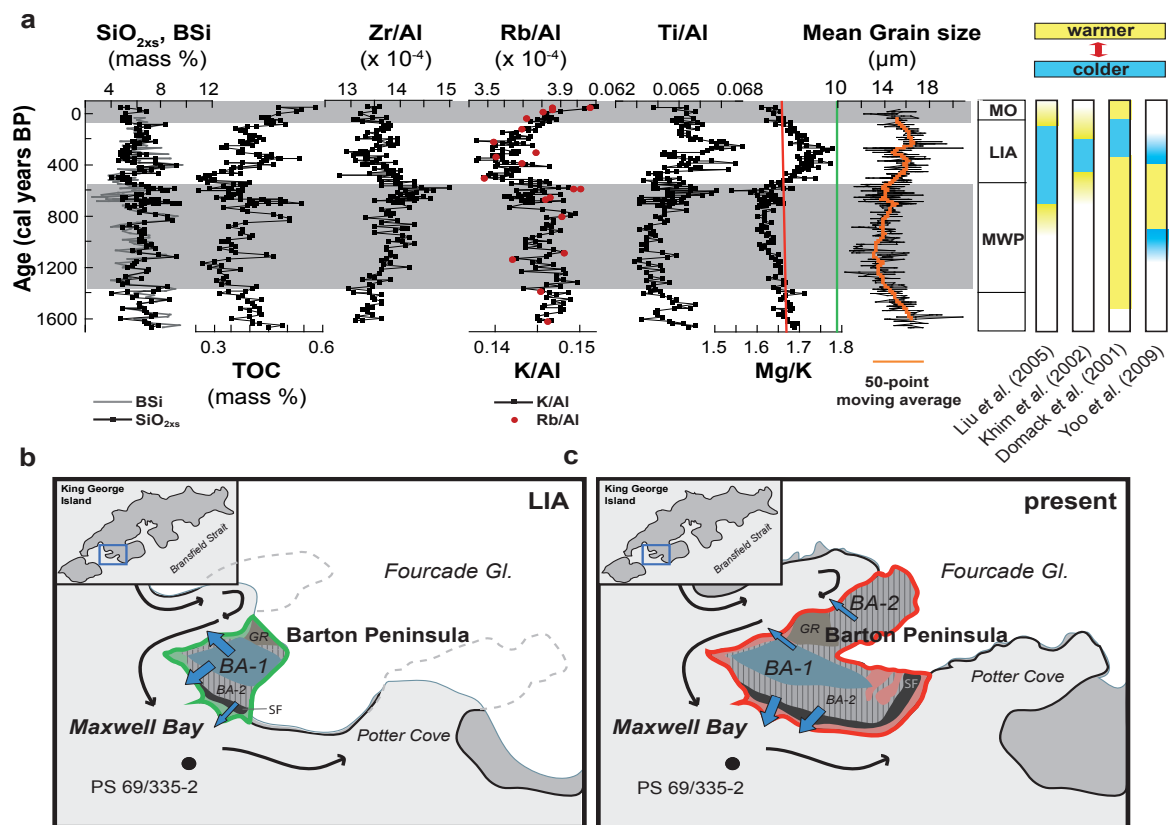


Fig. 3.7. a) Comparison between selected bioproductivity proxies ($\text{SiO}_{2\text{xs}}$, BSi, TOC), Zr/Al, K/Al, Rb/Al, Ti/Al, and Mg/K ratios vs age (cal yr BP) in Maxwell Bay sediments and recorded climatic events of several studies along the WAP. BSi values (grey solid line) are calculated from opal data taken from Hass et al. (2010). The green and red vertical lines represent the average Mg/K ratio of outcrops on Barton Peninsula, b) during the LIA, and c) at present. BA-1 = basaltic andesite 1, BA-2 = basaltic andesite 2, SF = Sejong Formation, GR = granodiorite, MO = Modern optimum, LIA = Little Ice Age, MWP = Medieval Warm Period. Mean grain size data are from Hass et al. (2010). Tephra layers were excluded from this plot for a better illustration of the trends.

siliceous bioproduction. For the period from 1,700 cal yr BP to present, continuous cyclic fluctuations in TOC (0.26–0.58%) and $\text{SiO}_{2\text{xs}}$ were determined. Maxima in TOC for example at c. 700, c. 825, c. 1,120, and 1,665 cal yr BP are paralleled by the $\text{SiO}_{2\text{xs}}$ record. Their uniform trends terminate at c. 350 cal yr BP where a gradual increase in TOC up to 0.58% occurs that is not reflected in $\text{SiO}_{2\text{xs}}$ and BSi.

3.5.5. Geochemistry of sulphur and redox sensitive elements

Figure 3.8 shows the vertical distribution of some redox sensitive parameters (TOC, TS, U/AI) in core PS 69/335. A significant increase with depth is visible in the vertical distribution of U/AI. At the top of the core U/AI values are within the range of average soils represented by the dashed vertical line (0.12×10^{-4} , estimated after Lee et al., 2004), but follow the TOC profile in deeper sediments. Highest values are found between 5 and 8 mcd (610–1,110 cal yr BP) and at 9.46 mcd (1,650 cal yr BP, 0.28×10^{-4}), making U the element with the highest enrichment factor (2.4) compared to local bedrock and soils. The element showing the highest downcore variability is sulphur. Whereas TS is quite low in the upper c. 3 mcd (present to 384 cal yr BP, average = 0.19%), sulphur contents of 0.8% are present between 3 and 8 mcd (375–1,200 cal yr BP) before varying on midlevel in the lowest

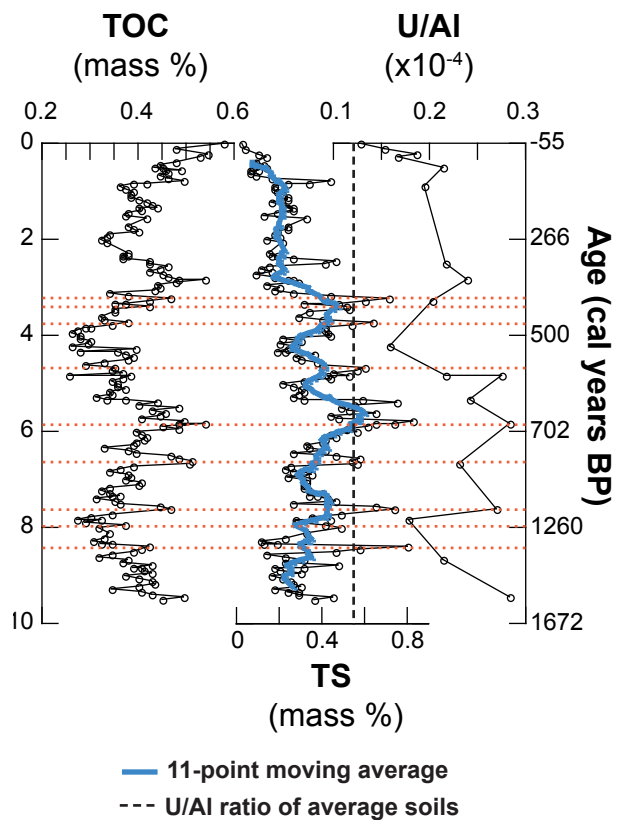


Fig. 3.8. Vertical distribution of TS, TOC, and U/AI vs depth (mcd) and age (cal yr BP) of core PS 69/335. Dashed vertical line represents U/AI ratios of average soils on Barton Peninsula estimated after Lee et al. (2004).

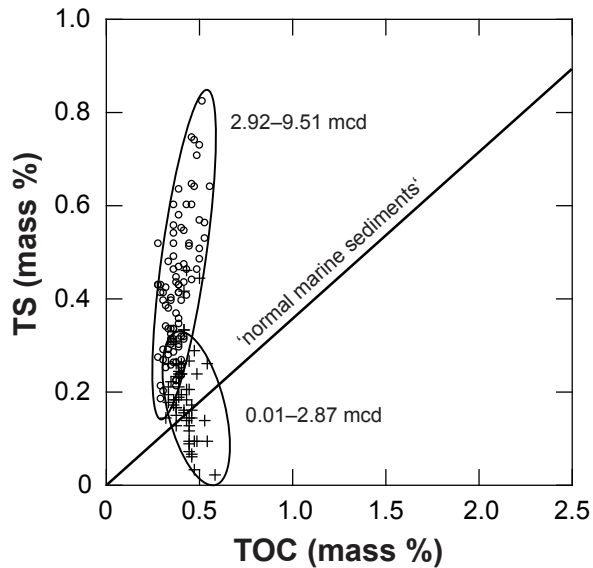


Fig. 3.9. Cross plot of TOC and TS of Maxwell Bay sediments. Samples are represented by crosses (0.01 and 2.87 mcd) and open circles (2.92 and 9.51 mcd). The solid line represents the TOC/TS ratio of 'normal marine sediments' (c. 2.8) after Berner & Raiswell (1983).

1.5 m (c. 1,200–1,670 cal yr BP, average = 0.29%). Particularly in the bottom part, maxima of TS coincide with TOC maxima (e.g., 3.21, 5.76, 6.56, and 7.61 mcd).

A TS vs TOC cross plot moreover reveals that TOC/TS ratios in surface sediments (<~3 mcd, -56 to 384 cal yr BP) are predominantly in the range of 'normal marine sediment', but reach lower values in the basal part (Fig. 3.9). It should be noted that the TS concentrations only represent a minimum estimation

since a possible sulphate reduction in deeper parts of the core would result in an overcorrection of the salt-corrected sedimentary sulphur. Assuming a complete depletion of sulphate in the pore water, TS contents in the basal part would on average be 20% higher, which would also lead to even lower TOC/TS ratios (-16%).

3.5.6. Chemical weathering

In Fig. 3.10a the $\text{CaO}^* + \text{Na}_2\text{O} - \text{K}_2\text{O} - \text{Al}_2\text{O}_3$ diagram of the samples from Maxwell Bay and the average composition of the dominant bedrock types of the Barton Peninsula after Lee et al. (2004) is shown. The CIA ranges between 53.6 and 59.5 (average = 56.9) and follows the weathering trend of basaltic andesite 2. Within the vertical distribution no clear trend is visible. Maximum values occur at 499, 589, and 1,259 cal yr BP, while minima are detected during times most probably influenced by volcanic material (442 and 744 cal yr BP, Fig. 3.10b).

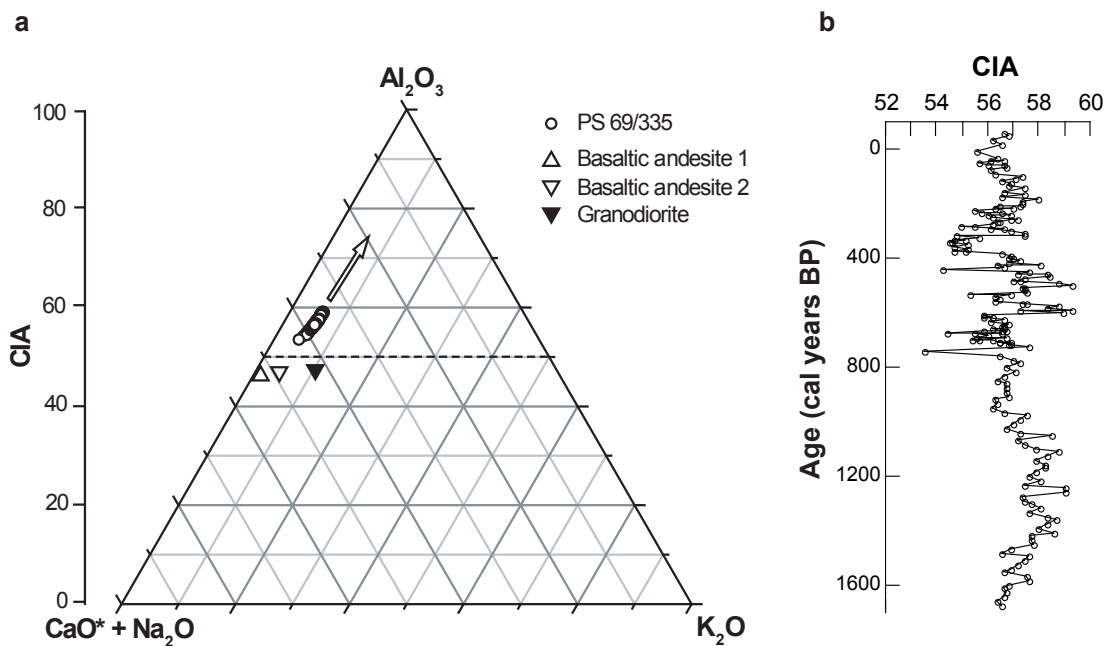


Fig. 3.10. a) $CaO^*+Na_2O-K_2O-Al_2O_3$ diagram of the samples from Maxwell Bay and the average composition of the dominant bedrock of the Barton Peninsula. The arrow indicates the weathering trend of basaltic andesite 2 rocks. b) Vertical distribution of the CIA vs age (cal yr BP) of core PS 69/335.

3.6. Discussion

3.6.1. Lithogenic background and tephrochronology

The results of this study suggest that the geochemical composition of the Maxwell Bay sediments is mostly determined by the lithogenic background of Barton Peninsula and adjacent areas. It is characterised by tholeiitic basaltic andesite rocks (Fig. 3.4) showing a Nb trough in their NMORB normalised element distribution (Fig. 3.5), which is typical for rocks evolved from subduction zone magmas (Machado et al., 2005). In addition, several tephra layers were identified by their geochemical characteristics using quantitative XRF, and were verified by photomicrography. Most of the minerals, found in at least two ash bearing deposits (442 and 744 cal yr BP), are characterised by sharp edged contours and inclusions of rapidly quenched volcanic glasses (Fig. 3.6). Thus, this material has not experienced significant mechanical reworking during transport. Although a dilution by local bedrock complicates the correlation

between sink and source of these ashes to a certain extent, an aeolian transport from Deception Island seems to be the most probable origin for these tephras (Baker et al., 1975; Matthies et al., 1990). Two of the tephra layers found in core PS 69/335 (3.56 mcd, c. 442 cal yr BP; 6.36 mcd, 744 cal yr BP) may even be related to the tephra horizons AP2 (c. 450 ¹⁴C cal yr BP) and AP3 (c. 750 ¹⁴C cal yr BP), which were observed by Björck et al. (1991d) in four lakes along the Antarctic Peninsula region.

3.6.2. Alteration of potential proxies by early diagenesis

Diagenesis is one of the main factors complicating the reconstruction of the palaeoclimate via bioproductivity proxies like TOC and BSi/opal. Howe et al. (2007) showed that in surface sediments from the deep Bransfield Strait and Weddell Sea, organic matter degradation can lead to diagenetic alteration of the primary climatic signals. Effects of sub- to anoxic diagenesis should therefore be considered when investigating the sediments closer to the coast, since melt water and nutrient discharge might induce an even higher primary productivity in these proximal settings, resulting in higher organic matter export to the sediments and even more intense early diagenesis.

The downcore profile of a redox sensitive proxy like the U/Al ratio (Fig. 3.8) may give a first indication of the depositional conditions in this area (Klinkhammer and Palmer, 1991). Changes in U/Al may be caused by a shift in source rock composition towards more uranium bearing granodiorites (U/Al = 0.32×10^{-4} (granodiorites), $0.07\text{--}0.13 \times 10^{-4}$ (basaltic andesites), after Lee et al., 2004) However, this appears to be very unlikely considering the fact that these granodiorites are only found at a small area in the central north of Barton Peninsula. Consequently, the hypothesis of U enrichment under reducing conditions within the sediment has to be taken into account. Mobilised as U⁶⁺ in an oxic environment, uranium may be precipitated and fixed in sediments as U⁴⁺ under more reducing conditions, as a result of microbially

induced processes below the sediment-water interface (Klinkhammer and Palmer, 1991). Apart from the upper layers where U/Al is close to lithogenic background, the ratio follows the distribution of TOC, which is explained by the affinity of reduced U^{4+} towards organic particles under reducing conditions (Anderson et al., 1989). This supports the assumption that uranium comes from oxic seawater and precipitates at depth along a redox gradient, which is controlled by the oxygen penetration depth (Klinkhammer and Palmer, 1991). Similar observations were also made by Santos et al. (2007) in the nearby Admiralty Bay. In oxygen depleted environments early diagenetic formation of pyrite must also be considered as this is strongly linked to microbial sulphate reduction. Whereas sedimentological investigations confirm the occurrence of sulphidic spots within the sediments of core PS 69/335, the occurrence of slightly higher amounts of sulphur in deeper layers is an indication of the formation of iron sulphides.

Further clues to the pathway of early diagenetic oxidation of TOC are given by the TOC vs TS cross plot shown in Fig. 3.9. The fact that the upper section of core PS 69/335 is generally characterised by TOC/TS values \geq c. 2.8 suggests that oxidants such as oxygen, nitrate, or manganese oxides are primarily responsible for TOC metabolism. In contrast, significantly lower TOC/TS values found in the bottom section of the core PS 69/335 reveal the fingerprint of sulphate reduction, which is supported by sulphate measurements of the filtered washing solution of the sediments. We are aware that this method cannot compensate for the lack of pore water data, because during core storage calcium-sulphate phases may have precipitated which were not redissolved by our leaching procedure. However, assuming that precipitation is negligible or comparable in all samples, the results indicate that SO_4^{2-}/Cl^- ratios in these filtrates gradually decrease downcore from surface sediments and reach 50% of the seawater value in a depth of c. 3.50–3.75 mcd (c. 435–467 cal yr BP, data not shown). This certainly is a minimum estimate, since sulphide (pyrite) oxidation would lead to increases in SO_4^{2-}/Cl^- ratio

as well. Whereas Khim & Yoon (2003) assumed that additional sulphur within Maxwell Bay sediments was probably related to the detrital supply of pyrite from pyrite bearing rocks of hydrothermal origin, the close relationship between TOC and TS in this setting as it is shown in Fig. 3.8 rather suggests authigenic pyrite formation, which is mainly controlled by the quantity of metabolisable organic matter. During future investigations, pore water analyses may give further useful information about early diagenetic processes in WAP sediments. In any case, these first results emphasise that the alteration of potential proxies, such as TOC, may complicate the palaeoclimate reconstruction in this area.

3.6.3. Controlling factors of bioproductivity in the coastal WAP region: reduced sea ice coverage and reduced sunlight penetration

In several studies along the WAP, TOC and particularly BSi/opal have successfully been used as proxies for palaeoproductivity. In this context the sensitive character of this area, which has experienced alternating periods of more extensive sea ice coverage and relatively ice-free open water conditions since the LGM, has already been demonstrated by several sedimentary, geochemical and diatom records (e.g., Khim et al., 2002; Yoon et al., 2010). The palaeoproductivity proxy records of core PS 69/335 (TOC, $\text{SiO}_{2\text{xs}}$) support the evidence for changing ice conditions through time by reflecting synchronous fluctuations that may provide the first evidence for short-term changes in marine primary production and climatic conditions during the past c. 1,750 yr.

According to Taylor et al. (2001), high TOC and BSi contents in marine sediments of the WAP region are primarily associated with increased bioproductivity during warmer periods and minimal sea ice. Several factors influencing primary production have to be taken into consideration in nearshore areas where melt water streams from retreating glaciers directly affect the chemistry and physics of the water column. In addition to water column stabilisation by the drainage of freshwater, an increased

import of nutrients, iron in particular, is predicted (e.g., Raiswell et al., 2006; Schloss et al., 2002). Both factors generally support plankton bloom development. However, particularly in enclosed fjords and coastal areas, a negative effect of increased melt water discharge on bioproductivity because of higher turbidity and low light penetration is also possible (Schloss et al., 2002). Hass et al. (2010), for example, showed that lower TOC values in Maxwell Bay sediments are correlated to some extent with finer grained deposits, which characterise warmer periods and reflect reduced bioproductivity due to higher amounts of suspended particulate sediment material in the water column. However, whereas they could clearly identify the Medieval Warm Period (MWP, 1,400–550 cal yr BP) and the Little Ice Age (LIA, 550–50 cal yr BP) as a main neoglacial event using granulometric data, these long-term climatic periods could not acceptably be reconstructed with the bioproductivity proxy records alone (Fig. 3.7a). Our data imply that the effect of light attenuation on primary production in Maxwell Bay caused by increased input of particulate matter during warmer periods and longer sea ice coverage during colder periods may have a similar influence.

3.6.4. Proxies for changes in provenance and glacier extents on Barton Peninsula

More reliable information about long-term changes in local climate may be provided by inorganic geochemical data of core PS 69/335 sediments that have been corrected for sea salt, tephra layers and biogenic material, like biogenic opal and TOC. Figure 3.7a reveals that particularly the downcore profile of Mg/K generally follows the grain size distribution. After Hass et al. (2010) the granulometric data evidence colder conditions between 550 and 50 cal yr BP and a warmer phase between c. 1,400 and 550 cal yr BP. The existence of a colder period within the Late Holocene, for example, that is equivalent in timing with the LIA of the Northern Hemisphere has moreover been demonstrated by several studies at different locations along the WAP, although timing and duration varies regionally (Fig.

3.7a). Magnetic susceptibility records from Palmer Deep sediments suggest a LIA equivalent between c. 700 and 100 cal yr BP (Domack et al., 2001), which is widely consistent with glacial geological results from South Georgia and the sub-Antarctic islands (Clapperton and Sugden, 1988). Changes in the penguin population on Ardley Island indicate a cold period from c. 450 to 200 cal yr BP (Liu et al., 2005), whereas Khim et al. (2002) found evidence for a cooling starting at c. 400 cal yr BP in a sediment core from the eastern Bransfield Basin, following a warmer phase between c. 900 and 400 cal yr BP. The fact that Mg/K seems to reflect these climatic events could have several reasons. This parameter may, for example, be used as a measure of basaltic melts modified by fractional crystallisation. As it has already been shown earlier the geochemical signature of core PS 69/335 strongly suggests that Barton Peninsula is the most probable origin of these sediments (Figs 3.4 and 3.5). This is additionally evidenced by median Mg/K ratios found in core PS 69/335 (1.7) and in rock samples from the different peninsulas (Barton Peninsula = 1.5, Weaver Peninsula = 10.7, Fildes Peninsula = 3.9; see Table S2). However, slight changes in several element/aluminium ratios between 550 and 50 cal yr BP (e.g., Ti/Al, Zr/Al, Rb/Al) supports the assumption that small-scale alternations in supply areas reflecting different stages of glacier extents on Barton Peninsula may be responsible for this (Fig. 3.7a). Geochemical data of particulate matter discharged from different melt water streams are not available, which complicates provenance analyses. However, based on the bedrock data provided by Yeo et al. (2004) retreated glaciers during warmer periods (e.g., MWP, 1,400–550 cal yr BP) would lead to a higher influence of Mg-poor and K-rich primary source rocks (BA-2, average Mg/K = 1.8) and the volcanoclastic Sejong Formation (SF, average Mg/K = 1.1) (Fig. 3.7c). This in turn would cause a lower average Mg/K ratio of the outcrops of 1.67 (Fig. 3.7a, red line; Table S2). In contrast to that, as is shown in Fig. 3.7b, re-advanced glaciers between c. 550–50 cal yr BP would have resulted in a shift towards less fractionated basaltic andesites (BA-1, Mg/K = 6.6) and a higher average Mg/K ratio

of the uncovered bedrock of 1.79 (Fig. 3.7a, green line; Table S2). This is also in line with the values found in PS 69/335 (see Fig. 3.7a, MWP average = 1.71, LIA average = 1.63). Furthermore, we would expect a trend towards lower Rb/Al and Zr/Al ratios during colder periods when the influence of basaltic andesite 1 rocks is higher (see Table 3), which is exactly what we see in our sediments (Fig. 3.7a). Whereas Seong et al. (2009) were not able to reconstruct a glacier advance at Barton Peninsula in this period, our result is consistent with the study from Hall (2007) who described a re-advance of the Collins Glacier (Fildes Peninsula) at c. 650 cal yr BP using radiocarbon dates of incorporated moss.

However, changes in sediment geochemistry can also indicate sorting effects, particularly in high-energy environments. In this case one would expect winnowing processes to favour the simultaneous accumulation of coarser grained material and heavy minerals, such as rutile and zircon (Rittenhouse, 1943). This does not seem to be true for Maxwell Bay sediments where Zr/Al rather shows an opposing trend ($r = -0.39$). Moreover, chemical weathering processes may play an important role. Thus, Mg/K ratios possibly reflect climatic processes in that Mg is residing in chemically more unstable minerals such as pyroxenes, and K is present in stable minerals such as potassium feldspars. During warmer periods increased chemical weathering would as a result lead to lower Mg/K ratios in coastal sediments. Considering the fact that K/Al shows a significant decrease during these periods (Fig. 3.7a) and that this temporal trend is not visible in the CIA record (Fig. 3.10b), such an explanation appears to be rather unlikely. In general, the geochemical data does not show any evidence for significant chemical weathering in this area, which is consistent with results from a couple of other studies along the WAP region (Lee et al., 2004; Santos et al., 2007) and favours changing provenance and glacier extents as an explanation for shifts in Mg/K.

3.6.5. Geochemical proxies for the recent rapid warming along the WAP

Yoo et al. (2009) argued that granulometric and sedimentological data from the continental shelf of the northern SSI document a return to warmer conditions since c. 50 cal yr BP. Within the same period decreasing Mg/K ratios in Maxwell Bay sediments were observed indicating a higher influence of BA-2 source rocks, possibly triggered by the rapid recent glacier retreat at the Barton Peninsula (Fig. 3.7c). An additional indicator for rapid recent warming is derived from bulk sediment mass accumulation rates obtained from ^{210}Pb determinations of surface sediments. A gradual retreat of glaciers north of 64°S has been observed since the 1940s (Cook et al., 2005), which is reflected by an enhanced input of sediment laden melt water and a significant increase in MAR_{BS} in Maxwell Bay (Fig. 3.3b). Evidence for a faster retreat of the Fourcade Glacier (KGI) between 1956 and 1988 was found by Braun and Gossmann (2002). They also stated that in the following decade no significant glacier retreat and even slight advances were observed for the major glaciers at nearby Admiralty Bay, which would explain the relative constant MAR_{BS} calculated for the same period. Although no cooling was detected during this time period, anomalous slowing of glacier retreat was found in several areas along the WAP (Cook et al., 2005). However, recent studies came to the conclusion that the retreat of glaciers has accelerated during the last decade (e.g., Cook et al., 2005; Rignot et al., 2008) leading to higher particle fluxes in the water column and increasing MAR_{BS} . If air temperatures will continuously rise, as predicted in the latest IPCC report (Solomon et al., 2007), the input of particulate matter via melt water streams may increase even further. It is liable that this in turn will also have consequences for nearshore marine ecosystems. Moline et al. (2004), for example, could show that these melt water induced changes in light regime, nutrient availability and salinity have already affected the planktonic community in recent decades.

3.7. Conclusions

In this study the first comprehensive geochemical characterisation of sediments from the WAP is presented. Radiocarbon and ^{210}Pb data reveal that a composite core from Maxwell Bay (KGI) comprises a sedimentary record of the last c. 1,750 years with high sedimentation rates ranging from 0.2–1.7 cm yr⁻¹. Ten tephra layers, most probably derived from Deception Island, were detected by quantitative XRF measurements and verified by microscopic methods. The layers at 442 and 744 cal yr BP may directly be linked to previous eruptions and/or reported tephra layers in nearby lacustrine records. The sediment composition is mainly controlled by the lithogenic background of the study area, consisting of tholeiitic basaltic andesites most probably derived from the nearby Barton Peninsula. The primary composition of the sediments is moreover affected by early diagenetic processes (e.g., U and TS) and by fluctuations in bioproductivity (TOC, BSi/SiO_{2xs}) in the overlying water column. Palaeoclimatic interpretation of the sediment proxies let us infer that the study site has experienced short-term alternations in regional climate during the last c. 1,750 years, which may be a result of the climatically sensitive character of this area. Despite the low downcore variability of most elements, there is evidence that the supply area has changed during periods of retreat and re-advance of glaciers on Barton Peninsula. Changes in selected element ratios allow identification of two main climatic events during the Late Holocene that are equivalent in timing to the LIA (c. 550–50 cal yr BP) and the MWP (c. 1,400–550 cal yr BP) of the Northern Hemisphere. Although the study site nowadays is characterised by a warmer climate, no significant increase in proxies indicating chemical weathering could be found. Since the end of the 1930s, MAR_{BS} have almost tripled up to the present (0.66 g cm⁻² yr⁻¹), which documents a gradual glacier retreat and input of eroded particulate material because of the rapid regional warming trend observed in the last decades. With rising air temperatures predicted for the future the particle flux in the water column may further increase. However, the resulting severe consequences

for nearshore marine ecosystems in this sensitive area are hard to predict.

3.8. Acknowledgements

The authors extend their gratitude to the shipboard scientists and crew of the RV Polarstern. We also thank the technical assistants Eleonore Gründken, Carola Lehnert, Martina Schulz (Institute for Chemistry and Biology of the Marine Environment, Oldenburg), Rita Fröhling and Ute Bock (Alfred Wegener Institute for Polar and Marine Research, Bremerhaven). Special thanks go to Willard S. Moore for help in ^{210}Pb modelling and Andreas Klügel (Bremen University) for his assistance with petrological analyses. The authors are in particular indebted to Kathy Licht and Sandra Passchier for their enthusiastic and critical reviews.

3.9. Supplementary material

Three Supplementary tables will be found at [www.journals.cambridge.org/jid_](http://www.journals.cambridge.org/jid_ANS)ANS.

4. Penguin colony expansion on the western Antarctic Peninsula during Holocene warm phases curtailed by volcanic activity

Patrick Monien^{a,*}, Stephen J. Roberts^{b,*}, Julia Lofffield^a, Bernhard Schnetger^a, Emma P. Hocking^c, Dominic A. Hodgson^b, Michael J. Bentley^c, Peter Fretwell^b, Ryszard Ochyra^d, Anna R. Hey^{e,b}, Claire S. Allen^b, Steve Moreton^f, Hans-Jürgen Brumsack^a

^a Institute for Chemistry and Biology of the Marine Environment (ICBM), P.O. Box 2503, D-26111 Oldenburg, Germany.

^b British Antarctic Survey (BAS), Natural Environmental Research Council (NERC) High Cross, Madingley Road, Cambridge, CB3 0ET, UK

^c Durham University, Department of Geography, Science Laboratories, South Road, Durham, DH1 3LE, UK

^d Institute of Botany, Polish Academy of Sciences, ul. Lubicz 46, 31-512 Kraków, Poland

^e School of Earth and Ocean Sciences, Cardiff University, Main Building, Park Place, Cardiff CF10 3AT, UK

^f NERC Radiocarbon Facility (Environment), Scottish Enterprise Technology Park, Rankine Avenue, East Kilbride, Scotland, G75 0QF, UK.

* These authors contributed equally to this work

This chapter will be submitted to *Nature Geoscience*.

4.1. Introduction

Since the middle of the last century, mean annual air temperatures on the western Antarctic Peninsula (WAP) have increased by 3°C (Meredith and King, 2005) making it one of the most rapidly warming regions on Earth. This warming has already been linked to marked changes in the distribution of some of the regions' fauna, such as the Adélie, Gentoo and Chinstrap penguins, through its impacts on sea-ice cover, snow accumulation, primary production and the availability of breeding habitats (Baroni and Orombelli, 1994; Wilson et al., 2001; Fraser and Hofmann,

2003; Ducklow et al., 2007; Bricher et al., 2008). Previous studies from abandoned penguin rookeries (Baroni and Orombelli, 1994; Emslie et al., 2007) and changes in lake sediment geochemistry (Sun et al., 2000; Sun et al., 2004; Huang et al., 2011) have suggested longer term relationships between late Holocene climate and penguin population change. However, the spatial distribution and temporal coverage of these records (Emslie, 2001) limits our ability to use them as a basis for predicting future changes. Here we present the earliest evidence of penguin occupation on the Antarctic Peninsula from a high-resolution and well-dated Holocene lake sediment record from Ardley Island, WAP. Using bio-geochemical markers uniquely associated with penguin guano, we show that penguins were present from 7.4 cal kyr BP, with population maxima at 6.1–5.2, 4.3–3.4 and 2.0–1.4 cal kyr BP, during the warmest parts of the Holocene. Population change was driven by multiple factors, principally deglaciation and relative sea level change, which determine nesting site availability, and changes in sea-ice distribution, which determine access to prey species. Eruptions from the nearby Deception Island volcano caused near total extinctions of the local penguin population on several occasions in the last 8,000 years. Penguin populations are currently below Holocene maximum levels, but our results imply that they could rise if the Antarctic Peninsula continues to warm.

4.2. Results and Discussion

Penguin populations change in complex ways, responding rapidly to changes in their local-regional environment, which, in Antarctica, are closely coupled to variations in global climate and oceanographic conditions. For example, the observed decline in Adélie penguin (*Pygoscelis adélieae*) populations on the northern Antarctic Peninsula in recent decades has been linked to reduced period of sea-ice and proximity to prey species (Smith et al., 1999). In contrast, populations of Gentoo penguins (*P. papua*) are stable or increasing across the Antarctic Peninsula (Woehler et al., 2001). As an ‘ice-avoiding’ species favouring generally ‘warmer’ conditions than Adélie penguins,

their 'expansion' has been associated with the well-documented recent warming of the Antarctic Peninsula, where reduced sea-ice, ice shelves, and terrestrial glacier mass, have increased the availability of food closer to terrestrial habitats suitable for nesting (Ducklow et al., 2007).

All observational records of penguin population change in Antarctica are very short-term. Therefore, to reconstruct a longer and high-resolution history of penguin population change during the Holocene, we analysed major and trace elements in a 9,000 year radiocarbon dated lake sediment record from Ardley Island, WAP ($62^{\circ} 12.774$, $58^{\circ} 56.398$; Fig. 4.1, Supplementary Fig. 4.S1) and compared it with other regional records of past penguin occupation and palaeoclimate along the WAP.

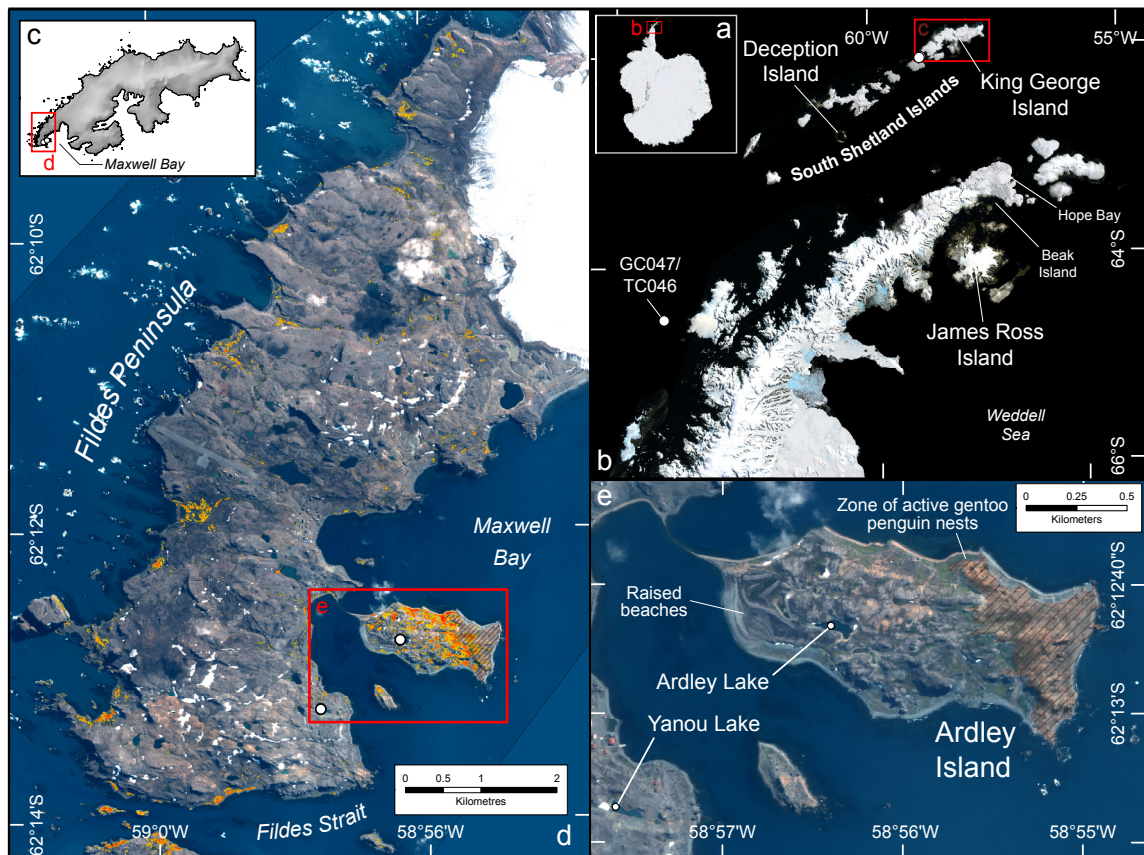


Fig. 4.1. Study Site. Overview maps showing a) Antarctica with b) the location of the western Antarctic Peninsula with the sampling site of core GC047/TC046 and the South Shetland Islands, c) King George Island (KGI) with d) the Fildes Peninsula and e) the sampling sites at Yanou Lake (KGI) and Ardley Lake, Ardley Island. Vegetated areas of increasing intensity shown in yellow-orange were determined from analysis of satellite data (see supplementary information).

Previous studies around Antarctica have shown that areas occupied by penguins have significantly higher concentrations of certain elements found in, or associated with, penguin guano (namely, As, Ba, Ca, Cd, Cu, P, S, Se, Sr, and Zn) (Liu et al., 2013; Supplementary Table 4.S1). Since these elements are considered immobile in soils and lake sediments (Sun et al., 2000; Huang et al., 2011) they are good proxies for historical changes in penguin presence (Sun et al., 2000). To further control for biochemical inputs associated with the underlying geology, soils and natural lake development, we undertook the same analyses on a sediment record from nearby Yanou Lake (62° 13.243, 58° 57.591, Fig. 4.1, Supplementary Fig. 4.S2), which has not been occupied by penguins. We also compared terrestrial data with constrained changes in regional sea-ice during the Holocene using a new diatom proxy ratio record from the nearest available marine sediment core taken from the Anvers Shelf (Fig. 4.1b).

The penguin colony in Ardley Island in the South Shetland Islands is dominated by Gentoo penguins. With c. 5,000 breeding pairs (Fig. 4.1e), it is one of the largest breeding Gentoo penguin colonies in the Antarctic (ATCM, 2009). Inter-mingled, there are also c. 300 breeding pairs of Adélie penguins and <50 breeding pairs of Chinstrap penguins (*P. antarctica*), but these two latter species account for <10% of total population (ATCM, 2009). Every breeding season, approximately 139 tonnes (dry mass) of penguin guano is discharged onto Ardley Island (Sun et al., 2004), some of which accumulates in the island's lakes and melt water ponds.

Sediment cores extracted from Ardley Lake (ARD), the only permanent water body on Ardley Island, record changes in the concentration of the unique assemblage of biochemical elements associated with changing inputs of penguin guano (Fig. 4.2). An R-mode cluster analysis performed on the inter-correlation coefficients of major and trace element concentrations in core ARD clearly separated guano-elements (Sr, Cu, Zn, Se, Ca, Se, P, C, N, S) and guano-associated elements (Cd, As, Hg) from lithogenic elements (e.g., Al, Mg, Si, Sc, Ti, Zr, Y, and REE) derived from

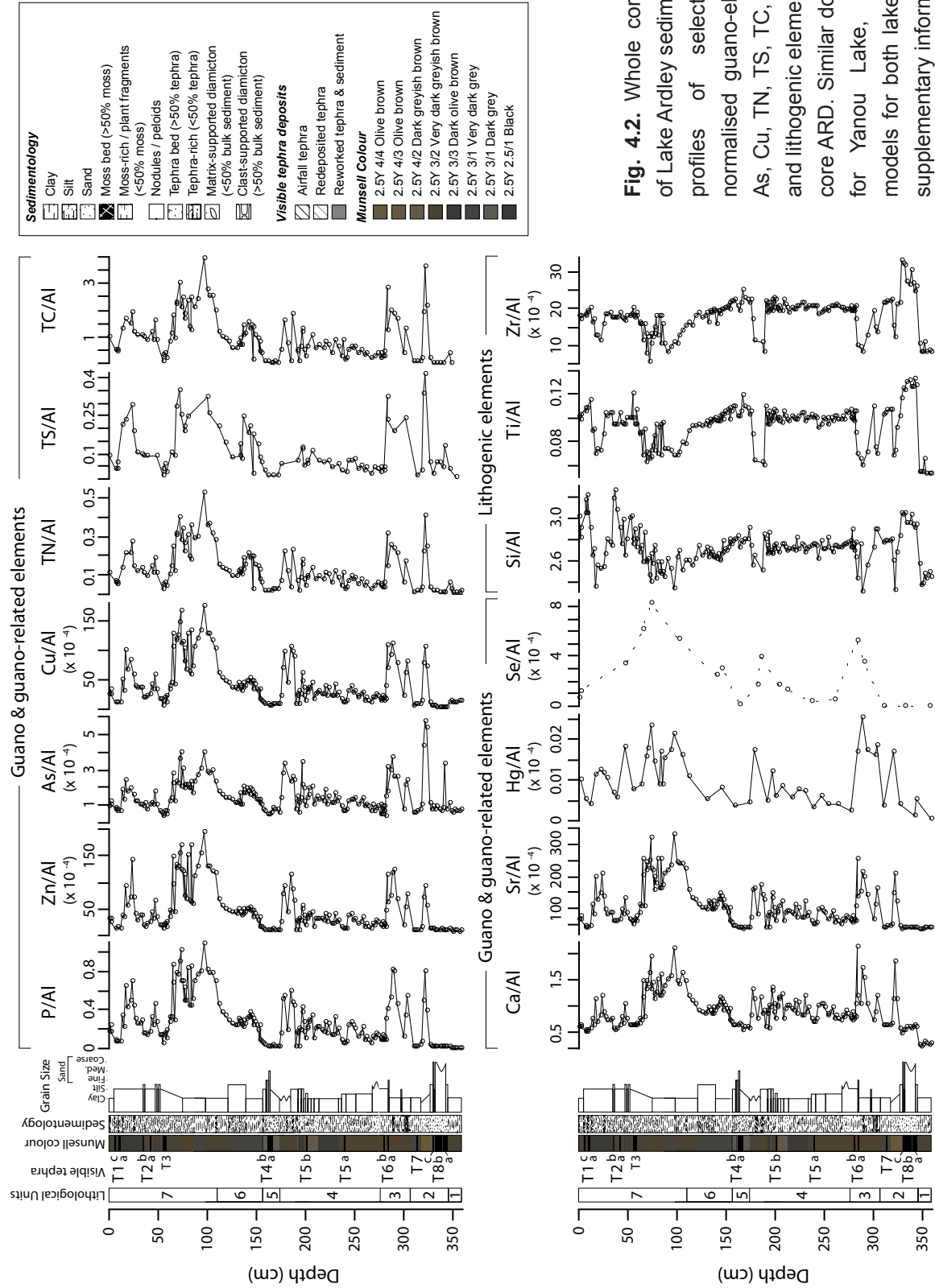


Fig. 4.2. Whole core geochemistry of Lake Ardley sediments. Downcore profiles of selected aluminium normalised guano-elements (P, Zn, As, Cu, TN, TS, TC, Ca, Sr, Hg, Se) and lithogenic elements (Si, Ti, Zr) of core ARD. Similar downcore profiles for Yanou Lake, and age-depth models for both lake records are in supplementary information.

weathering of volcanic bedrock in the Ardley Lake record (Supplementary Fig. 4.S4, Supplementary Table 4.S3). No such clear distinction existed in the Yanou Lake record (Supplementary Fig. 4.S4, Supplementary Table 4.S4). The presence of penguin guano in sediment samples from Ardley Lake is further supported by their C/N and C/P ratios, which are close to the ratios known for guano and humus in ornithogenic (bird formed) soils, but differ significantly from ratios found in phytoplankton and local plants (Supplementary Fig. 4.S5). Bi-plots of selected EI/Al ratios show that Ardley Lake sediments are generally located on a mixing line between ornithogenic soils and eroded local bedrock end members (Supplementary Fig. 4.S6). Therefore, the mean fraction of ornithogenic soils in Ardley Lake sediments ($F_{o.s.}$) can be estimated by using a simple mixing equation (see supplementary information) and used as a proxy of past penguin population change (Fig. 4.3e).

Our data show that Ardley Lake sediments began accumulating c. 8.8 cal kyr BP (Supplementary Fig. 4.S1; Supplementary Table 4.S2) when the previously more extensive South Shetland Islands ice cap had separated into individual ice caps on each of the islands (Mäusbacher et al., 1989; Watcham et al., 2011) and retreated from this part of the Fildes Peninsula between 10.1 to 8.2 cal kyr BP (Milliken et al., 2009).

High concentrations of guano-elements show the first occupation of the catchment by penguins occurred c. 7.4–7.2 cal kyr BP (Fig. 4.3e), suggesting good availability of relatively flat, ice-free nesting sites around Ardley Lake, with good, sea-ice free access for short foraging trips. This is the oldest evidence of penguin occupation on the WAP, preceding occupation of nesting sites along mid-southern WAP from c. 6 kyr BP, and the northern WAP sector from 5.5 to 0.6 kyr BP (Fig. 4.3g, h; Zale, 1994; Emslie, 2001).

Following this initial occupation of Ardley Island, penguin populations have fluctuated in response to a range of environmental changes including climate, sea-ice extent, as well as glaciation, relative sea level and volcanic activity (Fig. 4.3).

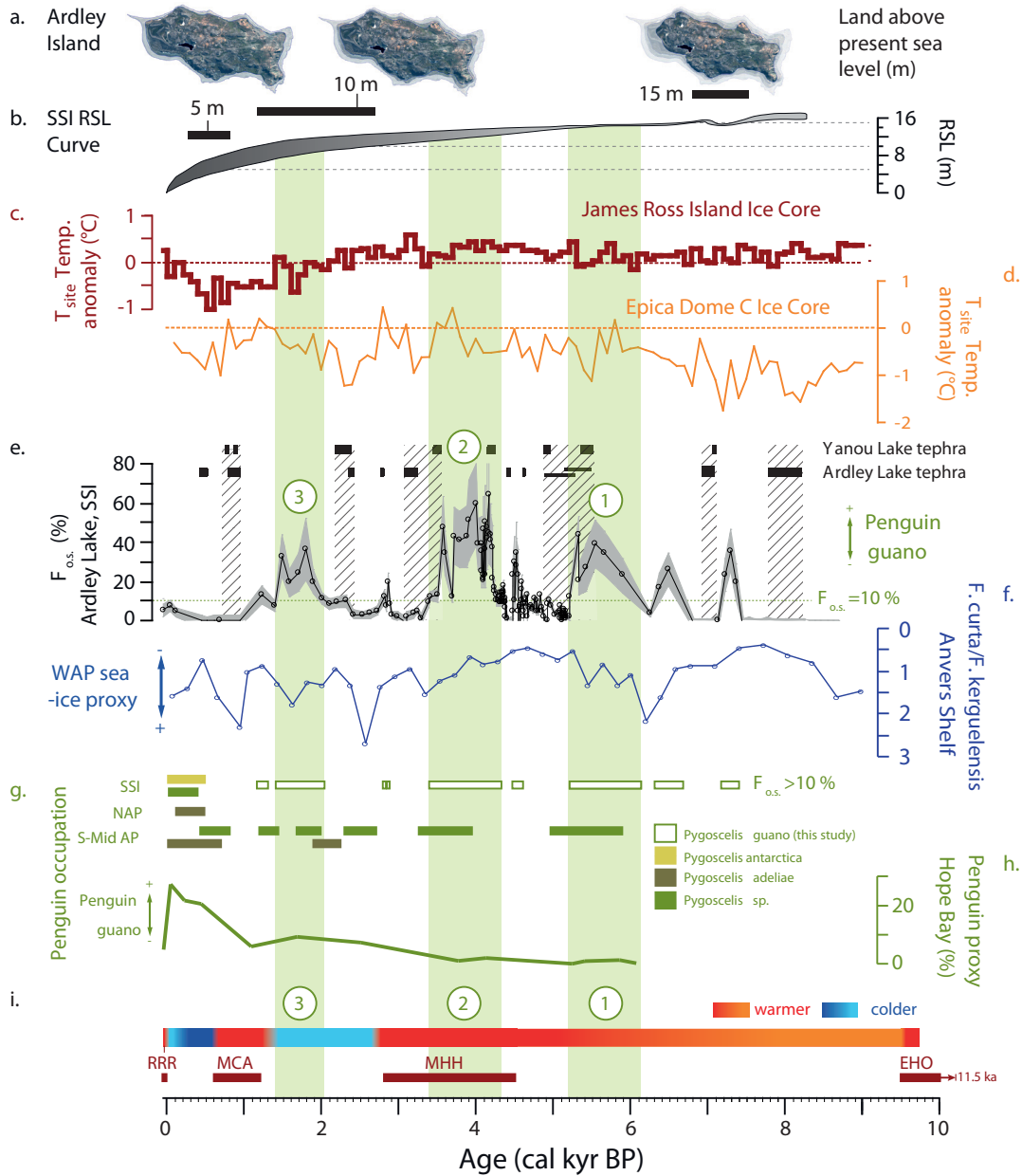


Fig. 4.3. Proxies for changes in penguin occupation, sea-ice and Holocene climate at the Antarctic Peninsula. a) Changes in available Ardley Island land mass with changing relative sea levels during the Holocene; Land above present sea level (a.p.s.l.), 5 m a.p.s.l., 10 m a.p.s.l., and 15 m a.p.s.l. (mapped using data from the King George Island Digital Elevation Model); b) Relative sea level (RSL) curve for the South Shetland Islands (Watcham et al., 2011); c) Temperature anomaly (compared to present day) from the James Ross Island (JRI) ice core record (Mulvaney et al., 2012); d) Temperature anomaly based on the Epica Dome C ice core record (Stenni et al., 2010); e) Calculated fractions of ornithogenic soils in core ARD ($F_{0.5}$); shaded zones represent key visible ash deposits in Ardley and Yanou lakes associated with a reduction in biogeochemical elements in Lake Ardley sediments; f) The nearest available sea-ice diatom proxy record from core GC047/TC046; g) Summary of penguin occupation on the Antarctic Peninsula (Emslie, 2001); h) Penguin population proxy based on bioelement concentrations in lake sediments from Hope Bay, north-eastern Antarctic Peninsula (Zale, 1994); i) Climate synthesis for the Antarctic Peninsula (Bentley et al., 2009).

Throughout the Ardley Lake record a long-term relationship between penguin populations and regional sea-ice persists, suggested by a broadly inverse relationship between guano-element concentrations (and therefore $F_{o.s.}$) and the nearest available diatom-based record of regional sea-ice changes during the Holocene from the Anvers Shelf (Fig. 4.3f).

The first peak in penguin populations is associated with a reduction in regional WAP sea-ice during a period of early Holocene warming 8–7 cal kyr BP following deglaciation. This coincides with lower *F. Curta* / *F. Kerguelensis* ratios found in the Anvers Shelf record between 8.3–6.6 cal kyr BP (Fig. 4.3f), which is interpreted as a period of warm water conditions and reduced regional sea-ice cover. Increased sea-ice is associated with increased food availability for most species of penguins (Croxall et al., 2002; Forcada et al., 2006). However, for Gentoo penguins, warmer conditions and reductions in sea-ice cover are particularly beneficial as they need to feed closer to their colony compared to other species (e.g., Adelie penguins) to support their relatively long breeding-nurturing cycle (Forcada et al., 2006). Gentoo penguins are known to favour coastal ice-free nesting sites, but can suddenly abandon existing nests due to the accumulation of too much guano. On Ardley Island, this and the increasing availability of coastal land as relative sea level fell during the Holocene (Fig. 4.3a) probably explains some sudden reductions of guano concentrations in Ardley Lake sediments.

Sporadically, volcanic activity appears to have had a devastating impact on the size of the penguin colony on Ardley Island. Low guano-element concentrations followed volcanic eruptions at c. 8–7.5 and 7 cal kyr BP from Deception Island (Fig. 4.3e). A short-lived recovery occurred in between these eruptions, but guano-element concentrations remained low after the c. 7 cal kyr BP eruption until c. 6.5 cal kyr BP, even though regional sea-ice was relatively reduced, and relative sea level remained constant at c. 15–16 m above present sea level (Fig. 4.3a, e, f). The general absence of reworked tephra in the ARD core during this period suggests population change

and not geochemical dilution was the controlling factor. A two-phase recovery of the penguin population occurred from 6.5 cal kyr BP, likely associated with regional sea-ice minima and continued warm climate, which allowed populations to reach their first major peak (with $F_{o,s}$ values >50%) at around 5.5 cal kyr BP. This peak population was brought to a rapid and catastrophic collapse by another volcanic eruption (or series of eruptions) from Deception Island between 5.5–4.8 cal kyr BP, which either deposited a significant amount of tephra directly onto Ardley Island and across King George Island, creating unsuitable nesting habitats across a wide area, or possibly caused disruption to local-regional climate and/or marine and terrestrial ecosystems in the build up to the Mid Holocene Hypsithermal. A minor dilution factor could be present in the sediments after this eruption, but the prolonged absence of guano-elements suggests the effect of these eruptions combined with extremely reduced sea-ice conditions could have reduced available food sources for Gentoo penguins in this part of the WAP for up to c. 900 years.

Following the 5.5–4.8 cal kyr BP eruption(s), populations remained low between 5.2 and 4.3 cal kyr BP, likely due to a phase of colder regional climate marked by glacier re-advances on King George Island 6.0–4.0 kyr ago (Mäusbacher et al., 1989; Watcham et al., 2011) and James Ross Island 6.4–3.2 kyr ago (Sterken et al., 2012). After, a substantial increase in the population occurred from 4.3–3.4 cal kyr BP (Fig. 4.3e), reaching the highest levels in the Mid-Holocene at c. 4.15 cal kyr BP. This coincides with relatively low regional sea-ice levels, coupled with a phase of peak-warmth during the Mid-Holocene Hypsithermal (MHH) detected in adjacent Yanou Lake through increased biological production (Supplementary Fig. 4.S3), in lake sediments records from Livingston Island, Elephant Island, Beak Island and James Ross Island (Bentley et al., 2009; Sterken et al., 2012), marine records from the Antarctic Peninsula (Bentley et al., 2009; Pike et al., 2013) and ice cores (Masson-Delmotte et al., 2011) (Fig. 4.3). Relative sea levels at this time were 8–12 m higher than present, which would likely have forced the expanding colony into the catchment

of Ardley Lake (Fig. 4.3a, b). The end of the Mid-Holocene penguin optimum was abrupt and broadly coincided with a renewed phase of volcanic activity between c. 3.0–3.5 cal kyr BP. Populations then remained low with the onset of a colder phase (the so-called ‘Neoglacial’) across the Antarctic Peninsula (Domack et al., 2001; Milliken et al., 2009) after c. 2.5 kyr BP (Fig. 4.3). The initiation of this cooling phase is seen in the James Ross Island ice core record (Mulvaney et al., 2012; Fig. 4.3c), the most prominent peak in the regional WAP sea-ice proxy record (Fig. 4.3f), periods of more intense (seasonally persistent) sea-ice in the Palmer Deep marine diatom record (Taylor and Sjunneskog, 2002) and episodic re-advances of local glaciers (Domack et al., 2001; Milliken et al., 2009).

The last sustained Holocene increase in penguin population on Ardley Island occurred c. 2.0–1.4 cal kyr BP, in line with a previous study from a nearby, but shallower water body on Ardley Island (Sun et al., 2000). At this time, bioproductivity proxies in Yanou Lake show generally higher concentrations (Supplementary Fig. 4.S3), but the control remains unclear. A locally warmer climate has been suggested from some regional marine records (Majewski et al., 2012), but is absent from the James Ross Island ice core record (Fig. 4.3c). The number of breeding penguins influencing the catchment of Ardley Lake at this time was likely driven upwards, initially at least, by a decline in regional sea-ice following the 2.5 kyr maximum (Fig. 4.3e, f). However, lower concentrations of penguin guano in the Ardley Lake sediments suggests either a relatively smaller population compared to the MHH optimum or reflects the increased availability of breeding space outside the Ardley Lake catchment due to the continued rapid fall in relative sea level (Watcham et al., 2011). After 1.2 cal kyr BP colder conditions and increased sea-ice (Fig. 4.3c, d, f, i) appear to lead to a reduction in the number of breeding penguins influencing the catchment of Ardley Lake. Only a relatively minor increase in the penguin population occurred during the last century on Ardley Island. This increase appears comparatively smaller than other Northern Peninsula breeding colonies in, for example, Hope Bay,

but these are dominated by Adelie penguins, which favour what were 'better-than-average' Holocene sea ice conditions up until very recently.

In summary, whilst we cannot assess some factors that determine breeding success such as pressure from predators (Emslie et al., 1995), the ability to change diet (Emslie and Patterson, 2007), or recent anthropogenic impacts (Bricher et al., 2008), this study has revealed the key factors influencing penguin populations on Ardley Island through the Holocene. Populations appear to be generally linked to changes in regional climate and sea-ice extent but have experienced several rapid and catastrophic crashes as a result of volcanic eruptions. The highest populations were detected at 6.1–5.2 cal kyr BP, 4.3–3.4 cal kyr BP during the Mid-Holocene Hypsithermal, and at 2.0–1.4 cal kyr BP. This suggests that Gentoo penguin colonies expanded to occupy more inland areas of Ardley Island during 'warmer' periods, particularly during the Mid-Holocene Hypsithermal. In addition to volcanic activity, low population episodes appear to have coincided with colder phases with the expansion of land and sea-ice creating unfavourable breeding conditions for Gentoo penguins. Despite recent links between increased Gentoo penguin populations and the warming climate (Ducklow et al., 2007), penguin populations on Ardley Island appear to be still well below their Holocene optima.

4.3. Supplementary Information

4.3.1. Supplementary Material and Methods

4.3.1.1. Site description and sampling

Ardley and Yanou Lake are two freshwater lakes situated on Ardley Island and the nearby Fildes Peninsula at the southern coast of King George Island, South Shetland Islands, western Antarctic Peninsula (WAP) (Fig. 4.1). The geology of both islands is dominated by Meso-Cenozoic volcanic rocks of basaltic and basaltic andesite composition (Machado et al., 2008). Both lakes are surrounded by yellow-green carpet moss (*Sanonia uncinata*), lichens (*Usnea antarctica*) and vascular plants (e.g., *Deschampsia antarctica*) covering most of the catchment areas. At present, the study area has a maritime cold climate which is more humid, warmer, and more seasonally variable than most other regions of continental Antarctica. Regionally, the WAP is characterised by a high relative humidity (90%), an annual precipitation rate of 630 mm water equivalent and a mean annual air temperature of -2.6°C (Liu et al., 2011a). With summer temperatures frequently above 0°C it is one of only a few Antarctic regions with considerable summer melting (Pritchard and Vaughan, 2007).

Ardley Lake is the only permanent lake on Ardley Island, which is connected to King George Island by a narrow isthmus at low tide (Fig. 4.1). It is bounded by a high steep ridge to the north and a more subdued ridge to the east whereas a scree-covered steep mound confines the lake to the south. During periods of high water level, outflow over the sill (17.82 m above mean sea level), from the west, is possible. At present there is no inflow, but a dry 'channelled depression' running to the east could indicate the presence of a former underground or surface inflow. A square-rod Livingston piston corer (Wright, 1967) was used to extract five overlapping main cores (ARD 1A–1E) from a core site at the deepest flat area at a water depth of 4.85–5.19 m near the centre of the ice-covered Ardley Lake (Fig. 4.1e).

In addition, a surface sediment core (ARD-SUR) with a length of 10 cm was taken at the same location by means of a 50 cm long Russian corer. The five overlapping main cores were combined into one master core (ARD) with a total sediment depth of 359 cm composite depth (Supplementary Fig. 4.S1).

Yanou is a freshwater lake on the southeast of Fildes Peninsula, King George Island, situated around 500 m from the sea to the east, directly opposite Ardley Lake (Fig. 4.1). It is bounded to the south and southwest by a steep scree-covered flat-topped ridge. To the north are a series of raised beaches, the highest of which forms the sill (16.56 m above mean sea level). A small desiccation pond is located around 40 m to the east. The lake receives a small inflow from an adjacent lake (Gaoshan Lake), at higher altitude to the west, and has no surface outflows. However, two dry 'channelled depressions' run out to the north, either side of the sill, which could mark the position of underground drainages. A UWITEC piston corer was used to extract three c. 1.9 m long overlapping cores (8A, 8B, 9B) from the deepest part of a dual basin, with a water depth of 4.9 m. Cores were cut at 1 m for transport into two sections per core. Consolidated surface sediments were recovered using a 50 cm long Russian corer which was able to penetrate a c. 3–5 cm thick living moss layer carpeting the surface. Four overlapping cores (YAN 8A-1 and YAN 8A-2, 9B-1, 8B-2) were combined into a master core (YAN) with a total sediment depth of 355 cm composite depth (Supplementary Fig. 4.S2). No evidence of slumping was found in the ARD and YAN sedimentary records.

4.3.1.2. Laboratory methods

4.3.1.2.1. Geochemistry

Cores were transported and stored at -20°C; samples were taken at 1 cm interval, lyophilised and ground with an agate ball mill and manually with an agate pestle and mortar. ARD samples were analysed for total carbon (TC), total sulphur (TS) and total nitrogen (TN) using a CNS analyser (vario EL Cube, Elementar, Germany)

equipped with a solid-state infrared and a heat conductivity detector. TC and TS measurements were conducted on YAN sediments by means of an ELTRA CS analyser. For 69 selected samples the content of total inorganic carbon (TIC) was determined coulometrically by a CM 5012 CO₂ coulometer coupled to a CM 5130 acidification module (UIC, USA) while total organic carbon was then calculated as the difference between TC and TIC (TOC% = TC% - TIC%) according to Babu et al. (1999).

In core ARD, and in the terrestrial section of core YAN adjusted for the volcanic ash layer (0–31 and 190–208 cm), TC and TOC are highly correlated ($r^2 = 0.9998$ and $r^2 = 0.9997$). TIC concentrations (av. 0.10 and <0.01 mass%) are further negligible compared to TC values in both cores (av. 6.2 and 2.5 mass%). Henceforth, therefore, TC is considered to reflect the amount of organic carbon in Ardley Lake sediments and the terrestrial section of core YAN. In addition, Loss-on-ignition (LOI) data was collected for YAN samples using standard/well-established procedures (Dean, 1974). For this sediment samples were given in preweighed crucibles, dried for 24 hours at 105°C followed by LOI analysis at 550°C for 2 hours, and 950°C for 4 hours (LOI₅₅₀ is used to estimate changes in organic carbon).

Quantitative XRF analysis for major and trace elements (SiO₂, Al₂O₃, CaO, K₂O, Na₂O, P₂O₅, As, Ba, Cu, Co, Ni, Sr, Y, Zn, Zr) was carried out with a conventional wavelength dispersive X-ray fluorescence (WD-XRF) spectrometer (Philips PW 2400). Glass beads were prepared following standard procedures (Eckert et al., 2013). Measurements were undertaken in random order to avoid artificial trends. Trace element analysis (Cd, REE) of selected samples was performed by Inductively Coupled Plasma Mass Spectrometry (ICP-MS, Element 2 mass spectrometer, Thermo Fisher GmbH, Germany) at 2500-fold dilution. For acid digestions 100 mg of each sample was given in a closed polytetrafluoroethylene (PTFE) vessel system (Heinrichs et al., 1986) and preoxidised with 0.5 mL HClO₄ (70%, suprapur®, Merck, Germany) at 180°C for two hours. After 3 mL HF (40%, suprapur®, Merck, Germany)

have been added samples were heated at 180°C for six hours. In the following the acids were evaporated at 180°C on heating blocks while the residuals (200 µL) were re-dissolved with 3 mL 6-N HCl (subboiled) for three times. Subsequently 1 mL HNO₃ (65%, subboiled) and 10 mL ultra-pure (18.2 MΩ) water were added to the residuals and samples were simmered at 60°C for one hour. Concluding the solutions were again heated at 180°C in closed vessels for another eight hours to achieve a total digestion and diluted to 25 mL afterwards. For additional details concerning XRF and ICP-MS measuring conditions see Schnetger et al. (2000) and Schnetger (1997). Selenium was determined on acid digestions by graphite atomic absorption spectrometry using a Unicam 939 QZ AA spectrometer and a Zeeman-effect background correction. A Milestone DMA-80 Direct Mercury Analyser was used for the measurement of mercury via cold vapor atomic absorption spectroscopy (CV-AAS).

4.3.1.2.2. *Diatom analysis*

Quantitative slides for diatom assemblage analyses were prepared following the method of Scherer (1994). Samples taken at 8 cm intervals throughout core TC36/GC47 were dried thoroughly in a warm oven at ~30°C; 5–20 mg of bulk sediment were sub-sampled into 30 mL vials; samples were cleaned and disaggregated using 3 mL of hydrogen peroxide (30%), 1 mL dilute hydrochloric acid (5%) and Calgon solution for a minimum of 12 hours in a water bath at ~50°C; settled through a >10 cm water column onto cover slips for at least 4 hours; cover slips were allowed to dry before being mounted onto microscope slides using Norland Optical Adhesive (refractive index = 1.56).

At least 300 diatom specimens were counted at x1000 magnification, using an Olympus BH2 Light Microscope with x10 magnification eye pieces and an Olympus S Plan x100 oil immersion lens. Species identifications were based on descriptions by Tomas (1997) and Scott and Marchant (2005). Relative abundances of the Antarctic

sea-ice diatom *Fragilariopsis curta* and the open ocean diatom *Fragilariopsis kerguelensis* were calculated and used in a ratio to represent a gradient from sea-ice to open ocean environments to infer changes in the dominant oceanic conditions over time.

4.3.1.2.3. Chronology

Chronologies for lake sediment cores were established by AMS radiocarbon (^{14}C) dating of macrofossils, in preferential order: 1) moss layers (consisting primarily of hand-picked fine strands aquatic moss *Drepanocladus longifolius* (Mitt.) Paris, but also occasional layers of *Campylium polygamum* (Schimp.) Lange & C.E.O. Jensen, and some unidentifiable/mixed species moss fragments – considered more likely to have been reworked); 2) terrestrial algae; 3) organic-rich bulk sediments and, near the base of each core: 4) bulk glaciolacustrine or glaciomarine sediments. Bulk glaciolacustrine and marine sediments were only dated when macrofossils were completely absent from a key section of core. Paired macrofossil and bulk samples were measured in the surface sediment of the cores to check for any systematic offsets between the age of the carbon incorporated in different macrofossil and bulk sediment fractions.

Macrofossils were hand-picked from frozen bulk material after overnight defrosting at 5°C ; then immersed in ultra-pure ($18.2\text{ M}\Omega$) water, sealed and placed in an ultrasonic bath for an hour, sieved to remove fine particles, and picked under a binocular microscope and dried/refrozen. Samples were sent frozen or dried to the Scottish Universities Environmental Research Centre (SUERC) and Beta Analytic (Miami, Florida, USA) for accelerator mass spectrometry (AMS) radiocarbon dating. Moss samples analysed by SUERC were soaked overnight in cold 0.5 M HCl , filtered and rinsed free of mineral acid with deionised water. As samples were small, they were placed directly into quartz tubes inserts containing quartz wool and dried by freeze drying. Microbial mat samples were digested in 2 M HCl (80°C for 8 hours),

washed free from mineral acid with distilled water then dried and homogenised. All other SUERC-samples were heated in 2 M HCl (80°C for 8 hours), rinsed in deionised water, until all traces of acid had been removed, and dried in a vacuum oven. The total carbon in a known weight of all pre-treated samples was recovered as CO₂ by heating with CuO in a sealed quartz tube. The CO₂ was converted to graphite by Fe/Zn reduction. Samples dated by Beta Analytic were leached with a 0.5 M to 1.0 M HCl bath to remove carbonates, heated to 70°C for 4 hours. Leaching was repeated until no carbonate remained, followed by rinsing to neutral 20 times with deionised water, then placed in 0.5% to 2% solution of NaOH for 4 hours at 70°C and rinsed to neutral 20 times with deionised water. The process was repeated until no additional reaction (typically indicated by a colour change in the NaOH liquid) was observed. Samples were then leached again in a 0.5 M to 1.0 M HCl bath to remove any CO₂ absorbed from the atmosphere by the NaOH soakings and to ensure initial carbonate removal was complete, and then dried at 70°C in a gravity oven for 8–12 hours.

Marine cores TC046 and GC047 were spliced together using the magnetic susceptibility record. The spliced record comprises the top 0.4 m of TC046 together with the whole of GC047. All depths in the text are provided as composite depths, i.e. for GC047, depths provided are the original core depth plus 0.4 m. The chronology for TC046/GC047 is based on four AMS radiocarbon dates. A minor age reversal occurred between 4.0 and 4.19 m (composite depth; minimum reversal 262 years, maximum 714 years).

For freshwater samples, calibration of terrestrial ¹⁴C ages was carried out in OXCAL v. 4.2 (Bronk Ramsey, 2009) using the SHCal04.14C Southern Hemisphere atmosphere dataset (McCormac et al., 2004; Reimer et al., 2004). Absolute percentage of modern carbon (pMC) data were corrected according to ¹³C/¹²C isotopic ratios from measured pMC, where a “modern” pMC value is defined as 100% (AD 1950), and the ‘present day’ pMC value is defined as 107.5% (AD 2010).

In the marine-influenced sections of the Yanou Lake sediment core, MARINE09 (100%) marine and a mixed MARINE09/SHCal04.14C (50% marine) (Reimer et al., 2009) calibration curves were compared, with an Antarctic marine reservoir effect for this locality of ΔR value of 664 ± 10 years ($1,064 \pm 10$ years minus the global marine reservoir of 400 years) based on the ages of contemporary water samples reported from Maxwell Bay (Watcham et al., 2011), which has a similar coastal setting in the west Antarctic Peninsula region and is also subject to seasonal melt water from tidewater glaciers. Only MARINE09 (100%) results are shown for clarity. Radiocarbon data from the Anvers Shelf record were calibrated using MARINE09 (100%) calibration curve, with a ΔR value of $1,470 \pm 70$ years, which represents the $1,870 \pm 70$ surface age obtained for this core minus the global marine reservoir of 400 years. The core top age of $1,870$ ^{14}C years was subtracted from the remainder of the dates before calibration to account for the total reservoir effect. The resulting age model shows the composite core spans 12,250 to 84 cal yr BP. We consider the use of a larger reservoir effect at this location to be appropriate because it is a deeper and more open water locality than Maxwell Bay.

Radiocarbon age data are reported as conventional radiocarbon years BP (^{14}C yr BP) $\pm 1\sigma$, and as two-sigma (95.4%) calibrated age ranges, mean $\pm 1\sigma$, and median calibrated ages (cal yr BP relative to AD 1950) (Supplementary Table 4.S2). Calibrated ages are rounded to the nearest 5 years where measured radiocarbon age errors were less than ± 50 radiocarbon years and to the nearest 10 years where measured radiocarbon age errors were greater than ± 50 radiocarbon years.

Classical age-depth modelling was undertaken using CLAM v2.1 software (Blaauw, 2010). Interpolated ages in the text were rounded to the nearest 10 years and derived from the 'best-fit' age of the CLAM age-depth model, with interpolated 2- σ (95%) calibrated age ranges shown in brackets, also rounded to the nearest 10 years. Calibrated ^{14}C ages are in, or are very close to, chronological order with respect to sediment depth in both cores, except for the age reversal at 22 cm in the ARD

core which has an anomalous high age of 3,480 cal yr BP, caused by re-working of older organic material from the catchment (Supplementary Fig. 4.S1). This sample was not included in the CLAM age-depth modelling exercise. In the ARD core, linear sedimentation rates (LSR) range between 7 and 86 cm kyr⁻¹. Significantly higher values with up to 260 cm kyr⁻¹ present between 4,070-5,125 cal yr BP (74–281 cm) in laminated sediments (with no evidence for slumping) were either due to higher sediment input into the lake following a volcanic eruption from nearby Deception Island at c. 4.8–5 kyr (Willmott et al., 2006), or ‘flat’ regions of radiocarbon calibration during this time period (Blaauw and Christen, 2011). Away from marine or marine influenced sediments, a large reworked tephra deposit creates a similar same age-depth profile in the YAN core (Supplementary Fig. 4.S2). We did not date samples within the c. 5,000-year tephra deposit in the YAN record. There were no terrestrial macrofossils present because Yanou Lake was at or below sea level at the time of this eruption and these sediments were overwhelmingly composed of volcanic ash and therefore contained insufficient carbon for dating.

4.3.1.3. *Statistical analysis*

At least 7-fold measurements of several carefully selected in-house (PS-S, UT-S, TW-TUC, Loess, BB-TUC, ICBM-B) and international reference standards (AGV-1, GSS-6, GSD-2, BE-N, NIST-1515 Apple Leaves) were conducted in order to warrant the precision and accuracy of the methods. To determine the degree of statistical spread and therefore the precision of a method the relative standard deviation (RSD) was used (Skoog and Leary, 1996). In case of TC, TS, TN, and XRF analyses multiple determinations of reference material were performed to calculate the pooled relative standard deviation (RSD_{pooled}) (Skoog and Leary, 1996). To get an idea of the accuracy of a method the relative error f representing the variation from the certified value is determined (Skoog and Leary, 1996). Precision was better than 1.5% for major elements (Si, Ti, Al, Fe, Mn, Mg, Ca, K, P) and <5% for bulk

parameters (TS, TN, TC, TIC) and minor elements (Ba, Co, Hg, Sr, V, Y, Zr, Zn, REE). Exceptions are given by As, Cu and Ni ($RSD_{\text{pooled}} < 8\%$) In general, accuracy is ranging from -3.1 to 4.5% (major elements and bulk parameter) and -8.2 to 5.1% (minor elements), except for Na_2O (9.2%), MgO (7.7%), Cu (7.8%), and Gd (-10.8%). Where $f > 5\%$ (major elements) and $f > 10\%$ (trace elements) correction factors were calculated based on the reference samples in order to minimise systematic errors. Correlation analysis was undertaken using R 2.15.2 (R Foundation of Statistical Computing). Hierarchical R-mode cluster analyses were conducted with the R package 'Pvclust' version 1.2-2 (Suzuki and Shimodaira, 2006) using average method and a correlation-based dissimilarity matrix. Based on multiscale bootstrap resampling (number of bootstrap: 10,000) approximately unbiased p -values were further calculated to assess the uncertainties in cluster analysis.

4.3.1.4. Calculation of the average fraction of ornithogenic soils in lake sediments

As evidenced by selected element-aluminium crossplots (Supplementary Fig. 4. S6) Ardley Lake sediments clearly represent a mixture between two end members, eroded Ardley Island bedrock on the one hand and ornithogenic soils from the lake's catchment on the other hand, Therefore, the average relative proportion of ornithogenic soils in Ardley Lake sediments ($F_{\text{o.s.}}$) can be estimated by using a mixing equation modified after Shultz and Calder (1976):

$$F_{\text{o.s.}}(\text{rel.}\%) = \frac{\left(\sum_{\text{El}=\text{Cu,Sr,Zn,P}} \frac{\text{El}/\text{Al}_{\text{smp}} - \text{El}/\text{Al}_{\text{bgd}}}{\text{El}/\text{Al}_{\text{o.s.}} - \text{El}/\text{Al}_{\text{bgd}}} \right)}{4} \cdot 100 \quad (4.S1)$$

$\text{El}/\text{Al}_{\text{smp}}$ is the element/aluminium ratio of selected bio-elements (Cu, P, Sr, Zn) in Ardley Lake sediments and $\text{El}/\text{Al}_{\text{bgd}}$ (mean Ardley Island bedrock; Machado et al., 2005) and $\text{El}/\text{Al}_{\text{o.s.}}$ (guano-bearing ornithogenic soils; Tatur et al., 1997) represent the respective ratios in both end members. Aluminium was used for standardisation

because of its low solubility in common soil solutions with normal pH values, thus representing an ideal immobile element for the lithogenic background, which is not affected by biogenic or diagenetic processes (Brumsack, 1989; Calvert and Pedersen, 1993; Young and Nesbitt, 1998). In order to minimise misinterpretation of this proxy, the average fraction of ornithogenic soils in the lake sediments was calculated using a combination of four chemically unrelated El/Al ratios which provides a buffering effect on possible variations in ornithogenic soil and bedrock composition over time. The resultant $F_{o.s.}$ value, for example 20%, means that 20% of the sediment sample is ornithogenic soil and 80% eroded bedrock. However, it should be noted that a fraction of ornithogenic soil in the lake sediments of 20% does not necessarily mean that there were twice as many penguins in the catchment compared to a value of 10%, only that the input of guano-influenced soils during this respective period was doubled.

Theoretically, every $F_{o.s.}$ value $>0\%$ is evidence for guano/ornithogenic soil input above the terrigenous background level. Therefore, the $F_{o.s.}$ value of 10% or more was used to indicate presence of penguins around Ardley Lake. (dotted line in Fig. 4.3d). Given that measurement errors are $<1\%$, this is considered to be a very conservative estimate of penguin guano input and 'penguin occupation' in the lake's catchment area.

4.3.1.5. Satellite analysis of present day vegetation

The distribution of present day vegetation shown in Fig. 4.1 is calculated from Very High Resolution Quickbird2 satellite (image number 1010010004D26100) taken on the 21st of February 2006 with an on-the-ground resolution of 2.4 m per pixel. The results show NDVI (Normalised Difference Vegetation Index) values from the uncorrected imagery where values are above a 0.06 NDVI, a ratio found to be representative of the cut-off between poorly vegetated and bare ground in Antarctic vegetation assemblages (Fretwell et al., 2011). NDVI analysis returns a

ratio indicating the amount of live green vegetation in each pixel of the satellite image based upon the relative amounts of red and infra-red light. The cell structure of chlorophyll containing cells absorbs red light whilst reflecting light in the infra-red part of the spectrum, a number of commonly used remote sensing indices are based upon this relationship; NDVI being the most common of these (Gates, 1980). The ratio gives an indication of verdancy of vegetation in an area, however not all lichens can be identified using this index as some species shield the chlorophyll contained in their algal cells. The results shown here show a number of areas of vegetation on Ardley Island with NDVI values over 0.30 (displayed in red on the map), these are likely to be verdant moss banks or stands of *Deschampsia*. The analysis shown here is part of a larger on-going effort to use remote sensing methods to identify and map vegetation on the Antarctic Peninsula using satellite data.

4.3.2. Supplementary Results and Discussion

4.3.2.1. *Summary core descriptions*

In the Ardley Lake sediment record, seven major lithological units, consisting mainly of alternating olive-grey to black organic mud layers and fine laminated grey to black organic silt, were identified (Supplementary Fig. 4.S1). The base of the core (333-359 cm) is characterised by black coarse sands and light grey clay with medium-coarse sand and gravel clasts. Five main lithological units were identified in the Yanou Lake record. Units 1-2 are glaciomarine and lagoonal sediments, with the gravel-rich diamicton, overlain by fine sediments with shallow marine diatoms, deposited when Yanou Lake was below sea level. The short-lived phase of terrestrial lagoonal sedimentation at the base of Unit 2 and the airfall tephra deposit has been linked to a stalled phase of deglaciation at this location during the Early Holocene. Unit 3 is composed of fine terrestrial sediments and moss layers, with fresh-brackish diatoms. Unit 4 is a c. 130 cm thick deposit composed of airfall and reworked volcanic ash and silty-clay sediment with the occasional sand grain size layer. Unit 5

is composed fine terrestrial sediments, tephra and moss layers, with fresh-brackish diatoms associated with Yanou Lake's proximity to the coast.

4.3.2.2. *C/N and C/P ratios*

Results of bio-element assemblages indicating the presence of guano in Lake Ardley sediments are supported by their C/N and C/P ratios we compared with a range of ornithogenic (bird formed) soils, phytoplankton and local plants (Supplementary Fig. 4.S4). The C/N ratios of catchment mosses, lichens, liverworts and vascular plants, such as *Deschampsia antarctica* (Fig. 4.1) are significantly higher (C/N ratios = 21-114; Lee et al., 2009) than Ardley Lake sediments (C/N = av. 6.6; Supplementary Fig. 4.S4), and nearby ornithogenic soils (av. 6.3; Tatur et al., 1997). Mean Ardley Lake sediment C/P ratios of 3.3 suggest that the biogenic fraction is derived from a mixture of guano (av. = 1.2; Tatur et al., 1997) and ornithogenic soils (av. = 3.7; Tatur et al., 1997).

4.3.2.3. *Bio-element assemblages and their usability as proxy for ornithogenic soil input*

Our penguin proxy is based on previous studies around Antarctica which have shown that ornithogenic (bird formed) soils and lake sediments in areas occupied by penguins have significantly higher concentrations of guano-related elements compared with control sites (Supplementary Table 4.S1). Lake sediments from Hope Bay, Antarctic Peninsula, for instance, were found to be highly enriched in Ca, Cd, Cu, P, Sr, and Zn, which was linked to a fluctuating input of guano into the lake (Zale, 1994). Geochemical studies on soils of active penguin rookeries in the Seabee Hook area of Cape Hallett in northern Victoria Land, East Antarctica revealed a significant enrichment in elements, like As, Ca, Cu, P, S, and Zn (Hofstee et al., 2006). Similarly, in the Vestfold Hills higher concentrations of As, Cd, Cu, F, Mg, Ni, P, Se, Sr, TC TN, TS, Zn are found in ornithogenic soils (Huang et al.,

2009; Huang et al., 2011). At Cape Bird and on Beaufort Island (Ross Sea region) ornithogenic sediments are typically enriched in As, Cu, Cd, Cu, P, TS, and Zn (Liu et al., 2013). Margin sediments from ponds located on Ardley Island influenced by penguin droppings are shown to be characterised by enhanced concentrations of Ba, Ca, Cu, F, P, Se, Sr, TC, S, Zn (Sun et al., 2000; Liu et al., 2005). In another study the flux ratio vs depth profiles of P, Zn, Cu, Se, F, As, Cd, and Ni over Al was used to reconstruct the historical seabird population in the catchment area of Mochou Lake, Larsemann Hills (Liu et al., 2007). There are several reasons why these bio-element assemblages represent ideal proxies for changes in ornithogenic soil input. First, since the relative proportion of penguin influenced soils and lithogenic material in the overland runoff is expected to be stable, changes in bio-element concentrations in the lake sediments are rather an indicator for variations in ornithogenic soil input than to changing erosive rates (Liu et al., 2011b). In addition, the high inter-correlation of chemically different bio-elements ensures that simultaneous changes in their concentrations are directly related to fluctuations in guano input and do not just reflect post-depositional processes or changes in provenance (Zale, 1994). Related to that many of the bio-element assemblages found in this and previous studies are considered to be immobile in (Antarctic) lake sediments (Dearing, 1986; Sun et al., 2000; Huang et al., 2011), which is due to several factors. Phosphates, like struvite ($\text{Mg}(\text{NH}_4)\text{PO}_4 \times 6 \text{H}_2\text{O}$), leukoposphite and in particular hydroxylapatite ($\text{Ca}_5(\text{PO}_4)_3(\text{OH})$) are one of the dominant compounds found in ornithogenic soils at King George Island (Tatur and Barczuk, 1985). The high correlation between Mg and P in ornithogenic soils from Vestfold Hills may indicate the present of struvite (Huang et al., 2011), but in the Ardley Lake sediments Mg is likely derived from the bedrock lithology (Supplementary Fig. 4.S4). The more positive correlation between Ca and P ($r = 0.63$, $p < 0.001$; Supplementary Table 4.S3) suggests that hydroxylapatite is the main phosphate phase in core ARD. During the precipitation of apatites an exchange between Ca^{2+} , PO_4^{3-} , F^- and OH^- on the one side and elements, like Ag, Br, Ba, Cd,

Cu, Cr, I, Na, Mg, Mo, Pb, S, Se, Sr, U, V, Y and Zn on the other side is possible (Jarvis et al., 1994; Sauer et al., 1997; Abratis et al., 2004; Tribovillard et al., 2006), and this is coupled to microbial mediated degradation of solid phases (Jarvis et al., 1994). Consequently, trace elements, which have naturally higher concentrations in penguin guano are enriched in these phosphate phases and immobilised during this substitution process. Heavy metals, like Cu, Hg and Cd are often bio-accumulated in top predators, such as mammals and sea birds due to their high Cu, Cd and Hg dietary intake (Rainbow, 1989; Ancora et al., 2002). Thus, penguin or sea mammal droppings can be a source for these elements. In contrast, the behaviour of Hg in sediments is more complex. In its methylated form, mercury is highly mobile and gradually released from the sediments after deposition (Mercone et al., 1999). However, since Se and Hg showing similar trends in ARD sediments (see Fig. 4.2) the formation of more stable HgSe (tiemannite) and CdSe, which is an end product of biochemical detoxification, is possible (Magos and Webb, 1980).

Geochemical shifts found in the Ardley Lake record are not related to marine or brackish to freshwater transitions since the assemblage of elements found has only previously been found in guano-influenced deposits. Furthermore, no such assemblage exists in the Yanou Lake record, which has a well-defined marine-brackish-freshwater transition (Watcham et al., 2011).

In summary, we concluded that simultaneous changes in bio-element concentrations in our lake sediments directly reflect the amount of ornithogenic soils present in the catchment area and are, therefore, indirectly linked to the number of penguins present in the catchment.

4.3.3. Supplementary Figures

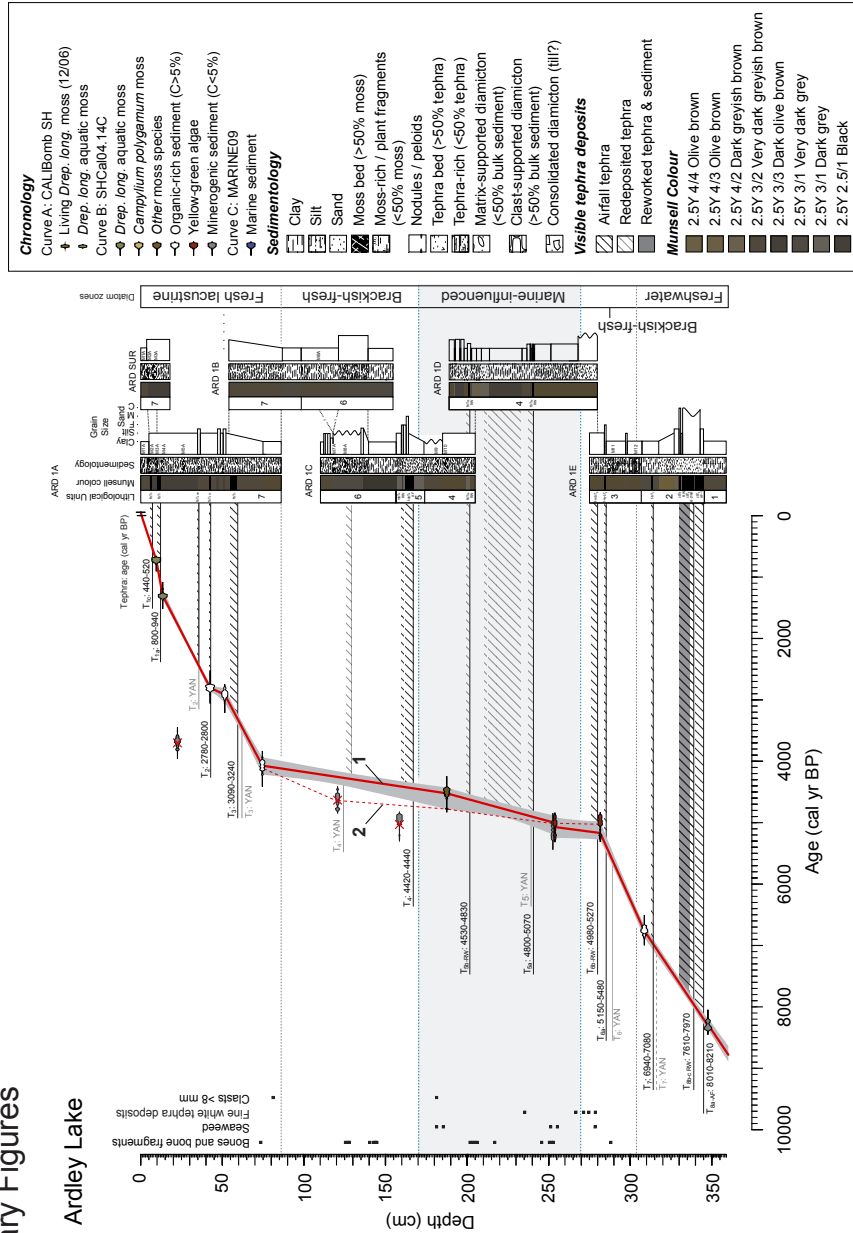


Fig. 4.S1. Classical age model, linear sedimentation rates (LSR) and lithology of the Ardley Lake cores. Composite X-rays for these cores are shown in Watcham et al.(2011). Age depth modelling was undertaken in CLAM v.2.1 (100,000 iterations; interpolated curves and material dated as in key and S-Table 4.S2). The Ardley Lake is curve based on 5,833 models without reversals. There is no significant statistical difference overall between age-depth profiles for the ARD core produced using classical (CLAM; Blaauw, 2010) and Bayesian (BACON; Blaauw et al., 2011) age-depth modelling techniques ($r^2=0.988$) (see Table 4.S2). Grey area represents the 95% confidence interval; red crosses indicate outliers, which were not taken into consideration for age model 1. Of two possible models for core ARD, model 1 was considered the most likely, a conclusion reinforced by Bayesian age-depth modelling analysis. Tephra deposits are shown by a diagonal line shading and parts of the core containing >50% reworked tephra deposits are shaded in dark grey, together with a comparison between the ARD and YAN ages for the main tephra deposits (Fig. 4.S2).

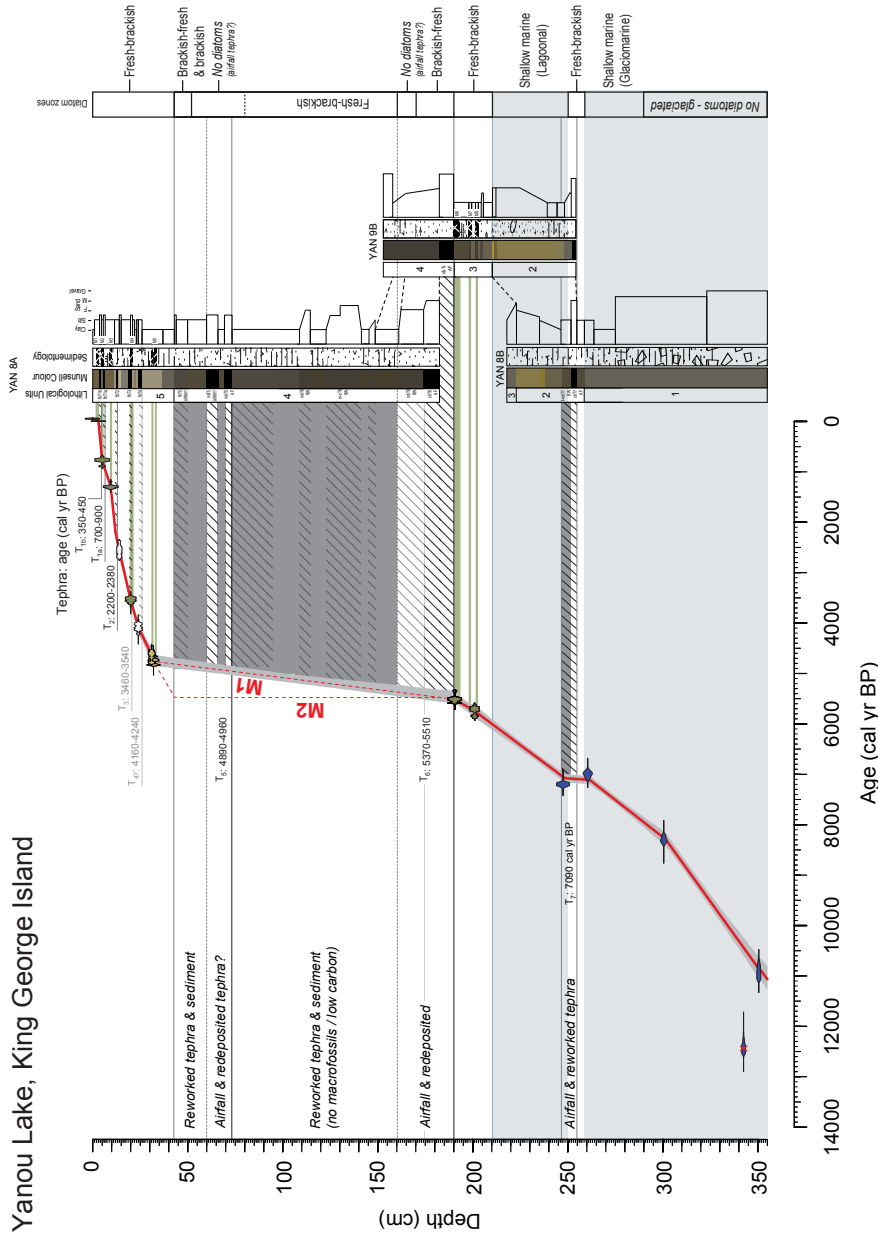


Fig. 4.S2. Classical age model, linear sedimentation rates (LSR) and lithology of the Yanou Lake cores. Composite X-rays for these cores are shown in Watcham et al. (2011). Age depth modelling was undertaken in CLAM v. 2.1 (100,000 iterations; interpolated curves and material dated as in key and S-Table 4.S2). The Yanou Lake curve is based on 559 models without age reversals and two possible models for the core section composed of >50% airfall and reworked tephra. Grey area represents the 95% confidence interval; red crosses indicate outliers, which were not taken into consideration for age model 1. Of the two possible models shown, model 1 is considered the most likely. Tephra deposits are shown by a diagonal line shading and main moss layers by green shading; parts of the core containing >50% reworked tephra deposits are shaded in dark grey.

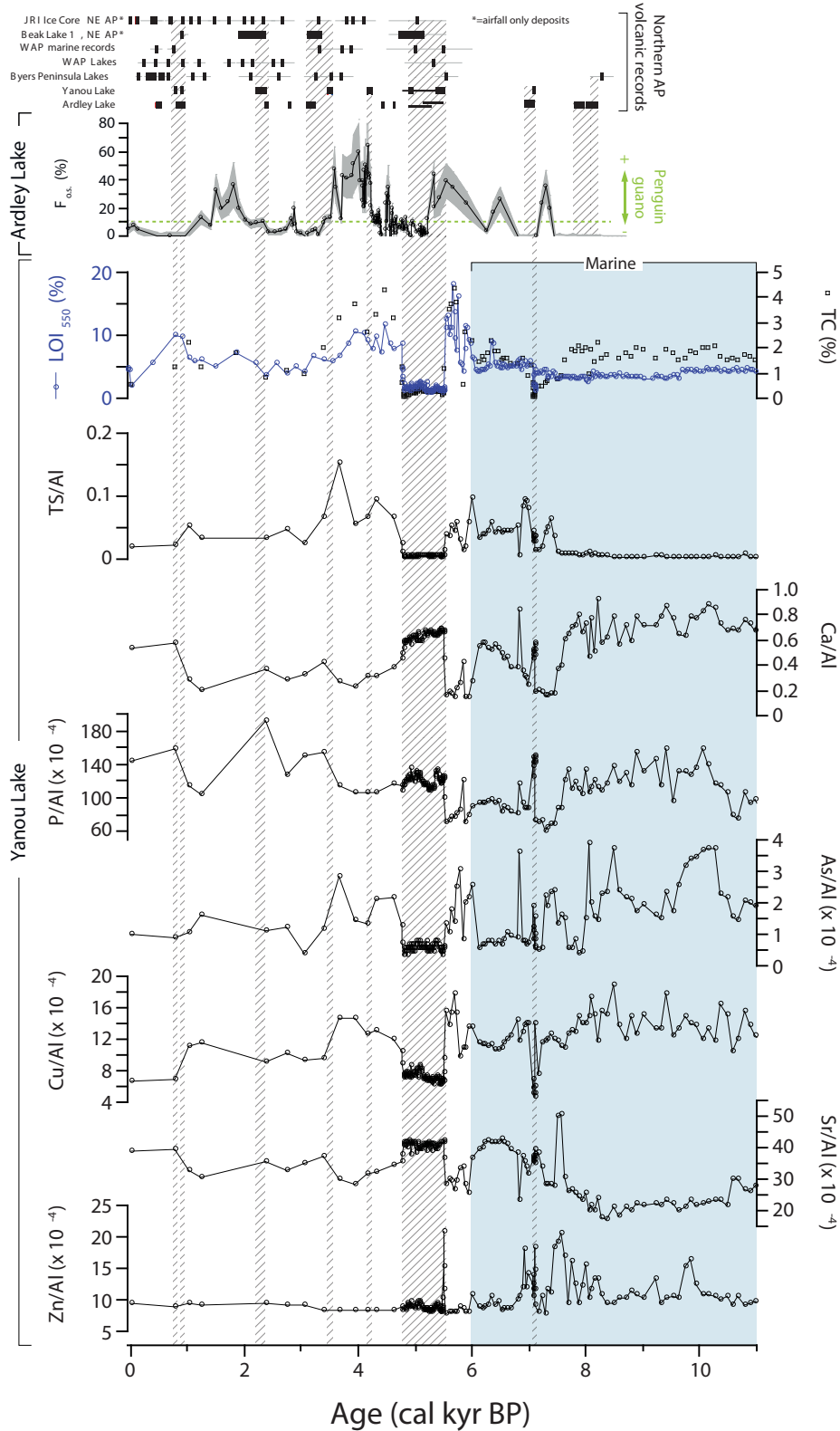
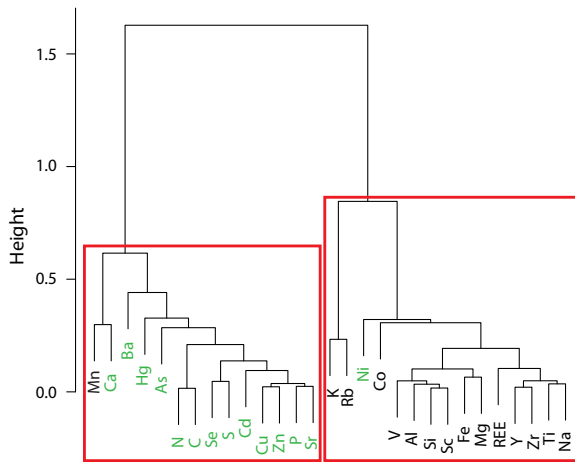


Fig. 4.S3. Whole core geochemistry of core YAN from Yanou Lake. Developing regional tephrochronology for the Antarctic Peninsula region, ARD core $F_{o.s.}$ profile from Ardley Lake (Fig. 4.3) compared to TOC, LOI_{550} and guano-associated bioelement/aluminium ratios vs age (cal yr BP) in core YAN. Volcanic ash data is from Roberts et al. (2011), Björck et al. (1991d), and Toro et al. (2013).

a. Ardley Lake (ARD)



b. Yanou Lake (YAN)

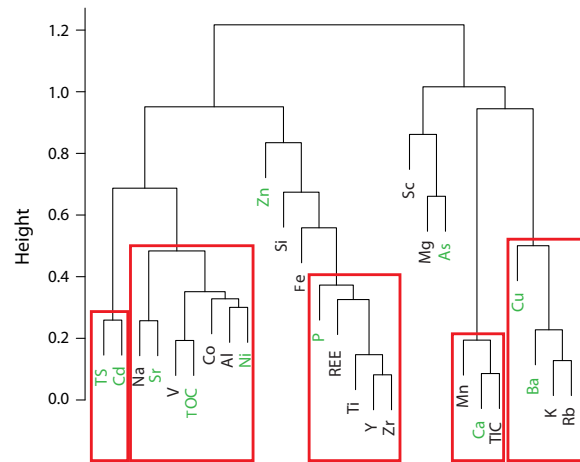
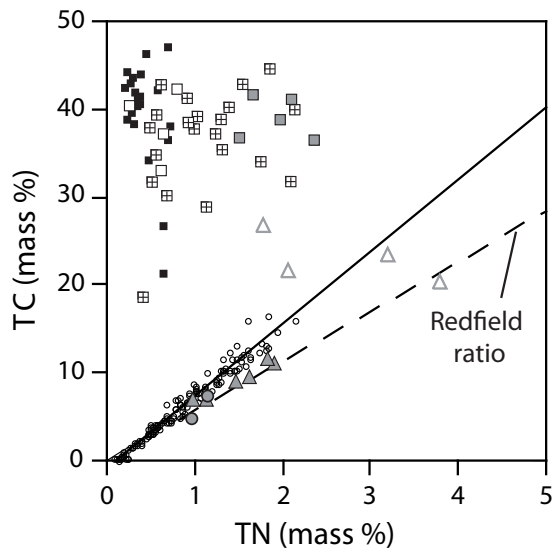
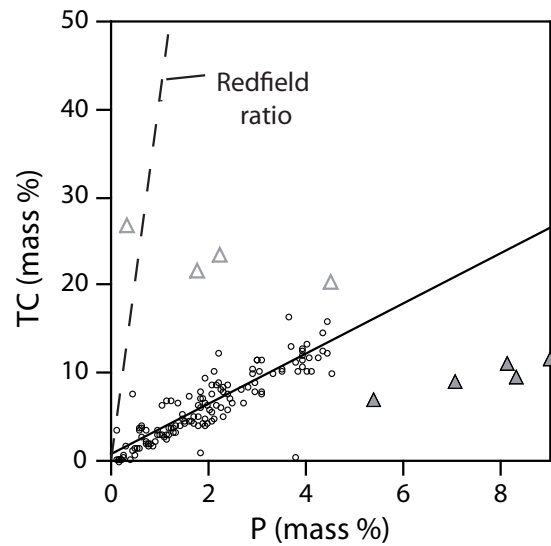


Fig. 4.S4. R-mode cluster analysis of cores ARD and YAN. Results of R-mode cluster analysis for measured major and trace elements of a) core ARD and b) core YAN. Red values at the edge of each cluster represent AU (approximately unbiased) p -values (%) for the null hypothesis H_0 'the cluster does not exist'. Clusters with AU p -values larger than 99% are highlighted by red rectangles. Major and trace elements known to be enriched in guano and ornithogenic soils are marked in green.

a



b



○ ARD samples □ liverworts ■ vascular plants ■ moss ■ lichens △ ornithogenic soils (guano) △ ornithogenic soils (humus) ● ornithogenic soils (phosphatic clay)

Fig. 4.S5. Comparison of C/N and C/P ratios. a) C/N and b) C/P ratios b) of Ardley Lake sediments (open circles), local lichens (e.g. *usnea antarctica*), liverworts (*cephalozia varians*), mosses, vascular plants (*Deschampsia antarctica*) (Lee et al., 2009) and different types of ornithogenic soils (Tatur et al., 1997). The solid and the dashed line represent the linear correlation curve of the samples from core ARD and the general C/N and C/P ratios of phytoplankton according to the Redfield ratio, respectively.

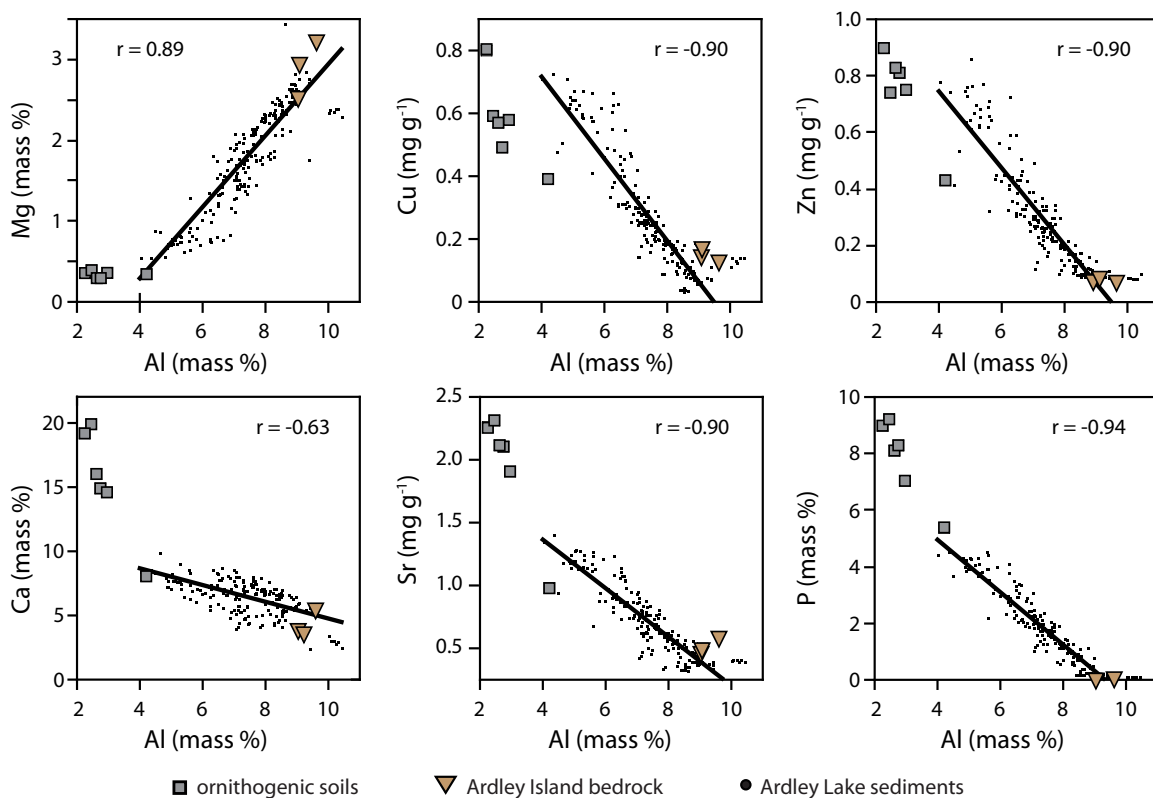


Fig. 4.S6. Element crossplots. Biplots of selected element/aluminium ratios of Ardley Lake sediments (this study), ornithogenic soils (Tatur et al., 1997) and local bedrock (Machado et al., 2005).

4.3.4. Supplementary Tables

Table. 4.S1. Bioelements present in guano around Antarctica. Comparison of bio-elements found in ornithogenic sediments and penguin guano around Antarctica. *n.d.*: not determined. Data is from Zale (1994)^a, Hofstee et al. (2006)^b, Huang et al. (2011)^c, Huang et al. (2009)^d, Liu et al. (2013)^e, Sun et al. (2000)^f, Liu et al. (2005)^g and Liu et al. (2007)^h.

Location	Sample type	Cu	P	S	As	Se	Zn	Cd	F	Sr	Ca	Mg	Ni	Ba
Lake Boeckella, Hope Bay ^a	ornithogenic sediments	x	x			<i>n.d.</i>	x	x	<i>n.d.</i>	x	x			
Seabee Hook, Cape Hallett, northern Victoria Land ^b	penguin guano	x	x	x	x		x	x			x	x		<i>n.d.</i>
Zolotov Island, Vestfold Hills ^c	ornithogenic sediments	x	x	x	<i>n.d.</i>	<i>n.d.</i>		x		<i>n.d.</i>		x		<i>n.d.</i>
Gardner Island, Vestfold Hills ^d	ornithogenic sediments	x	x	x	x	x		<i>n.d.</i>	x	x				
Beaufort Island & Cape Bird, Ross Sea region ^e	ornithogenic sediments	x	x	x	x	x	x	x	<i>n.d.</i>					
Lake Y2, Ardley Island, South Shetland Islands ^f	ornithogenic sediments	x	x	x		x	x	<i>n.d.</i>	x	x	x			x
Lake Y4, Ardley Island, South Shetland Islands ^g	ornithogenic sediments	x	x	x		x	x	<i>n.d.</i>	x	x	x			
Mochou Lake, Larsemann Hills, East Antarctica ^h	ornithogenic sediments	x	x		x	x	x	x	x				x	
Lake Ardley, Ardley Island, South Shetland Islands (this study)	ornithogenic sediments	x	x	x	x	x	x	x	<i>n.d.</i>	x	x			

Table 4.S2. Radiocarbon age data for sediment cores. Radiocarbon ages for a) the Ardley Lake sediment core, b) the Yanou Lake sediment core and c) marine cores from the Anvers Trough referred to in this paper, showing conventional radiocarbon ages, marine reservoir corrected ages and 2- σ calibrated age data. Pre-treatment: AAA = acid-alkali-acid; AW = acid washes; * = estimated isotopic values due to small samples size; Calibration curves: A=SH1Bomb; B= SHCal04.14C; C=MARINE09 with $\Delta R=664\pm 10$ ^{14}C yr (100% marine); D=MARINE09 with $\Delta R=1,470 \pm 10$ ^{14}C yr (100% marine); rw = reworked.

Laboratory & Sample codes	Core section: Core depth (cm)	Stratigraphic depth (cm)	Material dated & carbon source	Pre-treatment	Carbon content (%)	$\delta^{13}\text{C}_{\text{org}}$ (‰ ± 0.1)	Measured [Absolute] pMC (% modern ± 1 σ)	Conventional Radiocarbon Age (years BP ± 1 σ)	OxCal 95.4% calibration data (cal yr BP)		Reject (x) & Reason
									Max. - Min.	Mean ± 1 σ Median Curve	
SUERC-22305	ARD-SUR: 0-1	0 - 1	Living Drepanocladus longifolius (Mitt.) Paris aquatic moss	AAA	13.2	-23.8	104.23 ± 0.48	modern	-6	-7 -6 ± 1 -6	A
BETA-338226	ARD-SUR: 9-10	9 - 10	Drepanocladus longifolius (Mitt.) Paris aquatic moss layer	AAA	-	-25.6	89.85 ± 0.34	860 ± 30	790	675 725 ± 30 725	B
BETA-338227	ARD1A:13-14	13 - 14	Drepanocladus longifolius (Mitt.) Paris aquatic moss strands	AAA	-	-25.0*	83.59 ± 0.42	1440 ± 40	1380	1185 1305 ± 35 1305	B
BETA-271284	ARD1A:22-23	22 - 23	Organic-rich sediment (moss free)	AW	10.4*	-25.7	64.84 ± 0.32	3480 ± 40	3830	3570 3685 ± 70 3680	B
BETA-271285	ARD1A:42-43	42 - 43	Organic-rich sediment (moss free)	AW	8.2*	-23.6	71.01 ± 0.35	2750 ± 40	2880	2740 2805 ± 40 2800	B
BETA-271287	ARD1A:51-52	51 - 52	Organic-rich sediment (moss free)	AW	-	-24.0	70.04 ± 0.35	2860 ± 40	3060	2780 2910 ± 60 2905	B
BETA-271286	ARD1A:74-75	74 - 75	Organic-rich sediment (moss free)	AW	-	-25.8	62.47 ± 0.31	3780 ± 40	4235	3925 4070 ± 70 4070	B
SUERC-22315	ARD1B:42-43	119.8 - 121.4	Mineral-rich sediment (no macrofossils)	AW	4.4	-26.4	59.61 ± 0.26	4155 ± 36	4825	4445 4635 ± 100 4620	B
SUERC-18922	ARD1C:48-49	158 - 159	Mineral-rich sediment (no macrofossils)	AW	0.6	-25.9	57.59 ± 0.27	4433 ± 37	5215	4845 4980 ± 80 4940	B
SUERC-22307	ARD1C:77-78	187 - 188	Moss strands	AW	30.8	-23.9	60.09 ± 0.27	4091 ± 36	4790	4415 4520 ± 85 4505	B
SUERC-22316	ARD1D:63-64	252 - 253	Mineral-rich sediment (no macrofossils)	AW	9.0	-9.2	56.99 ± 0.26	4517 ± 37	5300	4890 5120 ± 110 5125	B
SUERC-22308	ARD1D:63.5-64.5	253.5 - 254.5	Yellow-green algae	AW	47.2	-22.3	57.23 ± 0.27	4484 ± 38	5280	4885 5055 ± 120 5025	B
SUERC-22309	ARD1D:92-93	281 - 282	Yellow-green algae	AW	48.5	-20.5	57.33 ± 0.27	4469 ± 38	5280	4860 5020 ± 115 4995	B
SUERC-18948	ARD1E:33-34	308 - 309	Organic-rich sediment (no macrofossils)	AW	13.3	-25.5	47.44 ± 0.21	5990 ± 35	6885	6665 6760 ± 55 6760	B
SUERC-22317	ARD1E:72-73	347 - 348	Mineral-rich sediment (no macrofossils)	AW	4.1	-18.2	39.06 ± 0.19	7552 ± 39	8390	8195 8305 ± 55 8320	B

a)

Table 4.S2 (continued). Radiocarbon age data for sediment cores. Radiocarbon ages for a) the Ardley Lake sediment core, b) the Yanou Lake sediment core and c) marine cores from the Anvers Trough referred to in this paper. showing conventional radiocarbon ages, marine reservoir corrected ages and 2-σ calibrated age data. Pre-treatment: AAA = acid-alkali-acid; AW = acid washes; * = estimated isotopic values due to small samples size; Calibration curves: A=SH1Bomb; B= SHCal04.14C; C=MARINE09 with ΔR=664±10 ¹⁴C yr (100% marine); D=MARINE09 with ΔR=1,470 ± 10 ¹⁴C yr (100% marine); rw = reworked.

Laboratory & Sample codes	Core section: Core depth (cm)	Stratigraphic depth (cm)	Material dated & carbon source	Pre-treatment	Carbon content (%)	δ ¹³ C _{org} (‰ ± 0.1)	Measured (Absolute) pMC (% modern ± 1σ)	Conventional Radiocarbon Age (years BP ± 1σ)	OXCAL 95.4% calibration data (cal yr BP)		Reject (x) & Reason		
									Max. - Min.	Median Curve			
b)													
SUERC-22325	YANSC:1.5-3	1.5 - 3	Drepanodactylus longifoliusaquatic moss	AAA	1.7	-16.7	104.53 ± 0.46	modern	-6	-7 ± 1	-6	A	
							[103.79 ± 0.46]			[1956.3-1957.8 AD or >2004 AD]			
SUERC-18934	YAN8A-1.5-5.5	5 - 5.5	Drepanodactylus longifoliusaquatic moss	AW	10	-25.0*	89.32 ± 0.41	907 ± 37	905	680 ± 50	770	B	
BETA-316286	YAN8A-1.9.5-10	9.5 - 10	Drepanodactylus longifoliusaquatic moss	AAA	-	-25.3	83.69 ± 0.31	1430 ± 30	1350	1185 ± 25	1295	B	
BETA-271289	YAN8A-1.14-15	14 - 15	Bulk organic sediment (lake)	AW	-	-15	72.89 ± 0.36	2540 ± 40	2725	2360 ± 95	2570	B	
BETA-316287	YAN8A-1.20-20.5	20 - 20.5	Drepanodactylus longifoliusaquatic moss	AAA	-	-29	65.74 ± 0.25	3370 ± 30	3640	3455 ± 50	3535	B	
BETA-271290	YAN8A-1.24-25	24 - 25	Bulk organic sediment (lake)	AW	-	-16.6	62.39 ± 0.31	3790 ± 40	4240	3930 ± 75	4085	B	
BETA-316288	YAN8A-1.31-31.5	31 - 31.5	Campyllum polygamum moss layer	AAA	-	-23.2	59.50 ± 0.22	4170 ± 30	4825	4520 ± 90	4640	B	
SUERC-18935	YAN8A-1.32-32.5	32 - 32.5	Campyllum polygamum moss layer	AW	20	-25.0*	58.75 ± 0.27	4273 ± 37	4860	4585 ± 70	4740	B	
SUERC-22310	YAN8B-1.37.5-38	190.5 - 191	Campyllum polygamum? moss layer	AAA	39.5	31.9	54.69 ± 0.25	4847 ± 37	5605	5330 ± 60	5515	B	
SUERC-22311	YAN9B-1.48-49	201 - 202	Campyllum polygamum? moss strands	AAA	13.6	-26.5	53.33 ± 0.25	5051 ± 38	5895	5610 ± 75	5725	B	
SUERC-22326	YAN8B-1.29-30	247 - 248	Bulk organic sediment (marine-influenced)	AW	1.7	-20.7	40.17 ± 0.19	7326 ± 37	7290	7100 ± 45	7200	C	
SUERC-22327	YAN8B-1.42-43	260 - 261	Bulk organic sediment (marine)	AW	0.3	-27.1	41.04 ± 0.19	7155 ± 38	7135	6885 ± 65	6985	C	
BETA-271291	YAN8B-1.82-83	300 - 301	Bulk organic sediment (marine)	AW	-	-25.9	34.71 ± 0.30	8500 ± 70	8440	8150 ± 75	8300	C	
BETA-271292	YAN8B-2.24-25	342 - 343	Mineral-rich sediment (marine)	AW	-	-24.2	23.69 ± 0.21	11570 ± 70	12605	12120 ± 115	12425	C x-rw	
BETA-271293	YAN8B-2.32-33	350 - 351	Mineral-rich sediment (marine)	AW	-	-25.3	26.63 ± 0.23	10630 ± 70	11130	10675 ± 10915	125 10925	C	
c)													
OxA-3249_0	TC04601:0	0 - 1	Bulk sediment (marine)	AW	-	-24.8	-	1870 ± 70	250	-	110 ± 80	90	D
OxA-3250_281	GC04702:241-242	281 - 282	Bulk sediment (marine)	AW	-	-34.9	-	7780 ± 90	7070	-	6480 ± 140	6780	D
SUERC-16254_400	GC04703:360-361	400 - 401	Bulk sediment (marine)	AW	0.76	-22.8	20.04 ± 0.19	12768 ± 76	13070	-	12580 ± 120	12780	D x-rw
OxA-3251_419	GC04704:379-380	419 - 420	Bulk sediment (marine)	AW	-	-22.8	-	12280 ± 150	12860	-	11440 ± 270	12220	D

Table 4.S3. Correlation matrix of core ARD. Correlation coefficients between the elements in Lake Ardley sediments. Bold values mark correlation coefficients $r > 0.9$ and $r < -0.9$; ** Correlation is significant at the 0.01 level (2-tailed); * Correlation is significant at the 0.05 level (2-tailed).

	Si	Ti	Al	Fe	Mn	Mg	Ca	Na	K	P	As	Ba	Cd	Co	Cu	Hg	Ni	Sc	Se	Sr	V	Y	Zn	Zr	ΣREE	TC	TS	TN
Si	1	0.87**	0.95**	0.84**	-0.44**	0.87**	-0.64**	0.88**	0.49**	-0.96**	-0.73**	-0.43**	-0.91**	0.69**	-0.95**	-0.78**	0.62**	0.98**	-0.98**	-0.95**	0.93**	0.82**	-0.94**	0.81**	0.83**	-0.94**	-0.85**	-0.95**
Ti		1	0.78**	0.86**	-0.16*	0.87**	-0.35**	0.96**	0.27**	-0.87**	-0.63**	-0.72**	-0.86**	0.63**	-0.92**	-0.77**	0.65**	0.73**	-0.84**	-0.84**	0.85**	0.96**	-0.86**	0.96**	0.91**	-0.92**	-0.75**	-0.85**
Al			1	0.86**	-0.39**	0.89**	-0.62**	0.82**	0.49**	-0.94**	-0.70**	-0.35**	-0.84**	0.75**	-0.90**	-0.79**	0.67**	0.98**	-0.94**	-0.90**	0.95**	0.73**	-0.90**	0.72**	0.79**	-0.94**	-0.85**	-0.93**
Fe				1	-0.05	0.93**	-0.41**	0.87**	0.39**	-0.90**	-0.51**	-0.55**	-0.84**	0.70**	-0.87**	-0.80**	0.70**	0.93**	-0.89**	-0.84**	0.92**	0.82**	-0.85**	0.85**	0.68**	-0.85**	-0.69**	-0.84**
Mn					1	-0.09	0.70**	-0.11	-0.15*	0.33**	0.53**	-0.12	0.23	-0.12	0.29**	0.41**	0.03	-0.39	0.28	0.37**	-0.27**	-0.07	0.31**	-0.05	-0.39	0.30**	0.36**	0.34**
Mg						1	-0.33**	0.88**	0.34**	-0.91**	-0.62**	-0.63**	-0.89**	0.73**	-0.91**	-0.79**	0.84**	0.95**	-0.92**	-0.85**	0.92**	0.81**	-0.88**	0.84**	0.79**	-0.90**	-0.83**	-0.89**
Ca							1	-0.33**	0.63**	0.50**	-0.10	0.45	-0.37**	0.55**	0.48**	0.03	-0.73**	0.70**	0.70**	-0.57**	-0.37**	0.59**	-0.28**	-0.62**	0.47**	0.41**	0.47**	0.41**
Na								1	0.40**	-0.88**	-0.62**	-0.64**	-0.85**	0.64**	-0.89**	-0.79**	0.69**	0.87**	-0.88**	-0.84**	0.86**	0.93**	-0.85**	0.95**	0.89**	-0.92**	-0.79**	-0.86**
K									1	-0.40**	-0.17*	0.28**	-0.42	0.31**	-0.32**	-0.18	0.30**	0.67**	-0.57**	-0.40**	0.43**	0.30**	-0.36**	0.31**	0.43	-0.41**	-0.47**	-0.43**
P										1	0.67**	0.51**	0.90**	-0.66**	0.97**	0.80**	-0.64**	-0.97**	0.95**	0.98**	-0.95**	-0.82**	0.97**	-0.82**	-0.81**	0.89**	0.81**	0.91**
As											1	0.43**	0.83**	-0.49**	0.68**	0.51**	-0.46**	-0.92**	0.95**	0.64**	-0.62**	-0.57**	0.63**	-0.54**	-0.84**	0.74**	0.72**	0.63**
Ba												1	0.38	-0.30**	0.61**	0.64**	-0.59**	-0.14	0.40	0.46**	-0.43**	-0.67**	0.53**	-0.71**	-0.32	0.57**	0.53**	0.42**
Cd													1	-0.75**	0.94**	0.48**	-0.66**	-0.89**	0.91**	0.91**	-0.91**	-0.77**	0.91**	-0.81**	-0.76**	0.50**	0.77	0.68**
Co														1	-0.63**	-0.42**	0.63**	0.82**	-0.80**	-0.61**	0.72**	0.60**	-0.56**	0.60**	0.73**	-0.73**	-0.51**	-0.71**
Cu															1	0.79**	-0.64**	-0.91**	0.96**	0.95**	-0.93**	-0.86**	0.98**	-0.87**	-0.78**	0.87**	0.82**	0.90**
Hg																1	-0.63**	-0.67	0.74	0.72**	-0.75**	-0.71**	0.75**	-0.76**	-0.28	0.72**	0.74**	0.73**
Ni																	1	0.76**	-0.70**	-0.56**	0.65**	0.61**	-0.61**	0.66**	0.67**	-0.76**	-0.62**	-0.69**
Sc																		1	-0.96**	-0.96**	0.98**	0.73**	-0.92**	0.66*	0.82**	-0.71*	-0.98**	-0.78**
Se																			1	0.97**	-0.94**	-0.82**	0.94**	-0.75**	-0.80**	0.66*	0.95**	0.74**
Sr																				1	-0.92**	-0.81**	0.96**	-0.79**	-0.89**	0.85**	0.78**	0.89**
V																					1	0.79**	-0.93**	0.79**	0.77**	-0.92**	-0.79**	-0.93**
Y																						1	-0.81**	0.98**	0.92**	-0.87**	-0.73**	-0.80**
Zn																							1	-0.81**	-0.76**	0.83**	0.79**	0.87**
Zr																								1	0.86**	-0.90**	-0.73**	-0.81**
ΣREE																								1	-0.74**	-0.99**	-0.65**	
TC																									1	0.91**	0.98**	
TS																										1	0.87**	
TN																											1	0.87**

Table 4.S4. Correlation matrix of core YAN. Correlation coefficients between the elements in Lake Yanou sediments. Bold values mark correlation coefficients $r > 0.9$ and $r < -0.9$; **, ** Correlation is significant at the 0.01 level (2-tailed); * Correlation is significant at the 0.05 level (2-tailed).

	Si	Ti	Al	Fe	Mn	Mg	Ca	Na	K	P	As	Ba	Cd	Co	Cu	Ni	Sc	Sr	V	Y	Zn	Zr	ΣREE	TC	TS	
Si	1																									
Ti	0.65**	1																								
Al	-0.62**	0.50**	1																							
Fe	-0.12	-0.75**	0.48**	1																						
Mn	0.34**	0.48**	0.66**	0.94**	1																					
Mg	0.53**	0.59**	0.94**	0.94**	0.94**	1																				
Ca	0.94**	0.80**	0.94**	0.94**	0.94**	0.94**	1																			
Na	0.80**	0.41**	0.83**	0.90**	0.90**	0.90**	0.80**	1																		
K	-0.80**	0.41**	0.83**	0.90**	0.90**	0.90**	0.80**	0.80**	1																	
P	-0.30**	-0.19	0.77**	0.33	0.41**	0.41**	0.41**	0.41**	0.43**	1																
As	0.77**	0.33	0.41**	0.33	0.16	0.79**	0.79**	0.79**	0.49**	0.43**	1															
Ba	0.41	0.41	0.12	0.93**	0.60**	-0.22	-0.87**	0.87**	-0.63**	-0.22	0.87**	1														
Cd	-0.28	0.54	-0.24	-0.07	-0.55	0.09	0.15	-0.31	-0.52	0.34	0.96**	0.93**	1													
Co	0.04	0.34**	-0.04	0.23	0.03	0.13	-0.14	-0.03	-0.88**	-0.29	0.92**	0.83**	0.07	1												
Cu	0.04	0.34**	-0.04	0.23	0.03	0.13	-0.14	-0.03	-0.88**	-0.29	0.92**	0.83**	0.07	-0.88**	1											
Ni	0.47**	-0.66**	0.44**	-0.08	0.58**	0.07	-0.55**	-0.60**	0.47**	-0.66**	0.44**	-0.08	0.58**	0.07	-0.55**	1										
Sc	0.36**	-0.08	0.36	0.33	0.37	0.74	-0.50	-0.16	0.36**	-0.08	0.36	0.33	0.37	0.74	-0.50	-0.16	1									
Sr	0.84**	0.32	-0.88**	-0.80**	0.84**	0.32	-0.88**	-0.80**	0.84**	0.32	-0.88**	-0.80**	0.84**	0.32	-0.88**	-0.80**	0.84**	1								
V	0.81**	0.87	-0.76**	-0.20	0.71**	0.68**	0.71**	0.68**	0.81**	0.87	-0.76**	-0.20	0.71**	0.68**	0.71**	0.68**	0.81**	0.87	1							
Y	0.81**	0.87	-0.76**	-0.20	0.71**	0.68**	0.71**	0.68**	0.81**	0.87	-0.76**	-0.20	0.71**	0.68**	0.71**	0.68**	0.81**	0.87	0.81**	1						
Zn	0.01	0.02	0.06	-0.25	0.01	0.06	-0.25	0.01	0.06	-0.25	0.01	0.06	-0.25	0.01	0.06	-0.25	0.01	0.06	0.01	0.02	1					
Zr	0.41	0.41	0.41	0.41	0.41	0.41	0.41	0.41	0.41	0.41	0.41	0.41	0.41	0.41	0.41	0.41	0.41	0.41	0.41	0.41	0.41	1				
ΣREE	0.41	0.41	0.41	0.41	0.41	0.41	0.41	0.41	0.41	0.41	0.41	0.41	0.41	0.41	0.41	0.41	0.41	0.41	0.41	0.41	0.41	0.41	1			
TC	0.18	0.18	0.18	0.18	0.18	0.18	0.18	0.18	0.18	0.18	0.18	0.18	0.18	0.18	0.18	0.18	0.18	0.18	0.18	0.18	0.18	0.18	0.18	1		
TS	0.50**	-0.50**	0.50**	-0.50**	0.50**	-0.50**	0.50**	-0.50**	0.50**	-0.50**	0.50**	-0.50**	0.50**	-0.50**	0.50**	-0.50**	0.50**	-0.50**	0.50**	-0.50**	0.50**	-0.50**	0.50**	-0.50**	0.50**	1

4.4. Acknowledgements

We are grateful to the British Antarctic Survey (BAS) Field Operations staff and HMS Endurance for their logistic support and the generous hospitality at Chinese Great Wall Station during the field campaign. We thank H. Biester and T. Riedel from Braunschweig University, Germany, for their help with Hg analyses, technical assistants at the Institute for Chemistry and Biology of the Marine Environment (ICBM) and at BAS, and S. Xu at the SUERC AMS Radiocarbon Dating Facility. This study forms part of the ESF-funded IMCOAST project, specifically AP-6 led by SJR, and was funded by a NERC core programme grant to DH and the German Research Foundation (DFG project no. BR 775/25-1).

5. Redox conditions and trace metal cycling in coastal sediments from the maritime Antarctic

Patrick Monien^{a*}, Donata Monien^a, Sanja Asendorf^a, Karsten Lettmann^a,
Heng Chai Lim^a, Bernhard Schnetger^a, Hans-Jürgen Brumsack^a

^aInstitute for Chemistry and Biology of the Marine Environment (ICBM), Carl-von-Ossietzky
Straße 9-11, 26129 Oldenburg, Germany.

This chapter has been submitted to *Geochimica Cosmochimica Acta*.

5.1. Abstract

Redox-sensitive trace metals (Mn, Fe, U, Mo, Re), nutrients and terminal metabolic products (NO_3^- , NH_4^+ , PO_4^{3-} , total alkalinity) were for the first time investigated in pore waters of Antarctic coastal sediments. The results of this study reveal a high spatial variability in redox conditions in surface sediments from Potter Cove, King George Island, western Antarctic Peninsula. Particularly in the shallower areas of the bay the significant correlation between sulphate depletion and total alkalinity, the inorganic product of terminal metabolism, indicates sulphate reduction to be the major pathway of organic matter mineralisation. In contrast, dissimilatory metal oxide reduction seems to be prevailing in the newly ice-free areas and the deeper troughs, where concentrations of dissolved iron of up to 700 μM were found. We suggest that the increased accumulation of fine-grained material with high amounts of reducible metal oxides in combination with the reduced availability of metabolisable organic matter and enhanced physical and biological disturbance by bottom water currents, ice scouring and burrowing organisms favours metal oxide reduction over sulphate reduction in these areas. Based on modelled iron reduction rates we calculate an Antarctic shelf derived input of potentially bioavailable iron to the Southern Ocean

of 1.2–18 mg m² yr⁻¹. This contribution is in the same order of magnitude as the flux provided by icebergs and significantly higher than the input by aeolian dust. For this reason suboxic shelf sediments form a key source of iron for the high nutrient-low chlorophyll (HNLC) areas of the Southern Ocean. In view of rising temperatures at the WAP accompanied by enhanced glacier retreat and the accumulation of melt water derived iron-rich material on the shelf this source may become even more important in the future.

5.2. Introduction

The microbially mediated mineralisation of organic material forms a major process controlling the redox conditions and therefore the cycling of trace metals and nutrients in marine sediments (e.g., Elderfield et al., 1985; Shaw et al., 1990). Since the oxidation of carbon is coupled to the reactivity and availability of electron acceptors, like O₂, nitrate, Mn(IV), Fe(III) or sulphate, their occurrence or absence in pore waters provides valuable information on redox conditions in the sediment (e.g., Beck et al., 2008b; Canfield and Thamdrup, 2009). Redox-sensitive trace metals (Fe, Mn, V, Mo, U, Re) and nutrients (NO₃⁻, NO₂⁻, NH₄⁺, PO₄³⁻) have therefore been successfully used to decipher the redox state and biogeochemical processes in a wide range of coastal marine and deep-sea sediments of the North Atlantic, the North Pacific, the North Sea and off Peru (Froelich et al., 1979; Shaw et al., 1990; Canfield et al., 1993; Morford et al., 2005; Beck et al., 2008a; Beck et al., 2008b; Scholz et al., 2011; Morford et al., 2012). Several studies have shown that in the neritic zone, where the aerobic layer is often only a few millimetres thick, sulphate reduction is considered to be the dominant pathway of anaerobic organic matter degradation, which accounts for up to 92% of carbon oxidation (Jørgensen, 1982; Thamdrup and Canfield, 1996; Kostka et al., 1999). In contrast, the importance of other electron acceptors, like nitrate, manganese or iron is often neglected although in areas with Mn and Fe-rich surface sediments metal oxide reduction may play a

major role as well (Canfield et al., 1993; Thamdrup and Canfield, 1996; Rysgaard et al., 1998; Vandieken et al., 2006).

To date there are only a few studies dealing with geochemical processes and organic matter degradation in coastal marine sediments in the sub-Antarctic or Antarctic. Hartnett et al. (2008), for example, calculated benthic oxygen fluxes and denitrification rates from pore water profiles collected close to Anvers Island at the western Antarctic Peninsula. They could show that O_2 consumption rates on the Antarctic continental margin are comparable to rates found in other typical continental margin sediments. The influence of bioturbation on nutrient (NH_4^+ , NO_3^-) exchange rates between the sediment-water interface were analysed in sediments from Factory Cove, Signey Island, South Orkney Islands by Nedwell and Walker (1995). Further studies dealt with sulphate reduction rates in Subantarctic sediments off Signey Island (Nedwell, 1989) and in Ellis Fjord, Vestfold Hills, East Antarctica (Franzmann et al., 1988). However, investigations about early diagenetic processes and the behaviour of redox-sensitive trace elements in Antarctic pore waters are rare and restricted to deep sea regions of the Southern Ocean (e.g., King et al., 2000). This gap is astonishing as the Southern Ocean is known to be a high nutrient-low chlorophyll (HNLC) region where primary production is limited by the availability of bioavailable iron (e.g., Martin et al., 1990; Boyd et al., 2007). Consequently, the recycling of trace metals in Antarctic shelf sediments and their subsequent release into the water column could possibly represent an important source of bioavailable iron to the Southern Ocean, as it has been proposed by several authors (Lancelot et al., 2009; Tagliabue et al., 2010; Shaw et al., 2011; de Jong et al., 2012).

In this study we for the first time report data on redox-sensitive trace metals (Mn, Fe, Mo, U, Re), nutrients (NO_3^- , PO_4^{3-}), sulphate and terminal metabolic products (NH_4^+ , H_2S , total alkalinity) determined in pore waters from Potter Cove, King George Island, maritime Antarctica. In combination with solid-phase data (bulk parameters, like TOC and TS) we intend to shed light on controlling factors of early diagenetic

processes and redox conditions at different locations in this model area. Moreover, using a modelling approach the potential of Antarctic shelf sediments as a significant source of bioavailable iron for the Southern Ocean will be discussed.

5.3. Trace element geochemistry

5.3.1. Iron

In oxic environments iron is naturally occurring as solid Fe(II) and Fe(III) bearing silicates and (hydr)oxides (Poulton and Raiswell, 2005; Schroth et al., 2009). During early diagenetic processes in the sediment microbially mediated reduction and dissolution of reactive Fe (oxyhydr)oxides can occur leading to an enrichment of dissolved Fe(II) in the pore water (e.g., Canfield et al., 1993). Whereas in the presence of H₂S Fe (hydr)oxides (e.g., ferrihydrite or lepidocrocite) rapidly react to insoluble Fe(II) phases, like FeS and finally pyrite (FeS₂), residual Fe silicates require more than 10⁵ years for a significant sulphidisation due to their slower reaction kinetics (Canfield, 1989; Canfield et al., 1992; Raiswell and Canfield, 1996).

5.3.2. Manganese

While stable in its oxidised and solid form in oxic seawater, Mn(IV) oxides are reduced to dissolved Mn(II) (and Mn(III)) in suboxic sediments (Stumm and Morgan, 1981; Trouwborst et al., 2006; Madison et al., 2013). With increasing alkalinity production in deeper, anoxic sediment layers Mn(II) is fixed again to the sediments by precipitation of mixed Ca–Mn carbonates (Middleburg et al., 1987; Jakobsen and Postma, 1989; Mucci, 2004). Mn (hydr)oxides are associated with Fe and some trace elements (e.g., As, Co, Mo, Ni, V) which are either incorporated or adsorbed on their surface and whose cycling is directly linked to dissolution and precipitation processes of the respective (hydr)oxide (e.g., Shaw et al., 1990; Burdige, 1993).

5.3.3. Rhenium

Rhenium is characterised by its conservative behaviour in marine waters, presumably present as an oxyanion (Re(VII)O_4^-) at 39.8 ± 0.2 pM (corrected to 35‰ salinity, Anbar et al., 1992; Colodner et al., 1995). In suboxic pore water ReO_4^- is probably reduced to Re(IV) and adsorbed or precipitated into sediments where conducive conditions for organic matter oxidation by Fe(III) and sulphate reduction are persisting (Colodner et al., 1993; Morford et al., 2012).

5.3.4. Molybdenum

Being conservative in oxic marine environments, molybdenum is present as dissolved molybdate (Mo(IV)O_4^{2-}) showing concentrations of around 110 nM at a salinity of 35‰ (Morris, 1975; Algeo and Tribovillard, 2009). In reducing sediments when hydrogen sulphide concentrations in the pore water exceed 50-250 μM (Helz et al., 1996; Zheng et al., 2000) MoO_4^{2-} is subsequently transformed into dissolved thiomolybdates ($\text{MoO}_x\text{S}_{4-x}^{2-}$, $x = 0$ to 3) and finally scavenged as particle-reactive tetrathiomolybdate (MoS_4^{2-}) by iron sulphides and/or humic materials (Bertine and Turekian, 1973; Erickson and Helz, 2000; Tribovillard et al., 2004; Vorlicek et al., 2004). Furthermore, an association between pore water Mo and the formation or reductive dissolution of iron and manganese oxihydroxides was found (Crusius et al., 1996; Helz et al., 1996).

5.3.5. Uranium

Uranium shows a conservative behaviour in oxygenated seawater where it is present as soluble U(VI) carbonate complex ($\text{UO}_2(\text{CO}_3)_3^{4-}$) at approximately 13 nM (Ku et al., 1977; Langmuir, 1978). According to Klinkhammer & Palmer (1991) 75% of the removal of dissolved U from the ocean is related to the diffusion of U into suboxic sediments. Below the iron reduction zone and mediated by bacterial Fe and sulphate reduction it is reduced to U(IV) or U(III) and finally deposited as stable

UO₂ (Lovley et al., 1991; Sani et al., 2004). Several studies moreover underline the evident association between U and Fe oxides, which seem to co-cycle in suboxic sediments (Barnes and Cochran, 1990; Church et al., 1996; Duff et al., 2002; Morford et al., 2007).

5.4. Regional Setting

Potter Cove is a 4 km long and 2.5 km wide tributary inlet at the southwestern end of King George Island (KGI, 62°23'S, 58°27'W), the largest of the South Shetland Islands. A shallow (<30 m) transversal sill separates the inner (~3.0 km²) from the outer cove (~3.5 km²), which is characterised by a broad intertidal area with water depths between 100 and 200 m in the southeast and extensive underwater macroalgal forests on hard bottom at its coasts (Klöser et al., 1994; Iken et al., 1998). In the inner cove, in contrast, where water depths do not exceed 50 m, soft substrate is dominant. While Fourcade Glacier has covered half of the inner cove in the 1950s, its tidewater front has been retreating more than 1 km to the east and is grounding on the shore since c. 2008 (Rückamp et al., 2011). Nowadays, high glacial cliffs grounded on bedrock surround the cove in the northern and eastern sector, whereas a broad sandy beach delimits the bay in the south. Between July/August and October Potter Cove is completely covered by ice, which starts to break up end of October/early November (Yoon et al., 2004). During the rest of the year the cove is ice-free and the hydrology of Potter Cove is dominated by saline and cold subsurface waters (34.0–34.5 psu, <0°C) from the adjacent Maxwell Bay, which enters the cove in the northwestern part in a generally wind-driven cyclonic circulation pattern (Roese and Drabble, 1998). It is overlain by a surface layer of less saline and warmer water (<34 psu, 0–1°C) influenced by seasonally and interannually varying freshwater discharge from the melting Fourcade glacier and surface runoff (Khim and Yoon, 2003). Three main streams with different regimes (snowy-lacustrine in the southwest and snowy-glacial in the south-east) carrying sediment-laden melt

water meander through the southern shore. By these streams about 0.14 kg m^{-3} of fine-grained suspended particulate material ($0.0042\text{--}0.532 \text{ kg s}^{-1}$) is transported into coastal waters during the melting period (Schloss et al., 2002).

5.5. Material and Methods

5.5.1. Sampling

During austral summers 2009/2010 and 2010/2011 103 surface sediment samples were taken in Potter Cove, King George Island on a regular grid at c. 200 m distance intervals using a Van Veen grabber (Fig. 5.1, Table 5.1). Moreover, 46 sediment cores, characterised by an overlying water column showing no evidence for resuspended sediment and a clearly defined sediment-water interface were retrieved at different locations. Sampling was done using a modified sediment corer (UWITEC, Austria)

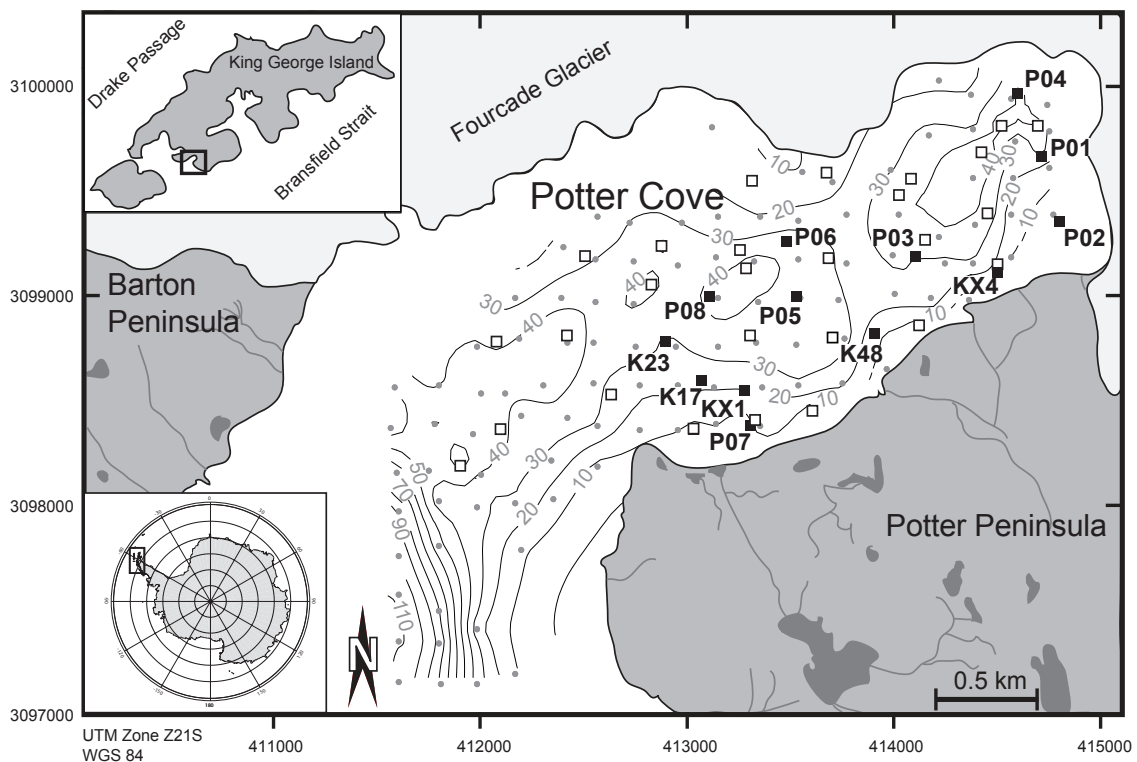


Fig. 5.1. Map of the study site with sampling locations. Sediment cores (squares) and surface samples (grey dots) were taken during austral summers 2009/2010 and 2010/2011. Black squares mark sediment cores where pore water data are available.

Table 5.1. Overview of pore water core locations, including sampling date, UTM coordinates (Zone Z21E; WGS84), water depth, coring gear and core length (recovery in brackets). GC: gravity corer, PC: push corer.

Core name	Sampling Date	Grid	Easting	Northing	Water Depth (m)	Gear	Core length (cm)
PC/P01	28.12.2011	21E	414712	3099674	~30	GC	29.0
PC/P02	17.01.2011	21E	414796	3099363	9.7	GC	45.0 (44.0)
PC/P03	04.02.2011	21E	414146	3099280	32	GC	45.0 (44.0)
PC/P04	04.02.2011	21E	414593	3099976	43	GC	43.0
PC/P05	08.01.2011	21E	413518	3099007	36	GC	30.0 (28.0)
PC/P06	20.01.2011	21E	413473	3099270	37	GC	27.0
PC/P07	20.01.2011	21E	413256	3098391	4.7	GC	26.0
PC/P08	01.02.2011	21E	413100	3099000	42	GC	37.0
PC/K17	11.02.2010	21E	413075	3098606	23	GC	27.0 (25.0)
PC/K23	28.01.2010	21E	412888	3098794	29	GC	29.0
PC/K48	01.03.2010	21E	413906	3098827	12	PC	17.5 (16.0)
PC/KX1	03.02.2010	21E	413304	3098560	21	PC	18.5 (18.0)
PC/KX4	18.02.2010	21E	414493	3099121	10	PC	27.0 (24.0)

with an additional weight of 12 kg (GC) and push corers (PC) operated by the Argentine Diving Division, with a diameter of 5.7 and 5.4 cm, respectively (Fig. 5.1, Table 5.1). Directly after core recovery sediment cores were transported to the field lab avoiding any kind of vibration. 13 of these cores were immediately sampled for pore waters in 1- (0–5 cm), 2- (7–27 cm) and 5-cm resolution (≥ 30 cm). Therefore ultrapure water-washed rhizons (0.15 μm mean pore size, Rhizosphere Research Products, The Netherlands) were inserted simultaneously into the core liner through pre-drilled holes that were covered by transparent adhesive tape and pore waters were collected in 12 mL syringes. One aliquot of each pore water sample was filled in 5 mL polypropylene (PP) tubes (conditioned with 2% HNO_3 conc. (subboiled)), acidified with nitric acid ($\geq 69\%$, TraceSelect[®], Sigma Aldrich, Germany) to pH < 2 , stored at 4°C and transported to the home lab for further analyses. A second aliquot was directly measured for nutrients and total alkalinity (TA) at Carlini station within one hour after core sampling. For selected cores (P02–P08) a third aliquot of 1.5 mL was directly given in a 2 mL PP tube (Eppendorf, Germany) already filled with 0.6 mL

of a 50 mM Zn acetate solution for H₂S analysis. Sediments of parallel cores were sampled at 1-cm resolution, filled in pre-weighed polyethylene (PE) bags, weighed, lyophilised and weighed again to calculate the water content of each sample. Where no parallel cores could be recovered (K17, K23, K48, KX1, KX4, P03) sediment samples were taken directly after the cores have been sampled for pore water following the procedures described above. Original depths of sediment samples were then estimated by using a correction factor (core length before pore water sampling divided by the core length after pore water sampling) to account for the loss in core length during pore water sampling.

5.5.2. Pore water analyses

Nutrients (NO₂⁻, NO_x⁻, NH₄⁺) and TA were measured on pore water samples directly on-site with a Multiscan GO microplate spectrophotometer (Thermo Fisher Scientific, Finland) following the procedures after Miranda et al. (2001), Benesch and Mangelsdorf (1972) and Sarazin et al. (1999) with slight modifications. Whereas ammonia analyses were done on HgCl₂ poisoned samples (Kattner, 1999) two weeks after pore water sampling, all other parameters were determined within 1 h of sampling on non-poisoned sample aliquots. Nitrate (NO₃⁻) was calculated from the difference between NO_x⁻ and NO₂⁻. H₂S was analysed following the method described by Cline (1969), which was adapted to microtiter plate wells. Major and trace elements (Na, Fe, Mn, SO₄²⁻ (as total sulphur), PO₄³⁻ (as total phosphorus)) were determined after a 2-fold dilution by inductively coupled plasma optical emission spectroscopy (iCAP 6000, Thermo Scientific, Germany) using a spiked seawater standard for calibration and several internal standards for matrix correction (see Beck et al., 2008b for further information). Further, trace element analyses (Fe, Mn, Mo, Re, U) of 20-fold diluted sample aliquots were performed using an Element 2 inductively coupled plasma mass spectrometer (Thermo Scientific, Germany) following the procedure of Rodushkin (1998).

5.5.3. Sediment analyses

Total sulphur (TS) and total carbon (TC) on sediment core samples were analysed on fine-ground samples (<0.125 mm in agate ball mills) by means of a CS analyser (ELTRA CS 500, Germany) equipped with a solid-state infrared detector. The content of total inorganic carbon (TIC) was determined coulometrically using a CM 5012 CO₂ coulometer coupled to a CM 5130 acidification module (UIC, Joliet, USA) whereas total organic carbon (TOC) was then calculated as the difference between TC and TIC (Babu et al., 1999). Based on the pore water salinity a correction for sea salt was carried out for all element concentrations. Where no pore water data were available sulphate concentrations were estimated using conventional seawater composition and a salinity of 34 psu.

5.5.4. Calculation of sulphate depletion

The depletion in sulphate ($SO_4^{2-}_{dep}$) representing the net amount of sulphate consumption via microbial SO_4^{2-} reduction was determined for each sediment depth using the following formula modified after (Weston et al., 2006):

$$SO_4^{2-}_{dep} = \left(\frac{Na^+_{PW}}{MR_{SW}} \right) - SO_4^{2-}_{PW} \quad (5.1)$$

where Na^+_{PW} and $SO_4^{2-}_{PW}$ are the measured molar concentration of sodium and sulphate in the pore water and MR_{SW} is the molar ratio of Na^+ and SO_4^{2-} which is assumed to be constant in oxic surface seawater ($MR = 16.6$). Since the ratio of Na^+_{PW} to MR_{SW} represents the 'expected' SO_4^{2-} concentration in the pore water with a given salinity, the difference between this concentration and $SO_4^{2-}_{PW}$ is consequently an estimate for the metabolic amount of sulphate reduction which is concomitantly corrected for slight changes in salinity due to fresh water input (e.g., atmospheric-, melt-, and ground water).

5.5.5. Estimation of sulphate and iron reduction rates

Sulphate (SRR) and iron reduction rates (FeRR) of selected cores were estimated using the REC (Rate Estimation from Concentrations) model after Lettmann et al. (2012). This numerical procedure is based on the 1-D steady state diagenetic transport reaction equation for dissolved compounds, which is inverted by Tikhonov regularisation, a common and robust technique for solving ill-conditioned inverse problems (Lettmann et al., 2012). In addition to the determined sulphate and iron concentrations in the pore water, a few other parameters were needed for reduction rate calculation. The effective diffusion coefficients in the pore water volume of the sediment (D_{Sed}) were calculated after Boudreau (1997) following equation 5.2:

where D represents the respective molecular diffusion coefficient of sulphate

$$D_{Sed} = \frac{D}{\theta^2} \quad (5.2)$$

(0.04662 m² s⁻¹; Boudreau, 1997) and iron (0.03162 m² s⁻¹; Boudreau, 1997) in the seawater at 0°C, 34 psu and 3 atm and θ is the tortuosity. According to Boudreau (1997) the tortuosity can be estimated from the porosity ϕ by:

where ϕ of each sediment layer was calculated using the following equation:

$$\theta = \sqrt{1 - \ln(\phi^2)} \quad (5.3)$$

where V is the volume (in cm³), m_w is the wet weight (in g) and m_d is the dry weight (in g) of each sample and ρ_{sw} is the density of seawater (in g cm⁻³).

$$\phi = \frac{(m_w - m_d)}{(V \cdot \rho_{sw})} \quad (5.4)$$

Moreover, bioturbation was considered in this model by using the bioturbation coefficient D_b , which was calculated after Tromp et al. (1995):

$$\log_{10}(D_b) = 1.63 + 0.85 \cdot \log_{10}\omega \quad (5.5)$$

assuming an average regional sedimentation rate of $\omega = 0.3 \text{ cm yr}^{-1}$ (Monien et al., 2011; Majewski et al., 2012).

5.5.6. Statistics

For validation of the methods carefully selected international and in-house (in italic) reference materials were measured for sediment (*Loess, Peru-1, UT-S*) and pore water analyses (NASS-5, CASS-5 (both NRC, Canada), spiked Atlantic Seawater (Osil, UK), single-element standard solutions (Alfa Aesar, U.S.)). The pooled relative standard deviation (RSD_{pooled}) after Skoog and Leary (1996) was used to determine the degree of statistical spread and therefore the precision of a method. To get an idea of the accuracy of a method the relative error f representing the variation from the certified value is determined (Skoog and Leary, 1996). The results of the statistical evaluation are given in Table 5.2. The precision of sediment analyses (TS, TC, TIC) was $\leq 5\%$ and accuracy ranged from -0.6 to 2.5% (TOC: -1.2%). In case of pore water analyses precision was better than 5% except for Re (7.5%) and very

Table 5.2. Precision and accuracy of pore water (Fe, Mn, Mo, Na, Re, U, PO_4^{3-} , NO_x^- , NO_2^- , NH_4^+ , SO_4^{2-}) and solid phase (TS, TC, TIC) analyses of Potter Cove sediments. Precision is given as relative standard deviation (RSD%). In case of TOC and NO_3^- accuracy and precision represent the relative maximum errors.

	Precision (%)	Accuracy (%)
NO_x^-	5.0	2.0
NO_2^-	4.2	-2.6
NO_3^-	6.0	2.5
NH_4^+	2.9	1.3
TA	2.8	0.03
Na	1.4	5.7
PO_4^{3-}	1.0	0.2
SO_4^{2-}	1.4	-5.3
Mn	4.1	-2.0
Fe	3.0	-2.0
Mo	1.7	0.1
Re	7.5	-11.2
U	2.1	-1.7
TS	5.0	2.5
TC	1.2	-0.6
TIC	1.0	0.5
TOC	2.4	-0.8

low (<0.03 μM) Mn (17%) and Fe (36%) concentrations. Generally accuracy ranged between -5.3% and 5.7% with only Re showing a higher relative error (11%). Where $|f| > 5\%$ (major elements) and $|f| > 10\%$ (trace elements) correction factors were calculated based on one of the reference samples using other reference samples for validation in order to minimise systematic errors.

5.6. Results and Discussion

5.6.1. Pore water profiles and redox zonation of Potter Cove surface sediments

Nutrients (NO_3^- , NH_4^+ , PO_4^{3-}), sulphate, total alkalinity and redox-sensitive trace elements (Mn, Fe, U, Mo, Re) were studied in pore waters to evaluate the redox conditions and the major pathways of organic matter degradation in superficial coastal sediments from Potter Cove, maritime Antarctica. The pore water geochemistry of selected cores will be discussed on a site-to-site basis in order to get a general picture of redox conditions in three different zones in the studied bay. Locations include: a) the newly ice-free area close to the tidewater front at the northeast of Potter Cove (P04), b) the deeper (>40 m water depth) troughs in the central part of the bay (P05, P08) and c) a shallower zone influenced by melt water discharge at the southern coast (K48, P07). We explicitly abstain from the use of major and trace element data of the solid phase to get information about early diagenetic processes as resulting enrichments or depletions in the sediments would be completely masked due to the high sedimentation rate in this region (>1 cm yr^{-1} ; Milliken et al., 2009; Monien et al., 2011).

5.6.1.1. Inner cove close to the tidewater glacier front

At site P04, which is located close to the glacier front in the northeastern section of Potter Cove pore water profiles of redox-sensitive nutrients and trace metals indicate the typical sequence of redox reactions in hemipelagic sediments as proposed by Froelich et al. (1979) and Canfield & Thamdrup (2009).

As shown in figure 5.2 nitrate concentrations moderately decrease from bottom water concentrations (c. 25 μM) to near zero within the first 10 centimetres indicating subsequent denitrification under reducing conditions. Concurrently, Mn concentrations are steadily increasing in this core to 177 μM at 30 cmbsf and slightly decrease to 136 μM at the core bottom (Fig. 5.2). A similar trend is shown by Fe, where pore water concentrations start to rise at 2 cmbsf slightly below the onset of manganese reduction. Fe concentrations reach their maximum of 361 μM at 21 cmbsf before they show a gradual decrease to <10 μM at 35 cmbsf.

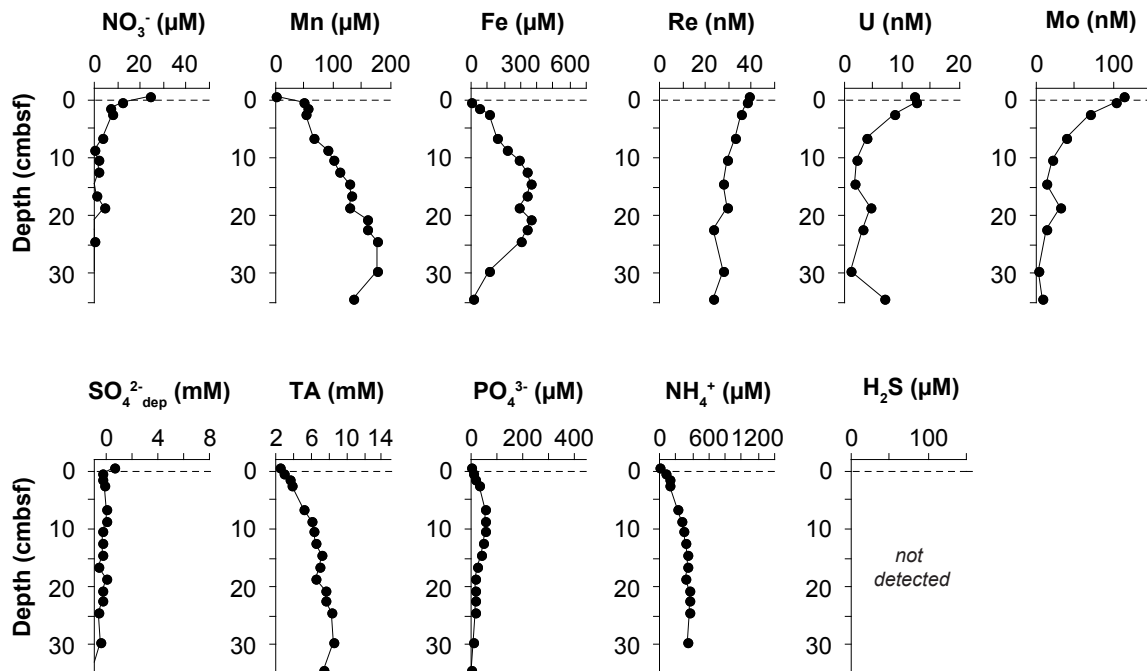


Fig. 5.2. Pore water profiles of nutrients (NO_3^- , NH_4^+ , PO_4^{3-}), redox-sensitive trace metals (Fe, Mn, Mo, U, Re), sulphate depletion (SO_4^{2-} dep), H_2S , and total alkalinity (TA) from core P04 close to the tidewater glacier front.

Generally, the broad ferruginous and manganous zones present in core P04 with high concentrations of dissolved Fe (>300 μM until 25 cmbsf) and Mn point to a rather 'suboxic' character of these sediments. This is in line with measured concentrations of terminal metabolic products of organic matter degradation, such as total alkalinity (TA), ammonia and phosphate. A steady but rather slow increase in alkalinity with

depth (8.9 mM at 30 cmbsf) and relatively low phosphate (<60 μM) and ammonia concentrations (<370 μM) in P04 pore waters only suggest a moderate microbial activity and recycling of nutrients in these sediments under suboxic conditions (Fig. 5.2). Although no evidence for a significant depletion in sulphate was found (Fig. 5.2), it is likely that the removal of dissolved Fe from the pore water at the base of core P04 gives first evidence for the abiotic reduction of iron oxides by sulphide (Canfield and Thamdrup, 2009), although no smell of H_2S could be detected.

The behaviour of other redox-sensitive transition metals even suggests an earlier onset of sulphate reduction in core P04. Uranium, for instance, shows an exponential decrease from bottom water concentration (c. 12 nM) at the core top to near zero values at 15 cmbsf. The slight increases in U visible at 17 cmbsf and at the core bottom are possibly attributed to advection of small amounts of bottom water by bioirrigation or physical reworking by iceberg scouring. This would also explain enhanced concentration of other redox-sensitive elements and nutrients (Mo, Re, NO_3^-) in the same depth intervals (Fig. 5.2). Lovley et al. (1991) reported that microbial reduction of U(IV) is associated with Fe(III)-reducing microorganisms, which would support our finding that subsequent removal of U from pore water and Fe reduction would occur at similar depths in core P04. However, this is not true for Mo, which widely follows the profile of dissolved U in this core showing minimum pore water concentrations (<4 nM) at 30 cm depth (Fig. 5.2). It is generally accepted that Mo removal from pore water and authigenic Mo enrichment in sediments can only be explained by the presence of free H_2S (Helz et al., 1996; Zheng et al., 2000; Morford et al., 2005; Morford et al., 2007). This, in turn, would suggest an onset of sulphate reduction already in the upper 10 cm of the core, which is not supported by the SO_4^{2-} profile (Fig. 5.2). A similar finding was made by King et al. (2000) who observed a significant depletion in pore water Mo in sediments of the Atlantic sector of the Southern Ocean without any evidence of sulphidic conditions. Since we can exclude both, a sampling artifact and an intrusion of oxygen-rich bottom water that

would have led to higher Mo concentrations in the pore water in both cases, there are only two possibilities. On the one hand, nanomolar levels of sulphide produced in locally defined zones of sulphate reduction are possibly responsible for quantitative removal of Mo from the pore water. Considering that less than 450 nM of sulphide would be sufficient to transform 110 nM of Mo to particle reactive tetrathiomolybdate (MoS_4^{2-}) we would not necessarily see a significant decline in sulphate due to its high abundance in seawater (c. $27\text{--}28 \times 10^6$ nM). However, this assumption would neglect co-reactions of sulphides with, for instance, Fe, which may occur more rapidly. Furthermore, Helz et al. (1996) proposed a sulphide-controlled geochemical 'switch point' of 10 μM H_2S at which dissolved molybdate (MoO_4^{2-}) is abruptly transferred to MoS_4^{2-} . In contrast, according to Zheng et al. (2000) already at a threshold of 10 nM H_2S the removal of Mo via coprecipitation of Fe-Mo-S phases is possible. On the other hand, another non-sulphidic removal process for Mo in the pore water has to be taken into account as well. Whereas high concentrations in dissolved Mn would contradict a scavenging of Mo by Mn oxides as described by Shaw et al. (1990) a removal by residual organic particles may also be possible. Dellwig et al. (2007), for example, could show that a decline of Mo in coastal waters of the Wadden Sea (NW Germany) may be explained by the fixation of Mo in oxygen-depleted zones of organic aggregates formed by bacterially derived transparent exopolymer particles (TEP). However, in the context of this study a final explanation for the unusual behaviour of Mo in core P04 could not be found.

5.6.1.2. *The central inner cove*

Pore waters of sediments taken in the deeper (36–42 m water depth) central part of the inner cove (cores P05, P08) are characterised by a more condensed redox zonation compared to the stations close to the glacier front (Fig. 5.3). At both locations, nitrate is consumed within the first two cmbsf, even though slightly elevated concentrations are seen in core P05 between 9 and 17 cmbsf ($<8 \mu\text{M}$). Similar to

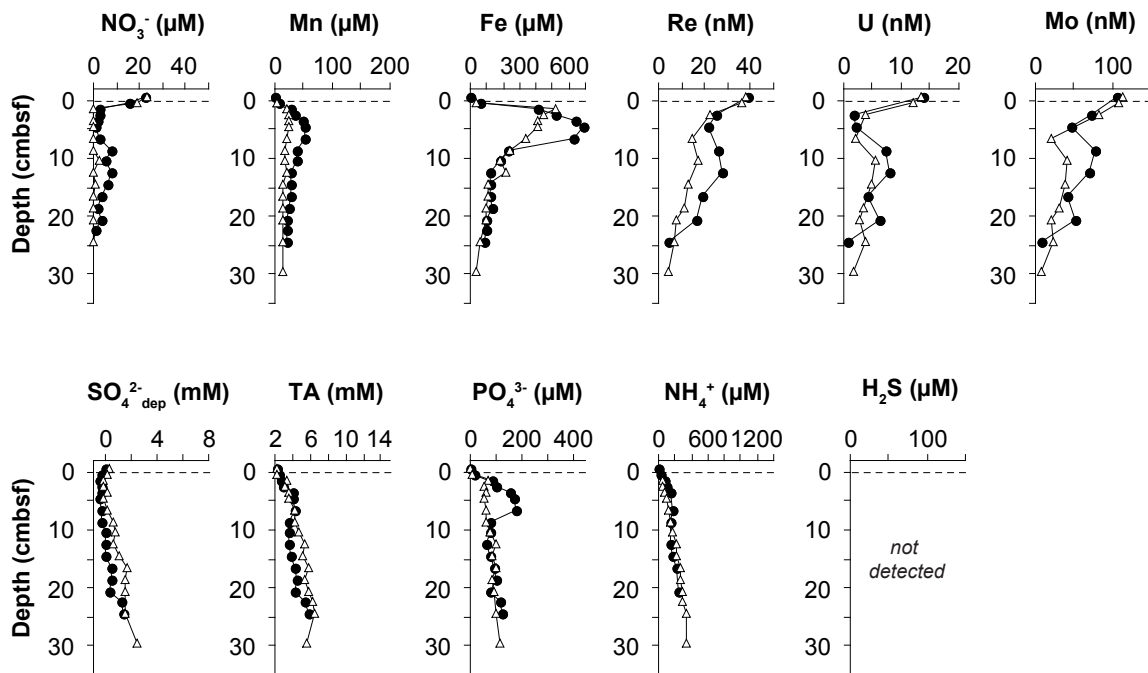


Fig. 5.3. Pore water profiles of nutrients (NO_3^- , NH_4^+ , PO_4^{3-}), redox-sensitive trace metals (Fe, Mn, Mo, U, Re), sulphate depletion (SO_4^{2-} dep), H_2S , and total alkalinity (TA) from cores P05 (black dot) and P08 (white triangle) obtained from the central Potter Cove.

core P04 advection of bottom water seems to be the most probable explanation for this considering the concurrent rise in concentrations of elements, like Mo, Re, and U in the same depth interval of this core. Particularly dissolved Fe reveals a relatively sharply bounded zone of enrichment in these pore waters peaking at c. 2–5 cmbsf before concentrations rapidly decrease to non-zero values towards the base of the core. This trend is to some extent paralleled by Mn, which shows a slower decline with increasing sediment depth. With 514 μM (P08) and 685 μM (P05), respectively, the central stations exhibit the highest concentrations of dissolved Fe found in Potter Cove sediments. The parallel decreases in Re, U, and Mo in core P08, which is accompanied by a gradual and moderate increase in terminal metabolism products, such as TA (6.5 mM), phosphate (116 μM) and NH_4^+ (349 μM) indicates organic matter degradation and nutrient recycling under progressively reducing conditions (Fig. 5.3). At station P05 a significant decline in Mo and Re is recognisable not until c. 15–19 cmbsf, which widely coincides with the lower boundary of the iron reduction

zone (Fig. 5.3). Like at station P08, TA, ammonia, and phosphate concentrations are moderately elevated in P05 pore waters with a phosphate maximum of 180 μM directly within the iron reduction zone. This peak value is probably associated with the dissolution of iron phosphate phases (Tribovillard et al., 2006). Although the removal of Fe and Mo from the fluid phase in deeper sediment layers at both locations strongly suggests the presence of sulphidic conditions, neither an H_2S odor nor a significant depletion in sulphate (c. 1–2 mM) could be detected (Fig. 5.3).

5.6.1.3. Inner cove close to the melt water stream outlets and Carlini Station

At the shallower southern coast of the cove pore water profiles show characteristic sequences of “compressed” redox zonation as expected for nearshore sediments. At station K48 located close to the Potter Creek melt water stream outlet the nitrate reduction zone is relatively narrow and is followed by enhanced concentrations of dissolved Mn and Fe reaching maxima of 33 and 189 μM in the first 10 cmbsf, respectively (Fig. 5.4). The concurrent decreases in Re, Mo, and U accompanied by a steady increase in SO_4^{2-} _{dep} (5 mM) and TA (11 mM) towards the base of the core let suggest more severe reducing conditions in these sediments compared to the other sites. Particularly the removal of iron from the pore water in deeper sediments (>11 cmbsf) seems to mark the beginning of the sulphidic zone, where dissolved iron is probably fixed as iron sulphide in the solid phase again. Even stronger anoxic conditions were found at station P07, which is situated in c. 5 m water depth in front of Carlini Station. Whereas nitrate is completely reduced and removed from the pore water system in the first centimetre, only marginal concentrations of dissolved iron (max. 21 μM) and manganese (max. 6.4 μM) were found (Fig. 5.4). Particularly, Fe in the reduction zone seems to be restricted to the first three cmbsf before Fe concentrations decline to near zero further down. Anoxic conditions present below 5 cmbsf are moreover supported by the rapid and simultaneous removal of U, Re, and Mo from the pore water, with Mo reaching a near-zero value around 6 nM at

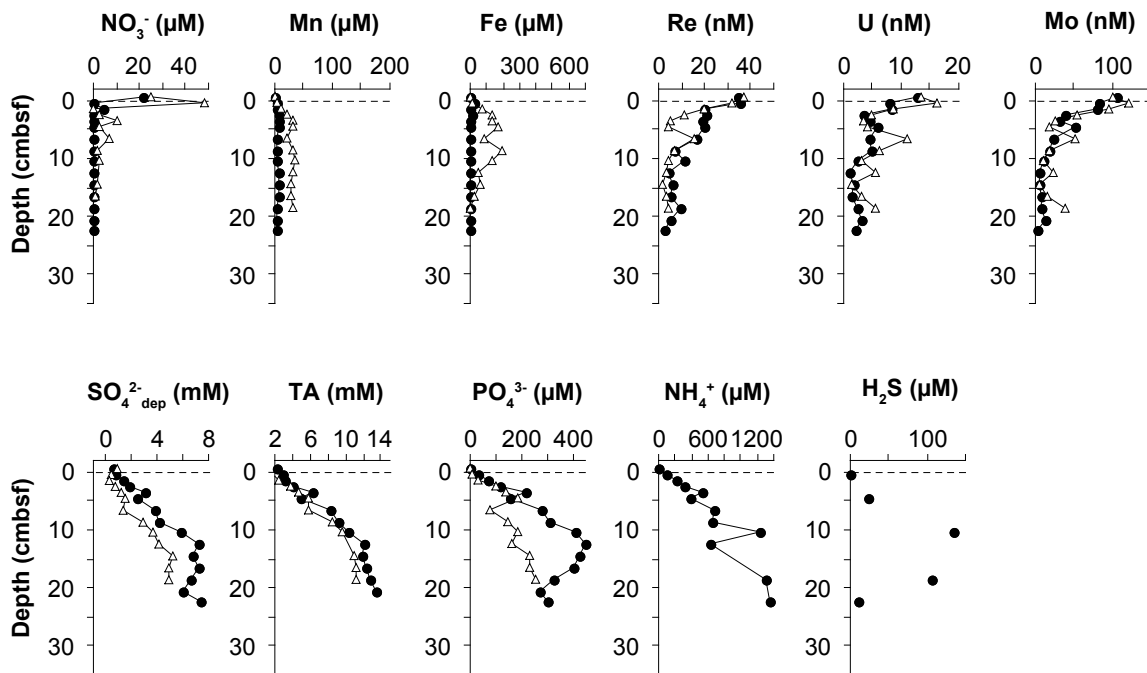


Fig. 5.4. Pore water profiles of nutrients (NO_3^- , NH_4^+ , PO_4^{3-}), redox-sensitive trace metals (Fe, Mn, Mo, U, Re), sulphate depletion (SO_4^{2-} dep), H_2S , and total alkalinity (TA) from cores P07 (black dot) and K48 (white triangle) obtained close to the southern coast of Potter Peninsula. Note that no NH_4^+ and H_2S data is available for core K48.

13 cmbsf (Fig. 5.4). Sulphidic conditions are on the one hand reflected by the gradual increase in SO_4^{2-} dep (7.4 mM in 20 cmbsf), and on the other hand by the presence of free H_2S in sediment depths below 5 cm (Fig. 5.4). It should be noted that free H_2S could not be detected in any other core analysed in this study. Accompanied by the removal of sulphate synchronous increases in total alkalinity (13.5 mM), ammonia (1,342 μM) and phosphate (450 μM) were observed indicating rapid mineralisation of organic matter in P07 surface sediments (Fig. 5.4).

5.6.2. Pore water stoichiometry and sulphate reduction rates

In order to identify the predominant organic matter mineralisation process in Potter Cove surface sediments at the different sampling locations regression analyses between SO_4^{2-} dep as an estimate for the metabolic amount of sulphate reduction and total alkalinity (TA) as a terminal metabolic products were conducted. Following the

GEOSECS Choice of Takahashi et al. (1982) in a marine environment the definition of TA can be simplified to:

$$\text{TA} = [\text{HCO}_3^-] + 2[\text{CO}_3^{2-}] + [\text{H}_2\text{BO}_3^-] \quad (5.6)$$

which would make TA a suitable substitute for dissolved inorganic carbon (DIC). This is in line with Beck et al. (2008a) who could show that TA equals DIC in deep pore waters obtained from intertidal flat sediments at the NW German coast. According to equation 5.6, although particularly valid for living marine phytoplankton (Redfield et al., 1963; Sholkovitz, 1973), we would expect a DIC:SO₄²⁻_{dep} (TA: SO₄²⁻_{dep}) ratio of 2 if the degradation of organic material is mainly linked to sulphate reduction.



Figure 5.5 reveals that sulphate depletion in Potter Cove pore waters is indeed positively correlated to total alkalinity in most of the cores located at the southeastern coast (KX4, K48, P03) and in the vicinity of the research station (P07, KX, K23). At these sites the TA: SO₄²⁻_{dep} ratio, which is given by the slope of the respective regression analysis ranges between 1.6 and 2.3 and is quite close to the expected value of 2 according to the Redfield ratio (Fig. 5.5). The presence of sulphate reducing conditions in Potter Cove sediments is not surprising. Several studies could already show that sulphate reduction is one of the main processes of organic matter degradation in coastal sediments, where the oxygen surface layer is often only a few millimetres thick and where it accounts for 10-92% of TOC oxidation (Jørgensen, 1982; Thamdrup and Canfield, 1996; Kostka et al., 1999; Gribsholt and Kristensen, 2003). Interestingly, this is not only true for temperate regions, but was also found in permanently cold coastal sediments from Svalbard, Arctic (Kostka et al., 1999) or from Signey Island, Subantarctic (Nedwell, 1989). Although we could show that sulphate reduction may represent the major pathway of organic matter mineralisation in this part of the bay, estimated sulphate reduction rates (SRR) are

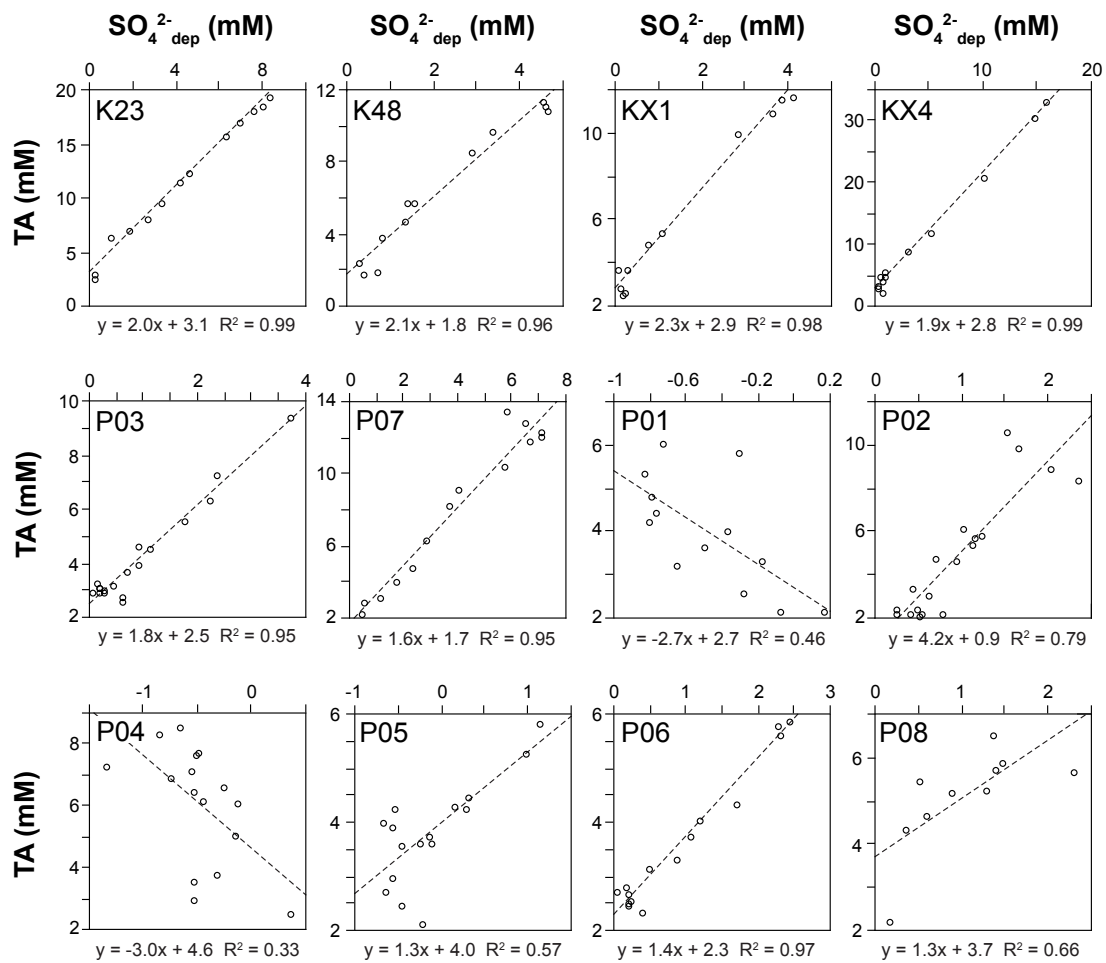


Fig. 5.5. Ratios of total alkalinity (TA) to sulphate depletion (SO_4^{2-} dep) in pore waters from Potter Cove sediments with best-fit linear regressions.

generally low. Using the numerical REC (Rate Estimation from Concentrations) model after Lettmann et al. (2012) integrated SRR of $0.23\text{--}0.56 \text{ mol m}^{-2} \text{ yr}^{-1}$ were calculated for the upper 20 cm of cores KX4, K23, K48 and P07, which show the highest depletion in sulphate (Fig. 5.6). These rates are significantly lower than SRR estimated for other subpolar or temperate regions, like Factory Cove, Signey Island ($2.5 \text{ mol m}^{-2} \text{ yr}^{-1}$; Nedwell, 1989), or the Danish coast ($0.95\text{--}5.5 \text{ mol m}^{-2} \text{ yr}^{-1}$; Sørensen et al., 1979), but comparable to SRR found in sediments off Greenland ($0.39 \text{ mol m}^{-2} \text{ yr}^{-1}$; Rysgaard et al., 1996). Probably this is due to the fact that particularly in the shallower areas close to the coast sediments are affected by enhanced physical disturbance, for example, by iceberg scouring. The resulting

intrusion of oxygenated seawater into deeper layers would inhibit sulphate reduction and lead to lower sulphate reduction rates at the surface.

In contrast, an entirely different picture is given for the cores that were taken in newly ice-free areas directly at the glacier front (P02, P01, P04) and in the deeper troughs (P05, P08) in the centre of the cove (>40 m) (Fig. 5.5). Here, correlations between sulphate depletion and TA are rather poor or even negative. Though redox-sensitive trace elements, like Mo may give evidence for negligible sulphate reduction in some of these cores this process alone seems not to be responsible for increases in total alkalinity/DIC and the reflected organic matter degradation. At these locations alternative metabolic pathways, involving nitrate, manganese and iron reduction may be more important as it could also be shown for Arctic sediments northeast of Svalbard (Vandieken et al., 2006).

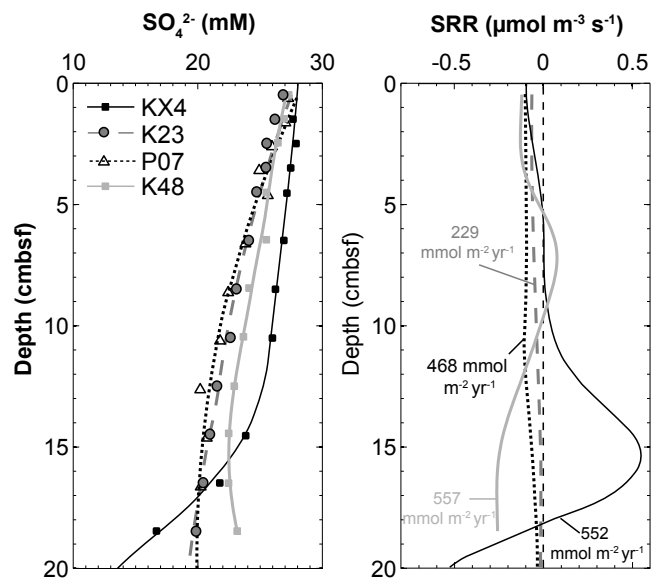


Fig. 5.6. a) Pore water profiles of sulfate (SO_4^{2-}) and b) modeled sulphate reduction rates (SRR) for the upper 20 cm of cores P07, KX4, K23, and K48 using the REC model after Lettmann et al. (2012) and a smoothing parameter λ of 10. For more information about λ see Lettmann et al. (2012).

5.6.3. Spatial distribution of redox conditions in Potter Cove surface sediments

The spatial distribution of selected pore water and solid phase parameters shows a picture of diverse redox conditions at different locations at the study site (Fig. 5.7). There is evidence for a significant reduction of sulphate in Potter Cove surface sediments (0-20 cmbsf) as high sulphate depletion is found along the southern coast of Potter Peninsula and in the northwestern area of the inner

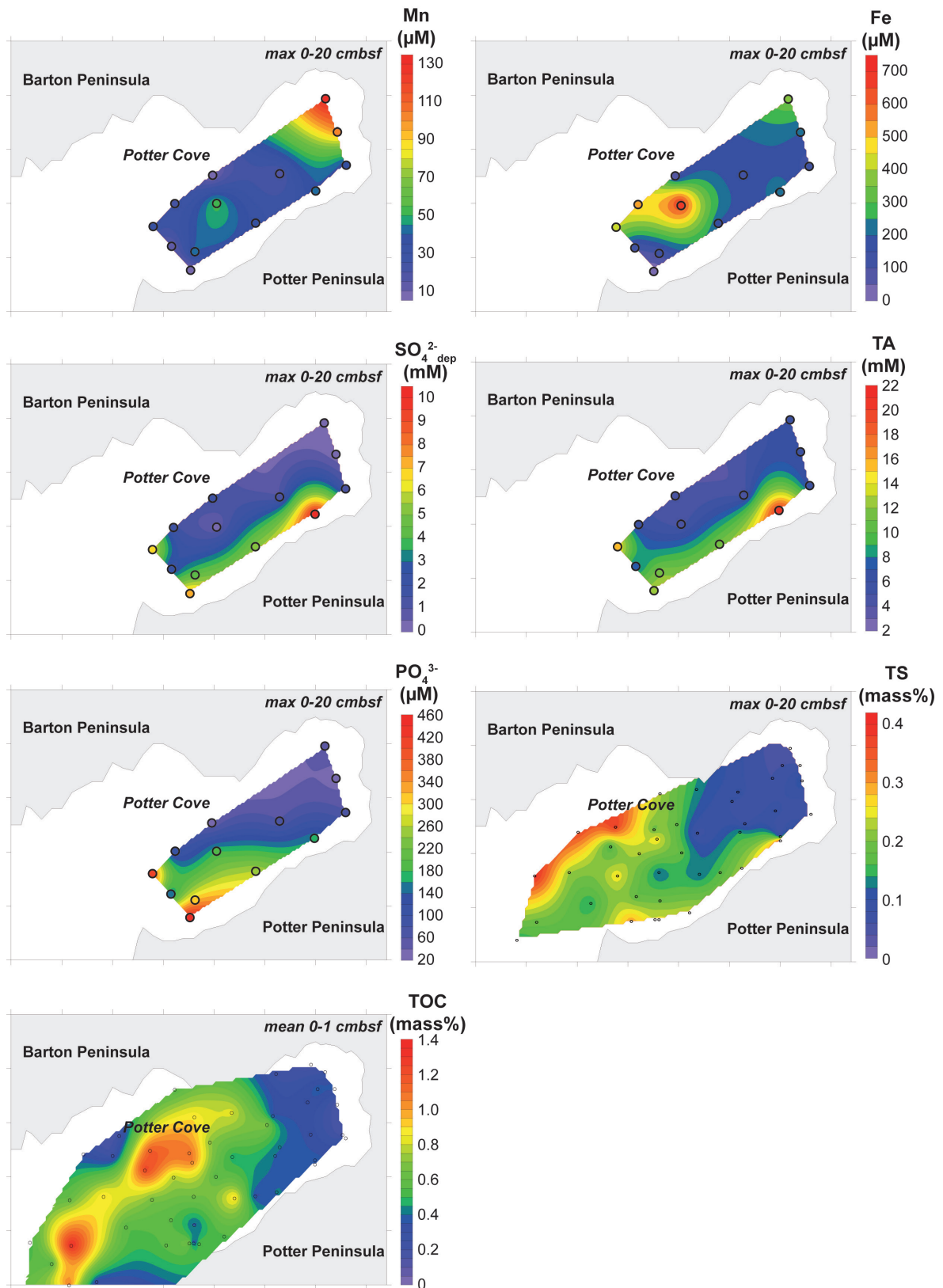


Fig. 5.7. Contourplots of several pore water (Fe, Mn, $\text{SO}_4^{2- \text{dep}}$, PO_4^{3-} , TA) and solid phase parameters (TOC, TS) of Potter Cove sediments.

cove. It is accompanied by enhanced microbial activity, which is reflected by an increased total alkalinity in the pore water. The presence of sulphidic conditions is moreover supported by higher maximum concentrations in total sulphur in the solid phase of these sediments indicating the formation of iron sulphides, like FeS_x and pyrite (Howarth and Jørgensen, 1984). Maxima of up to 0.4% TS were present in the shallower (<30 m) southeastern area of the bay where no pore water data are available. Considering that sea salt correction of solid phase sulphur may even be overestimated by assuming seawater composition of the pore water the solid phase data strongly suggest even more intense sulphidic conditions in surface sediments in this area.

In contrary, close to the glacier front and in the deeper troughs (>40 m) of the central cove concentrations of terminal products of metabolism, like TA and phosphate are generally lower and sulphate depletion does not exceed 4 mM (Fig. 5.7). On the other hand, these sediments are characterised by high amounts of dissolved iron in the upper 19 cmbsf. With average iron concentrations of >300 μM in the centre and at least >250 μM in the northeast of the cove metal oxide reduction seems to be prevailing in these areas as it has also been shown in section 5.6.2. Maximum values of dissolved iron found in Potter Cove surface sediments (c. 700 μM) are even significantly higher than in any other study conducted so far.

Morford et al. (2009), for example, reported Fe concentrations in coastal pore waters from Buzzard Bay, Massachusetts (USA) of up to 500 μM . Lower Fe concentrations were found in surface sediments in the California Borderland (<200 μM , Shaw et al., 1990) and from the Skagerak, Denmark (c. 180 μM , Canfield et al., 1993). Even in high-Arctic coastal marine sediments from Young Sound, Northeast Greenland, for instance, where iron reduction is considered to be a major pathway of organic matter degradation, concentrations of dissolved Fe in the pore water do not exceed 300 μM (Rysgaard et al., 1998).

5.6.4. Factors controlling redox conditions in Potter Cove sediments

There are several factors affecting redox conditions in (coastal) sediments, such as the oxygen concentrations in the overlying water column or the quantity and quality of organic matter supplied to the sediment (Beck et al., 2008b). But also the rate of sediment accumulation, the occurrence of sediment disturbance, either by burrowing organisms or physical re-working and the availability of respective electron acceptors may influence the biogeochemical processes in the sediment as well (e.g., Sholkovitz, 1973; Aller et al., 1986). In the following possible controlling factors for spatial differences in predominant organic matter mineralisation pathways and redox conditions in Potter Cove sediments are discussed.

5.6.4.1. Availability of substrate

The quantity of organic carbon, which is buried in the sediment, forms certainly one of the major controls on sedimentary redox processes. Jørgensen et al. (1982) could already show that metabolic rates, which are triggered by the amount of suitable substrate, are positively correlated to the level of reducing conditions. TOC concentrations in Potter Cove surface sediments (av. $0.53 \pm 0.30\%$) are relatively low even for siliceous muds and oozes from the Antarctic continental shelf and the Bransfield Basin (av. 1.2–1.5%; Dunbar et al., 1989; Barcena et al., 1998) but comparable to values found by Milliken et al. (2009) and Monien et al. (2011) in sediments from the nearby Maxwell Bay (av. 0.3–0.4%). Higher values are particularly present in the (north)western part of the cove (0.5–1.3%), whereas TOC concentrations are lower (<0.4%) or even near zero in the newly ice-free areas in the east close to the glacier front (Fig. 5.7). With average molar TOC/TN ratios close to the ratio expected for phytoplankton (c. 6.6; Redfield et al., 1963) and local macroalgae (5.8–11.7; Weykam et al., 1996), a predominantly marine source for the organic material in Potter Cove sediments (6.1 ± 1.5) is indicated. As this average ratio is significantly lower than TOC/TN values of local mosses (40 ± 19),

lichens (114 ± 46), liverworts (55 ± 3), grasses (21 ± 4) or freshwater algae from the adjacent lakes (8.3 ± 1.4) (Lee et al., 2009), an appreciable input of terrestrial and therefore less digestible organic matter from the enclosing peninsulas can be excluded. However, although primary production is generally high in the neritic zones around Antarctica (Martin et al., 1990), this is not the case for Potter Cove and adjacent areas where summer chlorophyll *a* (chl *a*) concentrations are generally below 1 mg m^{-3} (Schloss et al., 2012). Schloss et al. (2002) argue that a combination of several physical conditions, including an unfavourable depth of turbulent vertical mixing and the shading of surface waters by melt water derived suspended particulate matter may be a possible reason for relatively low phytoplankton growth in Potter Cove during austral summer. Therefore, it is more probable that macroalgae may represent a relevant contributor to the sedimentary TOC pool as it has already been proposed by Quartino et al. (2008). This may be supported by the fact that higher TOC concentrations are particularly found in surface sediments that are located adjacent to the hard bottom dominated areas in the outer and the western part of the inner cove (Fig. 5.7). In these zones, which are already ice-free since at least c. 60 years (Rückamp et al., 2011), high abundances of macroalgae are found whereas the newly ice free areas close to the glacier front are still only sparsely settled (Quartino et al., 2013). However, a higher accumulation of glacial material close to the glacier front, which would dilute the TOC content in the sediment has to be considered as well. In any case, the lack of metabolisable organic material in the surface sediments in the eastern coast close to the glacier may to some extent serve as an explanation for less reducing conditions present in the sediments in this area. However, it fails to clarify the dominance of metal oxide reduction processes in the deposits of the deeper troughs of the central cove (P05, P08). Interestingly, their TOC concentrations are comparable or even higher than to those present in surface sediments along the southern coast ($0.2\text{--}0.5\%$ vs $0\text{--}0.3\%$; Fig. 5.7).

5.6.4.2. *Availability and reactivity of electron acceptors*

Another controlling factor may be the availability and reactivity of respective electron acceptors, which are closely linked to organic matter mineralisation. According to Froelich et al. (1979) and Canfield and Thamdrup (2009) aerobic respiration is followed by the reduction of nitrate, Mn(IV), Fe(III), sulphate and finally methanogenesis. Their order of utilisation is based on the thermodynamics of the processes and the energy available to the organisms; an overlap between some of these processes is also possible (Canfield and Thamdrup, 2009). Whereas sulphate is practically non-limiting in marine subsurface sediments due to its high concentration in seawater (Jørgensen, 1982), this is not necessarily true for reducible Fe phases.

It is commonly accepted that only a fraction of the sedimentary iron is on the short-term available for microbially mediated iron reduction. Iron reactivity depends on factors, like mineralogy, crystallinity, and grain size (Postma, 1993 and references therein). Consequently, iron reduction will only dominate over sulphate reduction as long as the sediments still contain reactive iron (oxyhydr)oxide minerals, such as ferrihydrite, lepidocrocite, goethite and haematite, whose half-lives with respect to reductive dissolution and sulphidation range between some minutes and a couple of days (Canfield et al., 1992; Raiswell and Canfield, 1996; Poulton et al., 2004). However, when this pool of reactive metal oxides and iron (oxyhydr)oxides in particular is exhausted, as it is the case at some locations along the southern coast of the bay (P07), sulphate reduction is the predominant pathway of organic matter degradation. This is not only indicated by the lack of significant enrichments in dissolved Mn and Fe, but also by the occurrence of free H₂S in the pore water, which is no longer required for precipitating FeS₂ or its precursor FeS.

The situation is different in the central cove and close to the glacier front, where sulphate depletion seems to be negligible and where moderate increases in terminal products of metabolism (TA, PO₄³⁻) are linked to high Mn and Fe concentrations. A similar phenomenon was observed by Aller et al. (1986) who investigated muds from

the inner Amazon shelf. They related the presence of extensive iron reduction zones (>1 m), which showed no evidence of significant sulphate depletion, to the periodical regeneration of the reactive Fe pool by physical re-working. Particularly for shallower coastal Antarctic regions it is known that anchor ice, iceberg scouring and water turbulence produced by tides and waves are disturbance mechanisms affecting the surface sediments and the coastal biota (Arntz et al., 1994). It is probable that these mechanisms are also responsible for physical re-working of Potter Cove sediments although we would rather expect this for the shallower areas at the southern coast. Moreover, an enhanced activity of burrowing organisms in well-bioturbated surface sediments has to be considered as well.

A further and more likely possibility could be an enhanced deposition of reactive iron-rich material at these locations. Every year during the summer months c. 3,000 tonnes of fine-grained suspended particulate matter are transported into the cove by sediment laden melt water streams on Potter Peninsula (D. Monien, unpublished data). These calculations do not include the subglacial input of SPM from underneath the Fourcade Glacier front, which was estimated to be even higher (c. 24,000 tonnes yr⁻¹; D. Monien, unpublished data). Granulometric analyses let assume that most of this fine-grained material is deposited in the newly ice-free areas close to the glacier and in the deeper central cove (A. Wöfl, personal communication). This is in line with recent current models, which show that these deeper troughs possibly act as a kind of depocentre for this fine-grained material (Lim, 2013). In addition, leaching experiments have shown that this SPM contains appreciable amounts (2.1–2.9%) of dithionite and ascorbic acid leachable iron (D. Monien, unpublished data), which can potentially be reduced by microorganisms.

5.6.5. Coastal pore waters as a significant source of trace metals and micronutrients in the Antarctic region

Iron is considered to be an important micronutrient for marine primary producers (e.g., Martin et al., 1990; Coale et al., 2004). Particularly in regard to iron limitation in vast regions of the Southern Ocean controlling algae bloom development in this HNLC (high nutrient-low chlorophyll) area (Martin et al., 1990; Lancelot et al., 2009), the knowledge about contributors to the iron pool of this system is of utmost importance. In addition to aeolian input, upwelling of replete deeper water masses, release of terrigenous material from icebergs and iron-bearing subglacial streams, suboxic shelf sediments are discussed to be a potential source of bioavailable iron (Fe_b) to the ocean (Tagliabue et al., 2010; Shaw et al., 2011; de Jong et al., 2012). Only a small amount of microbially reduced and remobilised Fe(II), which diffuses from the sediment into the oxic water column will be stabilised by natural organic ligands as aqueous Fe(III) (Rue and Bruland, 1995), a form that is principally bioavailable (Chen and Wang, 2001). Most of the iron will be rapidly re-oxidised to Fe(III) and due to its low solubility in oxic seawater precipitated as extremely reactive nanoparticulate ferrihydrite (Raiswell and Anderson, 2005). These ferrihydrites are to some extent scavenged by suspended material and re-deposited in the sediment, where they can easily be reduced again. A certain amount may be kept in suspension and transported for longer distances across the shelf (Lam et al., 2012). By vertical diffusion or during upwelling events these reactive and labile iron phases may be delivered to the mixed surface layer and represent a key source of bioavailable iron as it could be shown by Lam and Bishop (2008) for the HNLC western Subarctic Pacific.

However, the relevance of this mechanism in terms of iron fluxes to the Southern Ocean is still unclear. Most of the calculations available for this area so far are not based on real pore water data but on fluxes measured by Elrod et al. (2004) on the California shelf. Using the REC model after Lettmann et al. (2012) we were

able to estimate Fe reduction rates in Potter Cove sediments ranging between c. 5 and 146 $\mu\text{mol m}^{-2} \text{yr}^{-1}$ (Table 5.3). It should be mentioned that this is still a conservative estimate since iron reduction may play a greater role in the deeper (c. 500 m) hemipelagic areas of the shelf. Furthermore, true Fe reduction rates may

Table 5.3. Iron reduction rates in the upper 20 cm of selected Potter Cove sediments estimated by using the REC model after Lettmann et al. (2012) and a smoothing parameter λ of 10. For more information about λ see Lettmann et al. (2012).

Core	Iron reduction rate ($\text{mmol m}^{-2} \text{yr}^{-1}$)
P01	20
P02	5
P04	16
P05	146
P08	121
KX4	17

be significantly underestimated considering that calculations are based on the Fe pore water profile neglecting the loss of dissolved iron by adsorption or precipitation of Fe-bearing minerals (Canfield et al., 1993). Even if we assume that only 1% of the Fe reduced in the sediments will reach the water column through the sediment-water interface, the Antarctic shelf areas (Timmermann et al., 2010) would contribute 1.2×10^4 to 3.6×10^5 tonnes per year to

the pool of bioavailable iron. Consequently, these shelf sediments would provide a Fe_b flux of $1.2\text{--}18 \text{ mg m}^{-2} \text{yr}^{-1}$ to the Southern Ocean (based on a total area of c. $20 \times 10^6 \text{ km}^2$; Shaw et al., 2011). This flux is significantly higher than the input by aeolian dust ($0.05\text{--}0.25 \text{ mg m}^{-2} \text{yr}^{-1} \text{Fe}_b$) and previous estimates of shelf-derived input of bioavailable iron, which range between 0.1 (Lancelot et al., 2009) and $1.2\text{--}3.2 \text{ mg m}^{-2} \text{yr}^{-1}$ (Tagliabue et al., 2010) Fe_b considering the same conservative export efficiency of 1%. In contrast, it is comparable to the contribution of iceberg-hosted material ($2\text{--}20 \text{ mg m}^{-2} \text{yr}^{-1} \text{Fe}_b$) as estimated by Shaw et al. (2011), which makes it a major source of bioavailable iron for the HNLC regions of the Southern Ocean.

5.7. Conclusions

For the first time, redox-sensitive trace elements and nutrients are used to describe redox conditions and biogeochemical processes in pore waters from coastal sediments at King George Island, western Antarctic Peninsula. We could show that sulphate reduction is the major pathway of organic matter mineralisation in the shallower areas at the southern coast of Potter Peninsula and on a transect towards the northwestern area of the inner Potter Cove. Sulphate reduction rates in the upper 20 cm of these sediments ($0.23\text{--}0.56\text{ mol m}^{-2}\text{ yr}^{-1}$) are comparable to rates found in coastal sediments off Greenland but an order of magnitude lower than known from nearshore deposits in other subantarctic or temperate regions. In contrast, microbial manganese and dissimilatory iron reduction processes are dominant in the deeper troughs of the central cove and in the newly ice-free area in glacial proximity. We suggest that a combination of enhanced physical and biological disturbance by bottom water currents, ice scouring and burrowing organisms, the increased accumulation of melt water derived, fine-grained material with high amounts of reducible metal oxides and the reduced availability of metabolisable organic matter favours metal oxide reduction over sulphate reduction in these respective regions. Based on modelled iron reduction rates we calculated an Antarctic shelf derived input of potentially bioavailable iron to the Southern Ocean of $1.2\text{--}18\text{ mg m}^{-2}\text{ yr}^{-1}$. The contribution is estimated to be in the same range than the flux provided by icebergs and significantly higher than the input by aeolian dust or previous estimates for the continental shelf. This makes the suboxic shelf sediments a key source of iron for the HNLC areas of the Southern Ocean. As a consequence of enhanced glacier retreat and melt water fluxes and the resulting rise of accumulation of iron-rich sediment on the shelf (Monien et al., 2011; Majewski et al., 2012), it can be assumed that the role of Antarctic shelf sediments for the natural iron fertilisation of the Southern Ocean may even gain more importance in the future.

5.8. Acknowledgements

This study forms part of the IMCOAST project and was funded by the German Research Foundation (DFG project no. BR 775/25-1) and the German Federal Ministry of Education and Research (BMBF, ref. no. 03F0617C). We are grateful to the Argentine Diving Division and the generous hospitality at Carlini Station during the field campaigns 2009/2010 and 2010/2011. Special thanks go to Oscar Gonzales (Instituto Antártico Argentino, Buenos Aires) for the scientific coordination of the project during both field campaigns. Finally, we gratefully acknowledge the technical assistants at the ICBM (Institute for Chemistry and Biology of the Marine Environment).

6. Influence of the pore water geochemistry on Fe and Mn assimilation in *Laternula elliptica* at King George Island (Antarctica)

Harald Poigner^a, Patrick Monien^b, Donata Monien^b, Michael Kriews^a, Hans-Jürgen Brumsack^b, Dorothee Wilhelms-Dick^a, and Doris Abele^a

^a Alfred Wegener Institute Helmholtz Centre for Polar and Marine Research, Am Handelshafen 12, 27570 Bremerhaven, Germany

^b Carl von Ossietzky University Oldenburg, Institute for Chemistry and Biology of the Marine Environment (ICBM), Carl-von-Ossietzky-Str. 9-11, 26129 Oldenburg, Germany

This chapter is published in a reviewer-edited version in *Estuarine, Coastal and Shelf Science*, **135**, 285-295 (2013).

6.1. Abstract

A high input of lithogenic sediment from glaciers was assumed to be responsible for high Fe and Mn contents in the Antarctic soft shell clam *Laternula elliptica* at King George Island. Indeed, withdrawal experiments indicated a strong influence of environmental Fe concentrations on Fe contents in bivalve hemolymph, but no significant differences in hemolymph and tissue concentrations were found among two sites of high and lower input of lithogenic debris. Comparing Fe and Mn concentrations of pore water, bottom water, and hemolymph from sampling sites, Mn appears to be assimilated as dissolved species, whereas Fe apparently precipitates as ferrihydrite within the oxic sediment or bottom water layer prior to assimilation by the bivalve. Hence, we attribute the high variability of Fe and Mn accumulation in tissues of *L. elliptica* around Antarctica to differences in the geochemical environment of the sediment and the resulting Fe and Mn flux across the benthic boundary.

6.2. Introduction

Iron and manganese contents in the tissues of the circum-Antarctic clam *Laternula elliptica* (King and Broderip, 1832) differ considerably among sites around Antarctica. This led scientists to search for the environmental sources of both metals to explain local differences. At King George Island (KGI; South Shetland archipelago, western Antarctic Peninsula (WAP)) several authors related relatively high contents of both metals in bivalve tissues to a high input of eroded bedrock material transported by melt water streams into the coastal areas (Abele et al., 2008; Curtosi et al., 2010; Husmann et al., 2012). Recently, Monien et al. (2011) reported a tripling of sediment accumulation rates in Maxwell Bay (KGI) during the last century, with the highest increase during the decade 1990–2000. The increased input of lithogenic debris coincides with intensified melt water discharge from retreating land glaciers on the Antarctic Peninsula as a consequence of the strong rise in air temperature in the WAP region during the last decades (Rignot and Thomas, 2002; Vaughan et al., 2003; Braun and Hock, 2004; Turner et al., 2005; Cook et al., 2005; Vaughan, 2006; Dominguez et al., 2007; Steig et al., 2009; Rückamp et al., 2011). Husmann et al. (2012) proposed the intensified sediment and melt water input at KGI to be responsible for the higher Fe accumulations in *L. elliptica* from KGI compared to individuals collected at Rothera Point (Adelaide Island). However, eroded bedrock material remains to be verified as source of high tissue Fe levels in *L. elliptica*.

Like other benthic deposit feeders, *L. elliptica* ingests particles and water from the benthic boundary layer. Trace metals are assimilated from both sources (Rainbow, 2002; Griscom and Fisher, 2004). The proportion of metal assimilation from the particulate and dissolved phase depends on the bioavailability of the metal in each fraction and on the physiological characteristics of the species (e.g., pH-conditions in the gut; Wang and Fisher, 1999; Rainbow and Wang, 2001; Griscom and Fisher, 2004). Large amounts of lithogenic sediment particles are ingested together with the nutrition. However, the assimilation efficiencies (AE) of metals are generally

higher for organic matter compared to inorganic matter, because organic particles are processed more intensely in the gut, due to their nutritional value (Willows, 1992; Decho and Luoma, 1996; Gagnon and Fisher, 1997; Lee and Luoma, 1998; Griscom and Fisher, 2004). Free metal ions are most easily absorbed and readily bioavailable to marine organisms (e.g., Bjerregaard and Depledge, 1994; Fisher et al., 1996).

Concentrations of Fe and Mn usually do not exceed low nanomolar levels in oxic ocean waters (Landing and Bruland, 1987; Bruland and Lohan, 2004; Middag et al., 2012), but bivalves accumulate trace metals even when exposed to low concentrations (Rainbow, 1990). In this work, Rainbow suggested sediment pore water as an alternative source of bioavailable metals for burrowing bivalves. Pore waters in the suboxic sediment zone (preferentially termed as manganous and ferruginous zones; Canfield and Thamdrup, 2009) generally show high concentrations of dissolved Mn(II) and Fe(II) due to the dissimilatory reduction of manganese oxides and iron (hydr)oxides during early diagenesis (e.g., Froelich et al., 1979; Berner, 1981; Lovley and Phillips, 1988; Rutgers van der Loeff et al., 1990; Canfield et al., 1993). Dissolved Fe(II) and Mn(II) diffuse into the benthic boundary layer or into the overlying water layers due to concentration gradients between pore water and seawater and depending on the content of organic matter in the sediment, remineralisation rate, oxygen penetration depth, and biological or physical reworking of the sediment (Lynn and Bonatti, 1965; Yeats et al., 1979; Sundby and Silverberg, 1985; Elrod et al., 2004; Laës et al., 2007; Pakhornova et al., 2007; Sachs et al., 2009; Severmann et al., 2010; Kowalski et al., 2012).

However, the assimilation of pore water derived Fe and Mn by *L. elliptica* contradicts earlier studies, which assumed a predominating assimilation of both elements from lithogenic particles, in particular eroded bedrock material transported by melt water streams from the glaciers to the cove (Abele et al., 2008; Curtosi et al., 2010; Husmann et al., 2012). We questioned this concept, since the highest metal

tissue contents of *Laternula elliptica* were found in animals from Deception Island (Deheyn et al., 2005). This island is only marginally covered with glaciers, but highly affected by geothermal influence (e.g., import of dissolved metals; Elderfield, 1972; Rey et al., 1995).

Hence, we wanted to clarify i) if the Fe and Mn accumulation by *L. elliptica* differs significantly among animals at sites of high sediment input (located in front of the melt water inlets) and lower sediment impact (outside of the cove) in Potter Cove (PC) and ii) if high concentrations of dissolved Fe and Mn in sediment pore water are an important source for the assimilation by *L. elliptica*, similar to the hydrothermal influence at Deception Island.

6.3. Material and Methods

6.3.1. Sample collection and experimental treatment

Individuals of the Antarctic clam *Laternula elliptica* were collected by scuba divers at seven stations in PC (Fig. 6.1) between January and March 2010. Five stations (B; Fig. 6.1c) located next to the discharge area of melt water streams were chosen pseudo randomly on a Universal Transverse Mercator (UTM)-grid (100 m grid point distance). One station was positioned in a newly ice free area (ID) and one in the outlet of PC to Maxwell Bay (C). Schloss and Ferreyra (2002) reported a decreasing concentration of terrigenous material in the water column with increasing distance to the discharge area. Consequently, station B is defined as highly impacted by sediment input compared to both other stations (C, ID).

At all stations only bivalves with a shell length >7.0 cm were collected, except for station ID, where only smaller individuals <6.4 cm were found. The age of 37 individual shells was determined by counting annual growth rings according to Brey et al. (2011). Modifications include the use of epoxy-metal (liquid metal, Toolcraft, Conrad Electronic SE, Germany) as embedment and carbon carbide grinding paper (Buehler-Met®II, Buehler, USA) in steps of P1000, P2500 and P4000 grades.

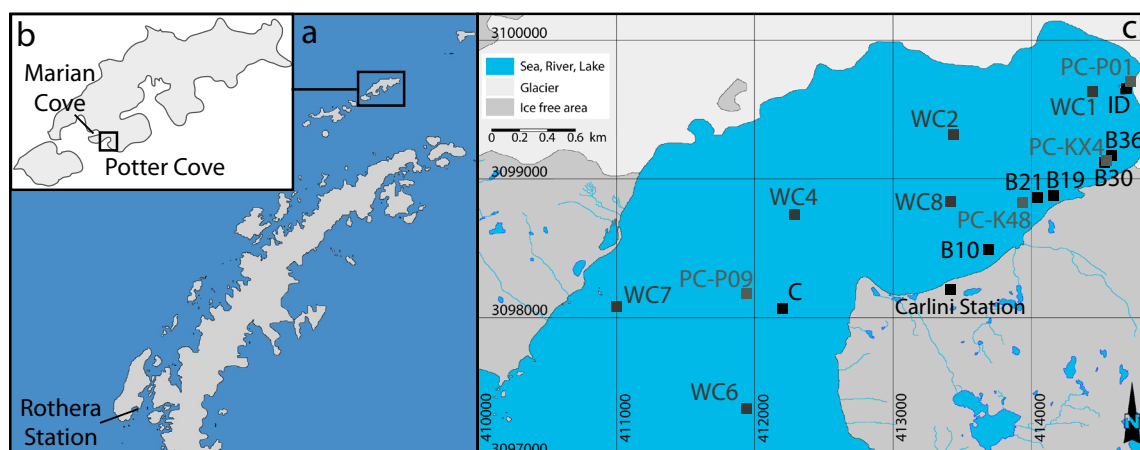


Fig. 6.1. a) Map of the Antarctic Peninsula with b) King George Island, and c) Potter Cove including the sampling stations (B, C, ID: stations for bivalve sampling; PC-K48, PC-KX4, PC-P01, PC-P09: sediment cores; WC: seawater samples; UTM grid: zone Z21E; WGS84).

Hemolymph and tissues (digestive gland (DG), gill, and mantle) were sampled from all animals within 12 hours after collection. Individuals used in starving experiments were acclimatised in natural seawater at 1°C at least for one week. 50% of the water was renewed every two days. Three replicates (EH1–EH3; one animal per aquarium) of *L. elliptica* were kept in 0.5 µm-filtered seawater (WFMB0.5-93/4 cartridge filter, Wolftechnik Filtersysteme GmbH, Germany) over a period of 14 days. A second treatment group of three individuals (EH4–EH6) was exposed to 0.5 µm-filtered seawater spiked with 10 µmol L⁻¹ Fe; dissolved as a Fe:EDTA complex. The Fe-EDTA solution was prepared by dissolving 100 µmol EDTA (≥99%, Sigma-Aldrich, Germany) in 100 mL of 18.2 MΩ water. After cooling, 100 µmol Fe (Ammonium iron(II) sulfate hexahydrate, ≥98%, Sigma-Aldrich, Germany) were added and diluted with 0.5 µm-filtered seawater to the final volume (10 L). Water of each aquarium and hemolymph of each bivalve were sampled at day 0, 5, 10, and 14. The water temperatures ranged between -0.5°C and 2°C.

Hemolymph (fluid and hemocyte cells) was taken from the posterior adductor muscle by using a G26x1 needle (Sterican®, B. Braun Melsungen AG, Germany) and a 1 mL or 10 mL syringe (Omnifix®, B. Braun Melsungen AG, Germany). This

stainless Cr-Ni-steel needle is coated by a thin silicone film, to avoid Fe contaminations due to the contact of blood and steel surface. Subsamples were centrifuged with 400 g (a force that did not lyse cellular material) for 15 min at 2°C (Centrifuge 5403, Eppendorf AG, German) to remove hemocytes from suspension to determine the Fe content of the hemolymph fluid. Afterwards original samples and centrifuged subsamples were acidified with 20 µL nitric acid (≥69%, TraceSelect®, Sigma Aldrich, Germany) per 1 mL sample and stored and transported at 4°C in 2 mL safe-lock-tubes (Eppendorf AG, Germany). Tissues were sampled using ceramic scissors and rinsed carefully with 18.2 MΩ water in order to remove seawater and sediment. This ensures that the body tissue metal concentrations represented only assimilated metals. Cleaned tissues were stored at -80°C and lyophilised.

6.3.2. Element analysis

All lab ware exposed to samples and standards was cleaned by soaking in >10% (v/v) HNO₃ (subboiled, 65%, Merck, Germany) for a minimum of 24 h, and rinsed subsequently with 18.2 MΩ water. PTFE (polytetrafluoroethylene) vessels were cleaned with 10 mL >30% HNO₃ and heated at 160°C for 2 h under recirculation and were also rinsed with 18.2 MΩ water prior to use. Before hydrolysis lyophilised tissues were powdered using an agate mortar and pestle and weighed into PTFE vessels (mainly 50–100 mg). Hemolymph (1–2 mL) was transferred to PTFE pots and sample vials were rinsed with 1 M bidistilled HNO₃ to ensure that the whole sample was transferred into the PTFE vessels.

First, 5 mL of HNO₃ (65%, subboiled) and 1 mL of H₂O₂ (30%, Suprapur®, Merck, Germany) were added. Due to strong outgassing, samples were kept at room temperature until outgassing ceased. Finally, 1 mL of HF (40%, Suprapur®, Merck, Germany) was added and vessels were heated under recirculation for 1 h at 60°C, 1 h at 100°C, and 8 h at 160°C. After cooling, 5 mL of 18.2 MΩ water were added and evaporated at 160°C to a residual volume of approx. 1 mL. Samples were filled

up with 1 M nitric acid (65%, bidistilled) to a final volume of 10 mL (hemolymph) or 50 mL (tissues) and transferred to polypropylene tubes.

Element concentrations of Ca, Fe, K, Mg, Mn, Na, and Sr were analysed by means of inductively coupled plasma - optical emission spectroscopy (ICP-OES; Iris Intrepid, Thermo Fisher Scientific Inc., USA). Additionally, Mn concentrations below the lowest calibration standard of the ICP-OES measurements ($0.01 \text{ mg L}^{-1} \text{ Mn}$) were analysed by ICP – mass spectrometry (ICP-MS; Perkin Elmer/Sciex, Elan6000, USA). Iron background concentrations of the aquarium waters during the experiment were determined after tenfold-dilution with 1 M bidistilled nitric acid by ICP-MS. The ICP-multi-element calibration standard IV (CertiPURE[®], Merck, Germany; used for ICP-OES), multi-element calibration standard 2 and 3 (Perkin Elmer, USA; used for ICP-MS), and rhodium(III) chloride solution (Merck, Germany) as internal standard were used for standardisation of the ICP-OES and ICP-MS system. All element concentrations analysed in this study are available at Pangaea (doi:10.1594/PANGAEA.776600).

6.3.3. Standard reference material

The standard reference materials IAEA-A13 (freeze dried animal blood) and IAEA407 (fish homogenate; International Atomic Energy Agency, Vienna, Austria) were hydrolysed during each digestion procedure to assure constant digestion quality (Table 6.1). Lyophilised animal blood (IAEA-A13) was chosen due to the lack of matrix matched reference material, although matrix discrepancies between samples (liquid, no hemoglobin) and reference material (lyophilised, hemoglobin) exist. Additional hydrolysis and analyses were done at the Institute of Soil Science of Temperate Ecosystems (University of Göttingen) for both reference materials and at the Institute for Chemistry and Biology of the Marine Environment (University of Oldenburg) for IAEA407 to prove the accuracy of our digestion procedure.

Concentrations were similar between institutes and ranged within the 95%

confidence interval (95%CI; Table 6.1) for most elements. For all elements precision ranged between 3.5% and 5.9% except for K (12.9%) in IAEA-A13 and between 5.2% and 8.9% in IAEA407.

Table 6.1. Results of the reference materials IAEA-A13 and IAEA407 analysed at two/three different laboratories (SD = standard deviation, 95% CI = 95% confidence interval, b.d.l. = values below detection limit, n.d. = not determined). All reference values are recommended values.

Element	Recommended		N	Alfred Wegener Institute Bremerhaven		University of Göttingen (N=8)		University of Oldenburg (N=1)	
	value	95% CI		Found concentration	SD	Found concentration	SD	Found concentration	
	[mg kg ⁻¹]			[mg kg ⁻¹]	[mg kg ⁻¹]	[mg kg ⁻¹]	[mg kg ⁻¹]	[mg kg ⁻¹]	
IAEA-A13	Ca	286	226 - 332	32	265	16	275	15	n.d.
	Fe	2400	2200 - 2500	34	2230	110	2110	73	n.d.
	K	2500	2100 - 2700	33	2040	260	2100	30	n.d.
	Na	12600	11600 - 13500	28	11070	390	10760	90	n.d.
IAEA 407	Ca	27000	25700 - 28300	13	26200	1700	26100	2160	25650
	Fe	146	143 - 149	12	132	12	129	10	b.d.l.
	K	13100	12200 - 14000	14	11000	710	11700	290	11500
	Mn	3.52	3.44 - 3.60	3	3.76	0.28	3.88	1.44	b.d.l.
	Sr	130	125 - 135	14	136	7	n.d.	n.d.	122

6.3.4. Pore water and seawater analysis

During austral summers 2009/2010 and 2010/2011 four sediment cores were retrieved close to the bivalve sampling stations (Fig. 6.1c) by using push corers (cores PC-K48 and PC-KX4) and a modified UWITEC gravity corer system (cores PC-P01 and PC-P09). Immediately after coring, sediments were directly sampled for pore water in 1 cm to 2 cm resolution (1 cm between 0–5 cm and 2 cm between 7–15 cm core depth) using 18.2 MΩ water-washed rhizons (0.15 µm mean pore size, Rhizosphere Research Products, The Netherlands) that were inserted simultaneously into the core liner through pre-drilled holes. Pore waters were then collected for up to 60 min under vacuum in 12 mL syringes. An aliquot of each

pore water sample was transferred to 5 mL polypropylene tubes (conditioned with 2% (v/v) subboiled HNO₃ conc.) and acidified with nitric acid (≥69%, TraceSelect®, Sigma Aldrich, Germany) to pH <2.

Seawater samples were taken from 5 m and 30 m depth (Fig. 6.1c) during the austral summer 2010-2011. All samples were acidified with subboiled nitric acid (65 %, Merck, Germany) to a final concentration of 2% after filtration (0.45 µm pore diameter; Sartorius AG, Göttingen, Germany). All water samples were stored and transported at 4°C to the home laboratory at the ICBM (Oldenburg, Germany) for element analyses.

Pore water Fe and Mn concentrations were determined at two-fold dilution by ICP-OES (iCAP 6000, Thermo Scientific, Germany). In case of low Fe and Mn concentrations (<0.9 µmol L⁻¹ (Fe) and <0.5 µmol L⁻¹ (Mn)) further analyses on ten-fold diluted sample aliquots were performed with an Element 2 ICP-MS (Thermo Scientific, Germany) to validate the results obtained by ICP-OES. In order to guarantee precision and accuracy of the methods international reference materials were measured, namely Atlantic Seawater (ASW, Osil, UK; N=17) and CASS-5 (NRCC, Canada; N=7), which were both spiked with single-element standard solutions (Alfa Aesar, U.S.). Solution containing 71.6 µmol L⁻¹ Fe and 72.8 µmol L⁻¹ Mn was added to ASW and solution containing 0.895 µmol L⁻¹ Fe and 0.910 µmol L⁻¹ Mn was added to CASS-5. Accuracy and precision were better than 4% for both elements. Seawater element concentrations were analysed in diluted (1:1) seawater samples by ICP-OES (Ca, K, Mg, Na, Sr) and on ten-fold diluted sample aliquots by ICP-MS (Fe, Mn). In order to verify the correctness of the measuring process the international seawater reference materials CASS-5 (Fe, Mn; N=31) and NASS-5 (Fe, Mn, via salinity: K, Mg, Ca, Na, Sr, N=11; NRCC, Canada) were analysed. Accuracy and precision were better than 4% for Ca, K, Mg, Na, and Sr. Accuracy and precision were 3.5% and 10% for Mn, respectively. Due to the very low Fe concentrations in seawater in some cases a standard correction was carried out and validated by

spiked standard reference material. Precision was better than 10% and accuracy better than 3.6%.

6.3.5. Statistical analysis

Since stations B10–B36 are representing the discharge area of melt water streams all five substations were pooled to one station B, now represented by N=25 bivalves. Element tissue contents [mg kg^{-1} dry weight] were normalised to bivalve shell volume to enable the comparison of sampling sites with non-overlapping animal size ranges. Since the shell does not grow exclusively along the anterior-posterior axis, the volume of an ellipsoid calculated from shell length, height, and width (Equation 6.1) was chosen as a more conservative approximation.

$$V_{Shell} = \frac{4}{3} \pi \times \frac{length_{Shell}}{2} \times \frac{height_{Shell}}{2} \times width_{Shell} \quad (6.1)$$

The ellipsoid proxy was also favoured over shell weight, because sediment particles were frequently enclosed between the shell layers in the siphon area of the shell (compare Harper et al., 2012), which would have biased shell weight as a normalisation proxy.

Descriptive statistics were computed by Origin 8.5.1 (OriginLab Corporation, USA). In order to identify and diminish outliers the Q-test after Dean and Dixon (1951) for $N < 10$ was applied. Differences in means were tested on significance between stations by the nonparametric Kruskal-Wallis-test (using R 2.12.1; R Development Core Team, 2011) and Nemenyi-test (computed manually). Equality of variances was tested by the Levene's test implemented in the lawstat package (Noguchi et al., 2009). An alpha level of 5% was chosen as statistically significant.

6.4. Results

Animals from stations B and C (N=28) were older than 13 years, whereas animals collected at ID (N=9) reached a maximum age of only five years. The lack of older individuals at station ID indicates a colonisation of the southern side of the island (close to station ID; Fig. 6.1) during the austral summer 2004/05. The island was covered by the Fourcade Glacier until 2002/03, and the results from station ID provide first evidence that benthic colonisation around the rocky island commenced only after the glacial retreat. As maturation in *L. elliptica* sets in at around 8 years (Dick et al., 2007), animals collected at station ID with a maximum age of 5 years are referred to as juveniles.

6.4.1. Iron withdrawal experiments

During the experiment Fe water concentrations ranged constantly between 2.1 $\mu\text{mol L}^{-1}$ and 2.8 $\mu\text{mol L}^{-1}$ (except EH2 day 5 (1.7 $\mu\text{mol L}^{-1}$) and EH3 day 14 (3.7 $\mu\text{mol L}^{-1}$) in the aquaria EH1–EH3 (filtered seawater) and between 8.1 $\mu\text{mol L}^{-1}$ and 11.6 $\mu\text{mol L}^{-1}$ in EH4–EH6 (Fe spiked filtered seawater). Figure 6.2a shows hemolymph Fe concentrations over time with regression lines for the Fe-withdrawal experiment, in which the bivalves were kept in Fe-depleted filtered seawater. Only two replicates are shown since a third replicate was excluded due to the inconsistency of the measured hemolymph Fe concentrations over time.

In the experiment where bivalves were kept in Fe-spiked filtered seawater (10 $\mu\text{mol L}^{-1}$ Fe; Fig. 6.2b), replicate EH4 showed increasing blood Fe concentration between day 0 (58.7 $\mu\text{mol L}^{-1}$) and day 5 (64.4 $\mu\text{mol L}^{-1}$), with concentrations declining consistently after day 5. In all other replicates of both treatments the Fe concentration decreased continuously and rapidly over time. We therefore assume the initial Fe concentration of EH4 to be higher than the Fe concentrations of the following samples (day 5, 10, and 14) and interpret the value of day 0 as non-credible result.

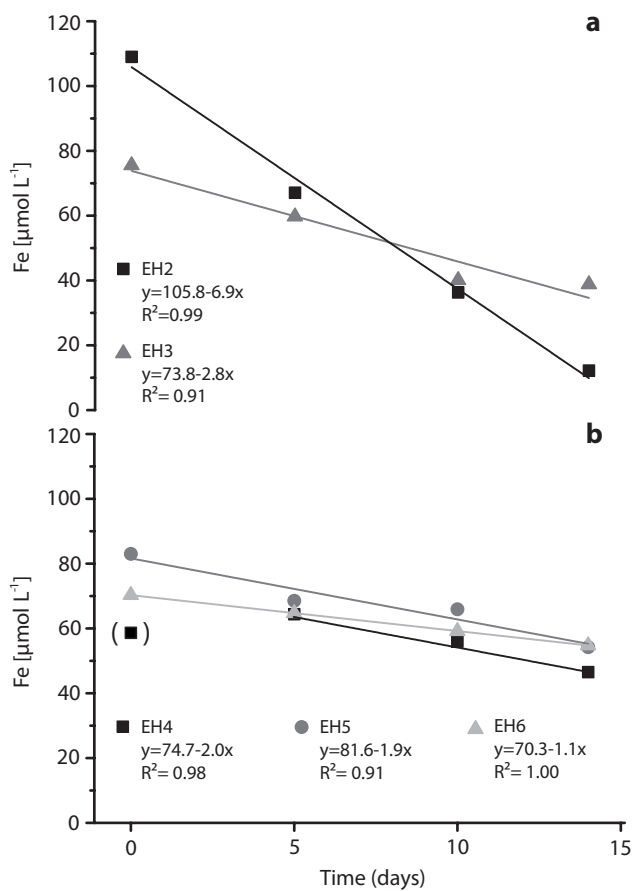


Fig. 6.2. Iron concentrations in bivalve hemolymph during a 14 day withdrawal experiment in a) filtered seawater and b) filtered seawater spiked with 10 $\mu\text{mol L}^{-1}$ Fe. Equations and adjusted R^2 are given for the linear regression lines. Day 0 of EH4 was not considered for linear regression.

The half-lives of Fe in EH2 and EH3 (8 days, 13 days) were lower than for replicates EH4 to EH6, which ranged from 19 to 31.5 days (half-life in EH4 was calculated without day 0). The adjusted determination coefficient (R^2) exceeds 0.91 for all replicates (EH4 was calculated without day 0). Iron contamination during sampling can be excluded due to this highly linear regression. Thus in both treatments the Fe concentration declined strongly over time.

6.4.2. Element concentrations of hemolymph, pore water, and seawater samples

The mean concentrations of Ca, Na, and Sr in hemolymph were similar to mean concentrations in pore water and seawater (Table 6.2; means over all stations). The mean K concentration in hemolymph samples (11.2 mmol L^{-1}) was

The slopes of the regression lines of the experimental setup (a) (replicates kept in filtered seawater; Fig. 6.2a) decline more steeply (slopes: -6.9 (EH2) and -2.8 (EH3)) than for the regression lines of the experimental setup (b) (replicates kept in Fe-spiked seawater, Fig. 6.2b, EH4–EH6: slopes: -0.9 to -1.8). Steeper slopes are also found in bivalves with higher initial Fe hemolymph concentrations. The half-lives of Fe in EH2 and EH3 (8 days, 13 days) were lower than for replicates EH4 to EH6, which ranged from 19 to 31.5 days (half-life

Table 6.2. Mean and range of Ca, Fe, K, Mn, Na, and Sr concentrations in bivalve hemolymph (stations B, C, and ID), pore water (cmbsf = cm below seafloor), and seawater.

Element	Hemolymph		Pore water (0 - 5 cmbsf)		Sea water (5 & 30 m water depth)	
	Mean	Range	Mean	Range	Mean	Range
Ca [mmol L ⁻¹]	10.6	8.9 - 11.7	10.6	10.1 - 11.4	10.4	9.0 - 10.8
K [mmol L ⁻¹]	11.2	8.9 - 12.6	10.3	9.7 - 10.7	10.3	8.8 - 10.7
Na [mmol L ⁻¹]	429	347 - 465	460	444 - 476	452	413 - 470
Sr [μmol L ⁻¹]	93	79.5 - 104	90	88.7 - 92.5	91	79 - 94
Fe [μmol L ⁻¹]	134	5.6 - 458	84	1.4 - 192	0.11	0.01 - 0.76
Mn [μmol L ⁻¹]	< 0.4	0.1 - 4.0	18.8	0.8 - 60	0.02	0.01 - 0.09

marginally higher than the maximum pore water and seawater concentrations (10.7 mmol L⁻¹). Hemolymph Fe concentrations of bivalves from different sampling locations (B, C, ID) are shown in figure 6.3. Significant differences in mean hemolymph Fe concentrations were only found between Station B ($169 \pm 51 \mu\text{mol L}^{-1}$) and station ID ($36 \pm 13 \mu\text{mol L}^{-1}$). Fe concentrations at station C ($141 \pm 108 \mu\text{mol L}^{-1}$) were

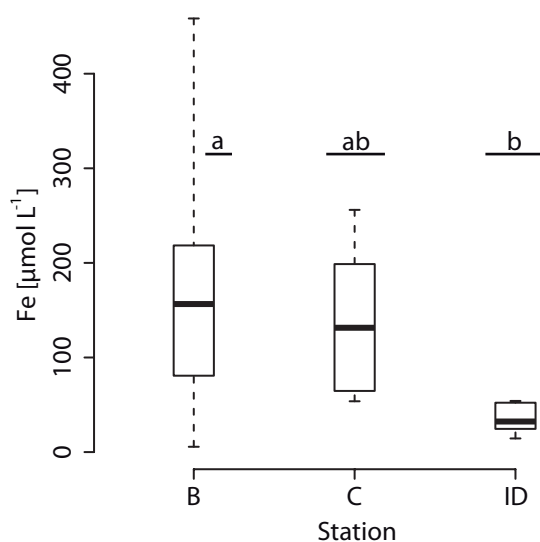


Fig. 6.3. Iron concentrations in bivalve hemolymph (N= 22(B)/ 5(C)/ 8(ID)). Boxplot whiskers represent the range. Different letters denote significant differences at an alpha level of 5%.

similar to both other stations. Centrifuged hemolymph samples contained $71\% \pm 10\%$ (N=29, across stations) of the total Fe concentration in hemolymph (data are not shown in the tables), which means that approximately 30% of total Fe in hemolymph is bound in cells.

In contrast to Fe, Mn concentrations were below the ICP-MS detection limit ($<0.1 \mu\text{mol L}^{-1}$) in most hemolymph samples. At station B the maximum Mn concentration was $3.9 \mu\text{mol L}^{-1}$, and thus identical to station ID ($4.0 \mu\text{mol L}^{-1}$), but higher than at station C ($2.4 \mu\text{mol L}^{-1}$).

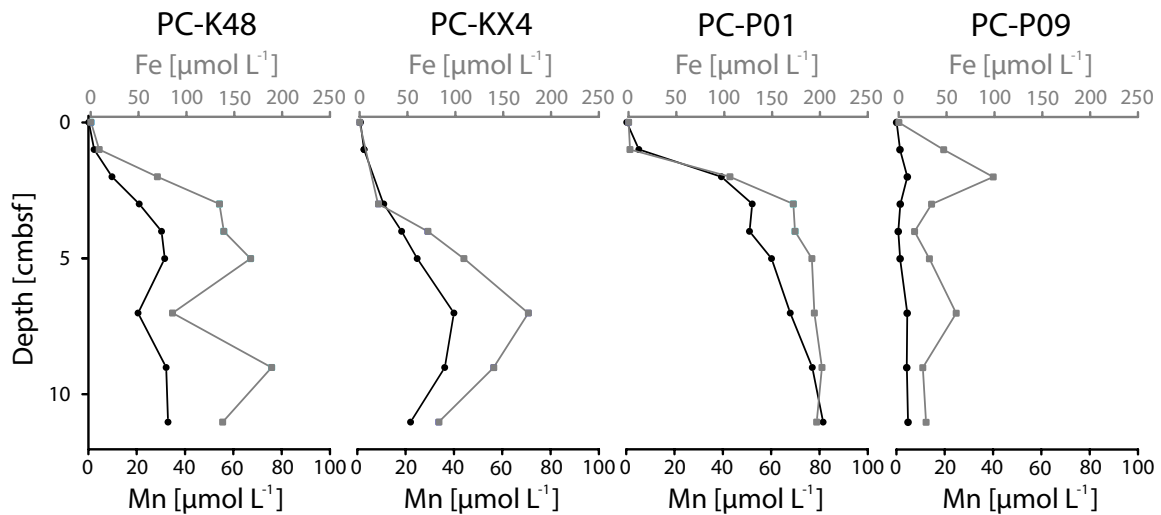


Fig. 6.4. Pore water profiles of Fe and Mn down to 11 cm below seafloor (cmbsf) of four stations related to the sampling sites of *L. elliptica* (PC-K48, PC-KX4 correspond to animals collected at stations B, PC-P01 to station ID, and PC-P09 to animals collected at station C).

Iron concentrations in hemolymph were considerably higher than in seawater and bottom water, whereas Mn hemolymph concentrations were similar to concentrations in bottom water ($0.1\text{--}1.3\ \mu\text{mol L}^{-1}$) and pore water within the first centimetre below seafloor (cmbsf; $1.5\text{--}5.0\ \mu\text{mol L}^{-1}$). Pore water profiles down to 11 cmbsf are shown in figure 6.4. At station B (PC-K48, PC-KX4) Fe and Mn concentrations changed similarly with depth and peaked in 5 cmbsf (PC-K48; $167\ \mu\text{mol L}^{-1}$ Fe, $32\ \mu\text{mol L}^{-1}$ Mn) and 7 cmbsf (PC-KX4; $176\ \mu\text{mol L}^{-1}$ Fe, $40\ \mu\text{mol L}^{-1}$ Mn). Only within the first 3 cmbsf Fe and Mn concentrations increased faster at site PC-K48 compared to PC-KX4. At Station ID (PC-P01), close to the glacier, the highest maximum concentrations ($202\ \mu\text{mol L}^{-1}$ Fe in 9 cmbsf, $82\ \mu\text{mol L}^{-1}$ Mn in 11 cmbsf) were found for both elements, with the strongest increase between 1 cm and 3 cm depth. Compared to the other cores, core PC-P09 from the outer cove (station C) had the lowest peak Fe and Mn concentrations ($99\ \mu\text{mol L}^{-1}$ Fe in 2 cmbsf, $4.8\ \mu\text{mol L}^{-1}$ Mn in 11 cmbsf).

6.4.3. Tissue element analysis (Fe, Mn)

Manganese contents in DG and mantle ranged mostly between the detection limit (defined as three times the single standard deviation, SD) and the lowest calibration standard and are therefore not shown in figure 6.5. Differences in Fe and Mn contents between station B and the two reference stations (C, ID) were tested after normalisation to shell volume according to equation (6.1) to account for size

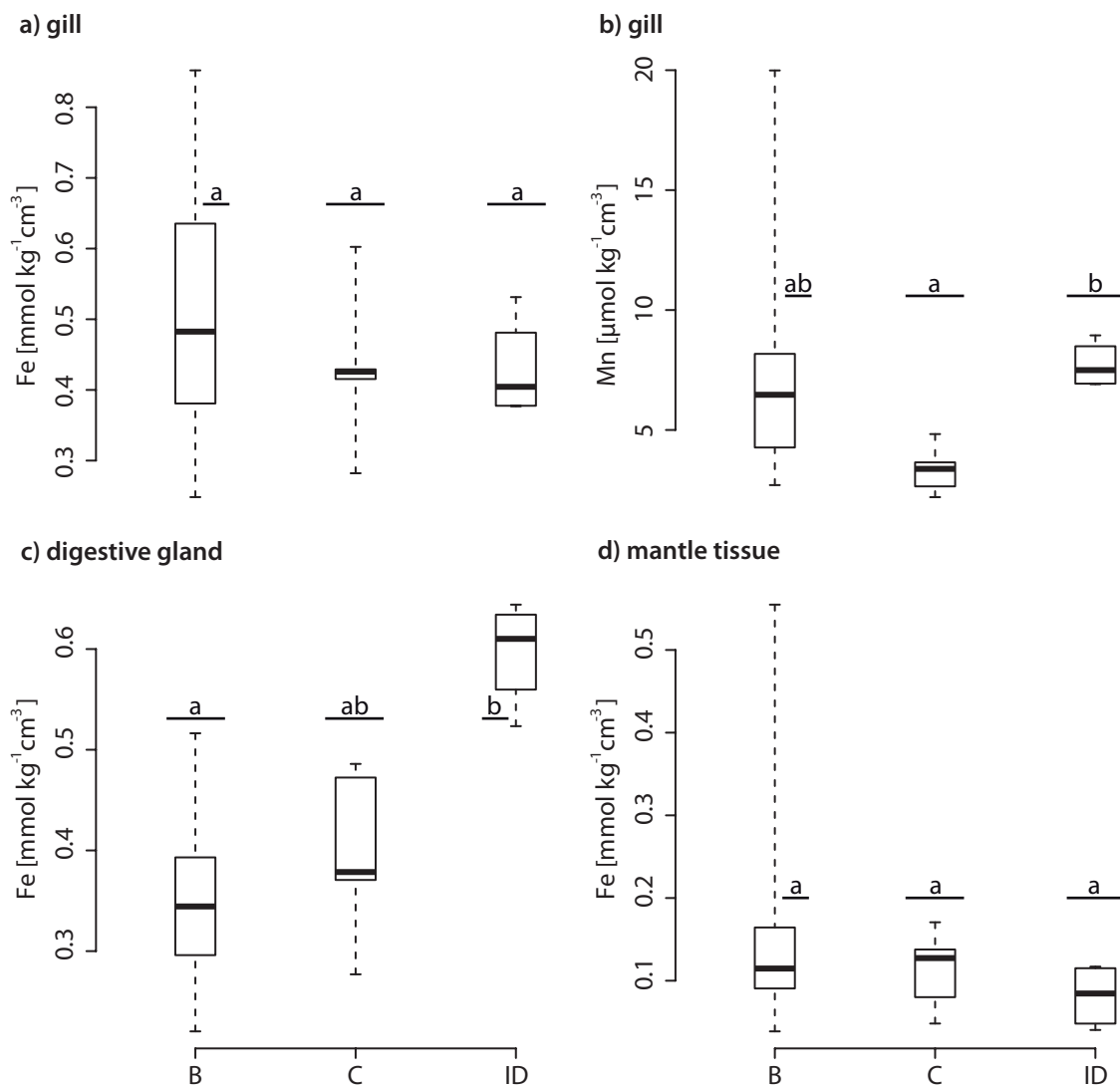


Fig. 6.5. Shell volume normalised Fe and Mn tissue contents: a) Fe contents in gills, b) Mn contents in gills, c) Fe contents in DG, d) Fe contents in mantle tissues. Mn contents in DG and mantle tissue are between the detection limit and lowest calibration standard and are therefore not shown. Tissue sample sizes (N) were 25 (B), 5 (C) and 4 (ID) for all elements, except for Fe contents in mantle tissues at station B (N=19). Boxplot whiskers represent the range. Different letters denote significant differences at an alpha level of 5%.

and age effects (e.g., individual life times, metabolic rates). Fe and Mn contents in gills did not differ significantly between stations B and C and B and ID (Fig. 6.5a, b). Mn contents differed significantly between stations C and ID. Particularly at station B tissue contents of both elements varied strongly. Fe contents in the DG were highest at station ID and the mean Fe content differed significantly between station ID and B (Fig. 6.5c). Mantle Fe contents did not differ significantly between all three stations (Fig. 6.5d).

6.5. Discussion

6.5.1. What controls Fe accumulation in *L. elliptica*?

Bivalves are basically iso-osmotic to the surrounding water, resulting in hemolymph concentrations of major seawater ions (e.g., Na^+ , Cl^- , SO_4^{2-}) similar to the environmental concentrations, as long as the clams' siphons (or shells of a mussel) remain open (Robertson, 1949; Robertson, 1953; Shumway, 1977; Willmer et al., 2000). In line with this, the major ion concentrations (Ca, K, Na, Sr; Table 6.2) in the hemolymph of *L. elliptica* did not differ from either seawater or pore water concentrations, and can, therefore, not be used to determine the source of hemolymph ions (pore water vs seawater). In contrast, in situ Fe hemolymph concentrations in *L. elliptica* from Potter Cove were several orders of magnitude above seawater concentrations and in the same order of magnitude as sediment pore water.

However, trace metal concentrations (e.g., Fe and Mn) in bivalve hemolymph are difficult to interpret with respect to their environmental sources, since they represent the product of cutaneous (gills) and intestinal (digestive tract) assimilation and the compartmentalisation into several tissues with varying turnover rates (George et al., 1976; Simkiss and Taylor, 1981; Simkiss and Mason, 1983). Once having entered the blood, Fe and Mn ions are bound to ligands (e.g., proteins, enzymes) to avoid cytotoxic effects (reviewed in Simkiss and Mason, 1983; Viarengo, 1985;

Gonzales et al., 2010; Gonzales and Puntarulo, 2011) and to initiate further storage, distribution or excretion (reviewed in Simkiss and Mason, 1983; Rainbow, 1990; Kadar et al., 2010). *Laternula elliptica* expresses the Fe storage protein ferritin in large quantities in DG, gills, and hemocyte cells (Husmann, 2013), which binds and thereby detoxifies cutaneously and intestinally assimilated Fe. Our results show that ~30% of the total Fe content in hemolymph of *L. elliptica* are bound in hemocytes, whereas ~70% are present in the plasma. The extracellular Fe fraction is likely more responsive to changing Fe concentrations in the immediate environment of the bivalves and explains the fast, linear decline in hemolymph Fe concentrations during the experimental exposure of *L. elliptica* to low concentrations of dissolved Fe. The faster decline of hemolymph Fe concentrations in filtered seawater compared to Fe spiked seawater reflects a strong dependence of hemolymph Fe concentrations on the levels of dissolved Fe in the incubation water. This linearity in declining Fe concentrations and the short half-lives of around ten days found in the hemolymph of *L. elliptica* are remarkably consistent to the results, which have been reported for the mussel *Mytilus edulis*.

George and Coombs (1977) investigated the Fe excretion during starvation in filtered seawater after the assimilation of particulate Fe(OH)₃ and dissolved Fe-EDTA. The authors found a linear decline in Fe content of the whole soft tissue of *M. edulis* after exposure to both Fe species, showing half-lives of ten days. Only animals treated with Fe(OH)₃ showed a fast Fe release during the first 24 h, due to the loss of non-absorbed Fe by feces, followed by the linear decline. Prolonged starvation did not reduce the mean Fe content below 20–25 mg kg⁻¹, which represented the permanent store (Hobden, 1967). Pentreath (1973) investigated the half-lives for Fe in several tissues in *M. edulis*, which ranged between 10 and 14 days, except for gills (21 days). The Fe residence times further remained constant with increasing Fe accumulation, due to an increasing excretion and a changing Fe distribution among tissues (George et al., 1976; George and Coombs, 1977). Beyond that Fe

accumulation in the whole tissue of *M. edulis* was linear to seawater concentrations of both $\text{Fe}(\text{OH})_3$ and Fe-EDTA during 25 days of exposure.

Hence, we interpret the Fe hemolymph concentrations and tissue contents as a function of the environmental bioavailable Fe, mediated by the Fe binding capacities of the different tissues. However, increasing metal concentrations are able to induce the synthesis of detoxifying ligands (metallothioneines; Viarengo, 1985). Rainbow (2002) further stated that there is no shortage of potential binding sites, due to the high affinity of trace metals to S and N, which are important components of amino acids and thus of proteins. Moreover, the toxicity of a metal is related to a species specific threshold concentration of metabolically available rather than the total metal concentration, because the binding of metals prevents proteins or other molecules from functioning in their metabolic role (Rainbow, 2002). Simplified, the detoxified Fe store includes physiologically essential Fe and non-labile Fe deposits (e.g., metal rich granules with high residence times), to which is added a variable amount of Fe in excess (temporary, metabolically available store), which is potentially toxic and needs to be excreted (see Rainbow, 2002). However, the accumulation and excretion of this temporarily and rapidly mobilised Fe store can be, but is not necessarily, linear for different tissues, as demonstrated for *M. edulis* and *L. elliptica*.

6.5.2. Combined geochemical and physiological interpretation of Fe accumulation pattern in *L. elliptica*

Based on the references above and our experimental results for *L. elliptica*, we expected a strong impact of bioavailable Fe sources in the immediate environment of the bivalve on its hemolymph concentrations. However, the hemolymph concentrations were considerably lower at station ID (juveniles), despite highest Fe pore water concentrations at this station (PC-P01). This discrepancy is attributed to a higher Fe incorporation into the shell related to lifetime mass specific respiration during the first years of lifetime (Dick et al., 2007) and, in particular, to a lower Fe

binding capacity, due to a smaller Fe-ligand pool in juveniles. Hemocyte cells of *L. elliptica* express the Fe storage protein ferritin in large quantities (Husmann, 2013), but hemolymph of younger individuals (<5.5 cm) contains only half the hemocytes (cells mL⁻¹) compared to adults (Husmann et al., 2011). Since our results showed that only ~30% of the total Fe in the hemolymph of *L. elliptica* is bound in hemocyte cells, age dependent differences are likely also applying to the binding of Fe in the extracellular ligand pool (e.g., extracellular ferritin, enzymes, proteins). In the DG ferritin is stronger expressed in juveniles than in adults (Husmann, 2013), which explains the significantly higher normalised Fe contents in DG at station ID.

In contrast, neither hemolymph Fe concentrations nor normalised Fe tissue contents differed significantly among adult animals from station B (melt water inlets) and C (outer cove). This agrees with the pore and bottom water profiles of dissolved Fe, which has been proposed as important sources of dissolved metals for the deposit feeding clam *Macoma balthica* (Griscom and Fisher, 2004 and references therein). Iron concentrations were similar among stations in bottom water (0.1–0.3 μmol L⁻¹ Fe) and roughly in pore water down to 5 cmbsf (100–170 μmol L⁻¹ Fe).

Numerous geochemical studies have demonstrated the release of dissolved Fe (and Mn) from pore water into the benthic boundary layer and overlying water by diffusion or advection (Elderfield, 1976; Sundby and Silverberg, 1981; Sundby and Silverberg, 1985; Slomp et al., 1997; Dellwig et al., 2007; Beck et al., 2008b; Severmann et al., 2010; Kowalski et al., 2012), even though bioturbative/irrigative fluxes are more important than diffusive fluxes (Raiswell and Canfield, 2012). However, as soon as dissolved, inorganic Fe(II) enters oxic sediment layers or seawater, it immediately oxidises to the more stable oxidation state Fe(III), which is affected by strong hydrolysis and precipitates as nanoparticulate iron (oxyhydr) oxides (Ahrland, 1975; Millero et al., 1995; Waite, 2001), particularly as metastable ferrihydrite (Fe₄HO₈ x 4 H₂O, earlier specified as Fe(OH)₃; reviewed in Raiswell and Canfield, 2012). This mineral forms poorly ordered nanoparticles

(1–5 nm), which are characterised by a high solubility and reactivity and are, thus, highly bioavailable (Raiswell and Canfield, 2012). Since bivalves assimilate Fe nanoparticles via endocytosis by specific epithelial cells in gills and viscera (George et al., 1976; Kadar et al., 2010), an assimilation of precipitated pore water Fe as ferrihydrite explains the coexistence of high Fe contents in the bivalve and low Fe concentrations in the bottom water. However, the assimilation of particulate Fe is likely restricted to easily dissolvable ferrihydrite, since ferrihydrites aggregate or alter to several other iron (oxyhydr)oxides (e.g., goethite, haematite) of lower solubility and poor bioavailability (Raiswell and Canfield, 2012) and the pH in the DG of *L. elliptica* (5.8–6.5; Poigner, unpublished) appears to be too high, to degrade crystalline Fe oxides or silicates (compare Thomas and Bendell-Young, 1998 for the clam *M. balthica*; Turner and Olsen, 2000 for the plaice *Pleuronectes platessa*).

Aqueous Fe(II) is further discharged by anoxic subglacial waters into oxic seawater or surface freshwaters, where it rapidly oxidises to ferrihydrite nanoparticles (Raiswell et al., 2006; Raiswell et al., 2008). In PC high particle loads are restricted to the upper seven metres in the water column and associated to low salinities, due to the import by melt water streams (Monien et al., 2013). Even though these suspended particles are rich in easily dissolvable iron (oxyhydr)oxides, most of it is transported to the Southern Ocean rather than being deposited in PC (Monien et al., 2013). Hence, we interpret differences in sedimentation of terrigenous, lithogenic material (represented by station B, C) as insignificant for the overall explanation of Fe accumulation pattern in PC, contrary to other authors before (Abele et al., 2008; Curtosi et al., 2010; Husmann et al., 2012). A potential influence is locally restricted to substation B21, since it is located in only five metres depth in front of melt water inlets and accounts for the higher variation in Fe tissue contents and hemolymph concentrations of station B.

Absolute tissue Fe and Mn contents (gills, DG, mantle) in adults (station B, C) are in the same order of magnitude as reported earlier for adults from KGI (Table 6.3)

and variations in mean contents among different KGI studies are likely a result of lacking normalisation, although adult shell lengths were similar. Philipp et al. (2008) showed a high inter-individual variability in the shell length-age relationship. An age range between 10 and 36 years was, for instance, observed for individuals with

Table 6.3. Mean contents \pm 95% confidence intervals [mg kg^{-1} dry weight] of Fe and Mn in tissues (DG = digestive gland, MAN = mantle tissue) of *L. elliptica* for all three stations. Sample sizes were 25 for station B and 5 for each of station C and ID, except mantle tissue samples of station B (N=19). Results of this study are compared with tissue concentrations of previous studies (mean \pm SD).

Location	Fe			Mn			Shell length [mm]	Source
	DG [mg kg^{-1} dw]	Gill [mg kg^{-1} dw]	MAN [mg kg^{-1} dw]	DG [mg kg^{-1} dw]	Gill [mg kg^{-1} dw]	MAN [mg kg^{-1} dw]		
B	1444 \pm 154	2060 \pm 305	764 \pm 315		29 \pm 8.3		73.2 - 90.7	this study
C	1864 \pm 668	2006 \pm 678	549 \pm 385		15 \pm 2.6		85.0 - 101.8	this study
ID	981 \pm 404	639 \pm 233	119 \pm 58		11 \pm 3.4		56.9 - 63.8	this study
Deception Island			9200 \pm 2200			700 \pm 400	-	Deheyn, 2005
Maxwell Bay (KGI)	2000 \pm 720	2000 \pm 650		18.6 \pm 7.5	44.7 \pm 16.3		72 - 95	Ahn et al., 1996
Potter Cove (KGI)	1660 \pm 653	1360 \pm 360	572 \pm 484	9.2 \pm 6.6	11.4 \pm 3.2	7.4 \pm 3.8	76 \pm 8	Husmann et al., 2012
Potter Cove (KGI)	1150 \pm 310	350 \pm 64	377 \pm 102	11.9 \pm 3.8	7.1 \pm 0.8	5.9 \pm 1.4	43 \pm 6	Husmann et al., 2012
Potter Cove (KGI)	1070 \pm 50			4.1 \pm 0.4			>70	Curtosi et al., 2010
Rothera Point	422 \pm 19	371 \pm 25	98.5 \pm 7.7	3.3 \pm 0.07	4.2 \pm 0.15	1.42 \pm 0.04	59.2 - 83.5	Lohan et al., 2001
Terra Nova Bay	145 \pm 58	178 \pm 56		4.5 \pm 0.4	5.1 \pm 0.7		-	Nigro et al., 1997

a shell length of 76 mm (hence we normalised on shell volume). Therefore, we conclude that lifetime integrated accumulation can vary greatly across homogenous shell length classes at one and the same site and also between different sampling sites.

However, adults from KGI (Marian Cove, PC) have tissue contents (Fe, Mn) up to ten times higher than animals from Adelaide Island and Terra Nova Bay (Ahn et al., 1996; Nigro et al., 1997; Lohan et al., 2001; Curtosi et al., 2010; Husmann et al., 2012; this study), which had even distinctly lower Fe contents than juveniles from PC (Table 6.3). Highest Fe and Mn accumulations have been reported in the mantle of *L. elliptica* found at Deception Island (9,200 mg kg⁻¹ dry weight), even though the mantle is the tissue of lowest Fe accumulation (Husmann et al., 2012; this study) and ferritin expression (Husmann, 2013). These high metal loads arise from volcanic geothermal activity (Deheyn et al., 2005), which releases dissolved metals via diffuse sources ('non-point source') into the benthic environment and elevates seawater concentrations (3.2 µmol L⁻¹ Fe, 0.5–2.3 µmol L⁻¹ Mn; Elderfield, 1972; Rey et al., 1995). Geothermal waters appear analog to pore waters according to the diffusion of bioavailable, dissolved metals towards the benthic boundary. Hence, the ingestion of freshly precipitated ferrihydrites from leaking geothermal or pore waters at the sediment surface could explain the high Fe contents in *L. elliptica* at Deception Island and PC.

6.5.3. Manganese assimilation by *L. elliptica*

Although Mn is also essential for enzyme activation and cellular processes in bivalves (Carmichael et al., 1980; Simkiss and Mason, 1983; Park et al., 2009), tissue and hemolymph concentrations of *L. elliptica* are remarkably low compared to Fe, which can be explained by a smaller Mn reservoir for the assimilation by *L. elliptica*.

The kinetic oxidation of dissolved Mn²⁺ to solid MnO₂ is slow compared to Fe (Knox and Turner, 1980; Roits et al., 2002) and its complexation to organic ligands (e.g., Knox and Turner, 1980; Roitz and Bruland, 1997; L'Her Roux et al., 1998) and adsorption onto hydrous Fe oxides (Sholkovitz, 1978) is considered as inconsequential. Consequently, Mn remains primarily as free Mn²⁺ and MnCl⁺ in the

water column (Roitz et al., 2002) and behaves independently from Fe (Knox and Turner, 1980). Since silicate bound Mn is not bioavailable to the bivalve (compare chapter 6.4.2), dissolved Mn around the benthic boundary constitutes the major Mn source for *L. elliptica*. This also explains the conformity of hemolymph (0.1–4.0 $\mu\text{mol L}^{-1}$ Mn; Tab. 6.2), bottom water (0.2–1.2 $\mu\text{mol L}^{-1}$ Mn; Fig. 6.5) and pore water Mn concentrations down to 0.5 cmbsf (1.5–5 $\mu\text{mol L}^{-1}$ Mn; Fig. 6.5). Further, normalised Mn gill contents were significantly higher at station ID than at station C, which correspond to the higher Mn pore water concentrations and the steeper gradient of dissolved Mn at station ID (PC-P01; Fig. 6.4). This likely reflects a higher assimilation at this site, since dissolved ions are primarily assimilated via the gills (reviewed in Simkiss and Mason, 1983; Rainbow, 1990; Kadar et al., 2010) and accumulation effects due to different lifetimes were eliminated by normalisation. This observed proportionality between Mn concentrations in hemolymph and pore/bottom water is difficult to explain physiologically, although linearity between tissue metal accumulation and environmental concentrations was observed for Mn and other elements and different species (reviewed in Simkiss and Mason, 1983; Metian et al., 2009).

In case of *L. elliptica* one possible explanation may be a limited pool of Mn-ligands, to complex free Mn-ions as soon as they enter the hemolymph after cutaneous or intestinal assimilation. Although Mn-containing enzymes exist in *L. elliptica* (e.g., Mn-SOD; Park et al., 2009), no analogue to the high-capacity Fe storage protein ferritin (Husmann, 2013) is known for Mn. Thus, other tissues may be of minor importance for Mn-storage and Mn is predominately transferred to excretion sites (kidney). In this case, an increased Mn turnover could keep Mn hemolymph concentrations low (e.g., at or lower environmental levels) and avoid toxic effects due to unbound Mn or Mn excess. Dissolved Mn concentrations lethal to 50% of the test individuals (LC-50) were $\sim 0.55 \text{ mmol L}^{-1}$ (48 h) for larvae of *Mytilus edulis* (Morgan et al., 1986) and $\sim 5.5 \text{ mmol L}^{-1}$ (168 h) for *Mya arenaria* (Eisler, 1977). Hence, Mn pore water

concentrations in Potter Cove are far below the reported LC-50 concentrations.

Nevertheless, the assumptions above are supported by remarkable small half-lives (7–26 days) of Mn in *Mytilus edulis* reflecting a very dynamic state (Pentreath, 1973). Further, Mn tissue contents (gills, mantle, foot, muscle) were mostly unaffected during starvation (Pentreath, 1973) indicating a low exchange among hemolymph and tissues. In the kidney, Mn is accumulated and primarily excreted as inorganic, metal-rich granules (reviewed in Simkiss and Mason, 1983).

Although the presented concept explains the observations for *L. elliptica* in PC, it remains speculative, since detailed studies concerning Mn distribution and residence times in tissues are lacking for *L. elliptica*.

6.6. Conclusions and Outlook

In figure 6.6 we summarise the Fe and Mn uptake pathways for *L. elliptica* in PC. For both elements we assume the flux of Fe- and Mn-rich pore water into the oxic sediment layer or across the benthic boundary as important source for the bivalve, even though the assimilation may differ. Since Mn oxidation is relatively slow compared to the oxidation of Fe and Mn concentrations in hemolymph were as low as in bottom water or in the pore water of the first cmbsf, we expect a predominant assimilation of dissolved Mn(II). In contrast, Fe hemolymph concentrations were considerable higher than bottom water concentrations, indicating an additional assimilation route, due to the strong impact of environmental Fe concentrations on hemolymph concentrations shown in our experiments. This bioavailable Fe is likely provided by bioavailable iron (oxyhydr)oxides, in particular ferrihydrite nanoparticles, precipitated from dissolved Fe after diffusion into the oxic sediment or bottom water layer. A minor fraction of bioavailable iron (oxyhydr)oxides is potentially provided by scavenging after precipitation in the water column or by the import via melt water at very shallow locations close to the inlets of melt water streams (e.g., substation B21).

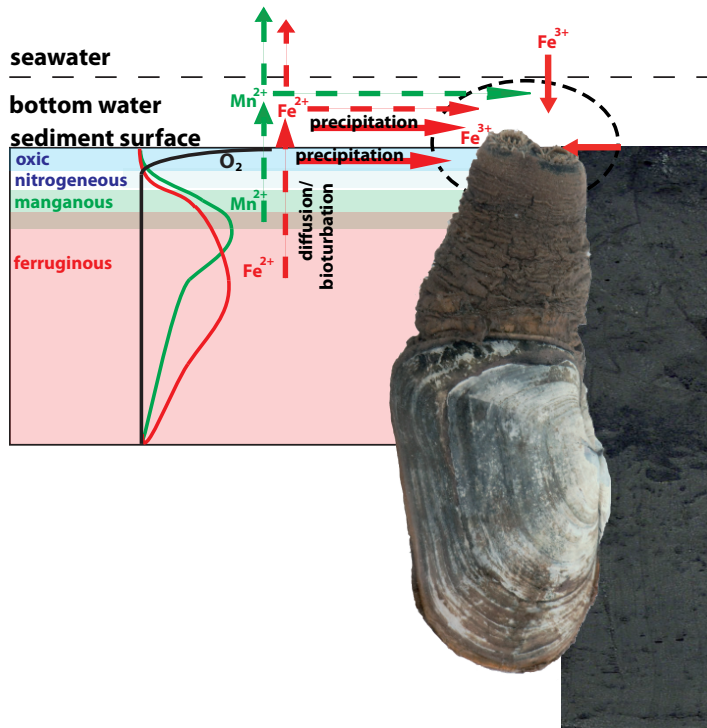


Fig. 6.6. Possible Fe and Mn uptake pathways for *L. elliptica* in Potter Cove related to diagenetic processes in the upper sediment layers. Dashed lines represent the fluxes of aqueous Fe(II) (red) and Mn(II) (green). Solid, red lines represent the assimilation of precipitated Fe (oxyhydr)oxides, in particular ferrihydrite. Chemical zonation of the diagenetic series after Froelich et al. (1979) and Canfield and Thamdrup (2009).

However, in this study significant differences in Fe accumulation were related to age-specific changes in physiology, particularly to Fe-binding capacities and Fe incorporation into the shell. Further, no significant differences related to the geochemical influence on metal contents in *L. elliptica*

were found in PC. This contrasts earlier studies, which assumed the high input of lithogenic sediment from glaciers into the cove to be causal of high Fe contents

in *L. elliptica*. Hence, our results challenge the proposed potential of Fe (and Mn) as proxy for the melt water import of eroded bedrock material into the cove. Although pore water data are lacking for other sites (Adelaide Island, Terra Nova Bay), we assume that differences in the geochemical environment cause the variations in Fe and Mn accumulation in *L. elliptica* around Antarctica, as it was discussed for Deception Island (geothermal influence) and PC (non-active volcanic site).

6.7. Acknowledgements

We would like to thank Stefanie Meyer (AWI) for her support during expedition preparations. Further we would like to thank her and Ilsetraut Stölting (AWI) for their

help in the laboratories. The divers and the crew of the Argentinean Antarctic Station Carlini are thanked for their logistic help. Additional analysis of reference materials were done by Norman Lofffield (Institute of Soil Science of Temperate Ecosystems, University of Göttingen) to prove the correctness of our digestion procedure. This work was supported by the German Research Foundation (DFG) under grants AB 124/11-1 and BR 775/25-1 in the framework of priority program 1158 – Antarctic Research and is associated to the IMCOAST project. Dorothee Wilhelms-Dick acknowledges the DFG for financial support (GRK 717: Proxies in Earth History). We also thank the two anonymous reviewers and the editor who greatly improved the manuscript.

7. Climate fluctuations during the past two millennia as recorded in sediments from Maxwell Bay, South Shetland Islands, West Antarctica

H. Christian Hass^a, Gerhard Kuhn^b, Patrick Monien^c, Hans-Jürgen Bumsack^c, Matthias Forwick^d

^a Alfred Wegener Institute for Polar and Marine Research, Wadden Sea Research Station, Hafenstrasse 43, D-25992 List, Germany

^b Alfred Wegener Institute for Polar and Marine Research, Am Alten Hafen 26, D-27568 Bremerhaven, Germany

^c ICBM, Oldenburg University, P.O. Box 2503, D-26111 Oldenburg, Germany

^d Department of Geology, University of Tromsø, N-9037 Tromsø, Norway

This paper is published in *Geological Society, London, Special Publications*, **344**, 243-260 (2010).

Abstract

The climate evolution of the South Shetland Islands during the last c. 2,000 years is inferred from the multiproxy analyses of a long (928 cm) sediment core retrieved from Maxwell Bay off King George Island. The vertical sediment flux at the core location is controlled by summer melting processes that cause sediment-laden melt water plumes to form. These leave a characteristic signature in the sediments of NE Maxwell Bay. We use this signature to distinguish summer and winter-dominated periods. During the Medieval Warm Period, sediments are generally finer which indicates summer-type conditions. In contrast, during the Little Ice Age (LIA) sediments are generally coarser and are indicative of winter-dominated conditions. Comparison with Northern and Southern Hemisphere, Antarctic, and

global temperature reconstructions reveals that the mean grain-size curve from Maxwell Bay closely resembles the curve of the global temperature reconstruction. We show that the medieval warming occurred earlier in the Southern than in the Northern Hemisphere, which might indicate that the warming was driven by processes occurring in the south. The beginning of the LIA appears to be almost synchronous in both hemispheres. The warming after the LIA closely resembles the Northern Hemisphere record which might indicate this phase of cooling was driven by processes occurring in the north. Although the recent rapid regional warming is clearly visible, the Maxwell Bay record does not show the dominance of summer-type sediments until the 1970s. Continued warming in this area will likely affect the marine ecosystem through melt water induced turbidity of the surface waters as well as an extension of the vegetation period due to the predicted decrease of sea ice in this area.

8. A new Holocene relative sea level curve for the South Shetland Islands, Antarctica

Emma P. Watcham^a, Michael J. Bentley^{a,b}, Dominic A. Hodgson^b, Stephen J. Roberts^b, Peter T. Fretwell^b, Jerry M. Lloyd^a, Robert D. Larter^b, Pippa L. Whitehouse^a, Melanie J. Leng^c, Patrick Monien^d, Steven G. Moreton^e

^a Durham University, Department of Geography, Science Laboratories, South Road, Durham DH1 3LE, UK

^b British Antarctic Survey, High Cross, Madingley Road, Cambridge CB3 0ET, UK

^c NERC Isotope Geosciences Laboratory, British Geological Survey, Nottingham NG12 5GG, UK

^d University of Oldenburg, Institute for Chemistry and Biology of the Marine Environment, Department of Microbiogeochemistry, D-26111 Oldenburg, Germany

^e NERC Radiocarbon Facility, Scottish Enterprise Technology Park, Rankine Avenue, East Kilbride, Glasgow G75 0QF, UK

This paper is published in *Quaternary Science Reviews*, **30**, 3152-3170 (2011).

Abstract

Precise relative sea level (RSL) data are important for inferring regional ice sheet histories, as well as helping to validate numerical models of ice sheet evolution and glacial isostatic adjustment. Here we develop a new RSL curve for Fildes Peninsula, South Shetland Islands (SSIs), a sub-Antarctic archipelago peripheral to the northern Antarctic Peninsula ice sheet, by integrating sedimentary evidence from isolation basins with geomorphological evidence from raised beaches. This combined approach yields not only a Holocene RSL curve, but also the spatial pattern of how RSL change varied across the archipelago. The curve shows a mid-Holocene RSL highstand on Fildes Peninsula at 15.5 m above mean sea level between 8,000 and 7,000 cal yr BP. Subsequently RSL gradually fell as a consequence of isostatic uplift

in response to regional deglaciation. We propose that isostatic uplift occurred at a non-steady rate, with a temporary pause in ice retreat ca. 7,200 cal yr BP, leading to a short-lived RSL rise of ~1 m and forming a second peak to the mid-Holocene highstand. Two independent approaches were taken to constrain the long-term tectonic uplift rate of the SSIs at 0.22–0.48 m kyr⁻¹, placing the tectonic contribution to the reconstructed RSL highstand between 1.4 and 2.9 m. Finally, we make comparisons to predictions from three global sea level models.

9. The influence of sedimentation on metal accumulation and cellular oxidative stress markers in the Antarctic bivalve *Laternula elliptica*

Gunnar Husmann^a, Doris Abele^b, Donata Monien^c, Patrick Monien^c, Michael Kriews^b, Eva E.R. Philipp^a

^aInstitute of Clinical Molecular Biology, Christian-Albrechts University Kiel, Schittenhelmstraße 12, 24105 Kiel, Germany

^bAlfred Wegener Institute for Polar and Marine Research, Am Handelshafen 12, 27570 Bremerhaven, Germany

^cInstitute for Chemistry and Biology of the Marine Environment (ICBM), Dep. of Microbiogeochemistry, Carl von Ossietzky University Oldenburg, P.O. Box 2503, 26111 Oldenburg, Germany

This paper is published in *Estuarine, Coastal and Shelf Science*, **111**, 48-59 (2012).

Abstract

Recent rapid climate warming at the western Antarctic Peninsula (WAP) results in elevated glacial melting, enhanced sedimentary run-off, increased turbidity and impact of ice-scouring in shallow coastal areas. Discharge of mineral suspension from volcanic bedrock ablation and chronic physical disturbance is expected to influence sessile filter feeders such as the Antarctic soft shell clam *Laternula elliptica* (King and Broderip, 1832). We investigated effects of sedimentary run-off on the accumulation of trace metals, and together with physical disturbance, the cumulative effect on oxidative stress parameters in younger and older *L. elliptica* from two stations in Potter Cove (King George Island, Antarctica) which are distinctly

impacted by turbidity and ice-scouring. Fe, Mn, Sr, V and Zn concentrations were slightly higher in sediments of the station receiving more sediment run-off, but not enriched in bivalves of this station. The only element that increased in bivalves experimentally exposed to sediment suspension for 28 days was Mn. Concentration of the waste accumulation biomarker lipofuscin in nervous tissue was higher in *L. elliptica* from the “exposed” compared to the “less exposed” site, whereas protein carbonyl levels in bivalve mantle tissue were higher at the less sediment impacted site. Tissue metal content and lipofuscin in nervous tissue were generally higher in older compared to younger individuals from both field stations. We conclude that elevated sediment ablation does not per se result in higher metal accumulation in *L. elliptica*. Instead of direct absorbance from sediment particles, metal accumulation in gills seems to indicate uptake of compounds dissolved in the water column, whereas metals in digestive gland appear to originate from enriched planktonic or detritic food. Accumulation of cellular waste products and potentially reactive metals over lifetime presumably alters *L. elliptica* physiological performance with age and may contribute to higher stress susceptibility in older animals.

10. On the phytoplankton bloom in coastal waters of southern King George Island (Antarctica) in January 2010: An exceptional feature?

I. R. Schloss^{a,b,c}, A. Wasilowska^d, D. Dumont^c, G.O. Almandoz^{e,b}, M.P. Hernando^f, C.-A. Michaud-Tremblay^c, L. Saravia^g, M. Rzepecki^h, P. Monienⁱ, D. Monienⁱ, E.E. Kopczyńska^j, V. Bers^k, G.A. Ferreyra^c

^a Instituto Antártico Argentino, Ciudad de Buenos Aires, Argentina

^b Consejo Nacional de Investigaciones Científicas y Técnicas, Ciudad de Buenos Aires, Argentina

^c Institut des sciences de la mer, Université du Québec à Rimouski, Rimouski, Canada

^d Warsaw University, Faculty of Geology, Warsaw, Poland

^e División Ficología, Facultad de Ciencias Naturales y Museo, Universidad Nacional de La Plata, La Plata, Argentina

^f Comisión Nacional de Energía Atómica, San Martín, Buenos Aires, Argentina

^g Área Biología y Bioinformática, Instituto de Ciencias, Universidad Nacional de General Sarmiento, Los Polvorines, Buenos Aires Argentina

^h Centre for Ecological Research, Polish Academy of Sciences, Poland

ⁱ Institute for Chemistry and Biology of the Marine Environment, Carl-von-Ossietzky University Oldenburg, Oldenburg, Germany

^j Institute of Biochemistry and Biophysics, Polish Academy of Science, Department of Antarctic Biology, Warsaw, Poland

^k Alfred-Wegener-Institute for Polar and Marine Research, Bremerhaven, Germany

This paper is published in *Limnology & Oceanography*, **59**(1), 195-210 (2014).

Abstract

Since the early 1990s, phytoplankton has been studied and monitored in Potter Cove (PC) and Admiralty Bay (AB), King George/25 de Mayo Island (KGI), South Shetlands. Phytoplankton biomass is typically low compared to other Antarctic shelf

environments, with average spring - summer values below 1 mg chlorophyll *a* (Chl *a*) m⁻³. The physical conditions in the area (reduced irradiance induced by particles originated from the land, intense winds) limit the coastal productivity at KGI, as a result of shallow Sverdrup's critical depths (Z_c) and large turbulent mixing depths (Z_t). In January 2010 a large phytoplankton bloom with a maximum of around 20 mg Chl *a* m⁻³, and monthly averages of 4 (PC) and 6 (AB) mg Chl *a* m⁻³, was observed in the area, making it by far the largest recorded bloom over the last 20 yr. Dominant phytoplankton species were the typical bloom-forming diatoms that are usually found in the western Antarctic Peninsula area. Anomalously cold air temperature and dominant winds from the eastern sector seem to explain adequate light:mixing environment. Local physical conditions were analysed by means of the relationship between Z_c and Z_t , and conditions were found adequate for allowing phytoplankton development. However, a multi-year analysis indicates that these conditions may be necessary but not sufficient to guarantee phytoplankton accumulation. The relation between maximum Chl *a* values and air temperature suggests that bottom-up control would render such large blooms even less frequent in KGI under the warmer climate expected in the area during the second half of the present century.

11. Summary & Outlook

The western Antarctic Peninsula (WAP) is one of the most sensitive and dynamic areas on Earth, where ecological and cryospheric systems respond rapidly to climate changes. During the last six decades this region has experienced a unique rapid recent warming trend, which is related to dramatic changes in the extent of sea and land ice, sea level, community structures and food chains. This, in turn, has put an increased scientific focus on this specific region. In order to understand long-term trends in climate variability and to test climate models used to predict future climate changes, reconstructions of the past climate are fundamental.

This thesis focuses on the reconstruction of the palaeoenvironmental conditions at the northern WAP during the Holocene using inorganic geochemical proxies in marine and lacustrine sedimentary archives. In addition, another emphasis was put on biogeochemical processes in WAP sediments and their recent impact on local benthic and pelagic communities.

The chemical composition of seabird influenced lacustrine archives was used to reconstruct a high-resolution history of penguin populations on Ardley Island, which was compared with other regional records of past penguin occupation and palaeoclimate along the WAP during the last 9,000 years. Sediments from two neighbouring lakes on Ardley Island and Fildes Peninsula, King George Island, WAP, were therefore analysed for biogeochemical markers (As, Ba, Ca, Cd, Cu, Hg, P, TS, Se, Sr, and Zn) uniquely associated with penguin guano (chapter 4). The results indicate that penguins occupied Ardley Island since 7.4 cal kyr BP and that their colonies have undergone several fluctuations in the following millenia. While some factors that determine breeding success such as pressure from predators, the ability to change diet, or recent anthropogenic impacts could not be assessed,

this study has revealed the key factors influencing penguin populations on Ardley Island through the Holocene. It is strongly suggested that local penguin colonies appear to be generally associated with variations in regional climate and sea-ice extent. Furthermore, they have experienced several rapid and catastrophic crashes as a result of volcanic eruptions. The highest populations were detected at 6.1–5.2 cal kyr BP, 4.3–3.4 cal kyr BP during the Mid-Holocene Hypsithermal, and at 2.0–1.4 cal kyr BP. There is evidence that Gentoo penguin colonies expanded to occupy more inland areas of Ardley Island during ‘warmer’ phases. In addition to volcanic activity, low population episodes seem to have coincided with colder periods with the expansion of land and sea-ice creating unfavourable breeding conditions for Gentoo penguins. Despite recent links between increased Gentoo penguin populations and the warming climate, penguin populations on Ardley Island nowadays appear to be still well below their Holocene optima.

The variability in regional Holocene climate was moreover documented by a comprehensive geochemical dataset of marine sediments from the WAP region (chapter 3). Radiocarbon and ^{210}Pb data revealed that the composite core taken from Maxwell Bay, King George Island, WAP comprises a palaeoclimatic record of the past two millennia with high sedimentation rates ranging from 0.2 to 1.7 cm yr⁻¹. The age model was validated by ten tephra layers, which were detected by quantitative XRF measurements and microscopic methods and could directly be linked to previous eruptions from nearby Deception Island. Major and trace element distribution patterns of the sediments suggest that their composition is mainly controlled by the lithogenic background of the study area, consisting of tholeiitic basaltic andesites most probably derived from the nearby Barton Peninsula. However, some geochemical indicators give also evidence that the primary composition is influenced by early diagenetic processes (U, TS) and by a changing primary production (TOC, biogenic silica/ $\text{SiO}_{2\text{xs}}$) at the study site. Palaeoclimatic interpretation of the sediment proxies indicates that the study site has experienced short-term alternations in regional climate during the

last c. 2,000 yr, which underlines the climatically sensitive character of this area. Periods of retreating and re-advancing of glaciers on the nearby Barton Peninsula probably led to changes in the supply area. Variations in selected element ratios as well as in the mean grain size allowed to identify two main climatic events during the Late Holocene that are equivalent in timing to the Little Ice Age (~550–50 cal yr BP) and the Medieval Warm Period (~1,400–550 cal yr BP) of the Northern Hemisphere. Moreover, the recent rapid regional warming trend is reflected in this sedimentary sequence. Using ^{210}Pb data from Maxwell Bay surface sediments, it could be shown that since the end of the 1930s mass accumulation rates have almost tripled up to the present day ($0.66 \text{ g cm}^{-2} \text{ yr}^{-1}$). This clearly documents the enhanced input of eroded particulate material into coastal areas and could directly be linked to the concurrent glacier retreat at the WAP as described by Cook et al. (2005). If air temperatures will continuously rise, as predicted in the latest IPCC report (Solomon et al., 2007), the input of particulate matter via melt water streams may further increase. This in turn may have severe consequences for local marine ecosystems in this sensitive region.

The possible influence of enhanced sediment accumulation on benthic communities and trace metal cycling in coastal sediments was discussed in some interdisciplinary studies (chapters 6 and 9) and in biogeochemical investigations of recent sedimentary deposits in Potter Cove, King George Island (chapter 5). In this context redox-sensitive trace elements, nutrients and terminal metabolic products were used to describe redox conditions and biogeochemical processes in pore waters from maritime Antarctica. Geochemical data obtained from 13 sediment cores, which were taken at different locations in the cove, revealed that sulphate reduction is the dominant pathway of organic matter oxidation. This is particularly true for the shallower zones at the southern coast of Potter Peninsula and on a transect towards the northwestern area of the inner cove. Modelled sulphate reduction rates ($0.23\text{--}0.56 \text{ mol m}^{-2} \text{ yr}^{-1}$) were found to be an order of magnitude lower than known

from coastal sediments in other sub-Antarctic or temperate regions (Nedwell, 1989; Sørensen et al., 1979) but comparable to those determined in coastal sediments off Greenland (Rysgaard et al., 1996). In contrast, microbial manganese and dissimilatory iron reduction processes seem to be prevailing in the deeper troughs (<40 m water depth) of the central cove and in the newly ice-free area near the glacier front. It is assumed that at these locations metal oxide reduction is favoured over sulphate reduction due to a combination of i) enhanced physical and biological disturbance by bottom water currents, ice scouring and burrowing organisms, ii) the increased accumulation of melt water derived, fine-grained material with high amounts of reactive metal oxides and iii) the reduced availability of metabolisable organic matter. Using a novel inverse method for the estimation of biogeochemical rates from measured pore water concentrations (Lettmann et al., 2012) iron reduction rates were calculated for the study area. These rates provided the basis for a first estimation of an Antarctic shelf-derived input of potentially bioavailable iron to the Southern Ocean. The contribution ($1.2\text{--}18\text{ mg m}^{-2}\text{ yr}^{-1}$) is in the same range than the flux from melting icebergs and significantly higher than the input by aeolian dust or previous estimates for the continental shelf. This supports the assumption that the ferruginous shelf sediments are probably a key source for this micronutrient in vast regions of the Southern Ocean, where iron still limits bioproductivity. In consequence of enhanced glacier retreat and melt water fluxes and the related increase in the accumulation of iron-rich sediments on the shelf, it can be assumed that the relevance of Antarctic shelf sediments for the natural iron fertilisation of the Southern Ocean may even increase.

Despite of the broad focus of this thesis on several geochemical topics, some open questions remain, which require further investigation. The knowledge about biogeochemical processes and trace metal cycling in nearshore surface sediments of the Antarctic may be important to shed more light on the relevance of local shelf sediments as a source for essential elements, like iron. Particularly considering that

estimates showed that the increase in Fe-induced productivity could have contributed about 30% to the 80-ppm drawdown in atmospheric CO₂ observed during glacial maxima by enhancing the ocean's biological pump (Sigman and Boyle, 2000). However, more studies including Fe isotope analyses are necessary to establish robust mathematical models to better estimate the Fe input to the Southern Ocean in a warming world.

Whereas the anthropogenic emission of greenhouse gases seems to be a major driver for the observed warming during the last decades (Oreskes, 2004; Solomon et al., 2007), the primary forcing mechanisms underlying the regional Holocene climate variability at the WAP are still not fully understood. Among changes in solar insolation and in the Southern Westerlies (Bentley et al., 2009; Khim et al., 2002; Leventer et al., 1996; Marshall et al., 2006), variations in the El Niño Southern Oscillation (ENSO) are discussed (e.g., Simmonds, 2003). Other authors relate changes in the North Atlantic thermohaline conditions and warm surface anomalies in the North Atlantic to AP climate variability (Broecker, 2001; Goosse et al., 2004; Nielsen et al., 2004). The influence of the Antarctic Circumpolar Current (ACC) and the associated upwelling of Circumpolar Deep Water (CDW) on the WAP continental shelf as an oceanographic mechanism possibly driving past and present changes in climate at the WAP (Bentley et al., 2009; Domack et al., 2003; Shevenell and Kennett, 2002) may further be of importance. To date the palaeoflow history of the CDW and its impact on variations in atmospheric circulations is not resolved. Geochemical provenance analyses complemented by investigations of stable metal isotopes (REE, Sr, Pb) in detrital and authigenic phases of glacio-marine sediments deposited along the WAP may therefore provide more insights into the changing influence of the CDW during the Holocene as an important factor for regional climate variability.

12. References

- Abele D., Atencio A., Dick D., Gonzalez O., Kriews M., Meyer S., Philipp E. and Stoelting I. (2008) Iron, copper and manganese discharge from glacial melting into Potter Cove and metal concentrations in *Laternula elliptica* shells. *Berichte zur Polar- und Meeresforschung* **571**, 39–46.
- Abraitis P. K., Patrick R. A. D. and Vaughan D. J. (2004) Variations in the compositional, textural and electrical properties of natural pyrite: a review. *Int. J. Miner. Process.* **74**, 41–59.
- Abram N. J., Mulvaney R., Wolff E. W., Triest J., Kipfstuhl S., Trusel L. D., Vimeux F., Fleet L. and Arrowsmith C. (2013) Acceleration of snow melt in an Antarctic Peninsula ice core during the twentieth century. *Nat. Geosci.* **6**, 404–411.
- Ahn I.-Y., Chung K. H. and Choi H. J. (2004) Influence of glacial runoff on baseline metal accumulation in the Antarctic limpet *Nacella concinna* from King George Island. *Mar. Pollut. Bull.* **49**, 119–127.
- Ahn I.-Y., Lee S. H., Kim K. T., Shim J. H. and Kim D.-Y. (1996) Baseline heavy metal concentrations in the Antarctic clam, *Laternula elliptica* in Maxwell Bay, King George Island, Antarctica. *Mar. Pollut. Bull.* **32**, 592–598.
- Ahrland S. (1975) Metal complexes present in seawater. In *The nature of seawater* (ed. E. Goldberg). Dahlem Workshop Report, Dahlem Konferenzen, Berlin. pp. 219–244.
- Algeo T. and Tribovillard N. (2009) Environmental analysis of paleoceanographic systems based on molybdenum–uranium covariation. *Chem. Geol.* **268**, 211–225.
- Aller R. C., Mackin J. and Cox R. (1986) Diagenesis of Fe and S in Amazon inner shelf muds: apparent dominance of Fe reduction and implications for the genesis of ironstones. *Cont. Shelf Res.* **6**, 263–289.
- Anbar A. D., Creaser R., Papanastassiou D. and Wasserburg G. (1992) Rhenium in seawater: Confirmation of generally conservative behavior. *Geochim. Cosmochim. Acta* **56**, 4099–4103.
- Ancora S., Volpi V., Olmastroni S., Focardi S. and Leonzio C. (2002) Assumption and elimination of trace elements in Adélie penguins from Antarctica: a preliminary study. *Mar. Environ. Res.* **54**, 341–344.

- Anderson J. B. (1999) *Antarctic marine geology.*, Cambridge University Press.
- Anderson R. F., Lehuray A. P., Fleisher M. Q. and Murray J. W. (1989) Uranium deposition in Saanich Inlet sediments, Vancouver Island. *Geochim. Cosmochim. Acta* **53**, 2205–2213.
- Appleby P. G. and Oldfield F. (1978) The calculation of lead-210 dates assuming a constant rate of supply of unsupported ^{210}Pb to the sediment. *Catena* **5**, 1–8.
- Aristarain A. J., Delmas R. J. and Stievenard M. (2004) Ice-core study of the link between sea-salt aerosol, sea-ice cover and climate in the Antarctic Peninsula area. *Clim. Chang.* **67**, 63–86.
- Aristarain A. J., Jouzel J. and Pourchet M. (1986) Past Antarctic Peninsula climate (1850-1980) deduced from an ice core isotope record. *Clim. Chang.* **8**, 69–89.
- Arntz W. E., Brey T. and Gallardo A. (1994) Antarctic zoobenthos. *Oceanogr. Mar. Biol., Annu. Rev.* **32**, 241–304.
- Ashcroft W. (1972) Crustal Structure of the South Shetland Islands and Bransfield Strait. *BAS Scientific Report* **66**, 43 pp.
- ATCM (2009) Final Report Part II, Measure 9: Management Plan for Antarctic Specially Protected Area No. 150. In *XXXII. Antarctic Treaty Consultative Meeting* Baltimore, United States, 13 pp.
- Babu C., Brumsack H.-J. and Schnetger B. (1999) Distribution of organic carbon in surface sediments along the eastern Arabian Sea: a revisit. *Mar. Geol.* **162**, 91–103.
- Baker P. E., Roobol M. J. A., Davies T. G., McReath I. and Harvey M. R. (1975) The geology of the South Shetland Islands: V. Volcanic evolution of Deception Island. *BAS Scientific Reports* **78**, 79 pp.
- Bakker D. C., Bozec Y., Nightingale P. D., Goldson L. E., Messias M.-J., de Baar H. J., Liddicoat M. I., Skjelvan I., Strass V. and Watson A. J. (2005) Iron and mixing affect biological carbon uptake in SOIREE and EisenEx, two Southern Ocean iron fertilization experiments. *Deep-Sea Res. I Oceanog. Res. Pap.* **52**, 1001–1019.
- Barbosa A., Benzal J., León A. and Moreno J. (2012) Population decline of chinstrap penguins (*Pygoscelis antarctica*) on Deception Island, South Shetlands, Antarctica. *Polar Biol.* **35**, 1453–1457.

- Barcena M. A., Gersonde R., Ledesma S., Fabres J., Calafat A. M., Canals M., Sierro F. J., Flores J. A., Bárcena M. A. and Fabrés J. (1998) Record of Holocene glacial oscillations in Bransfield Basin as revealed by siliceous microfossil assemblages. *Antarct. Sci.* **10**, 269–285.
- Barker P. and Griffiths D. (1972) The evolution of the Scotia Ridge and Scotia Sea. *Phil. Trans. R. Soc. A* **271**, 151–183.
- Barnes C. E. and Cochran J. K. (1990) Uranium removal in oceanic sediments and the oceanic U balance. *Earth Planet. Sci. Lett.* **97**, 94–101.
- Baroni C. and Orombelli G. (1994) Abandoned penguin rookeries as Holocene paleoclimatic indicators in Antarctica. *Geology* **22**, 23–26.
- Le Bas M. J., Le Maitre R. W., Streckeisen A., Zanettin B., Le Bas M. and Le Maitre R. (1986) A chemical classification of volcanic rocks based on the total alkali silica diagram. *J. Petrol.* **27**, 745–750.
- Beck M., Dellwig O., Holstein J. M., Grunwald M., Liebezeit G., Schnetger B. and Brumsack H.-J. (2008a) Sulphate, dissolved organic carbon, nutrients and terminal metabolic products in deep pore waters of an intertidal flat. *Biogeochemistry* **89**, 221–238.
- Beck M., Dellwig O., Schnetger B. and Brumsack H.-J. (2008b) Cycling of trace metals (Mn, Fe, Mo, U, V, Cr) in deep pore waters of intertidal flat sediments. *Geochim. Cosmochim. Acta* **72**, 2822–2840.
- Benesch R. and Mangelsdorf P. (1972) Eine Methode zur colorimetrischen Bestimmung von Ammoniak in Meerwasser. *Helgol. Wissenschaftliche Meeresunters.* **23**, 365–375.
- Bentley M. J., Hodgson D. A., Smith J. A., Cofaigh C. O., Domack E. W., Larter R. D., Roberts S. J., Brachfeld S., Leventer A., Hjort C., Hillenbrand C.-D. D. and Evans J. (2009) Mechanisms of Holocene palaeoenvironmental change in the Antarctic Peninsula region. *The Holocene* **19**, 51–69.
- Berner R. (1981) A new geochemical classification of sedimentary environments. *J. Sediment. Petrol.* **51**, 359–365.
- Berner R. A. and Raiswell R. (1983) Burial of organic carbon and pyrite sulfur in sediments over Phanerozoic time: a new theory. *Geochim. Cosmochim. Acta* **47**, 855–862.
- Bertine K. K. and Turekian K. K. (1973) Molybdenum in marine deposits. *Geochim. Cosmochim. Acta* **37**, 1415–1434.

- Beyer L., Pingpank K., Wriedt G., Bölter M. and Bolter M. (2000) Soil formation in coastal continental Antarctica (Wilkes Land). *Geoderma* **95**, 283–304.
- Birkenmajer K. (1992) Evolution of the Bransfield Basin and Rift, West Antarctica. In *Recent Progress in Antarctica Earth Science* (eds. Y. Yoshida, K. Kaminuma, and K. Shiraishi). Terra Scientific Publ. Co., Tokyo. pp. 405–410.
- Birkenmajer K. (1998a) Geology of volcanic rocks (Upper Cretaceous-Lower Tertiary) at Potter Peninsula, King George Island (South Shetland Islands, West Antarctica). *B. Pol. Acad. Sci-Earth* **46**, 147–155.
- Birkenmajer K. (1982) Late Cenozoic phases of block-faulting on King-George-Island (South-Shetland-Islands, West Antarctica). *Bulletin De L Academie Polonaise Des Sciences-Serie Des Sciences De La Terre* **30**, 21–32.
- Birkenmajer K. (1998b) Quaternary geology at Potter Peninsula, King George Island (South Shetland Islands, West Antarctica). *B. Pol. Acad. Sci-Earth* **46**, 9–20.
- Birkenmajer K. (2001) *Studia Geologica Polonica Vol. 118.*, Instytut Nauk Geologicznych, Krakow, 188 pp.
- Bjerregaard P. and Depledge M. (1994) Cadmium accumulation in *Littorina littorea*, *Mytilus edulis* and *Carcinus maenas* - The influence of salinity and calcium ion concentrations. *Mar. Biol.* **119**, 385–395.
- Björck S., Håkansson H., Zale R., Karlen W. and Jónsson B. L. (1991a) A late Holocene lake sediment sequence from Livingston Island, South Shetland Islands, with palaeoclimatic implications. *Antarct. Sci.* **3**, 61–72.
- Björck S., Hjort C., Ingólfsson O. and Skog G. (1991b) Radiocarbon dates from the Antarctic Peninsula - problems and potential. In *Radiocarbon dating: recent applications and future potential* (ed. J. J. Lowe). Quaternary Research Association, Cambridge. pp. 55–56.
- Björck S., Malmer N., Hjort C., Sandgren P., Ingólfsson Ó., Wallén B., Smith R. I. L., Jónsson B. L., Ingólfsson O., Wallén B. and Jónsson B. L. (1991c) Stratigraphic and Paleoclimatic Studies of a 5500-Year-Old Moss Bank on Elephant Island, Antarctica. *Arctic Alpine Res.* **23**, 361–374.
- Björck S., Olsson S., Ellis-Evans C., Håkansson H., Humlum O., de Lirio J. M., Ellis-Evans C., Håkansson H. and DeLirio J. M. (1996) Late Holocene palaeoclimatic records from lake sediments on James Ross Island, Antarctica. *Palaeogeogr. Palaeoclimatol. Palaeoecol.* **121**, 195–220.

- Björck S., Sandgren P. and Zale R. (1991d) Late Holocene tephrochronology of the northern Antarctic Peninsula. *Quaternary Res.* **36**, 322–328.
- Blaauw M. (2010) Methods and code for “classical” age-modelling of radiocarbon sequences. *Quat. Geochronol.* **5**, 512–518.
- Blaauw M. and Christen J. (2011) Flexible palaeoclimate age-depth models using an autoregressive gamma process. *Bayesian Anal.* **6**, 457–474.
- Blain S., Quéguiner B., Armand L., Belviso S., Bombled B., Bopp L., Bowie A. R., Brunet C., Brussaard C., Carlotti F., Christaki U., Corbière A., Dzrand I., Ebersbach F., Fuda J.-L., Garcia N., Gerringa L., Griffith B., Guigue C., Guillerm C., Jacquet S., Jeandel C., Laan P., Lefèvre D., Monaco C. Lo, Malits A., Mosseri J., Obernosterer I., Park Y.-H., Picherat M., Pondaven P., Remenyi T., Sandroni V., Sarthou G., Savoye N., Scouarnec L., Souhaut M., Thuiller D., Timmermans K., Trull T., Uitz J., van Beek P., Veldhuis M., Vincent D., Violler E., Vong L. and Wagener T. (2007) Effects of natural iron fertilization on carbon sequestration in the Southern Ocean. *Nature* **446**, 1070–1074.
- Böning P., Cuypers S., Grunwald M., Schnetger B. and Brumsack H.-J. (2005) Geochemical characteristics of Chilean upwelling sediments at ~36°S. *Mar. Geol.* **220**, 1–21.
- Borer P. M., Sulzberger B., Reichard P. and Kraemer S. M. (2005) Effect of siderophores on the light-induced dissolution of colloidal iron(III) (hydr) oxides. *Mar. Chem.* **93**, 179–193.
- Boudreau B. (1997) *Diagenetic models and their implectation: modelling transport and reactions in aquatic sediments.*, Springer-Verlag, Berlin, Heidelberg, New York, 414 pp.
- Boyd P. and Ellwood M. (2010) The biogeochemical cycle of iron in the ocean. *Nat. Geosci.* **3**, 675–682.
- Boyd P., Jickells T., Law C., Blain S., Boyle E., Buesseler K. O., Coale K. H., Cullen J., de Baar H. J., Follows M., Harvey M., Lancelot C., Levasseur M., Owens N., Pollard R., Rivkin R., Sarmiento J., Schoemann V., Smetacek V., Takeda S., Tsuda A., Turner S. and Watson A. (2007) Mesoscale iron enrichment experiments 1993-2005: Synthesis and future directions. *Science* **315**, 612–617.

- Braun M. and Gossmann H. (2002) Glacial changes in the area of Admiralty Bay and Potter Cove, King George Island, maritime Antarctica. In *Geoecology and Antarctic ice-free coastal landscapes* (eds. L. Beyer and M. Bölter). Springer, Berlin, Heidelberg. pp. 75–89.
- Braun M. and Hock R. (2004) Spatially distributed surface energy balance and ablation modelling on the ice cap of King George Island (Antarctica). *Global Planet. Change* **42**, 45–58.
- Brey T., Voigt M., Jenkins K. and Ahn I. (2011) The bivalve *Laternula elliptica* at King George Island - A biological recorder of climate forcing in the West Antarctic Peninsula region. *J. Marine Syst.* **88**, 542–552.
- Bricher P. . K., Lucieer A. and Woehler E. J. (2008) Population trends of Adélie penguin (*Pygoscelis adeliae*) breeding colonies: a spatial analysis of the effects of snow accumulation and human activities. *Polar Biol.* **31**, 1397–1407.
- Broecker W. S. (2001) Paleoclimate - was the medieval warm period global? *Science* **291**, 1497–1499.
- Bronk Ramsey C. (2009) Bayesian analysis of radiocarbon dates. *Radiocarbon* **51**, 337–360.
- Bruland K. W. and Lohan M. (2004) The control of trace metals in seawater. In *The oceans and marine geochemistry: Treatise on geochemistry* (eds. H. Holland and K. Turekian). Pergamon, Oxford, U.K. pp. 23–47.
- Brumsack H.-J. (1989) Geochemistry of recent TOC-rich sediments from the Gulf of California and the Black Sea. *Geol. Rundsch.* **78**, 851–882.
- Burdige D. J. (1993) The biogeochemistry of manganese and iron reduction in marine sediments. *Earth-Sci. Rev.* **35**, 249–284.
- Calvert S. and Pedersen T. (1993) Geochemistry of recent oxic and anoxic marine sediments: Implications for the geological record. *Mar. Geol.* **113**, 67–88.
- Canfield D. E. (1989) Sulfate reduction and oxic respiration in marine sediments: implications for organic carbon preservation in euxinic environments. *Deep-Sea Res. I Oceanog. Res. Pap.* **36**, 121–138.
- Canfield D. E., Raiswell R. and Bottrell S. H. (1992) The reactivity of sedimentary iron minerals toward sulfide. *Am. J. Sci.* **292**, 659–683.
- Canfield D. E. and Thamdrup B. (2009) Towards a consistent classification scheme for geochemical environments, or, why we wish the term “suboxic” would go away. *Geobiology* **7**, 385–392.

- Canfield D. E., Thamdrup B. and Hansen J. W. (1993) The anaerobic degradation of organic matter in Danish coastal sediments: iron reduction, manganese reduction, and sulfate reduction. *Geochim. Cosmochim. Acta* **57**, 3867–3883.
- Carmichael N., Squibb K., Engel D. and Fowler B. (1980) Metals in the molluscan kidney: Uptake and subcellular distribution of ^{109}Cd , ^{54}Mn and ^{65}Zn by the clam *Mercenaria mercenaria*. *Comp. Biochem. Physiol. A Physiol.* **65**, 203–206.
- Chang K. II, Jun H. K., Park G. T. and Eo Y. S. (1990) Oceanographic conditions of Maxwell Bay, King George Island, Antarctica (Austral summer 1989). *Korean Journal of Polar Res.* **1**, 27–46.
- Chen M. and Wang W.-X. (2001) Bioavailability of natural colloid-bound iron to marine plankton: Influences of colloidal size and aging. *Limnol. Oceanogr.* **46**, 1956–1967.
- Chun H. Y., Chang S. K. and Lee J. I. (1994) Biostratigraphic study on the plant fossils from the Barton Peninsula and adjacent area. *J. Paleont. Soc. Korea* **10**, 69–84.
- Church T., Sarin M., Fleisher M. and Ferdelman T. (1996) Salt marshes: An important coastal sink for dissolved uranium. *Geochim. Cosmochim. Acta* **60**, 3879–3887.
- Clapperton C. M. and Sugden D. E. (1988) Holocene glacier fluctuations in South America and Antarctica. *Quaternary Sci. Rev.* **7**, 185–198.
- Clarke A., Murphy E. J., Meredith M. P., King J. C., Peck L. S., Barnes D. K. A. and Smith R. C. (2007) Climate change and the marine ecosystem of the western Antarctic Peninsula. *Phil. Trans. R. Soc. B: Biological Sciences* **362**, 149–166.
- Cline J. (1969) Spectrophotometric determination of hydrogen sulfide in natural waters. *Limnol. Oceanogr.* **14**, 454–458.
- Coale K. H., Johnson K. S., Chavez F. P., Buesseler K. O., Barber R. T., Brzezinski M. a, Cochlan W. P., Millero F. J., Falkowski P. G., Bauer J. E., Wanninkhof R. H., Kudela R. M., Altabet M. a, Hales B. E., Takahashi T., Landry M. R., Bidigare R. R., Wang X., Chase Z., Strutton P. G., Friederich G. E., Gorbunov M. Y., Lance V. P., Hiltling A. K., Hiscock M. R., Demarest M., Hiscock W. T., Sullivan K. F., Tanner S. J., Gordon R. M., Hunter C. N., Elrod V. a, Fitzwater S. E., Jones J. L., Tozzi S., Koblizek M., Roberts A. E., Herndon J., Brewster J., Ladizinsky N., Smith G., Cooper D., Timothy D., Brown S. L., Selph K. E., Sheridan C. C., Twining B. S. and Johnson Z. I. (2004) Southern Ocean iron enrichment experiment: carbon cycling in high- and low-Si waters. *Science* **304**, 408–414.

-
- Colodner D., Edmond J. and Boyle E. (1995) Rhenium in the Black Sea: comparison with molybdenum and uranium. *Earth Planet. Sci. Lett.* **31**, 1–15.
- Colodner D., Sachs J., Ravizza G., Turekian K., Edmond J. and Boyle E. (1993) The geochemical cycle of rhenium: a reconnaissance. *Earth Planet Sci Lett* **117**, 205–221.
- Cook A. J., Fox A. J., Vaughan D. G. and Ferrigno J. G. (2005) Retreating glacier fronts on the Antarctic Peninsula over the past half-century. *Science* **308**, 541–544.
- Croxall J., Trathan P. and Murphy E. (2002) Environmental change and Antarctic seabird populations. *Science* **297**, 1510–1514.
- Crusius J., Calvert S., Pedersen T. and Sage D. (1996) Rhenium and molybdenum enrichments in sediments as indicators of oxic, suboxic and anoxic conditions of deposition. *Earth Planet. Sci. Lett.* **145**, 65–78.
- Curtosi A., Pelletier E., Vodopivec C., St Louis R. and Mac Cormack W. P. (2010) Presence and distribution of persistent toxic substances in sediments and marine organisms of Potter Cove, Antarctica. *Arch. Environ. Contam. Toxicol.* **59**, 582–592.
- Dean R. and Dixon W. (1951) Simplified statistics for small numbers of observations. *Anal. Chem.* **23**, 636–638.
- Dean W. (1974) Determination of carbonate and organic matter in calcareous sediments and sedimentary rocks by loss on ignition, comparison with other models. *J. Sediment. Petrol.* **44**, 242–248.
- Dearing J. (1986) Core correlation and total sediment influx. In *Handbook Of Holocene Palaeoecology and Palaeohydrology* (ed. B. Berglund). Wiley, Chicester. pp. 247–270.
- Death R., Wadham J., Monteiro F., Le Brocq A., Tranter M., Ridgwell A., Dutkiewicz S. and Raiswell R. (2013) Antarctic ice sheet fertilises the Southern Ocean. *Biogeosciences* **10**, 12551–12570.
- Decho A. and Luoma S. (1996) Flexible digestion strategies and trace metal assimilation in marine bivalves. *Limnol. Oceanogr.* **41**, 568–572.
- Deheyn D. D., Gendreau P., Baldwin R. J. and Latz M. I. (2005) Evidence for enhanced bioavailability of trace elements in the marine ecosystem of Deception Island, a volcano in Antarctica. *Mar. Environ. Res.* **60**, 1–33.

- Dellwig O., Beck M., Lemke A., Lunau M., Kolditz K., Schnetger B. and Brumsack H.-J. (2007a) Non-conservative behaviour of molybdenum in coastal waters: Coupling geochemical, biological, and sedimentological processes. *Geochim. Cosmochim. Acta* **71**, 2745–2761.
- Dellwig O., Bosselmann K., Koelsch S., Hentscher M., Hinrichs J., Boettcher M. E., Reuter R. and Brumsack H.-J. (2007b) Sources and fate of manganese in a tidal basin of the German Wadden Sea. *J. Sea Res.* **57**, 1–18.
- Dick D., Philipp E. E., Kriews M. and Abele D. (2007) Is the umbo matrix of bivalve shells (*Laternula elliptica*) a climate archive? *Aquat. Toxicol.* **84**, 450–456.
- Dierssen H. M., Smith R. C. and Vernet M. (2002) Glacial meltwater dynamics in coastal waters west of the Antarctic peninsula. *P. Natl. Acad. Sci. USA* **99**, 1790–1795.
- Ding Q. and Steig E. J. (2013) Temperature change on the Antarctic Peninsula linked to the tropical Pacific. *J. Climate* **26**, 7570–7585.
- Dold B., Gonzales-Toril E., Aguilera A., Lopez-Pamo E., Cisternas M., Bucchi F. and Amils R. (2013) Acid rock drainage and rock weathering in Antarctica: Important sources for iron cycling in the Southern Ocean. *Environ. Sci. Technol.* **47**, 6129–6136.
- Domack E. W., Burnett A. and Leventer A. (2003) Environmental setting of the Antarctic Peninsula. In *Antarctic Peninsula climate variability. Antarctic Research Series, vol. 79* (ed. E. W. Domack). American Geophysical Union, Washington, DC. pp. 1–13.
- Domack E. W., Foss D., Syvitski J. and McClennen C. E. (1994) Transport of suspended particulate matter in an Antarctic Fjord. *Mar. Geol.* **121**, 161–170.
- Domack E. W. and Ishman S. (1993) Oceanographic and physiographic controls on modern sedimentation within Antarctic fjords. *Geol. Soc. Am. Bull.* **105**, 1175–1189.
- Domack E. W., Ishman S. E., Stein A., McClennen C. E. and Julls A. T. (1995) Late Holocene advance of the Muller Ice Shelf, Antarctic Peninsula : sedimentological , geochemical and palaeontological evidence. *Antarct. Sci.* **7**, 159–170.
- Domack E. W., Leventer A., Dunbar R., Taylor F., Brachfeld S. and Sjunneskog C. (2001) Chronology of the Palmer Deep site, Antarctic Peninsula: a Holocene palaeoenvironmental reference for the circum-Antarctic. *The Holocene* **11**, 1–9.

- Dominguez C., Eraso A. and Domínguez M. del C. (2007) Substantial changes happened during the last years in the icecap of King George, Insular Antarctica. *Karst and Cryokarst* **45**, 87–110.
- Ducklow H. W., Baker K., Martinson D. G., Langdon B. Q., Ross R. M., Smith R. C., Stammerjohn S. E., Vernet M., Fraser W. R. and Quetin L. B. (2007) Marine pelagic ecosystems: the West Antarctic Peninsula. *Philos. T. Roy. Soc. B.* **362**, 67–94.
- Duff M., Coughlin J. and Hunter D. (2002) Uranium co-precipitation with iron oxide minerals. *Geochim. Cosmochim. Acta* **66**, 3533–3547.
- Dunbar R. B., Leventer A. R. and Stockton W. L. (1989) Biogenic sedimentation in McMurdo Sound, Antarctica. *Mar. Geol.* **85**, 155–179.
- Eckert S., Brumsack H.-J., Severmann S., Schnetger B., März C. and Fröllje H. (2013) Establishment of euxinic conditions in the Holocene Black Sea. *Geology* **41**, 523–524.
- Eisler R. (1977) Acute toxicities of selected heavy metals to the softshell clam *Mya arenaria*. *Bull. Environ. Contam. Toxicol.* **17**, 137–145.
- Elderfield H. (1972) Effects of volcanism on water chemistry, Deception Island, Antarctica. *Mar. Geol.* **13**, M1–M6.
- Elderfield H. (1976) Manganese fluxes to the oceans. *Mar. Chem.* **4**, 103–132.
- Elderfield H., Mackenzie A., Berner R. A., Meadows P., Jones J., Clemmey H., Murchison D., Durand B., Eglinton G. and Sarnthein M. (1985) Element cycling in bottom sediments. *Phil. Trans. R. Soc. B* **315**, 19–23.
- Elrod V. A., Berelson W., Coale K. and Johnson K. (2004) The flux of iron from continental shelf sediments: A missing source for global budgets. *Geophys. Res. Lett.* **31**, L12307.
- Emslie S. D. (2001) Radiocarbon dates from abandoned penguin colonies in the Antarctic Peninsula region. *Antarct. Sci.* **13**, 289–295.
- Emslie S. D., Baumann K. and van Tuinen M. (2011) Late Holocene occupation of Gentoo penguins (*Pygoscelis papua*) on Byers Peninsula, Livingston island, Antarctica. *Polar Biol.* **34**, 283–290.
- Emslie S. D., Coats L. and Licht K. (2007) A 45,000 yr record of Adelie penguins and climate change in the Ross Sea, Antarctica. *Geology* **35**, 61–64.
- Emslie S. D., Karnovsky N. and Trivelpiece W. Z. (1995) Avian predation at penguin colonies on King George Island, Antarctica. *Wilson Bull.* **107**, 317–327.

-
- Emslie S. D. and Patterson W. (2007) Abrupt recent shift in delta C-13 and delta N-15 values in Adelie penguin eggshell in Antarctica. *P. Natl. Acad. Sci. USA* **104**, 11666–11669.
- Emslie S. D. and Woehler E. J. (2005) A 9000-year record of Adélie penguin occupation and diet in the Windmill Islands, East Antarctica. *Antarct. Sci.* **17**, 57–66.
- Erickson B. E. and Helz G. R. (2000) Molybdenum(VI) speciation in sulfidic waters: Stability and lability of thiomolybdates. *Geochim. Cosmochim. Acta* **64**, 1149–1158.
- Fisher N., Teyssie J., Fowler S. and Wang W. (1996) Accumulation and retention of metals in mussels from food and water: A comparison under field and laboratory conditions. *Environ. Sci. Technol.* **30**, 3232–3242.
- Föllmi K. (1996) The phosphorus cycle, phosphogenesis and marine phosphate-rich deposits. *Earth-Sci. Rev.* **40**, 55–124.
- Forcada J., Trathan P. N., Reid K., Murphy E. J. and Croxall J. P. (2006) Contrasting population changes in sympatric penguin species in association with climate warming. *Glob. Chang. Biol.* **12**, 411–423.
- Franzmann P., Skyring G., Burton H. and Deprez P. (1988) Sulfate reduction rates and some aspects of the limnology of four lakes and a fjord in the Vestfold Hills, Antarctica. *Hydrobiologia* **165**, 25–33.
- Fraser W. R. and Hofmann E. E. (2003) A predator's perspective on causal links between climate change, physical forcing and ecosystem response. *Mar. Ecol. Prog. Ser.* **265**, 1–15.
- Fraser W. R., Trivelpiece W. Z., Ainley D. G. and Trivelpiece S. G. (1992) Increases in Antarctic penguin populations: reduced competition with whales or a loss of sea ice due to environmental warming? *Polar Biol.* **11**, 525–531.
- Fretwell P., Convey P., Fleming A., Peat H. and Hughes K. (2011) Detecting and mapping vegetation distribution on the Antarctic Peninsula from remote sensing data. *Polar Biol.* **34**, 273–281.
- Froelich P., Klinkhammer G., Bender M., Luedtke N., Heath G., Cullen D., Dauphin P., Hammond D., Hartman B. and Maynard V. (1979) Early oxidation of organic matter in pelagic sediments of the eastern Equatorial Atlantic - Suboxic diagenesis. *Geochim. Cosmochim. Acta* **43**, 1075–1090.

-
- Gagnon C. and Fisher N. (1997) The bioavailability of sediment-bound Cd, Co, and Ag to the mussel *Mytilus edulis*. *Can. J. Fish. Aquat. Sci.* **54**, 147–156.
- Gates D. (1980) *Biophysical Ecology.*, Springer, New York, 611 pp.
- George S. and Coombs T. (1977) Effects of high stability iron-complexes on the kinetics of iron accumulation and excretion in *Mytilus edulis* (L.). *J. Exp. Mar. Biol. Ecol.* **28**, 133–140.
- George S., Pirie B. and Coombs T. (1976) The kinetics of accumulation and excretion of ferric hydroxide in *Mytilus edulis* (L.) and its distribution in the tissues. *J. Exp. Mar. Biol. Ecol.* **23**, 71–84.
- Gohl K. (2007) The expedition ANT-XXIII/4 of the research vessel Polarstern in 2006. *Reports on Polar and Marine Research* **557**, 166.
- Gonzales P., Abele D. and Puntarulo S. (2010) Exposure to excess dissolved iron in vivo affects oxidative status in the bivalve *Mya arenaria*. *Comp. Biochem. Physiol. C. Toxicol. Pharmacol.* **152**, 167–174.
- Gonzales P. and Puntarulo S. (2011) Iron and nitrosative metabolism in the Antarctic mollusc *Laternula elliptica*. *Comp. Biochem. Physiol. C. Toxicol. Pharmacol.* **153**, 243–250.
- Goosse H., Masson-Delmotte V., Renssen H., Delmotte M., Fichetef F., Morgan V., van Ommen Ta., Khim B.-K. and Stenni B. (2004) A late medieval warm period in the Southern Ocean as a delayed response to external forcing? *Geophys. Res. Lett.* **31**, L06203.
- Gribsholt B. and Kristensen E. (2003) Benthic metabolism and sulfur cycling along an inundation gradient in a tidal spartina anglica salt marsh. *Limnol. Oceanogr.* **48**, 2151–2162.
- Griffith T. W. and Anderson J. B. (1989) Climatic control of sedimentation in bays and fjords of the northern Antarctic Peninsula. *Mar. Geol.* **85**, 181–204.
- Griscom S. and Fisher N. (2004) Bioavailability of sediment-bound metals to marine bivalve molluscs: An overview. *Estuaries* **27**, 826–838.
- Hall B. L. (2007) Late-Holocene advance of the Collins Ice Cap, King George Island, South Shetland Islands. *The Holocene* **17**, 1253–1258.
- Harper E., Clark M., Hoffman J., Philipp E. E., Peck L. S. and Morley S. (2012) Iceberg scour and shell damage in the Antarctic clam *Laternula elliptica*. *PLOS One* **7**, e46341.

- Hartnett H., Boehme S., Thomas C., DeMaster D. and Smith C. (2008) Benthic oxygen fluxes and denitrification rates from high-resolution porewater profiles from the Western Antarctic Peninsula continental shelf. *Deep-Sea Res. Pt II* **55**, 2415–2424.
- Hass H. C., Kuhn G., Monien P., Brumsack H.-J. and Forwick M. M. (2010) Climate fluctuations during the past two millennia as recorded in sediments from Maxwell Bay, South Shetland Islands, West Antarctica eds. J. A. Howe, W. E. N. Austin, M. Forwick, and M. Paetzel. *Geol. Soc. London, Spec. Pub.* **344**, 243–260.
- Heinrichs H., Brumsack H. J., Lofffield N. and König N. (1986) Improved pressure digestion system for biological and anorganic materials. *Z Pflanz Bodenkunde* **149**, 350–353.
- Helz G., Miller C., Charnock J., Mosselmans J., Patrick R., Garner C. and Vaughan D. J. (1996) Mechanism of molybdenum removal from the sea and its concentration in black shales: EXAFS evidence. *Geochim. Cosmochim. Acta* **60**, 3631–3642.
- Hemming S. R. S., van de Flierdt T., Goldstein S. L., Franzese A. M., Roy M., Gastineau G. and Landrot G. (2007) Strontium isotope tracing of terrigenous sediment dispersal in the Antarctic Circumpolar Current: Implications for constraining frontal positions. *Geochem. Geophys. Geosy.* **8**, Q06N13.
- Heroy D. C., Sjunneskog C. and Anderson J. B. (2008) Holocene climate change in the Bransfield Basin, Antarctic Peninsula: evidence from sediment and diatom analysis. *Antarct. Sci.* **20**, 69–87.
- Hjort C., Ingólfsson Ó., Möller P. and Lirio J. M. (1997) Holocene glacial history and sea-level changes on James Ross Island, Antarctic Peninsula. *J. Quaternary Sci.* **12**, 259–273.
- Hobden D. (1967) Iron metabolism in *Mytilus edulis*. I. Variation in total content and distribution. *J. Mar. Biol. Assoc. UK* **47**, 597–606.
- Hofstee E. H., Balks M. R., Petchey F. and Campbell D. I. (2006) Soils of Seabee Hook, Cape Hallett, northern Victoria Land, Antarctica. *Antarct. Sci.* **18**, 473–486.
- Houghton J. T., Ding Y., Griggs D. J., Noguer M., van den Linden P. J., Dai X., Maskell K. and Johnson C. A. (2001) *Climate change 2001: The Scientific Basis.*, Cambridge University Press, Cambridge, 892 pp.

- Howarth R. and Jørgensen B. B. (1984) Formation of ^{35}S -labelled elemental sulfur and pyrite in coastal marine sediments (Limfjorden and Kysing Fjord, Denmark) during short-term $^{35}\text{SO}_4^{2-}$ reduction measurements. *Geochim. Cosmochim. Acta* **48**, 1807–1818.
- Howe J. A. and Pudsey C. J. (1999) Antarctic Circumpolar Deep Water: a Quaternary paleoflow record from the northern Scotia Sea, South Atlantic Ocean. *J. Sediment. Res.* **69**, 847–861.
- Howe J. A., Wilson C. R., Shimmield T. M., Diaz R. J. and Carpenter L. W. (2007) Recent deep-water sedimentation, trace metal and radioisotope geochemistry across the Southern Ocean and Northern Weddell Sea, Antarctica. *Deep-Sea Res. Pt II* **54**, 1652–1681.
- Huang T., Sun L. G., Wang Y. H. and Kong D. M. (2011) Late Holocene Adélie penguin population dynamics at Zolotov Island, Vestfold Hills, Antarctica. *J. Paleolimnol.* **45**, 273–285.
- Huang T., Sun L., Wang Y., Liu X. and Zhu R. (2009) Penguin population dynamics for the past 8500 years at Gardner Island, Vestfold Hills. *Antarct. Sci.* **21**, 571–578.
- Husmann G. (2013) The bivalve *Laternula elliptica*: physiological and molecular response to changing coastal Antarctic environments. Doctoral Thesis, Christian-Albrecht-University, Kiel, 180 pp.
- Husmann G., Abele D., Monien D., Monien P., Kriews M. and Philipp E. E. (2012) The influence of sedimentation on metal accumulation and cellular oxidative stress markers in the Antarctic bivalve *Laternula elliptica*. *Estuar. Coast. Shelf S.* **111**, 48–59.
- Husmann G., Philipp E. E., Rosenstiel P., Vazquez S. and Abele D. (2011) Immune response of the Antarctic bivalve *Laternula elliptica* to physical stress and microbial exposure. *J. Exp. Mar. Biol. Ecol.* **398**, 83–90.
- Iken K., Quartino M., Barrera-Oro E., Palermo J., Wiencke C. and Brey T. (1998) Trophic relations between macroalgae and herbivores. In *The Potter Cove coastal ecosystem, Antarctica. Ber. Polarforsch.* 299 (eds. C. Wiencke, G. Ferreyra, W. Arntz, and C. Rinaldi). pp. 258–262.
- Ingólfsson Ó., Hjort C. and Humlum O. (2003) Glacial and climate history of the Antarctic Peninsula since the Last Glacial Maximum. *Arct. Antarct. Alp. Res.* **35**, 175–186.

- Jaccard S., Hayes C., Martínez-García A., Hodell D., Anderson R., Sigman D. and Haug G. (2013) Two modes of change in Southern Ocean Productivity over the past million years. *Science* **339**, 1419–1423.
- Jakobsen R. and Postma D. (1989) Formation and solid-solution behaviour of Carthodochrosites in marine muds of the Baltic Deeps. *Geochim. Cosmochim. Acta* **53**, 2639–2648.
- Jarvis I., Burnett W. C., Nathan Y., Almbaydin F. S. M., Attia A. K. M., Castro L. N., Flicoteaux R., Hilmy M. E., Husain V., Qutawnah A. A., Serjani A., N. Z. Y., Seriani A. and Zanin Y. N. (1994) Phosphorite geochemistry: state-of-the-art and environmental concerns. *Eclogae Geol. Helv.* **87**, 643–700.
- Jin X., Gruber N., Dunne J., Sarmiento J. and Armstrong R. (2006) Diagnosing the contribution of phytoplankton functional groups to the production and export of particulate organic carbon, CaCO₃, and opal from global nutrient and alkalinity distributions. *Global Biogeochem. Cycles* **20**, GB2015.
- Jones P. and Mann M. (2004) Climate over past millenia. *Rev. Geophys.* **42**, RG2002.
- Jones V., Hodgson D.A. and Chepstow-Lusty A. (2000) Palaeolimnological evidence for marked Holocene environmental changes on Signy Island, Antarctica. *The Holocene* **10**, 43–60.
- De Jong J., Schoemann V., Lannuzel D., Croot P., de Baar H. J. and Tison J.-L. (2012) Natural iron fertilization of the Atlantic sector of the Southern Ocean by continental shelf sources of the Antarctic Peninsula. *J. Geophys. Res.* **117**, G01029.
- Jørgensen B. B. (1982) Mineralization of organic matter in the sea bed - the role of sulphate reduction. *Nature* **296**, 643–645.
- Jwa Y.-J., Park B.-K. and Kim Y. (1992) Geochronology and geochemistry of the igneous rocks from Barton and Weaver peninsulas, King George Island: A review. In *Recent Progress in Antarctica Earth Science* (eds. Y. Yoshida, K. Kaminuma, and K. Shiraishi). Terra Scientific Publ. Co., Tokyo. pp. 439–442.
- Kadar E., Lowe D., Sole M., Fisher A., Jha A., Readman J. and Hutchinson T. (2010) Uptake and biological responses to nano-Fe versus soluble FeCl₃ in excised mussel gills. *Anal. Bioanal. Chem.* **396**, 657–666.
- Kattner G. (1999) Storage of dissolved inorganic nutrients in seawater: poisoning with mercury chloride. *Mar. Chem.* **67**, 61–66.

-
- Khim B. K., Park B. K. and Yoon H. II (1997) Oxygen isotopic compositions of seawater in the Maxwell Bay of King George Island, West Antarctica. *Geosci. J.* **1**, 115–121.
- Khim B.-K. K. and Yoon H. II (2003) Postglacial marine environmental changes in Maxwell Bay, King George Island, West Antarctica. *Polar Res.* **22**, 341–353.
- Khim B.-K. K., Yoon H. II, Kang C. Y. and Bahk J. J. (2002) Unstable Climate Oscillations during the Late Holocene in the Eastern Bransfield Basin, Antarctic Peninsula. *Quaternary Res.* **58**, 234–245.
- Kim H., Lee J., Choe M., Cho M., Zheng X., Sang H. and Qiu J. (2000) Geochronologic evidence for early Cretaceous volcanic activity on Barton Peninsula, King George Island, Antarctica. *Polar Res.* **19**, 251–260.
- King J. and Harangozo S. A. (1998) Climate change at the western Antarctic Peninsula since 1945: Observations and possible causes. *Ann. Glaciol.* **27**, 571–575.
- King P. and Broderip W. (1832) Description of the Cirripedia, Conchifera and Mollusca in a collection formed by the officers of HMS Adventure and Beagle employed between the years 1826 and 1830 in surveying the southern coasts of South America, including the straits of Magalhaens and the coast of Tierra del Fuego. *Zool. J.* **5**, 332–349.
- King S., Froelich P. N. and Jahnke R. (2000) Early diagenesis of germanium in sediments of the Antarctic South Atlantic: In search of the missing Ge sink. *Geochim. Cosmochim. Acta* **64**, 1375–1390.
- Klinkhammer G. and Palmer M. (1991) Uranium in the oceans: where it goes and why. *Geochim. Cosmochim. Acta* **55**, 1799–1806.
- Klöser H., Ferreyra G., Schloss I. R., Mercuri G., Laternus F. and Curtosi A. (1994) Hydrography of Potter Cove, a small fjord-like inlet on King George Island (South Shetlands). *Estuar. Coast. Shelf S.* **38**, 523–537.
- Knox S. and Turner D. (1980) Polarographic measurement of manganese(II) in estuarine waters. *Estuar. Coast. Shelf S.* **10**, 317–324.
- Koning E., Epping E., Raaphorst W. van and Van Raaphorst W. (2002) Determining biogenic silica in marine samples by tracking silicate and aluminium concentrations in alkaline leaching solutions. *Aquat. Geochem.* **8**, 37–67.

-
- Kostka J. E., Thamdrup B., Glud R. N. and Canfield D. E. (1999) Rates and pathways of carbon oxidation in permanently cold Arctic sediments. *Mar. Ecol. Prog. Ser.* **180**, 7–21.
- Kowalski N., Dellwig O., Beck M., Grunwald M., Durselen C., Badewien T. H., Brumsack H.-J., van Beusekom J. E. and Boettcher M. E. (2012) A comparative study of manganese dynamics in the water column and sediments of intertidal systems of the North Sea. *Estuar. Coast. Shelf S.* **100**, 3–17.
- Ku T.-L., Knauss K. G. and Mathieu G. G. (1977) Uranium in open ocean: concentration and isotopic composition. *Deep-Sea Res.* **24**, 1005–1017.
- L'Her Roux L., Le Roux S. and Appriou P. (1998) Behaviour and speciation of metallic species Cu, Cd, Mn and Fe during estuarine mixing. *Mar. Pollut. Bull.* **36**, 56–64.
- Laës A., Blain S., Laan P., Ussher S., Achterberg E., Treguer P. and de Baar H. J. (2007) Sources and transport of dissolved iron and manganese along the continental margin of the Bay of Biscay. *Biogeosciences* **4**, 181–194.
- Lam P. J. and Bishop J. K. (2008) The continental margin is a key source of iron to the HNLC North Pacific Ocean. *Geophys. Res. Lett.* **35**, L07608.
- Lam P. J., Ohnemus D. C. and Marcus M. A. (2012) The speciation of marine particulate iron adjacent to active and passive continental margins. *Geochim. Cosmochim. Acta* **80**, 108–124.
- Lancelot C., De Montety A., Goosse H., Becquevort S., Schoemann V., Pasquer B. and Vancoppenolle M. (2009) Spatial distribution of the iron supply to phytoplankton in the Southern Ocean: a model study. *Biogeosciences* **6**, 2861–2878.
- Landing W. and Bruland K. W. (1987) The contrasting biogeochemistry of iron and manganese in the Pacific Ocean. *Geochim. Cosmochim. Acta* **51**, 29–43.
- Langmuir D. (1978) Uranium solution-mineral equilibria at low temperatures with applications to sedimentary ore deposits. *Geochim. Cosmochim. Acta* **42**, 547–569.
- Lee B. and Luoma S. (1998) Influence of microalgal biomass on absorption efficiency of Cd, Cr, and Zn by two bivalves from San Francisco Bay. *Limnol. Oceanogr.* **43**, 1455–1466.

- Lee J. I., Hur S. D., Yoo C. M., Yeo J. P., Kim H., Hwang J., Choe M. Y., Nam S. H., Kim Y., Park B.-K., Zheng X. and Lopez-Martinez J. (2001) Explanatory text of the geologic map of Barton and Weaver Peninsulas, King George Island, Antarctica. In Korea Ocean Research and Development Institute. 28 pp.
- Lee Y. II, Lim H. S. and Yoon H. II (2004) Geochemistry of soils of King George Island, South Shetland Islands, West Antarctica: Implications for pedogenesis in cold polar regions. *Geochim. Cosmochim. Acta* **68**, 4319–4333.
- Lee Y. II, Lim H. S., Yoon H. II and Lee I. Y. (2009) Carbon and nitrogen isotope composition of vegetation on King George Island, maritime Antarctic. *Polar Biol.* **32**, 1607–1615.
- Lettmann K. A., Riedinger N., Ramlau R., Knab N., Böttcher M. E., Khalili A., Wolff J.-O. and Jørgensen B. B. (2012) Estimation of biogeochemical rates from concentration profiles: A novel inverse method. *Estuar. Coast. Shelf S.* **100**, 26–37.
- Leventer A., Domack E., Barkoukis A., McAndrews B. and Murray J. (2002) Laminations from the Palmer Deep: A diatom-based interpretation. *Paleoceanography* **17**, PAL 3-1–PAL 3-15.
- Leventer A. R., Domack E. W., Ishman S. E., Brachfeld S., McClennen C. E. and Manley P. (1996) Productivity cycles of 200–300 years in the Antarctic Peninsula region: Understanding linkages among the sun, atmosphere, oceans, sea ice, and biota. *GSA Bull.* **108**, 1626–1644.
- Lim C. H. (2013) Modelling waves and currents in Potter Cove, King George Island, Antarctica. Doctoral Thesis, Carl von Ossietzky University of Oldenburg, 113 pp.
- Liu S. M., Ye X. W., Zhang J. and Zhao Y. F. (2002) Problems with biogenic silica measurement in marginal seas. *Mar. Geol.* **192**, 383–392.
- Liu X. D., Nie Y., Sun L. and Emslie S. D. (2013) Eco-environmental implications of elemental and carbon isotope distributions in ornithogenic sediments from the Ross Sea region, Antarctica. *Geochim. Cosmochim. Acta* **117**, 99–114.
- Liu X. D., Sun J., Sun L. G., Liu W. Q. and Wang Y. H. (2011a) Reflectance spectroscopy: a new approach for reconstructing penguin population size from Antarctic ornithogenic sediments. *J. Paleolimnol.* **45**, 213–222.
- Liu X. D., Sun L. G., Li D. and Wang Y. H. (2011b) Rare earth elements in the ornithogenic sediments from the Maritime Antarctic: A potential new palaeoecology proxy. *Geochem. J.* **45**, 15–26.

- Liu X. D., Sun L. G., Xie Z. Q., Yin X. B. and Wang Y. H. (2005) A 1300-year record of penguin populations at Ardley Island in the Antarctic, as deduced from the geochemical data in the ornithogenic lake sediments. *Arct. Antarct. Alp. Res.* **37**, 490–498.
- Liu X., Sun L., Xie Z., Yin X., Zhu R. and Wang Y. (2007) A preliminary record of the historical seabird population in the Larsemann Hills, East Antarctica, from geochemical analyses of Mochou Lake sediments. *Boreas* **36**, 182–197.
- Liu X.-D. D., Li H.-C. C., Sun L.-G. G., Yin X.-B. B., Zhao S.-P. P. and Wang Y.-H. H. (2006) $\delta^{13}\text{C}$ and $\delta^{15}\text{N}$ in the ornithogenic sediments from the Antarctic maritime as palaeoecological proxies during the past 2000 yr. *Earth Planet. Sci. Lett.* **243**, 424–438.
- Lohan M., Statham P. and Peck L. (2001) Trace metals in the Antarctic soft-shell clam *Laternula elliptica*: Implications for metal pollution from Antarctic research stations. *Polar Biol.* **24**, 808–817.
- Lovley D. and Phillips E. (1988) Novel mode of microbial energy metabolism - Organic carbon oxidation coupled to dissimilatory reduction of iron or manganese. *Appl. Environ. Microbiol.* **54**, 1472–1480.
- Lovley D. R., Phillips E. J., Gorby Y. A. and Landa E. R. (1991) Microbial reduction of uranium. *Nature* **350**, 413–416.
- Lynn D. and Bonatti E. (1965) Mobility of manganese in diagenesis of deep-sea sediments. *Mar. Geol.* **3**, 457–474.
- Machado A., de Lima E. F., Chemale F., Alexandre F. M., Sommer C. A., Figueiredo A. M. G., Almeida D. del P. M. de and De Almeida D. D. P. M. (2008) Mineral Chemistry of Volcanic Rocks of South Shetland Archipelago, Antarctica. *Int. Geol. Rev.* **50**, 154–162.
- Machado A., Lima E. F. de, Chemale F., Morata D., Oteiza O., Almeida D. P. M. del P. M. de, Figueiredo A. M. G., Alexandre F. M., Urrutia J. L. and Chemale J. F. (2005) Geochemistry constraints of Mesozoic–Cenozoic calc-alkaline magmatism in the South Shetland arc, Antarctica. *J. S. Am. Earth Sci.* **18**, 407–425.
- Madison A., Tebo B., Mucci A., Sundby B. and Luther III G. W. (2013) Abundant porewater Mn(III) is a major component of the sedimentary redox system. *Science* **341**, 875–878.
- Magos L. and Webb M. (1980) The interactions of selenium with cadmium and mercury. *Crit. Rev. Toxicol.* **8**, 1–42.

- Majewski W., Wellner J. S., Szczuciński W. and Anderson J. B. (2012) Holocene oceanographic and glacial changes recorded in Maxwell Bay, West Antarctica. *Mar. Geol.* **326-328**, 67–79.
- Marshall G., Orr A., van Lipzig N. P. and King J. C. (2006) The impact of a changing Southern Hemisphere annular mode on Antarctic Peninsula summer temperatures. *J. Climate* **19**, 5388–5404.
- Martin J. H., Gordon R. M. and Fitzwater S. E. (1990) Iron in Antarctic waters. *Nature* **345**, 156–158.
- Masson-Delmotte V., Buiron D., Ekaykin A., Frezzotti M., Gallée H., Jouzel J., Krinner G., Landais A., Motoyama H., Oerter H., Pol K., Pollard D., Ritz C., Schlosser E., Sime L. C., Sodemann H., Stenni B., Uemura R., Vimeux F. and Gallee H. (2011) A comparison of the present and last interglacial periods in six Antarctic ice cores. *Clim. Past.* **7**, 397–423.
- Matthies D., Mäusbacher R. and Storzer D. (1990) Deception Island tephra: a stratigraphical marker for limnic and marine sediments in Bransfield Strait area, Antarctica. *Zent.bl. Geol. Paläontologie* **1**, 153–165.
- Mäusbacher R., Müller J. and Schmidt R. (1989) Evolution of postglacial sedimentation in Antarctic lakes (King-George-Island). *Z. Geomorphol.* **33**, 219–234.
- Mawji E., Gledhill M., Milton J. A., Tarran G. A., Ussher S., Thompson A., Wolff G. A., Worsfold P. J. and Achterberg E. P. (2008) Hydroxamate siderophores: Occurrence and importance in the Atlantic Ocean. *Environ. Sci. Technol.* **42**, 8675–8680.
- McCormac F. G., Hogg A. G., Blackwell P. G., Buck C. E., Higham T. F. G. and Reimer P. J. (2004) SHCal04 southern hemisphere calibration, 0-11.0 cal kyr BP. *Radiocarbon* **46**, 1087–1092.
- Measures C. I., Hatta M. and Grand M. M. (2012) Bioactive trace metal distributions and biogeochemical controls in the Southern Ocean. *Oceanography* **25**, 122–133.
- Mercone D., Thomson J., Croudace I. W. and Troelstra S. R. (1999) A coupled natural immobilisation mechanism for mercury and selenium in deep-sea sediments. *Geochim. Cosmochim. Acta* **63**, 1481–1488.
- Meredith M. P., Brandon M. A., Wallace M. I., Clarke A., Leng M. J., Renfrew I. A., van Lipzig N. P. M. and King J. C. (2008) Variability in the freshwater balance of northern Marguerite Bay, Antarctic Peninsula: Results from $\delta^{18}\text{O}$. *Deep-Sea Res. Pt II* **55**, 309–322.

- Meredith M. P. and King J. C. (2005) Rapid climate change in the ocean west of the Antarctic Peninsula during the second half of the 20th century. *Geophys. Res. Lett.* **32**, 1–5.
- Metian M., Warnau M., Hédouin L. and Bustamante P. (2009) Bioaccumulation of essential metals (Co, Mn and Zn) in the king scallop *Pecten maximus*: Seawater, food and sediment exposures. *Mar. Biol.* **156**, 2063–2075.
- Michalchuk B. R., Anderson J. B., Wellner J. S., Manley P. L., Majewski W. and Bohaty S. (2009) Holocene climate and glacial history of the northeastern Antarctic Peninsula: the marine sedimentary record from a long SHALDRIL core. *Quaternary Sci. Rev.* **28**, 3049–3065.
- Micol T. and Jouventin P. (2001) Long-term population trends in seven Antarctic seabirds at Pointe Géologie (Terre Adélie). *Polar Biol.* **24**, 175–185.
- Middag R., de Baar H. J., Laan P. and Huhn O. (2012) The effects of continental margins and water mass circulation on the distribution of dissolved aluminum and manganese in Drake Passage. *J. Geophys. Res.-Oceans* **117**, C01019.
- Middleburg J. J., de Lange G. J. and Vanderweijden C. H. (1987) Manganese solubility control in marine pore waters. *Geochim. Cosmochim. Acta* **51**, 759–763.
- Millero F. J., Yao W. and Aicher J. (1995) The speciation of Fe(II) and Fe(III) in natural waters. *Mar. Chem.* **50**, 21–39.
- Milliken K. T., Anderson J. B., Wellner J. S., Bohaty S. M. and Manley P. L. (2009) High-resolution Holocene climate record from Maxwell Bay, South Shetland Islands, Antarctica. *Geol. Soc. Am. Bull.* **121**, 1711–1725.
- Miranda K., Espey M. and Wink D. (2001) A rapid, simple spectrophotometric method for simultaneous detection of nitrate and nitrite. *Nitric Oxide* **5**, 62–71.
- Moline M. A., Claustre H., Frazer T. K., Schofield O. and Vernet M. (2004) Alteration of the food web along the Antarctic Peninsula in response to a regional warming trend. *Glob. Chang. Biol.* **10**, 1973–1980.
- Monien D., Kuhn G., von Eynatten H. and Talarico F. M. (2012) Geochemical provenance analysis of fine-grained sediment revealing Late Miocene to recent paleo-environmental changes in the western Ross Sea, Antarctica. *Global Planet. Change* **96-97**, 41–58.

- Monien D., Monien P., Bruenjes R. M., Widmer T., Schnetger B. and Brumsack H.-J. (2013) Sedimentary regimes at Potter Cove, King George Island, maritime Antarctica - from source to sink. *European Geosciences Union General Assembly 2013 - Geophysical Research Abstracts* **15**, 7454.
- Monien P. (2008) A geochemical comparison of Holocene sediments from Maxwell Bay and Potter Cove off King George Island (Antarctic Peninsula). Diploma Thesis, Carl von Ossietzky University, Oldenburg, 112 pp.
- Monien P., Schnetger B., Brumsack H.-J., Hass H. C. and Kuhn G. (2011) A geochemical record of late Holocene palaeoenvironmental changes at King George Island (maritime Antarctica). *Antarct. Sci.* **23**, 255–267.
- Montes-Hugo M., Doney S. C., Ducklow H. W., Fraser W., Martinson D., Stammerjohn S. E. and Schofield O. (2009) Recent changes in phytoplankton communities associated with rapid regional climate change along the western Antarctic Peninsula. *Science* **323**, 1470–1473.
- Morford J. L., Emerson S. R., Breckel E. J. and Kim S. H. (2005) Diagenesis of oxyanions (V, U, Re, and Mo) in pore waters and sediments from a continental margin. *Geochim. Cosmochim. Acta* **69**, 5021–5032.
- Morford J. L., Martin W. R. and Carney C. M. (2012) Rhenium geochemical cycling: Insights from continental margins. *Chem. Geol.* **324-325**, 73–86.
- Morford J. L., Martin W. R., François R. and Carney C. M. (2009) A model for uranium, rhenium, and molybdenum diagenesis in marine sediments based on results from coastal locations. *Geochim. Cosmochim. Acta* **73**, 2938–2960.
- Morford J. L., Martin W. R., Kalnejais L. H., François R., Bothner M. and Karle I.-M. (2007) Insights on geochemical cycling of U, Re and Mo from seasonal sampling in Boston Harbor, Massachusetts, USA. *Geochim. Cosmochim. Acta* **71**, 895–917.
- Morgan J., Mitchell D. and Chapman P. (1986) Individual and combined toxicity of manganese and molybdenum to mussel, *Mytilus edulis*, larvae. *Bull. Environ. Contam. Toxicol.* **37**, 303–307.
- Morris A. (1975) Dissolved molybdenum and vanadium in the northeast Atlantic Ocean. *Deep-Sea Res. Oceanogr. Abstr.* **22**, 49–54.
- Morris E. M. and Vaughan D. (2003) Spatial and temporal variation of surface temperature on the Antarctic Peninsula and the limit of viability of ice shelves. In *Antarctic Research Series* (eds. E. Domack, A. Burnett, and A. Leventer). AGU, Washington, DC. pp. 61–68.

- Mucci A. (2004) The behavior of mixed Ca-Mn carbonates in water and seawater: Controls of manganese concentrations in marine porewaters. *Aquat. Geochem.* **10**, 139–169.
- Mulvaney R., Abram N. J., Hindmarsh R. C., Arrowsmith C., Fleet L., Triest J., Sime L. C., Alemany O. and Foord S. (2012) Recent Antarctic Peninsula warming relative to Holocene climate and ice-shelf history. *Nature* **489**, 141–144.
- Myrcha A., Pietr S. and Tatur A. (1985) The role of pygoscelid penguin rookeries in nutrient cycles at Admiralty Bay, King George Island. In *Antarctic Nutrient Cycles and Food Webs* (eds. W. Siegfried, P. R. Condy, and R. M. Laws). Springer-Verlag, Berlin, Heidelberg, New York, Tokyo. pp. 156–162.
- Navas A., López-Martínez J., Casas J., Machín J., Durán J. J., Serrano E., Cuchi J.-A. A., Mink S., Lopez-Martinez J., Machin J. and Duran J. J. (2008) Soil characteristics on varying lithological substrates in the South Shetland Islands, maritime Antarctica. *Geoderma* **144**, 123–139.
- Nedwell D. (1989) Benthic microbial activity in an Antarctic coastal sediment at Signy Island, South Orkney Islands. *Estuar. Coast. Shelf S.* **28**, 507–516.
- Nedwell D. and Walker T. R. (1995) Sediment-water fluxes of nutrients in an Antarctic coastal environment: influence of bioturbation. *Polar Biol.* **15**, 57–64.
- Nesbitt H. W. and Young G. M. (1982) Early Proterozoic climates and plate motions inferred from major element chemistry of lutites. *Nature* **299**, 715–717.
- Nielsen S. H., Koc N. and Crosta X. (2004) Holocene climate in the Atlantic sector of the Southern Ocean: controlled by insolation or oceanic circulation? *Geology* **32**, 317–320.
- Nigro M., Regoli F., Rocchi R. and Orlando E. (1997) Heavy metals in Antarctic molluscs. In *Antarctic communities species and survival* (ed. B. Battaglia). Cambridge University Press, Cambridge. pp. 409–412.
- Nodwell L. M. and Price N. M. (2001) Direct use of inorganic colloidal iron by marine mixotrophic phytoplankton. *Limnol. Oceanogr.* **46**, 765–777.
- Noguchi K., Hui W., Gel Y., Gastwirth J. and Miao W. (2009) lawstat: An R package for biostatistics, public policy, and law. *R package version 2.3*.
- Oreskes N. (2004) The scientific consensus on climate change. *Science* **306**, 1686.
- Paillard D., Labeyrie L. and Yiou P. (1996) Macintosh program performs time-series analysis. *EOS* **77:379**.

- Pakhomov E. A., Fuentes V., Schloss I. R., Atencio A. and Esnal G. B. (2003) Beaching of the tunicate *Salpa thompsoni* at high levels of suspended particulate matter in the Southern Ocean. *Polar Biol.* **26**, 427–431.
- Pakhornova S., Hall P., Kononets M., Rozanov A., Tengberg A. and Vershinin A. (2007) Fluxes of iron and manganese across the sediment-water interface under various redox conditions. *Mar. Chem.* **107**, 319–331.
- Park H., Ahn I., Lee J., Shin S., Lee J. and Choy E. (2009) Molecular cloning, characterization, and the response of manganese superoxide dismutase from the Antarctic bivalve *Laternula elliptica* to PCB exposure. *Fish Shellfish Immun.* **27**, 522–528.
- Parkinson C. (2002) Trends in the length of the Southern Ocean sea ice season, 1979–1999. *Ann. Glaciol.* **34**, 435–440.
- Pentreath R. (1973) The accumulation from water of ^{65}Zn , ^{54}Mn , ^{58}Co and ^{59}Fe by the mussel, *Mytilus edulis*. *J. Mar. Biol. Assoc. UK* **53**, 127–143.
- Philipp E. E., Brey T., Voigt M. and Abele D. (2008) Growth and age of *Laternula elliptica* populations in Potter Cove, King George Island. *Berichte zur Polar- und Meeresforschung* **571**, 216–222.
- Pike J., Swann G. E., Leng M. J. and Snelling A. M. (2013) Glacial discharge along the west Antarctic Peninsula during the Holocene. *Nat. Geosci.* **6**, 199–202.
- Postma D. (1993) The reactivity of iron oxides in sediments: A kinetic approach. *Geochim. Cosmochim. Acta* **57**, 5027–5034.
- Poulton S. W., Krom M. D. and Raiswell R. (2004) A revised scheme for the reactivity of iron(oxyhydr)oxide minerals towards dissolved sulfide. *Geochim. Cosmochim. Acta* **68**, 3703–3715.
- Poulton S. W. and Raiswell R. (2005) Chemical and physical characteristics of iron oxides in riverine and glacial meltwater sediments. *Chem. Geol.* **218**, 203–221.
- Pritchard H. D. and Vaughan D. G. (2007) Widespread acceleration of tidewater glaciers on the Antarctic Peninsula. *J. Geophys. Res.* **112**, 1–10.
- Quartino M. L., Deregibus D., Campana G. L., Latorre G. E. J. and Momo F. R. (2013) Evidence of macroalgal colonization on newly ice-free areas following glacial retreat in Potter Cove (South Shetland Islands), Antarctica. *PLOS One* **8**, e58223.

-
- Quartino M. L. and de Zaixso A. L. B. (2008) Summer macroalgal biomass in Potter Cove, South Shetland Islands, Antarctica: Its production and flux to the ecosystem. *Polar Biol.* **31**, 281–294.
- R Developer Core Team (2011) R: A language and environment for statistical computing. R Foundation for Statistical Computing.
- Rack W. and Rott H. (2004) Pattern of retreat and disintegration of the Larsen B Ice Shelf. *Ann. Glaciol.* **39**, 505–510.
- Rainbow P. (1990) Heavy metal levels in marine invertebrates. In *Heavy metals in the marine environment* (eds. R. Furness and P. Rainbow). CRC Press, Inc., Boca Raton. pp. 67–79.
- Rainbow P. (2002) Trace metal concentrations in aquatic invertebrates: why and so what? *Environ. Pollut.* **120**, 497–507.
- Rainbow P. S. (1989) Copper, Cadmium and Zinc concentrations in oceanic amphipod and euphausiid crustaceans, as a source of heavy-metals to pelagic seabirds. *Mar. Biol.* **103**, 513–518.
- Rainbow P. and Wang W. (2001) Comparative assimilation of Cd, Cr, Se, and Zn by the barnacle *Elminius modestus* from phytoplankton and zooplankton diets. *Mar. Ecol. Prog. Ser.* **218**, 239–248.
- Raiswell R. and Anderson T. (2005) Reactive iron enrichment in sediments deposited beneath euxinic bottom waters: constraints on supply by shelf recycling. *Geol. Soc. London, Spec. Pub.* **248**, 179–194.
- Raiswell R., Benning L., Tranter M. and Tulaczyk S. (2008) Bioavailable iron in the Southern Ocean: The significance of the iceberg conveyor belt. *Geochem. Trans.* **9**, 7.
- Raiswell R. and Canfield D. E. (1996) Rates of reaction between silicate iron and dissolved sulfide in Peru Margin sediments. *Geochim. Cosmochim. Acta* **60**, 2777–2787.
- Raiswell R. and Canfield D. E. (2012) The iron biogeochemical cycle past and present. *Geochemical Perspectives* **1**, 1–220.
- Raiswell R., Tranter M., Benning L., Siegert M., De'ath R., Huybrechts P. and Payne T. (2006) Contributions from glacially derived sediment to the global iron (oxyhydr)oxide cycle: implications for iron delivery to the oceans. *Geochim. Cosmochim. Acta* **70**, 2765–2780.

- Redfield A. C., Ketchum B. H. and Richards F. A. (1963) The influence of organisms on the composition of sea-water. In *The Sea: Ideas and observations on progress in the study of the seas* (ed. N. M. Hill). Interscience Publishers, New York. pp. 26–77.
- Reimer P. J., Baillie M. G., Bard E., Bayliss A., Beck J. W., Bertrand C. J., Blackwell P. G., Buck C. E., Burr G. S., Cutler K. B., Damon P. E., Edwards R. L., Fairbanks R. G., Friedrich M., Guilderson T. P., Hogg A. G., Hughen K. A., Kromer B., McCormac G., Manning S., Bronk Ramsey C., Reimer R. W., Remmele S., Southon J. R., Stuiver M., Talamo S., Taylor F., van der Plicht J. and Weyhenmeyer C. E. (2004) INTCAL04 terrestrial radiocarbon age calibration, 0–26 cal kyr BP. *Radiocarbon* **46**, 1029–1058.
- Reimer P. J., Baillie M. G., Bard E., Bayliss A., Beck J. W., Blackwell P. G., Bronk Ramsey C., Buck C. E., Burr G. S., Edwards R. L., Friedrich M., Grootes P., Guilderson T. P., Hajdas I., Heaton T., Hogg A. G., Hughen K. A., Kaiser K., Kromer B., McCormac F. G., Manning S. W., Reimer R. W., Richards D., Southon J. R., Talamo S., Turney C., van der Plicht J. and Weyhenmeyer C. E. (2009) INTCAL09 and MARINE09 radiocarbon age calibration curves, 0–50,000 years cal BP. *Radiocarbon* **51**, 1111–1150.
- Rey J., Somoza L. and Martinezfrias J. (1995) Tectonic, volcanic, and hydrothermal event sequence on Deception Island (Antarctica). *Geo-Mar. Lett.* **15**, 1–8.
- Rignot E., Bamber J. L., Van Den Broeke M. R., Davis C., Li Y. H., van de Berg W. J. and van Meijgaard E. (2008) Recent Antarctic ice mass loss from radar interferometry and regional climate modelling. *Nat. Geosci.* **1**, 106–110.
- Rignot E., Casassa G., Gogineni P., Krabill W., Rivera A. and Thomas R. (2004) Accelerated ice discharge from the Antarctic Peninsula following the collapse of Larsen B ice shelf. *Geophys. Res. Lett.* **31**, -.
- Rignot E. and Thomas R. H. (2002) Mass balance of polar ice sheets. *Science* **297**, 1502–1506.
- Rittenhouse G. (1943) Transportation and deposition of heavy minerals. *Geol. Soc. Am. Bull.* **54**, 1725–1750.
- Roberts S. J., Hodgson D. A., Sterken M., Whitehouse P. L., Verleyen E., Vyverman W., Sabbe K., Balbo A., Bentley M. J. and Moreton S. G. (2011) Geological constraints on glacio-isostatic adjustment models of relative sea-level change during deglaciation of Prince Gustav Channel, Antarctic Peninsula. *Quaternary Sci. Rev.* **30**, 3603–3617.

- Robertson J. (1953) Further studies on ionic regulation in marine invertebrates. *J. Exp. Biol.* **30**, 277–296.
- Robertson J. (1949) Ionic regulation in some marine invertebrates. *J. Exp. Biol.* **26**, 182–200.
- Rodushkin I. (1998) Capabilities of high resolution inductively coupled plasma mass spectrometry for trace element determination in plant sample digests. *Fresen. J. Anal. Chem.* **362**, 541–546.
- Roese M. and Drabble M. (1998) Wind driven circulation in Potter Cove. In *The Potter Cove coastal ecosystem, Antarctica* (eds. C. Wiencke, G. A. Ferreyra, W. Arntz, and C. Rinaldi). Reports on Polar Research, 299. pp. 40–46.
- Roitz J. and Bruland K. W. (1997) Determination of dissolved manganese(II) in coastal and estuarine waters by differential pulse cathodic stripping voltammetry. *Anal. Chim. Acta* **344**, 175–180.
- Roitz J., Flegal A. and Bruland K. W. (2002) The biogeochemical cycling of manganese in San Francisco Bay: Temporal and spatial variations in surface water concentrations. *Estuar. Coast. Shelf S.* **54**, 227–239.
- Rott H., Rack W., Skvarca P. and De Angelis H. (2002) Northern Larsen Ice Shelf, Antarctica: Further retreat after collapse. *Ann. Glaciol.* **34**, 277–282.
- Rott H., Skvarca P. and Nagler T. (1996) Rapid collapse of northern Larsen Ice Shelf, Antarctica. *Science* **271**, 788–792.
- Rückamp M., Braun M., Suckro S. and Blindow N. (2011a) Observed glacial changes on the King George Island ice cap, Antarctica, in the last decade. *Global Planet. Change* **79**, 99–109.
- Rückamp M., Braun M., Suckro S. and Blindow N. (2011b) Surface lowering, accumulation and area changes of the King George Island ice cap, Antarctica. *Global Planet. Change* **79**, 99–109.
- Rue E. L. and Bruland K. W. (1995) Complexation of iron(III) by natural organic ligands in the Central North Pacific as determined by a new competitive ligand equilibration/adsorptive cathodic stripping voltammetric method. *Mar. Chem.* **50**, 117–138.
- Rutgers van der Loeff M. M., Meadows P. and Allen J. (1990) Oxygen in pore waters of deep-sea sediments. *Phil. Trans. R. Soc. A* **331**, 69–84.

- Rysgaard S., Finster K. and Dahlggaard H. (1996) Primary production, nutrient dynamics and mineralisation in a northeastern Greenland fjord during the summer thaw. *Polar Biol.* **16**, 497–506.
- Rysgaard S., Thamdrup B., Risgaard-Petersen N., Fossing H., Berg P., Christensen P. B. and Dalsgaard T. (1998) Seasonal carbon and nutrient mineralization in a high-Arctic coastal marine sediment, Young Sound, Northeast Greenland. *Mar. Ecol. Prog. Ser.* **175**, 261–276.
- Sachs O., Sauter E., Schlüter M., Rutgers van der Loeff M. M., Jerosch K. and Holby O. (2009) Benthic organic carbon flux and oxygen penetration reflect different plankton provinces in the Southern Ocean. *Deep-Sea Res. Pt I - Oceanog. Res. Pap.* **56**, 1319–1335.
- Sani R., Peyton B., Amonette J. and Geesey G. (2004) Reduction of uranium(VI) under sulfate-reducing conditions in the presence of Fe(III)-(hydr)oxides. *Geochim. Cosmochim. Acta* **68**, 2639–2648.
- Santos I. R., Fávaro D. I., Schaefer C. E. C., Silva-Filho E. V and Favaro D. I. T. (2007) Sediment geochemistry in coastal maritime Antarctica (Admiralty Bay, King George Island): Evidence from rare earths and other elements. *Mar. Chem.* **107**, 464–474.
- Sarazin G., Michard G. and Prevot F. (1999) A rapid and accurate spectroscopic method for alkalinity measurements in sea water samples. *Water Res* **33**, 290–294.
- Sauer G. R., Wu L. N., Iijima M. and Wuthier R. E. (1997a) The influence of trace elements on calcium phosphate formation by matrix vesicles. *J. Inorg. Biochem.* **65**, 57–65.
- Sauer G., Wu L., Iijima M. and Wuthier R. (1997b) The influence of trace elements on calcium phosphate formation by matrix vesicles. *J. Inorg. Biochem.* **65**, 57–65.
- Scambos T. A., Bohlander J. A., Shuman C. A. and Skvarca P. (2004) Glacier acceleration and thinning after ice shelf collapse in the Larsen B embayment, Antarctica. *Geophys. Res. Lett.* **31**, L18402.
- Scambos T., Hulbe C. and Fahnestock M. (2003) Climate-induced ice shelf disintegration in the Antarctic Peninsula. In *Antarctic Peninsula climate variability. Antarctic Research Series, vol. 79* (ed. E. W. Domack). American Geophysical Union, Washington, DC. pp. 79–92.

- Scherer R. P. (1994) A new method for the determination of absolute abundance of diatoms and other silt-sized sedimentary particles. *J. Paleolimnol.* **12**, 171–179.
- Schloss I. R., Abele D., Moreau S., Demers S., Bers A. V., González O. and Ferreyra G. A. (2012) Resonse of phytoplankton dynamics to 19-year (1991-2009) climate trends in Potter Cove (Antarctica). *J. Marine Syst.* **92**, 53–66.
- Schloss I. R. and Ferreyra G. A. (2002) Primary production, light and vertical mixing in Potter Cove, a shallow bay in the maritime Antarctic. *Polar Biol.* **25**, 41–48.
- Schloss I. R., Ferreyra G. A., Mercuri G. and Kowalke J. (1999) Particle flux in an Antarctic shallow coastal environment. a sediment trap study. *Sci. Mar.* **63**, 99–111.
- Schloss I. R., Ferreyra G. A. and Ruiz-Pino D. (2002) Phytoplankton biomass in Antarctic shelf zones: a conceptual model based on Potter Cove, King George Island. *J. Marine Syst.* **36**, 129–143.
- Schnetger B. (1997) Trace element analysis of sediments by HR-ICP-MS using low and medium resolution and different acid digestions. *Fresen. J. Anal. Chem.* **359**, 468–472.
- Schnetger B., Brumsack H.-J., Schale H., Hinrichs J. and Dittert L. (2000) Geochemical characteristics of deep-sea sediments from the Arabian Sea: a high-resolution study. *Deep-Sea Res. Pt II* **47**, 2735–2768.
- Scholz F., Hensen C., Noffke A., Rohde A., Liebetrau V. and Wallmann K. (2011) Early diagenesis of redox-sensitice trace metals in the Peru upwelling area - response to ENSO-related oxygen fluctuations in the water column. *Geochim. Cosmochim. Acta* **75**, 7257–7276.
- Schroth A. W., Crusius J., Sholkovitz E. R. and Bostick B. C. (2009) Iron solubility driven by speciation in dust sources to the ocean. *Nat. Geosci.* **2**, 337–340.
- Scott F. J. and Marchant H. J. (2005) *Antarctic Marine Protists*. eds. F. J. Scott and H. J. Marchant, Australian Biological Resources Study (ABRS). CSIRO Publishing, Canberra, 572 pp.
- Seong Y. B., Owen L. A., Lim H. S., Yoon H. Il, Kim Y., Lee Y. Il and Caffee M. W. (2009) Rate of late Quaternary ice-cap thinning on King George Island, South Shetland Islands, West Antarctica defined by cosmogenic ³⁶Cl surface exposure dating. *Boreas* **38**, 207–213.

- Severmann S., McManus J., Berelson W. and Hammond D. (2010) The continental shelf benthic iron flux and its isotope composition. *Geochim. Cosmochim. Acta* **74**, 3984–4004.
- Shaked Y., Kustka A. B. and Morel F. M. (2005) A general kinetic model for iron acquisition by eukaryotic phytoplankton. *Limnol. Oceanogr.* **50**, 872–882.
- Shaw T. J., Gieskes J. M. and Jahnke R. A. (1990) Early diagenesis in differing depositional environments: The response of transition metals in pore water. *Geochim. Cosmochim. Acta* **54**, 1233–1246.
- Shaw T. J., Raiswell R., Hexel C., Vu H., Moore W. S., Dudgeon R. and Smith K. L. (2011) Input, composition, and potential impact of terrigenous material from free-drifting icebergs in the Weddell Sea. *Deep-Sea Res. Pt II* **58**, 1376–1383.
- Shepard A., Wingham D., Payne T. and Skvarca P. (2003) Larsen Ice Shelf has progressively thinned. *Science* **302**, 856–860.
- Shevenell A. E., Domack E. W. and Kernan G. M. (1996) Record of Holocene paleoclimate change along the Antarctic Peninsula: evidence from glacial marine sediments, Lallenmand Fjord. In *Climatic Succession and Glacial Record of the Southern Hemisphere* (eds. M. R. Banks and P. G. Quilty). *Pap. Proc. R. Soc. Tasman.* 130. pp. 55–64.
- Shevenell A., Ingalls A., Domack E. W. and Kelly C. (2011) Holocene Southern Ocean surface temperature variability west of the Antarctic Peninsula. *Nature* **470**, 250–254.
- Shevenell A. and Kennett J. (2002) Antarctic Holocene climate change: a benthic foraminiferal stable isotope record from Palmer Deep. *Paleoceanography* **17**, 1019.
- Sholkovitz E. (1973) Interstitial water chemistry of the Santa Barbara Basin sediments. *Geochim. Cosmochim. Acta* **37**, 2043–2073.
- Sholkovitz E. (1978) The flocculation of dissolved Fe, Mn, Al, Cu, Ni, Co and Cd during estuarine mixing. *Earth Planet. Sci. Lett.* **41**, 77–86.
- Shultz D. J. and Calder J. A. (1976) Organic carbon $^{13}\text{C}/^{12}\text{C}$ variations in estuarine sediments. *Geochim. Cosmochim. Acta* **40**, 381–385.
- Shumway S. (1977) Effects of salinity fluctuation on osmotic-pressure and Na^+ , Ca^{2+} and Mg^{2+} ion concentrations in hemolymph of bivalve molluscs. *Mar. Biol.* **41**, 153–177.

-
- Sigman D. M. and Boyle E. A. (2000) Glacial/interglacial variations in atmospheric carbon dioxide. *Nature* **407**, 859–869.
- Simkiss K. and Mason A. (1983) Metal ions: Metabolic and toxic effects. In *The mollusca: Environmental biochemistry and physiology* (eds. P. Hochachka and K. Wilbur). Academic Press, Inc., New York. pp. 101–164.
- Simkiss K. and Taylor M. (1981) Cellular mechanisms of metal ion detoxification and some new indices of pollution. *Aquat. Toxicol.* **1**, 279–290.
- Simmonds I. (2003) Modes of atmospheric variability over the Southern Ocean. *J. Geophys. Res.* **108**, 8078.
- Skoog D. A. and Leary J. J. (1996) *Instrumentelle Analytik.*, Springer, Berlin, 900 pp.
- Slomp C., Malchaert J., Lohse L. and Van Raaphorst W. (1997) Iron and manganese cycling in different sedimentary environments on the North Sea continental margin. *Cont. Shelf Res.* **17**, 1083–1117.
- Smellie J. L., Pankhurst R. J., Thomson M., Davies R. E. S. and Thompson M. R. A. (1984) The geology of the South Shetland Islands. VI. Stratigraphy, geochemistry and evolution. *BAS Scientific Reports* **87**, 85 pp.
- Smith R. C., Ainley D., Baker K., Domack E., Emslie S., Fraser B., Kennett J., Leventer A., Mosley-Thompson E., Stammerjohn S. and Vernet M. (1999) Marine ecosystem sensitivity to climate change. *Bioscience* **49**, 393–404.
- Solomon S., Qin D., Manning M., Chen Z., Marquis M., Averyt K. B., Tignor M. and Miller H. L. (2007) *Climate change 2007: the physical science basis - Contribution of working group I to the fourth assessment report of the Intergovernmental Panel on Climate Change*. Cambridge, 996 pp.
- Sørensen J., Jørgensen B. B. and Revsbech N. P. (1979) A comparison of oxygen, nitrate, and sulfate respiration in coastal marine sediments. *Microb. Ecol.* **5**, 105–115.
- Stammerjohn S. E., Martinson D. G., Smith R. C. and Iannuzzi R. A. (2008) Sea ice in the western Antarctic Peninsula region: Spatio-temporal variability from ecological and climate change perspective. *Deep-Sea Res. Pt II* **55**, 2041–2058.
- Stammerjohn S. E., Massom R., Rind D. and Martinson D. (2012) Regions of rapid sea ice change: An inter-hemispheric seasonal comparison. *Geophys. Res. Lett.* **39**, L06501.

- Steig E. J., Schneider D., Rutherford S., Mann M., Comiso J. and Shindell D. (2009) Warming of the Antarctic ice-sheet surface since the 1957 International Geophysical Year. *Nature* **457**, 459–462.
- Stenni B., Masson-Delmotte V., Selmo E., Oerter H., Meyer H., Röthlisberger R., Jouzel J., Cattani O., Falourd S., Fischer H., Hoffmann G., Iacumin P., Johnsen S., Minster B. and Udisti R. (2010) The deuterium excess records of EPICA Dome C and Dronning Maud Land ice cores (East Antarctica). *Quaternary Sci. Rev.* **29**, 146–159.
- Sterken M., Roberts S. J., Hodgson D. A., Vyverman W., Balbo A. L., Sabbe K., Moreton S. G., Verleyen E., Whitehouse P. L. and Bentley M. J. (2012) Holocene glacial and climate history of Prince Gustav Channel, northeastern Antarctic Peninsula. *Quaternary Sci. Rev.* **31**, 93–111.
- Stumm W. and Morgan J. J. (1981) *Aquatic Chemistry*, 2nd ed., Wiley-Interscience, New York.
- Sun L. G., Zhu R. B., Yin X. B., Liu X. D., Xie Z. Q., Wang Y. H., Liguang S., Renbin Z., Xuebin Y., Xiaodong L., Zhouqing X. and Yuhong W. (2004) A geochemical method for the reconstruction of the occupation history of a penguin colony in the maritime Antarctic. *Polar Biol.* **27**, 670–678.
- Sun L. and Xie Z. (2001) Relics: penguin population programs. *Science Progress* **84**, 31–44.
- Sun L., Xie Z. and Zhao J. (2000) A 3,000-year record of penguin populations. *Nature* **407**, 858.
- Sun S. S. and McDonough W. F. (1989) Chemical and isotopic systematics of oceanic basalts: implications for mantle composition and processes eds. A. D. Saunders and M. J. Norry. *Geol. Soc. London, Spec. Pub.* **42**, 313–345.
- Sundby B. and Silverberg N. (1985) Manganese fluxes in the benthic boundary-layer. *Limnol. Oceanogr.* **30**, 372–381.
- Sundby B. and Silverberg N. (1981) Pathways of manganese in an open estuarine system. *Geochim. Cosmochim. Acta* **45**, 293–307.
- Suzuki R. and Shimodaira H. (2006) Pvclost: an R package for assessing the uncertainty in hierarchical clustering. *Bioinformatics* **22**, 1540–1542.

- Tagliabue A., Bopp L., Dutay J.-C., Bowie A. R., Chever F., Jean-Baptiste P., Bucciarelli E., Lannuzel D., Remenyi T., Sarthou G., Aumont O., Gehlen M. and Jeandel C. (2010) Hydrothermal contribution to the oceanic dissolved iron inventory. *Nat. Geosci.* **3**, 252–256.
- Takahashi T., Williams R. and Bos D. (1982) Carbonate chemistry. In *GEOSECS Pacific Expedition, Volume 3: Hydrographic Data 1973-1974* (eds. W. S. Broecker, D. W. Spencer, and H. Craig). National Science Foundation, Washington D.C. pp. 77–83.
- Talarico F. M. and Sandroni S. (2011) Early Miocene basement clasts in ANDRILL AND-2A core and their implications for paleoenvironmental changes in the McMurdo Sound region. *Global Planet. Change* **78**, 23–35.
- Tatian M., Sahade R., Mercuri G., Fuentes V. L., Antacli J., Stellfeldt A. and Esnal G. B. (2008) Feeding ecology of benthic filter-feeders at Potter Cove, an Antarctic coastal ecosystem. *Polar Biol.* **31**, 509–517.
- Tatur A. and Barczuk A. (1985) Ornithogenic phosphates on King George Island in the maritime Antarctic. In *Antarctic Nutrient Cycles and Food Webs* (eds. W. R. Siegfried, P. R. Condy, and R. M. Laws). Springer, Berlin. pp. 163–168.
- Tatur A. and Keck A. (1990) Phosphates in ornithogenic soils of the maritime Antarctic. *Proc. NIPR Symp. Polar Biol.* **3**, 133–150.
- Tatur A., Myrcha A. and Niegodzisz J. (1997) Formation of abandoned penguin rookery ecosystems in the maritime Antarctic. *Polar Biol.* **17**, 405–417.
- Taylor F. and Sjunneskog C. (2002) Postglacial marine diatom record of the Palmer Deep, Antarctic Peninsula (ODP Leg 178, Site 1098) 2. Diatom assemblages. *Paleoceanography* **17**, PAL 2–1–PAL 2–12.
- Taylor F., Whitehead J. and Domack E. W. (2001) Holocene paleoclimate change in the Antarctic Peninsula: evidence from the diatom, sedimentary and geochemical record. *Mar. Micropaleontol.* **41**, 25–43.
- Thamdrup B. and Canfield D. E. (1996) Pathways of carbon oxidation in continental margin sediments off central Chile. *Limnol. Oceanogr.* **41**, 1629–1650.
- Thomas C. and Bendell-Young L. (1998) Linking the sediment geochemistry of an intertidal region to metal bioavailability in the deposit feeder *Macoma balthica*. *Mar. Ecol. Prog. Ser.* **173**, 197–213.

- Timmermann R., Le Brocq A., Deen T., Domack E. W., Dutrieux P., Galton-Fenzi B., Hellmer H., Humbert A., Jansen D., Jenkins A., Lambrecht A., Makinson K., Niederjasper F., Nitsche F., Nøst O., Smedsrud L. and Smith W. (2010) A consistent data set of Antarctic ice sheet topography, cavity geometry, and global bathymetry. *Earth System Science Data* **2**, 261–273.
- Tomas C. (1997) *Identifying Marine Phytoplankton.*, Academic Press Inc., New York, 858 pp.
- Toro M., Granados I., Pla S., Giralt S., Antoniadou D., Galan L., Cortizas A. M., Lim H. S. and Appleby P. G. (2013) Chronostratigraphy of the sedimentary record of Linnopolar Lake, Byers Peninsula, Livingston Island, Antarctica. *Antarct. Sci.* **25**, 198–212.
- Torre L., Servetto N., Eöry M. L., Momo F., Tatián M., Abele D. and Sahade R. (2012) Respiratory responses of three Antarctic ascidians and a sea pen to increased sediment concentrations. *Polar Biol.* **35**, 1743–1748.
- Tribovillard N., Algeo T. J., Lyons T. and Riboulleau A. (2006) Trace metals as paleoredox and paleoproductivity proxies: An update. *Chem. Geol.* **232**, 12–32.
- Tribovillard N., Riboulleau A., Lyons T. and Baudin F. (2004) Enhanced trapping of molybdenum by sulfurized marine organic matter of marine origin in Mesozoic limestones and shales. *Chem. Geol.* **213**, 385–401.
- Trivelpiece W. Z., Hinke J. T., Miller A. K., Reiss C. S., Trivelpiece S. G. and Watters G. M. (2011) Variability in krill biomass links harvesting and climate warming to penguin population changes in Antarctica. *P. Natl. Acad. Sci. USA* **108**, 7625–7628.
- Tromp T., van Cappellen P. and Key R. (1995) A global model for the early diagenesis of organic carbon and organic phosphorus in marine sediments. *Geochim. Cosmochim. Acta* **59**, 1259–1284.
- Trouwborst R. E., Clement B. G., Tebo B. M., Glazer B. T. and Luther III G. W. (2006) Soluble Mn(III) in suboxic zones. *Science* **313**, 1955–1957.
- Turner A. and Olsen Y. (2000) Chemical versus enzymatic digestion of contaminated estuarine sediment: Relative importance of iron and manganese oxides in controlling trace metal bioavailability. *Estuar. Coast. Shelf S.* **51**, 717–728.
- Turner J., Colwell S. R., Marshall G. J., Lachlan-Cope T. A., Carleton A. M., Jones P. D., Lagun V., Reid P. A. and Lagovkina S. (2005) Antarctic climate change during the last 50 years. *Int. J. Climatol.* **25**, 279–294.

- Vandieken V., Nickel M. and Jørgensen B. B. (2006) Carbon mineralization in Arctic sediments northeast of Svalbard: Mn(IV) and Fe(III) reduction as principal anaerobic respiratory pathways. *Mar. Ecol. Prog. Ser.* **322**, 15–27.
- Vaughan D. G. (2006) Recent trends in melting conditions on the Antarctic Peninsula and their implications for ice-sheet mass balance and sea level. *Arct. Antarct. Alp. Res.* **38**, 147–152.
- Vaughan D. G., Marshall G. J., Connolley W. M., Parkinson C., Mulvaney R., Hodgson D. A., King J. C., Pudsey C. J. and Turner J. (2003) Recent rapid regional climate warming on the Antarctic Peninsula. *Clim. Chang.* **60**, 243–274.
- Viarengo A. (1985) Biochemical effects of trace metals. *Mar. Pollut. Bull.* **16**, 153–158.
- Vorlicek T. P., Kahn M. D., Kasuya Y. and Helz G. R. (2004) Capture of molybdenum in pyrite-forming sediments: Role of ligand-induced reduction by polysulfides. *Geochim. Cosmochim. Acta* **68**, 547–556.
- Wagener T., Guieu C., Losno R., Bonnet S. and Mahowald N. (2008) Revisiting atmospheric dust export to the Southern Hemisphere ocean: biogeochemical implications. *Global Biogeochem Cycles* **22**, GB2006.
- Waite T. (2001) Thermodynamics of the iron system in seawater. In *The biogeochemistry of Iron in seawater* (eds. D. Turner and K. Hunter). John Wiley & Sons Ltd., West Sussex, U.K. pp. 291–342.
- Wang W. and Fisher N. (1999) Delineating metal accumulation pathways for marine invertebrates. *Sci. Total Environ.* **237-238**, 459–472.
- Watcham E. P., Bentley M. J., Hodgson D. A., Roberts S. J., Fretwell P. T., Lloyd J. M. J. M., Larter R. D., Whitehouse P. L., Leng M. J., Monien P. and Moreton S. G. S. (2011) A new Holocene relative sea level curve for the South Shetland Islands, Antarctica. *Quaternary Sci. Rev.* **30**, 3152–3170.
- Weimerskirch H., Inchausti P., Guinet C. and Barbraud C. (2003) Trends in bird and seal populations as indicators of a system shift in the Southern Ocean. *Antarct. Sci.* **15**, 249–256.
- Weston N. B., Porubsky W. P., Samarkin V. A., Erickson M., Macavoy S. E. and Joye S. B. (2006) Porewater stoichiometry of terminal metabolic products, sulfate, and dissolved organic carbon and nitrogen in estuarine intertidal creek-bank sediments. *Biogeochemistry* **77**, 375–408.

- Weykam G., Gómez C., Wiencke C., Iken K. and Klöser H. (1996) Photosynthetic characteristics and C:N ratios of macroalgae from King George Island (Antarctica). *J. Exp. Mar. Biol. Ecol.* **204**, 1–22.
- Wilhelm S. W. (1995) The ecology of cyanobacteria in iron-limited environments: a review of physiology and implications for aquatic environments. *Aquat. Microb. Ecol.* **9**, 295–303.
- Williams T. D. (1995) *The penguins: Spheniscidae.*, Oxford University Press, Oxford, 295 pp.
- Willmer P., Stone G. and Johnston I. (2000) *Environmental physiology of animals.*, Blackwell Science Ltd., Oxford, U.K, 768 pp.
- Willmott V., Domack E. W., Canals M. and Brachfeld S. (2006) A high resolution relative paleointensity record from the Gerlache-Boyd paleo-ice stream region, northern Antarctic Peninsula. *Quaternary Res.* **66**, 1–11.
- Willows R. (1992) Optimal digestive investment - A model for filter feeders experiencing variable diets. *Limnol. Oceanogr.* **37**, 829–847.
- Wilson P. R., Ainley D. G., Nur N., Jacobs S. S., Barton K. J., Ballard G. and Comiso J. C. (2001) Adélie penguin population change in the Pacific sector of Antarctica: relation to sea-ice extent and the Antarctic Circumpolar Current. *Mar. Ecol. Prog. Ser.* **213**, 301–309.
- Woehler E. J., Cooper J., Croxall J., Fraser W. R., Kooyman G., Miller G., Nel D., Patterson D., Peter H.-U., Ribic C., Salwicka K., Trivelpiece W. Z. and Weimerskirch H. (2001) A statistical assessment of the status and trends of Antarctic and Subantarctic seabirds. In *SCAR* Cambridge.
- Wright H. E. (1967) A square-rod piston sampler for lake sediments. *J. Sediment. Petrol.* **37**, 975–976.
- Yeats P., Sundby B. and Bowers J. (1979) Manganese recycling in coastal waters. *Mar. Chem.* **8**, 43–55.
- Yeo J. P., Lee J. I., Hur S. D. and Choi B. G. (2004a) Geochemistry of volcanic rocks in Barton and Weaver Peninsulas, King George Island, Antarctica: implications for arc maturity and correlation with fossilized volcanic centers. *Geosci. J.* **8**, 11–25.
- Yeo J. P., Lee J. I., Hur S. D. and Choi B.-G. (2004b) Geochemistry of igneous rocks in Barton and Weaver peninsulas, King George Island, Antarctica: Correlation with ancient volcanic centers. *Geosci. J.* **8**, 11–25.

-
- Yoo C. M., Choe M. Y., Jo H. R., Kim Y. and Kim K. H. (2001) Volcaniclastic sedimentation of the Sejong Formation (late Paleocene-Eocene), Barton Peninsula, King George Island, Antarctica. *Ocean Polar Res.* **23**, 97–107.
- Yoo K.-C., Yoon H. II, Kim J.-K. and Khim B.-K. (2009) Sedimentological, geochemical and palaeontological evidence for a neoglacial cold event during the late Holocene in the continental shelf of the northern South Shetland Islands, West Antarctica. *Polar Res.* **28**, 177–192.
- Yoon H. II, Park B.-K., Domack E. and Kim Y. (1998) Distribution and dispersal pattern of suspended particulate matter in Maxwell Bay and its tributary, Marian Cove, in the South Shetland Islands, West Antarctica. *Mar. Geol.* **152**, 261–275.
- Yoon H. II, Park B.-K. K., Kim Y. and Kim D. (2000) Glaciomarine sedimentation and its paleoceanographic implications along the fjord margins in the South Shetland Islands, Antarctica during the last 6000 years. *Palaeogeogr. Palaeoclimatol. Palaeoecol.* **157**, 189–211.
- Yoon H. II, Yoo K.-C., Bak Y.-S. Y.-S., Lim H. S., Kim Y. and Lee J. II (2010) Late Holocene cyclic glaciomarine sedimentation in a subpolar fjord of the South Shetland Islands, Antarctica, and its paleoceanographic significance: Sedimentological, geochemical, and paleontological evidence. *Geol. Soc. Am. Bull.* **122**, 1298–1307.
- Yoon H. II, Yoo K.-C., Park B.-K., Kim Y., Khim B.-K. and Kang C.-Y. (2004) The origin of massive diamicton in Marian and Potter coves, King George Island, West Antarctica. *Geosci. J.* **8**, 1–10.
- Young G. and Nesbitt H. (1998) Processes controlling the distribution of Ti and Al in weathering profiles, siliciclastic sediments and sedimentary rocks. *J. Sediment. Res.* **68**, 448–455.
- Zale R. (1994) Changes in size of the Hope Bay Adelie penguin rookery as inferred from Lake Boeckella sediment. *Ecography* **17**, 297–304.
- Zheng Y., Anderson R. F., van Geen A. and Kuwabara J. (2000) Authigenic molybdenum formation in marine sediments: a link to pore water sulfide in the Santa Barbara Basin. *Geochim. Cosmochim. Acta* **64**, 4165–4178.
- Zhu R. B., Sun L. G., Yin X. B., Xie Z. Q. and Liu X. D. (2005) Geochemical evidence for rapid enlargement of a gentoo penguin colony on Barton Peninsula in the maritime Antarctic. *Antarct. Sci.* **17**, 11–16.

Danksagungen

Im Rahmen meiner Doktorarbeit habe ich viele Menschen kennengelernt, die mich bei der vorliegenden Arbeit auf verschiedenste Art und Weise unterstützt haben und denen ich zu tiefstem Dank verpflichtet bin.

Zunächst danke ich ganz besonders Prof. Dr. Hans-Jürgen Brumsack für die Möglichkeit, in der Arbeitsgruppe Mikrobiogeochemie über die Geochemie antarktischer Sedimente promovieren zu können. Seine fortwährende Unterstützung während dieser Zeit, sein Vertrauen, das er in mich gesetzt hat und sein Glaube an mich haben entscheidend zum Gelingen dieser Arbeit beigetragen. Mein Dank gilt ferner Prof. Dr. Jürgen Rullkötter für seine Bereitschaft, die vorliegende Arbeit als Korreferent zu begutachten. Dr. Bernhard Schnetger danke ich, dass er mir die Analytik und die Önologie nähergebracht und mir stets für fachliche Gespräche und bei analytischen Problemen zur Seite gestanden hat. Seine Motivation, sein analytisches Wissen und sein Bestreben, analytische Methoden immer weiter zu optimieren haben mir sehr viel bei dieser Arbeit geholfen und mich nachhaltig geprägt.

Auf diesem Wege möchte ich mich auch bei Dr. Melanie Beck, Dr. Christian März, Dr. Thomas Riedel, Dr. Philipp Böning, Sebastian Eckert, Ann-Katrin Meinhardt und der gesamten geochemischen Familie für die unvergesslich schöne Zeit in der Arbeitsgruppe und die vielen, interessanten Diskussionen in den vergangenen Jahren bedanken. Eleonore Gründken, Carola Lehnert und Martina Schulz danke ich für ihr großes Engagement und ihre unermüdliche Hilfe im Labor. Ein großes Dankeschön geht darüber hinaus an Thomas Claassen und den Mitarbeitern der Werkstätten der Carl-von-Ossietzky Universität in Oldenburg für die schnelle und unkomplizierte Unterstützung beim Bau der Probenahmesysteme.

Sanja Asendorf, Harald Poigner, Oscar Gonzales und den argentinischen Marinetauchern möchte ich meinen großen Dank für ihren Beitrag bei der Probenahme auf den zwei Antarktis-Landexpeditionen aussprechen. Desweiteren bedanke ich mich ganz herzlich bei Tamara Manograsso Czalbowski und Susana Vazquez für ihre tatkräftige Hilfe auf den Expeditionen und während meines Auslandsaufenthaltes in Argentinien und Dr. Stephen J. Roberts vom British Antarctic Survey für seine fachliche Unterstützung und die langen Diskussionsabende.

Meinen Eltern bin ich zu tiefstem Dank für ihr Vertrauen und den Rückhalt, den sie mir stets gegeben haben, verpflichtet. Besonders möchte ich mich bei meiner Frau Donata und meiner Tochter Antonia Marie bedanken, die mich die letzten Jahre über bedingungslos unterstützt haben und ohne die diese vorliegende Arbeit niemals möglich gewesen wäre.

Diese Arbeit wurde von der Deutschen Forschungsgesellschaft (DFG) unter der Projektnummer BR 775/25-1 gefördert.

Curriculum vitae

Persönliche Daten

Name	Patrick Monien
Geburtsdatum/-ort	15.02.1977, Oldenburg
Staatsangehörigkeit	Deutsch
Anschrift	Mittellinie 130, 26160 Bad Zwischenahn
Telefon	04486-3049864
E-Mail	patrick.monien@uni-oldenburg.de

Schulischer Werdegang

1983 - 1987	Grundschule Feldbreite, Rastede
1987 - 1989	Orientierungsstufe der Kooperativen Gesamtschule Rastede
1989 - 1992	Gymnasialzweig der Kooperativen Gesamtschule Rastede

Akademischer Werdegang

10.1997 - 09.1998	Ruprecht-Karls-Universität, Heidelberg, Chemie (Dipl.)
10.2004 - 12.2008	Carl von Ossietzky Universität, Oldenburg, Marine Umweltwissenschaften (Dipl.) Diplomarbeit in der AG Mikrobiogeochemie am Institut für Chemie und Biologie des Meeres (ICBM) mit dem Titel: „A geochemical comparison of Holocene sediments from Maxwell Bay and Potter Cove off King George Island (Antarctic Peninsula)“ Diplom: 01.12.2008
seit 02.2009	Wissenschaftlicher Mitarbeiter und Promotionstudent in der AG Mikrobiogeochemie am Institut für Chemie und Biologie des Meeres (ICBM)

Erklärung

Hiermit versichere ich, dass ich die vorliegende Arbeit unter Berücksichtigung der Leitlinien guter wissenschaftlicher Praxis an der Carl-von-Ossietzky Universität Oldenburg selbstständig angefertigt und keine anderen als die angegebenen Quellen und Hilfsmittel verwendet habe. Zusätzlich erkläre ich, dass diese Dissertation weder in ihrer Gesamtheit noch in Teilen einer anderen wissenschaftlichen Hochschule zur Begutachtung in einem Promotionsverfahren vorliegt oder vorgelegen hat, und dass im Zusammenhang mit dem Promotionsvorhaben keine kommerziellen Vermittlungs- oder Beratungsdienste in Anspruch genommen worden sind.

Oldenburg, im Oktober 2013

Patrick Monien